SOURCE APPORTIONMENT OF Pb IN PM_{10} FROM THE UPPER MEŽA VALLEY BY THE USE OF ADVANCED ANALYTICAL TECHNIQUES

Tjaša Žerdoner

Doctoral Dissertation
Jožef Stefan International Postgraduate School
Ljubljana, Slovenia

Supervisor: Assoc. Prof. Dr. Tea Zuliani, Jožef Stefan Institute, Ljubljana, Slovenia
Co-Supervisor: Asst. Prof. Dr. Janja Vidmar, Jožef Stefan Institute, Ljubljana, Slovenia

Evaluation Board:
Prof. Dr. Maja Ponikvar-Svet, Chair, Jožef Stefan Institute, Ljubljana, Slovenia
Asst. Prof. Dr. Ingrid Falnoga, Member, Jožef Stefan Institute, Ljubljana, Slovenia
Prof. Dr. Johanna Irrgeher, Member, Montanuniversität, Leoben, Austria

MEDNARODNA PODIPLOMSKA ŠOLA JOŽEFA STEFANA
JOŽEF STEFAN INTERNATIONAL POSTGRADUATE SCHOOL

Tjaša Žerdoner

SOURCE APPORTIONMENT OF Pb IN PM_{10} FROM THE UPPER MEŽA VALLEY BY THE USE OF ADVANCED ANALYTICAL TECHNIQUES

Doctoral Dissertation

DOLOČANJE IZVORA Pb V PM_{10} IZ ZGORNJE MEŽIŠKE DOLINE Z UPORABO NAPREDNIH ANALIZNIH TEHNIK

Doktorska disertacija

Supervisor: Assoc. Prof. Dr. Tea Zuliani

Co-Supervisor: Asst. Prof. Dr. Janja Vidmar

Ljubljana, Slovenia, July 2025

Acknowledgments

The successful completion of this dissertation was made possible thanks to the support and guidance of many individuals who, in different ways, contributed to my PhD journey.

First and foremost, I would like to express my sincere gratitude to my supervisor, Assoc. Prof. Dr. Tea Zuliani, for her continuous guidance, encouragement, and support throughout my doctoral studies, as well as for challenging me to strengthen my research. Her expertise and invaluable advice have been crucial to the completion of this work. I am also sincerely grateful to my co-supervisor, Asst. Prof. Dr. Janja Vidmar, for her insightful feedback, availability, and willingness to provide advice whenever needed. Their mentorship and extensive expertise enabled me to gain new knowledge and skills that will help me throughout my career.

I am also thankful to the members of my doctoral dissertation evaluation board, Prof. Dr. Maja Ponikvar-Svet, Asst. Prof. Dr. Ingrid Falnoga and Prof. Dr. Johanna Irrgeher, for their constructive comments, which greatly enriched this work. I would also like to acknowledge the support of the Slovenian Research and Innovation Agency, as being part of the Young Researchers programme made it possible to conduct this research and pursue my PhD.

My warm thanks go to the entire Research Group for Trace Elements Speciation at the Jožef Stefan Institute, including Prof. Dr. Radmila Milačič Ščančar, Prof. Dr. Janez Ščančar, Dr. Stefan Marković, Dr. Katarina Kozlica, Pia Leban, Mišel Gorenčič, and Miroslav Štrbac. I greatly appreciate the constructive discussions, technical assistance, and the collaborative environment that made my research experience both productive and enjoyable. I would particularly like to thank my colleague and office mate, Dr. Majda Nikezić, for all the support, discussions, laughs, and shared experiences.

Finally, I am deeply grateful to my family and friends for their unconditional support, love, and encouragement. I am especially thankful to my husband for his invaluable emotional support, love, patience, and understanding during my doctoral studies. Their love and support have been my greatest source of strength throughout this journey.

Abstract

Knowledge of the pollution activity at the mining and smelting sites and assessment of contamination levels at different sites is not always sufficient for reliable conclusions regarding lead (Pb) provenance and contributions from sources. Pb isotopes have long been used as 'fingerprints' of the source of Pb recorded in environmental archives, as its isotope composition is not significantly affected by physical-chemical fractionation processes.

Due to the long and intensive mining and processing activities of Pb and zinc (Zn) in the Upper Meža Valley, the area is excessively polluted with Pb, Zn, cadmium (Cd), and other potentially toxic elements (PTEs). After the closure of the mine and smelter and the introduction of severe remedial measures, the burden on the environment and people began to decrease. However, in recent years, a re-release of Pb and other PTEs has been observed. The focus of previous research in the Upper Meža Valley was mostly on the load of the environment with Pb and its distribution in the environment, while a more detailed study about the source apportionment of Pb in airborne particulate matter, with a diameter smaller than 10 µm (PM_{10}) and an assessment of the contribution of individual sources has not yet been done.

Therefore, the main purpose of the dissertation was to determine the source of Pb in PM_{10} from the Upper Meža Valley by applying advanced analytical techniques. First, the analytical method for the determination of Pb isotope composition by multicollector inductively coupled plasma mass spectrometry (MC ICP-MS) in different environmental samples (river water, sediments, soils, sand, road dust, mine waste, ores, PM_{10}, $PM_{2.5}$) was optimized. Special attention was devoted to appropriate sample preparation and Pb isolation from the matrix. The method was then applied to real samples collected in the Upper Meža Valley, while the total concentrations of different PTEs were also determined by ICP-MS. In this way, the local Pb sources were characterized. To investigate the concentration and size distribution of particles carrying Pb and other potentially present PTEs by single particle ICP-MS (spICP-MS), an analytical method for the extraction of nanoparticles (NPs) from PM_{10} samples was optimized and applied to the PM_{10} samples collected in the Upper Meža Valley.

The Pb isotope ratios of PM_{10} samples differed from the local background (soil, sand, mine waste) and approached values of an anthropogenic source present in the area (secondary Pb production). Anthropogenic contributions were estimated to account for (56–69) % of total Pb in PM_{10}. With spICP-MS analyses, both Zn- and Pb-containing NPs in PM_{10} samples were identified, with (0.6–3.8) % of total Zn and (0.3–1.7) % of total Pb extracted as NPs. This data served as an additional indicator of the Pb sources and, more importantly, as assistance in the estimation of potential health effects of Pb in PM_{10}.

Povzetek

Poznavanje onesnaženja na območjih rudnikov in talilnic, ter ocena ravni onesnaženosti na različnih lokacijah pogosto nista dovolj za zanesljivo določitev izvora svinca (Pb) in prispevka posameznih virov k onesnaženju. Tako se izotopi Pb že dolgo uporabljajo kot »prstni odtisi« za določanje vira Pb v okoljskih vzorcih, saj fizikalno-kemijski procesi ne vplivajo bistveno na njegovo izotopsko sestavo.

Zaradi dolgotrajnih in intenzivnih dejavnosti pridobivanja in predelave Pb in cinka (Zn) v Zgornji Mežiški dolini je tamkajšnje okolje močno obremenjeno s Pb, Zn, kadmijem (Cd) in drugimi potencialno strupenimi elementi (PTEs). Po zaprtju rudnika in talilnice ter uvedbi strogih sanacijskih ukrepov se je breme na okolje in ljudi začelo zmanjševati. V zadnjih letih pa je bilo zaznano ponovno sproščanje Pb in ostalih PTEs v okolje. Dosedanje raziskave v Zgornji Mežiški dolini so bile osredotočene predvsem na obremenitev okolja s Pb in njegovo porazdelitev v okolju, medtem ko podrobnejša analiza virov Pb v zračnih prašnih delcih s premerom manjšim od 10 µm (PM_{10}) in ocena prispevka posameznih izvorov do sedaj še ni bila izvedena.

Zato je bil glavni namen te doktorske disertacije z naprednimi analiznimi tehnikami določiti vire Pb v PM_{10} iz Zgornje Mežiške doline. Najprej smo optimizirali analizno metodo določanja izotopske sestave Pb z multikolektor induktivno sklopljeno plazmo z masno spektrometrijo (MC ICP-MS) v različnih okoljskih matricah (rečna voda, sediment, zemlja, pesek, cestni prah, rudniški odpad, ruda, PM_{10}, $PM_{2.5}$). Posebno pozornost smo namenili ustrezni pripravi vzorcev in izolaciji Pb iz matrice. Optimizirana metoda je bila nato uporabljena na realnih vzorcih iz Zgornje Mežiške doline, v katerih smo s pomočjo ICP-MS določili tudi celotne koncentracije določenih PTEs. Na ta način smo podrobno opredelili in okarakterizirali lokalne vire Pb. Za določanje koncentracije in velikostne porazdelitve delcev, ki vsebujejo Pb in druge potencialno prisotne PTEs, smo s pomočjo single particle ICP-MS (spICP-MS) optimizirali metodo ekstrakcije nanodelcev (NPs) iz PM_{10} vzorcev, ki so bili zbrani v Zgornji Mežiški dolini.

Izotopska razmerja Pb v PM_{10} so se razlikovala od vrednosti lokalnega ozadja (zemlja, pesek, rudniški odpad) in so se približala vrednostim antropogenega vira, prisotnega na območju (sekundarna proizvodnja Pb). Prispevek antropogenega vira k celotnemu Pb v PM_{10} je bil ocenjen na (56–69) %. S spICP-MS analizami so bile v PM_{10} vzorcih nanodelci, ki vsebujejo tako Pb kot tudi Zn, pri čemer je bilo (0.6–3.8) % celotnega Zn in (0.3–1.7) % celotnega Pb prisotnega v obliki NPs .Ti podatki so služili kot dodaten pokazatelj virov Pb in, še pomembneje, kot pomoč pri oceni potencialnih vplivov Pb v PM_{10} na zdravje.

Contents

List of Figures

List of Tables

Abbreviations

AFM ... atomic force microscopy
BSE ... backscattered electron mode
CRMs ... certified reference materials
DLS ... dynamic light scattering
EDF-HSI ... enhanced darkfield hyperspectral imaging
EF ... enrichment factor
ESA ... electrostatic analyzer
ETA ... electrothermal atomization
FAA ... flame atomic absorption
FTIR ... Fourier-transform infrared spectroscopy
ICP-MS ... inductively coupled plasma mass spectrometry
ICP-OES ... inductively coupled plasma optical emission spectroscopy
ICP-QMS ... inductively coupled plasma quadrupole mass spectrometry
ICP-SFMS ... inductively coupled plasma sector field mass spectrometry
IIF ... instrumental isotopic fractionation
LA ... laser ablation
LOD ... limit of detection
MC ICP-MS ... multicollector inductively coupled plasma mass spectrometry
m/z ... mass to charge ratio
NMR ... nuclear magnetic resonance
NPs ... nanoparticles
PEC ... probable effect concentrations
PEC-Q ... probable effect concentration quotient
PTEs ... potentially toxic elements
PM ... particulate matter
PM_{10} ... particulate matter with a diameter <10 µm
$PM_{2.5}$ ... particulate matter with a diameter <2.5 µm
$PM_{0.1}$ ... particulate matter with a diameter <0.1 µm
SE ... secondary electron mode
SEM-EDS ... scanning electron microscopy–energy dispersive spectroscopy
SIMS ... secondary ion mass spectrometry
spICP-MS ... single particle inductively coupled plasma mass spectrometry
TEM ... transmission electron microscopy
TIMS ... thermal ionization mass spectrometry
TOF ICP-MS ... time of flight inductively coupled plasma mass spectrometry
WFD ... EU Water Frame Directive
XRF ... X-ray fluorescence

Chapter 1

Introduction

1.1 Airborne Particulate Matter (PM)

The presence of persistent contaminants in the environment poses a global threat to human health. While natural processes contribute to the release of contaminants to a certain amount, human activities like agriculture, industry, including mining generate the majority of them. The main transport pathways of the contaminants are through air, water, soil, and organisms. Airborne transport, facilitated by suspended particles to which substances with low volatility may be attached, is an important pathway for the redistribution of contaminants. This process can move pollutants from localized sources such as industrial centers or mines to larger environmental areas, affecting ecosystems and the human population.

Airborne particulate matter (PM) is a mixture of various solids and/or liquid droplets suspended in air, which can originate from both natural and anthropogenic sources (*European Environment Agency Glossary*, 2025). Particles can occur in different sizes, shapes, and chemical compositions. They can be made of a single component or may comprise a mix of substances such as metals, sulfates, nitrates, ammonia, sodium chloride, carbon, mineral dust, and microorganisms. PM particles can be categorized into primary and secondary particles. Primary particles are directly emitted from sources like combustion processes, construction sites, mining and smelting, and unpaved roads. In contrast, secondary particles form in the atmosphere through chemical reactions involving gases like sulfur dioxide, nitrogen oxides, and volatile organic compounds (Perraud et al., 2012). PM may occur in three main size ranges: as coarse particles (PM_{10}, with a diameter of 10 µm or less), fine particles ($PM_{2.5}$, with a diameter of 2.5 µm or less), and ultrafine particles ($PM_{0.1}$), also known as nanoparticles (NPs, with a diameter of 100 nm or less) (Chifflet et al., 2018). PM_{10} and $PM_{2.5}$ particles can originate from various natural and anthropogenic sources, such as emissions from gasoline, oil, and wood combustion. PM_{10} may also include dust from construction sites, landfills and agriculture, wildfires and waste burning, industrial sources, wind-blown dust from open lands, pollen, and fragments of bacteria.

The hazard posed by PM to humans is highly dependent on its size and size distribution. PM particles are small enough to be inhaled into the respiratory system, causing or exacerbating respiratory diseases such as asthma, bronchitis, and other lung conditions. PM_{10} particles are more likely to be deposited on the surface in the upper region of the lungs, while $PM_{2.5}$ particles are more likely to be deposited in the deeper regions of the lungs. Prolonged exposure to high levels of PM_{10} has been linked to cardiovascular issues and can significantly affect vulnerable populations, including children, the elderly, and those with pre-existing health conditions (Bodor et al., 2021). $PM_{2.5}$ can cause lung cancer, respiratory, and cardiovascular diseases (Apte et al., 2015). The associations of inhalable PM_{10} with daily all-cause, cardiovascular, and respiratory mortality across more than 600 cities in multiple countries were investigated by Liu et al. (2019). The results showed that a 10 µg/m^3 increase in the 2-day average of PM_{10} concentration was associated with a 0.44 % rise in daily all-cause mortality, a 0.36 % increase in daily cardiovascular mortality, and a 0.47 % increase in daily respiratory mortality. The limit concentration recommended by the World Health Organization for PM_{10} in the air is 50 µg/m^3 in 24 h and 20 µg/m^3 for the annual average (with only 3–4 exceedance days per year), while for $PM_{2.5}$ the limit concentrations are even lower, 25 µg/m^3 in 24 h and 10 µg/m^3 for the annual average (*WHO Global Air Quality Guidelines*, 2021).

In addition to "traditional" contaminants, airborne metal-containing nanoparticles (NPs) are considered a new and emerging contaminant being introduced into the environment. They have a diameter of 100 nm or less, and compared to larger particles, they can remain suspended in the air for longer and be transported over longer distances. They may consist of either small metal particles (e.g., from ore) or metals that can be adsorbed onto particles with a large surface area. Due to their small size, they can be inhaled into much deeper regions of the lungs and can penetrate very quickly and efficiently into the bloodstream. NPs are also more susceptible to biological uptake and, therefore, most relevant in terms of bioavailability (Yang et al., 2016). Both natural processes, such as volcanic eruptions and cosmic dust, and processes in metalworking, chemical industries, and vehicle traffic may release NPs in the air (Jeevanandam et al., 2018; Sanderson et al., 2014). These NPs can then undergo chemical, physical, and biological transformations, including photocatalytic degradation, agglomeration, sedimentation, bio-oxidation, etc. (Lowry et al., 2012).

1.2 Potentially Toxic Elements (PTEs)

Potentially toxic elements (PTEs), such as Pb, Zn, As, Cd, Cr, Mn, Fe, Co, Ni, Cu, and Mo, naturally occur in the environment, however, the majority of their accumulation, particularly in soil and sediments, was due to anthropogenic activities. Even though some elements might be considered essential, all of them are potentially toxic in different concentrations. Some nonessential elements, such as Pb, As, and Cd, are toxic at relatively low concentrations and without any known beneficial biological function in humans (Thalassinos et al., 2023). PTEs are widely distributed in the environment and pose significant risks to both the environment and human health if present in elevated concentrations. They can be transported over long distances through atmospheric, hydrological, and food pathways, making it difficult to determine their sources.

Chronic exposure of aquatic organisms to PTEs may affect their growth, activity, and reproduction (Pan et al., 2018). In assessing the quality of river sediments or the degree of anthropogenic influences on PTEs pollution, different approaches such as probable effect concentrations (PEC) (MacDonald et al., 2000), probable effect concentration quotient (PEC-Q) (Long et al., 2006), enrichment factor (EF) (Larrose et al., 2010), and others (Essien et al., 2009; C. Wang et al., 2012) can be used. The PEC for different PTEs were determined by MacDonald et al. (2000) and are defined as concentrations above which harmful effects are likely to be observed. The PEC-Q approach has been used to evaluate possible risks from the simultaneous presence of several PTEs (Long et al., 2006).

On the other hand, mineral PM_{10} particles are of particular concern for human health due to their potential to contain PTEs. After the deposition of PM_{10}, PETs can accumulate in soil, water, and vegetation. The presence of elevated levels of these elements in PM_{10} poses an additional hazard, as inhalation can lead to PTEs accumulation in the human body, posing severe health risks. Some PTEs are carcinogenic (e.g., As, Cd, Cr) and can impact nervous function, damage vital organs, and cause DNA damage. Long-term exposure to these elements is linked to Alzheimer's and Parkinson's diseases, muscular dystrophy, and multiple sclerosis (Csavina et al., 2012). Chronic Pb exposure, although at relatively low levels, can cause neurological and developmental issues, especially in children (Ettler, 2016; Needleman, 2004). Airborne Pb can be emitted into the atmosphere by natural and anthropogenic processes. Natural sources may include volcanic emissions and dust derived from soil or desert, while anthropogenic sources may include mining and smelting of Pb and other metal ores, burning of coal, wood, and oil, waste incineration, and battery recycling (Graney et al., 2019). The annual limit value of Pb, As, Cd, and Ni in airborne PM is 500 ng/m^3, 6 ng/m^3, 5 ng/m^3, and 20 ng/m^3, respectively (*Directive 2008/50/EC*, 2008; *WHO Global Air Quality Guidelines*, 2021).

Numerous researchers have tried to identify the various sources and pathways of PTEs contamination by determining their elemental composition, analyzing concentration variances, ratios of elements, and enrichment factors compared to natural background levels (Beane et al., 2016; Doufexi et al., 2022; Yoshinaga et al., 2014). For tracing PTEs and identifying their origin, it is crucial to understand the link between natural and anthropogenic sources, their sinks, and geochemical cycling. Monitoring only PTEs concentrations at different locations and sample types, and knowing from which activities they may be released into the environment, is often not enough to determine the sources and contributions of individual sources to the overall pollution. For that, the stable isotope composition of different elements has been used in recent years.

1.3 Isotopes as Tracers

Isotopes are atoms of the same element with different numbers of neutrons in the nucleus. Elements have a natural isotope composition, which can vary for several reasons. One is mass-dependent isotope fractionation, which states that because of slight differences in mass, isotopes participate in chemical and physical processes with slightly different efficiencies. Therefore, variations in isotope ratios of elements in environmental samples occur because of fractionation processes, which result from evaporation/condensation, adsorption/desorption, dissolution/precipitation, redox processes, and biological cycling (L. Wang et al., 2021). This is observed in lighter elements (H, C, N, O, S), in metals such as Li and B, and to a smaller extent in all other elements, including heavier ones. The second reason is mass-independent fractionation, which states that in some isotopes, there is a slightly different interaction between the nucleus and the surrounding electron cloud. The reasons for this may be a different volume of the nucleus or its magnetic properties. Other reasons for variations in elements' natural isotope composition are radiogenic nuclides, extra-terrestrial materials, interactions of terrestrial materials with cosmic rays, and anthropogenic effects (Vanhaecke & Degryse, 2012).

Due to the development of mass spectrometry techniques, it is possible to detect small differences in the isotope composition of PTEs. Multicollector inductively coupled plasma mass spectrometry (MC ICP-MS) is a user-friendly and efficient technique for obtaining high-precision isotopic data – it enables the determination of isotope ratios with a measurement precision down to 0.001 % (Irrgeher & Prohaska, 2016).

One element, which isotope composition can provide valuable insight into its origin within a sample, is Pb (Dewan et al., 2015; Dong et al., 2017; Félix et al., 2015). The isotope composition of Pb is not significantly affected by physicochemical fractionation processes, therefore, it provides an efficient tool for determining the sources and pathways of Pb (Bollhöfer & Rosman, 2001; Shiel et al., 2010).

1.3.1 Pb isotopes

Pb is a naturally occurring, non-essential, and potentially toxic element. Elemental Pb has no odor, is silver in color, and has high density, malleability, ductility, corrosion resistance, and relatively poorly conducts electricity. Pb is most commonly found in two oxidation states, Pb(II) and Pb(IV). Its average elemental concentration in the upper and lower continental crust is 17 mg/kg and 12.5 mg/kg, respectively (Wedepohl, 1995). Its concentration in igneous and sedimentary rocks is between 1 mg/kg and 150 mg/kg. The main Pb-bearing mineral is galenite (PbS), however, different amounts of Pb are also present in various minerals, averaging between 11 mg/kg and 32 mg/kg in carbonaceous shale, siltstone, mudstone, claystone, sandstone, limestone, and dolomite (Kushwaha et al., 2018). In many cases, the naturally occurring Pb can be masked by anthropogenic Pb, which in the past came primarily from mining and smelting of Pb sulfide ores and the use of leaded gasoline. It was estimated that anthropogenic Pb on a global scale accounted for more than 96 % of total atmospheric Pb (Erel et al., 2001).

Pb has four stable isotopes: ^{204}Pb, ^{206}Pb, ^{207}Pb, and ^{208}Pb, with abundancies 1 %, 24 %, 23 % and 52 %, respectively. The isotopes ^{206}Pb, ^{207}Pb, and ^{208}Pb are end products of the decay chain of ^{238}U, ^{235}U, and ^{232}Th, respectively, and U, Th, and Pb have different abundances in the Earth's crust, geochemical behavior, and lifetimes (Komárek et al., 2008). In natural materials, the isotope composition of Pb can vary significantly depending on their age and origin. Different sources produce Pb with different isotope compositions (L. Wang et al., 2021). The isotope composition of Pb can be expressed in several ratios. In environmental sciences, ratios ^{206}Pb/^{204}Pb, ^{206}Pb/^{207}Pb, ^{208}Pb/^{206}Pb are commonly used. The ratio ^{206}Pb/^{207}Pb is the most preferred because it can be determined precisely, as the abundances of these isotopes are relatively high. However, the ratios ^{206}Pb/^{204}Pb and ^{208}Pb/^{204}Pb yield the largest variation between the reservoirs (Komárek et al., 2008). The isotope ratios of Pb are influenced by the duration for which Pb and its parent isotopes remained together before Pb was incorporated into the mineral. With time, the abundance of ^{207}Pb has changed very little compared to ^{206}Pb, as most ^{235}U has already decayed while ^{238}U still has a relatively high abundance (Erel et al., 2001). Old Pb ores are therefore characterized by a lower ^{206}Pb/^{207}Pb ratio compared to more recent ores, which have more radiogenic Pb (Komárek et al., 2008; Monna et al., 1997).

Correlations of different Pb isotope pairs are commonly used for determining the sources of Pb in the environment. The Pb isotope composition enables the determination of different sources of Pb, even if the sample represents a mixture of Pb from different sources. That is possible if all the potential Pb sources are identified and have specific ratios. Nowadays, the largest contribution to Pb in the environment is anthropogenic activities, while the natural contribution is minimal (Komárek et al., 2008). The isotope composition analysis of Pb was applied in many studies about tracing the origin of Pb as a geochemical tracer for food provenance (meat, wine, rice) (Epova et al., 2020; Evans et al., 2015; J. Wang et al., 2020) or as a tracer for identification of pollution sources (Kong et al., 2018; F. Li et al., 2018; F.-L. Li et al., 2012).

The isotope composition of Pb in soil is not significantly affected by physicochemical fractionation processes, and even when Pb enters the plants and the food chain, it is not fractionated by biological processes, so the ingested and then absorbed Pb has the same isotope composition as it had at the source. Geogenic exposure refers to Pb exposure that happened because of the interaction with a geological source, and Pb isotope composition can be used to geographically locate the place of exposure. This approach was used by Evans et al. (2015), who investigated Pb isotope composition in samples from farm livestock raised in three areas in Great Britain, outside cities and industrial areas. The results showed that Pb found in the meat was geogenic and that there was no evidence of anthropogenic Pb. Another example of using Pb isotopes as tracers of food's geographical origin is in the case of a study on the authenticity and geographical origin of Bordeaux wines, conducted by Epova et al. (2020). They compared Pb isotope composition in samples of authentic Bordeaux wines from France with that in some suspicious Bordeaux wines from China. A significant difference was observed in the Pb isotope composition, which means that this approach could be used to distinguish between different origins of wine. Pb isotope composition in Chinese wine was comparable to that of Asian atmospheric Pb, which has a specific composition because of the regional anthropogenic Pb. However, it would be nearly impossible to differentiate between an authentic and a fraudulent wine if both were produced in the same region.

Pb isotopes are particularly valuable in environmental sciences for identifying pollution sources and tracing the geographical origin of materials, providing insights into both natural and anthropogenic contributions to environmental contamination. By the use of Pb isotope composition and binary endmember mixing model, Li et al. (2012) investigated how natural and anthropogenic sources contribute to the accumulation of Pb in soil and vegetables grown in that soil. The samples of soil, vegetables, and rainwater were collected at three different sites. The results showed that there were differences in Pb isotope ratios of soils from three sampling sites, but no significant differences in Pb isotope ratios between vegetable species or between vegetables from different sampling sites were observed. The Pb isotope ratios measured in collected rainwater samples fitted well with those from coal combustion and from the emission of lead-ore-involved industry, which may suggest that these were the sources of atmospheric Pb. The binary endmember mixing model calculations showed that a large portion of Pb accumulated in vegetable leaves could come from atmospheric deposition. Uzu et al. (2010) found that a large number of Pb-rich particles appeared in the lettuce leaves after it was exposed to atmospheric Pb pollution for 43 days. The aim of the study by Gray et al. (2013) was to investigate metal deposition in Lake Ballinger (USA) sediment throughout the past several centuries. The results showed that Pb concentration and isotope composition in lake sediment changed after the start of the smelting operation and urbanization of the watershed. The contribution to Pb concentration in lake sediment was also attributed to gasoline-related emissions. To identify possible sources of pollution, Wen et al. (2015) studied the Pb isotope composition of soil samples and sulfide/oxide ore samples from the nearby Pb-Zn mining district in China. Based on the comparison of the isotope composition of both types of samples, they determined that the main source of Pb in the soils was the mining district, but there was another possible source present, with a distinct isotope composition. For most of the samples, the second source could be explained as background Pb concentrations in the soil. In another study, Li et al. (2018) studied the origin of Pb and Cd in urban dust by determining the isotope composition of Pb and metal ratios (Cd/Fe, Pb/Fe, Cd/Mn, Pb/Mn) in the samples of different types of dust (roof, exhaust, residential, and main road dust), collected in residential areas, city parks, main roads, and Botanic Garden in Hangzhou City, China. The results of Pb isotope composition indicated that the main source of Pb in residential dust was coal combustion, while the main source of Pb in road dust was automobile exhaust emission.

1.4 The Upper Meža Valley

In the Upper Meža Valley lies the largest Pb and Zn ore deposit in Slovenia with a long history of mining and ore processing. Mining in the Koroška region began in Roman times, while the first written source of lead ore excavation dates back to the 17th century. Lead production began to develop strongly during the time of Napoleon's Illyria, or rather, during the Napoleonic Wars, when the Mežica mine was considered to be the most important Austro-Hungarian lead mine. In the middle of the 19th century, the Bleiberger Bergwerks Union (BBU) incorporated most of the smaller mines and began to mine deliberately. A little later, sphalerite was identified in Mežica, and it was mined as an ore of zinc, and soon after, mining of wulfenite as a molybdenum ore began (Gregorač, 1965). The mine reached its highest production in the years between 1950 and 1955, more than 500000 tons of ore/year. In the history of mining in Mežica, 19 million tons of Pb and Zn ore were excavated, from which 1 million tons of Pb and 0.5 million tons of Zn were extracted (Rečnik et al., 2014).

Relatively small quantities of Pb ore and Pb extracted from the ore were produced until the first half of the 20th century, and the pollution was occurring only near small ore processing facilities. After that, all smelting operations were concentrated in Žerjav, which led to larger pollution of the environment and also many negative effects on people's health and quality of life (Gosar & Miler, 2011). During processing, a large amount of mine waste with high concentrations of Pb, Zn, As, Cd, and other PTEs was produced and deposited in abandoned mine shafts and near small streams along the Upper Meža Valley, with a total area spanning over 60 km^2 (Žibret et al., 2018). As a result, the Upper Meža Valley was excessively polluted with Pb, Zn, and other PTEs (Finzgar et al., 2014; Gošar et al., 2015; Gosar & Miler, 2011). In addition to mining, the secondary Pb production industry, more specifically for the production and recycling of lead batteries, has been present since 1956.

Released Pb and co-contaminating Zn had been deposited into the soil throughout the long history of Pb mining and smelting in the Upper Meža Valley and thus made the soil the most significant source of secondary contamination. As part of the project, Research on soil pollution in Slovenia (*Official Gazette RS 83/99*, 1999), monitoring of soil in 2007 showed that Pb concentrations present in the samples of topsoil layers from Slovenia ranged from 10 mg/kg to 2000 mg/kg. The limit value (85 mg/kg) was exceeded at 11 locations in Slovenia, including Podpeca and Žerjav. In Podpeca, the critical value (530 mg/kg) was also exceeded (Zupan et al., 2008). In 2013, samples of natural soil, road dust, and garden soil were taken at 23 locations in the Upper Meža Valley, a total of 56 samples. The critical value for Pb was exceeded in 27 samples, for Cd in 19 samples, and for Zn in 28 samples. In topsoil samples, critical values for Pb were exceeded in 7 samples, for Cd in 2 samples, and for Zn in 5 samples. The most exceeded critical values were in road dust and soil samples, taken at a depth of (20–30) cm. Analyses of soil samples taken at locations that underwent overlaying of the topsoil confirmed that heavy metal concentrations decreased after remediation. After two years, their concentrations were still very low. Concentrations of the analyzed elements increased after five years but were still much lower than before the overlay (Ivartnik et al., 2015). A review of the results from analyses of various samples collected in 2016, 2017, and 2018 revealed that the soil in the Upper Meža Valley was still heavily loaded with PTEs. The soil in some yards, gardens, and agricultural lands still exceeded the critical value (530 mg Pb/kg) (Ivartnik et al., 2017).

Elevated concentrations of Pb and other PTEs in the Meža River and its tributaries are the result of the leaching of material from landfills. Between 1914 and 1979, 150000 tons of floating sludge flowed into the Meža River. In 2000, Svete et al. (2001) collected sediments along the Meža River and its tributaries (Koprivna, Janžek rivulet, Topla, Helena rivulet, Bistra, Javorje rivulet, Jazbina rivulet, and Šumec) to investigate the extent of pollution with PTEs. The highest concentrations of Zn, Pb, and Cd were measured in sediments of the Helena rivulet (16300 mg/kg of Zn, 9300 mg/kg of Pb, and 130 mg/kg of Cd), which flows past the abandoned Pb and Zn mine, and in sediments from two locations at Meža River. Lower concentrations of Zn, Pb, and Cd were observed in sediments from the right-hand tributaries (Bistra and Javorje rivulet), and in sediments from locations that were further away from the influence of mining activities.

High concentrations of PTEs were also observed in the water from the Upper Meža Valley, in surface waters, and groundwater. In 1979, the concentrations of Pb in the water of the Meža River and its tributaries were around 700 mg/L (Kladnik, 2009). Gošar et al. (2015) studied concentrations of heavy metals in mine groundwater, in the Meža River, and its tributaries. They measured slightly higher concentrations of Cr, Cu, Pb, and Zn in the Helena stream, probably due to the presence of waste deposits, and slightly higher concentrations of Cd, Pb, and Zn in Meža River after Šumec, most probably due to the presence of a battery production and recycling plant and other metallurgic industry in this area. None of these concentrations exceeded any of the limit values in legislation (*Official Gazette RS 19/04*, 2004). Concentrations of PTEs in the groundwater in the Upper Meža Valley, in the first years after the flooding of the mine in 1994, were high and have diminished over time (Prestor et al., 2003). Between 1995 and 1997, Pb concentration was over the limit value for drinking water. After 1997, concentrations were below the established limit. A similar trend was observed for Zn. In 2002, the average concentration of Pb in river water was approximately 75 µg/L, and since 2015, the concentrations have been close to background concentrations (Gošar et al., 2015). As mine tailings began to be deposited in abandoned parts of the mine and with the construction of treatment plants, the concentration of Pb and other PTEs in the water began to decline. While the concentration of Pb in water has decreased, it was still high in sediments, ranging from 100 mg/kg to 3300 mg/kg (Gosar & Miler, 2011; Svete et al., 2001; Žibret et al., 2018).

In addition to the high concentrations of PTEs in the soil and sediments, the inhabitants of the area are exposed to these elements daily, mainly by inhalation and/or ingestion of dust. To decrease dust emissions from the smelting plant in Žerjav, systems of efficient bag filters were installed in 1978. After that, the daily quantity of released dust was reduced from 5000 kg to 70 kg, and the air Pb concentration from 80 µg/m^3 to 3 µg/m^3 (Jez & Lestan, 2015). While some measurements of Pb concentrations in PM_{10} have been done between 1972 and 1989, regular monitoring of PTEs concentrations in PM_{10} by the Slovenian Environment Agency has been carried out since 2007 with some interruptions, as part of the Ordinance on areas of maximum environmental impact and on the program of measures to improve the quality of the environment in the Upper Meža Valley (*Official Gazette RS 119/07*, 2007). The first quarterly monitoring of the PTEs concentrations in PM_{10} was carried out at three locations, Mežica, Črna na Koroškem, and Žerjav (Table 1.1, summarized after Results of the Three-Month Air Monitoring in the Upper Meža Valley (2007)). The results showed a significantly higher air load in Žerjav than in other measurement sites, so measuring continued only in Žerjav (Ivartnik et al., 2012).

Table 1.1: The average levels of Pb, As, Cd, and Ni in PM_{10} in Mežica, Žerjav, and Črna na Koroškem in the period from 18. 4. 2007 to 21. 6. 2007.

Monitoring site	Pb (ng/m^3)	As (ng/m^3)	Cd (ng/m^3)	Ni (ng/m^3)
Mežica	81	1.3	1.0	1.2
Žerjav	498	5.5	5.0	1.4
Črna na Koroškem	71	1.0	0.5	0.8

The average annual levels of Pb in PM_{10} sampled in Žerjav, where a Pb smelter used to operate and is now a site for Pb-recycling and Pb-battery production, from 1972 to 2022 are presented in Figure 1.1, while the average annual levels of As, Cd, and Ni are presented in Table 1.2. Even though Pb concentrations in PM_{10} decreased dramatically from 1972 to

2007, the results showed an increase in annual average concentrations from 250 ng/m^3 to 700 ng/m^3 between 2010 and 2021.

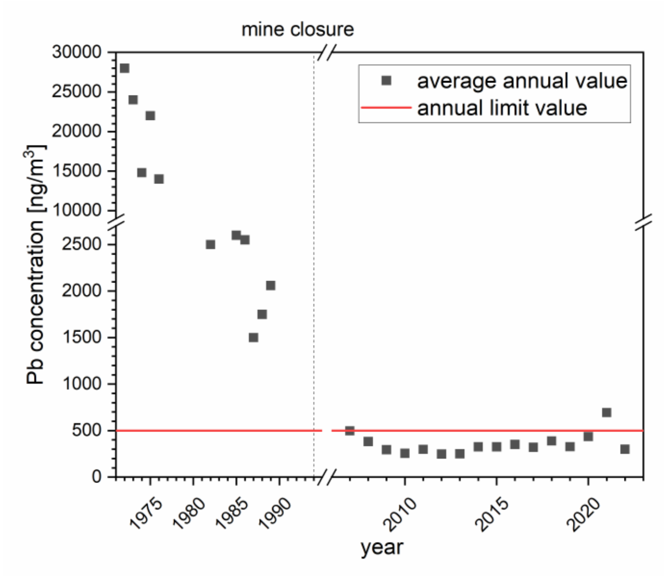

Figure 1.1: The average annual levels of Pb in PM_{10} sampled in Žerjav from 1972 to 2022. Data summarized after Ivartnik et al. (2012, 2015, 2017, 2022); Ivartnik, Pavlič, Hudopisk, Simetinger, Ploder, et al. (2019); Ivartnik, Pavlič, Hudopisk, Simetinger, Vindiš, et al. (2019); Koleša et al. (2008).

Table 1.2: The average annual levels of As, Cd, and Ni in PM_{10} sampled in Žerjav from 2009 to 2021. Data summarized after Ivartnik et al. (2012, 2015, 2017, 2022); Ivartnik, Pavlič, Hudopisk, Simetinger, Ploder, et al. (2019); Ivartnik, Pavlič, Hudopisk, Simetinger, Vindiš, et al. (2019); Koleša et al. (2008).

Time period	As (ng/m^3)	Cd (ng/m^3)	Ni (ng/m^3)
2009	2.7	2.6	1.7
2010	2.2	4.5	1.8
2011	1.9	2.3	2.4
2012	2.0	1.5	2.6
2013	1.7	2.2	3.0
2014	1.8	2.7	2.0
2016	1.9	5.7	<1.3
2017	/	/	/
2018	/	/	/
2019	/	/	/
2020	/	/	/
2021	2.3	2.7	1.7
Annual limit value	6	5	20

Due to past mining activities, the Upper Meža Valley has been extensively studied for the presence of PTEs, however, there are no reports of the presence of PTEs in the form of NPs. In the study by Beeston et al. (2010), the possible environmental conditions in the

Upper Meža Valley were artificially recreated by the production of PbS NPs by laser ablation, and their bioaccessibility to humans via respiration was studied *in vitro*. They found that inhaled PbS NPs are highly bioaccessible and thus pose a potential risk to human health.

As Pb is transmitted to the body through the inhalation and ingestion of contaminated dust particles, food, and water, workers and surrounding inhabitants have had high levels of Pb in their blood. In 1952, a study about Pb absorption was done, and the average Pb concentration in blood was 700 µg/L for inhabitants, 1000 µg/L for miners, and 1330 µg/L for smelter workers (Beritić, 1952). In 1971, those concentrations were between 336 µg/L and 898 µg/L for smelter workers (Fugaš, 1977). In a study from 1982, workers from different workplaces, such as the metallurgic section (production and maintenance workers), workers in the battery industry, and technical and auxiliary personnel, were included. The average Pb concentration in blood for all groups was between 449 µg/L and 790 µg/L (Prpić-Majić, 1982). Especially at risk were young children, so the first testing for Pb concentrations in blood was carried out from 1974 to 1976, and the median Pb concentration in the blood of preschool children was over 400 µg/L (Jez & Lestan, 2015). In 1990, the concentrations decreased to (41–284) µg/L. Regular biomonitoring in the area began in 2004, and an action program was introduced in 2007, with a goal of 95 % of children with Pb concentration in blood less than 100 µg/L (*Official Gazette RS 119/07*, 2007). On average, between 60 and 90 three-year-old children participated every year. The results in Figure 1.2 show that the trend of fast-decreasing Pb concentration in the blood of three-year-old children stopped. Comparison of periods 2006–2007, 2008–2009, and 2010–2011 shows that at the beginning, more than half of the children had a high content of Pb in the blood (>100 µg/L), which was then reduced to a fifth and later to a tenth of the children. From 2011, there was quite a fluctuation in the percentage of children with high Pb levels in the blood (from 4 % to 20 %), which was 9 % in 2011, 18 % in 2014, 20 % in 2017, and 5 % in 2019 and 2022 (Ivartnik et al., 2022; Ivartnik, Pavlič, Hudopisk, Simetinger, Ploder, et al., 2019). Based on this data from biomonitoring, Bavec et al. (2025) used the Integrated Exposure Uptake Biokinetic Model for Lead in Children (IEUBK) to predict mean blood lead levels and lead uptake from different sources. The results of the model showed that the primary exposure pathway in children from Žerjav could be from soil/dust, while in Mežica and Črna na Koroškem, the dietary exposure from locally grown foods predominates.

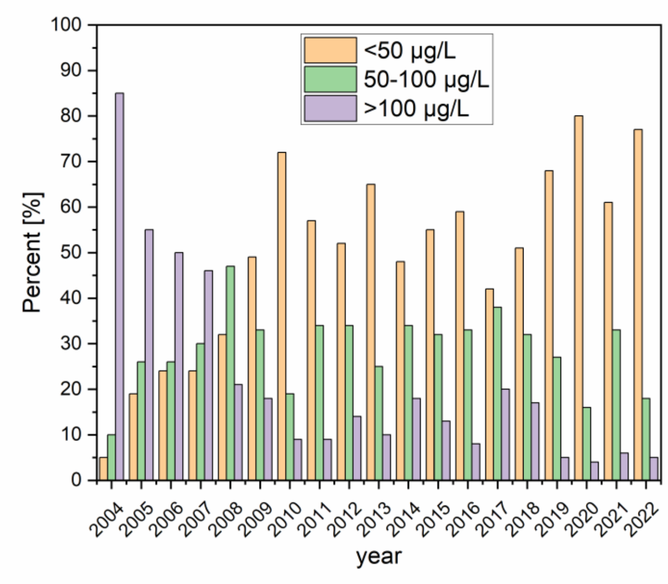

Figure 1.2: Comparison of proportions of three-year-old children from the Upper Meža Valley in terms of measured concentration of Pb in their blood. Data summarized after Ivartnik et al. (2022); Ivartnik, Pavlič, Hudopisk, Simetinger, Ploder, et al. (2019).

1.5 Advanced Analytical Techniques for Studying PM Sources

A combination of different advanced analytical techniques must be used to conduct a thorough PM source identification and characterization and to evaluate their contributions.

For the determination of total PTEs concentrations, different techniques can be used, such as flame atomic absorption (FAA), electrothermal atomization (ETA), X-ray fluorescence (XRF), inductively coupled plasma optical emission spectroscopy (ICP-OES), and inductively coupled plasma mass spectrometry (ICP-MS). FAA is a single-element technique that uses a flame to generate atoms of measured elements, which absorb light with a specific wavelength. The amount of absorbed light is used to determine the element concentration. It has a detection limit in the range of mg/L. ETA is usually a single-element technique, but can also be a multi-element technique that works on a principle similar to FAA, using a heated tungsten filament or graphite tube instead of a flame. It has a 100-times lower detection limit than the FAA (Thomas, 2003). XRF is a non-destructive technique that measures the secondary X-rays emitted from a sample, which was irradiated with high-energy primary X-rays. It has a detection limit in the range of (3–100) mg/L (Morgan et al., 2015). ICP-OES is a multi-element technique that excites atoms with plasma to the point that they emit photons with a specific wavelength. In radial-view, it has a similar detection limit to FAA, while in axial-view, the detection limit can be 2- to 10-times lower. One of the most frequently used techniques for total element concentration determination is ICP-MS. It is described in more detail in Chapter 1.5.1.3. The main difference from ICP-OES is that plasma is used to generate positively charged ions, which are then separated by the mass to charge ratio (m/z), and it has a detection limit in the range of ng/L. The lowest detection limits can be obtained with ICP-MS, followed by ETA, axial ICP-OES, radial ICP-OES, FAA, and XRF. The concentration range in which quantitative results can be obtained is the largest with ICP-MS and the lowest with ETA. As FAA and ETA are usually considered to be single-element techniques, their sample throughput is lower than that of ICP-OES and ICP-MS, which are multi-element techniques (Thomas, 2003).

ICP-MS techniques can also be used for Pb isotope determination, including ICP-MS with quadrupole (ICP-QMS), sector field (ICP-SFMS) (including multicollector ICP-MS (MC ICP-MS), described in more detail in Chapter 1.5.1.4), or time of flight mass analyzer (TOF ICP-MS). Additionally, thermal ionization mass spectrometry (TIMS) and secondary ion mass spectrometry (SIMS) can also be used. As opposed to ICP-MS, the formation of ions in TIMS is achieved on a heated filament, and the technique enables precise and accurate isotope determination. It requires extensive chemical treatment and optimization of evaporation and ionization of the sample, which prolongs the analytical procedure (Komárek et al., 2008). In SIMS, the surface of a solid sample is bombarded with a beam of primary ions, leading to sputtering and formation of secondary ions, which are then accelerated and transferred to a magnetic analyzer. Many solid matrices can be analyzed with SIMS, provided that the surface is flat, conductive, and compatible with ultrahigh-vacuum conditions. Additionally, the surface usually needs to be polished for high-precision isotope analyses. The detection limit of SIMS is in the range of mg/kg to µg/kg (Prohaska et al., 2014). ICP-QMS has lower accuracy and precision than TIMS, as different masses are not detected simultaneously. On the other hand, ICP-SFMS, especially MC ICP-MS, has a shorter measurement time than TIMS and a higher sample throughput. Compared to ICP-QMS, it can separate spectral interferences in high-resolution mode. MC ICP-MS has a similar isotope ratio precision as TIMS, with the advantage of the ability to ionize elements with higher ionization energies (Irrgeher & Prohaska, 2016).

The presence of NPs and their characterization can be assessed with many different techniques, some of them include electron microscopy, such as scanning electron microscopy (SEM) and transmission electron microscopy (TEM), enhanced darkfield hyperspectral imaging (EDF-HSI), dynamic light scattering (DLS), atomic force microscopy (AFM), Fourier-transform infrared spectroscopy (FTIR), nuclear magnetic resonance (NMR), and single particle ICP-MC (spICP-MS). Some properties of NPs can sometimes be studied only with one technique, while on the other hand, some parameters may be determined with multiple techniques. Electron microscopy techniques can visualize the NPs, giving information on their shape and size. If they are coupled with energy dispersive spectroscopy (EDS), they can also give information on their chemical structure. DLS gives information on hydrodynamic size and detects agglomerates. AFM can provide information about NPs' size, shape, dispersion in matrices, and quick examination of elemental composition. The surface composition of NPs and ligand binding can be studied with FTIR (Mourdikoudis et al., 2018). The most frequently used technique for quantification and size characterization of NPs suspensions in recent years is spICP-MS, which is described in more detail in Chapter 1.5.2.2.

1.5.1 Pb isotope determination

Pb isotope determination comprises three steps: sample preparation, Pb isolation from the matrix, and isotope measurement. Even though stable isotope analysis has proven effective for both quantitative and qualitative source identification, several challenges remain. For precise and accurate isotope ratio determination, samples must be properly prepared. It is of utmost importance that the matrix and possibly interfering elements are removed. An important isobaric interference for Pb on mass 204 is ^{204}Hg, and if the matrix is not removed, some non-spectral interferences and matrix effect can occur. With the correct pretreatment, systematic errors derived from matrix-induced interferences as well as changes in instrumental isotopic fractionation can be overcome.

1.5.1.1 Sample preparation

When liquid samples are analyzed, they are first evaporated, and then the dry remains are re-dissolved in an appropriate solution, depending on the isolation method applied. Few studies examined the possibility of extracting Pb from the water. Griffiths et al. (2020) tested and compared different combinations of Pb extraction from seawater. They tested the preconcentration of Pb by magnesium hydroxide ($Mg(OH)_2$) coprecipitation and solid-phase extraction of Pb using Nobias Chelate PA-1 resin. The results showed that solid-phase extraction had higher Pb yields than coprecipitation with $Mg(OH)_2$, but also higher blank contributions.

Solid samples first have to be digested, and the method of choice is usually microwave-assisted digestion. Different mixtures of acids (e.g., HNO_3, H_2O_2, HCl, and HF), duration of the program, and temperature are used depending on the matrix. The sample must be completely digested, as there cannot be any residue left. The next steps are the same as for liquid samples, namely, evaporation and Pb isolation from the matrix.

1.5.1.2 Pb isolation from the matrix

Commonly applied Pb separation methods involve the use of extraction chromatographic Pb Spec (De Muynck et al., 2008; Philip Horwitz et al., 1994), and Sr Spec resins (Gray et al., 2013; Pin et al., 2014), and ion exchange resins such as Dowex® 1X8 or AG50WX8 (Bing-Quan et al., 2001; F. Li et al., 2018; F.-L. Li et al., 2012; Zhao et al., 2015).

Both Pb Spec and Sr Spec resins contain the same crown ether (4,4’(5’)-di-t-butylcyclohexano18-crown-6), which is in 1-octanol on inert polymeric support in Sr Spec resin, and in isodecanol in Pb Spec resin. High retention of Pb on the Pb Spec resin can be achieved in the nitric acid concentrations from 0.1 mol/L to 10 mol/L (1 mol/L HNO_3 is usually used); similarly, high retention of Pb on the Sr Spec resin can also be achieved across a broad range of nitric acid concentrations (8 mol/L HNO_3 is usually used). Between these two resins, it is harder to remove Pb from the Sr Spec resin, which is why a lower amount of crown ether dissolved in a longer chain alcohol is used in the Pb Spec resin for easier stripping of Pb from the resin. Pb can be eluted from the Pb spec resin using different solutions, and De Muynck et al. (2008) evaluated the performance of Pb Spec resin and proposed a new procedure for Pb isolation. The improvements included less harmful chemicals and the possibility to regenerate the columns, without the influence on isotope ratios or a loss of separation efficiency. For the elution of Pb from the resin, they tested MilliQ, Na_4EDTA (0.1 mol/L), and ammonium oxalate (0.05 mol/L), and the latter proved to be the best choice. The results showed that Pb was quantitatively removed from the column after washing the resin with 5 mL of 0.05 mol/L ammonium oxalate. Dowex® 1X8 resin is a strong base anion exchange resin based on a copolymer of styrene and divinylbenzene, with the addition of an ion-active functional group (Cl^- ionic form). Both cross-linkage and ion exchange capacity play a role in the resin's capacity. High Pb retention on Dowex® 1X8 resin can be achieved in 0.5 mol/L HBr.

In general, the separation of Pb from the matrix comprises the following steps: washing of the resin, its activation or conditioning, loading of the sample, rinsing of the matrix, and Pb elution. The main differences between the separation procedures applying Pb Spec, Sr Spec, and Dowex® 1X8 resins are presented in Table 1.3, and include different number of steps in resin preparation (Sr Spec resin has the most steps and Pb Spec has the fewest), the amount of solvents used (Dowex® 1X8 uses the smallest amount), solvent used for Pb elution (Sr Spec and Dowex® 1X8 use HCl of different molarity, while Pb Spec uses ammonium oxalate). The advantage of Sr Spec resin is that it allows the isolation of Sr and Pb simultaneously. The most widely used is 1X8 resin (from producers Dowex® or BioRad), which has very high recovery rates (>90 %), uses the smallest amount of solvents, is easy to use, the time of the procedure is short, and is the least expensive.

Table 1.3: Comparison of Pb Spec, Sr Spec, and Dowex® 1X8 resin.

	extraction chromatographic resin		ion exchange resin
	Pb Spec	**Sr Spec**	**Dowex® 1X8**
the fewest steps in resin preparation	✓		
smallest amount of solvents used			✓
the shortest time of the procedure			✓
lowest cost			✓
simultaneous isolation of Sr and Pb		✓	
solvent used for Pb elution	ammonium oxalate	HCl	HCl

In a study of the simultaneous separation of Sr, Pb, and Nd from silicate rocks by extraction chromatography, Pin et al. (2014) used a combination of three resins, including Sr Spec. Separation of Sr and Pb from the matrix was achieved on Sr Spec resin, and recovery of Pb was reported as >90 %. The elution of Pb from the Sr Spec resin was achieved with 6 mol/L HCl. The Sr Spec resin was also used in a study about the identification of lake sediment contamination based on Hg and Pb isotope composition, by Gray et al. (2013). For determining isotope signatures of sources of atmospheric Pb, Zhao et al. (2015) used Dowex® 1X8 resin for the preparation of different samples (street dust, plant, vehicle exhaust, coal, soil, lake sediment, total suspended particles). The matrix was washed from the resin with HBr, and elution of Pb was achieved with HCl.

To achieve accurate and precise Pb isotope composition, the Pb isolation from the matrix should be complete. Therefore, the mass balance must be followed throughout all analytical steps, and ICP-MS is the technique of choice for Pb concentration determination. When no Pb is lost during sample preparation, it can be assumed that no isotope fractionation occurred, which would otherwise lead to biased results. As mentioned above, the MC ICP-MS has been the most used instrument in the last years for Pb isotope composition determination.

1.5.1.3 Inductively coupled plasma mass spectrometry (ICP-MS)

ICP-MS is a technique that is widely used for trace metal determination in environmental, geological, and biomedical fields. It has a very low detection limit (in the range of ng/L) and enables quantification in the range of mg/L and also µg/L. The main components of an ICP-MS instrument are a nebulizer, spray chamber, plasma torch, mass filter, and detector (Figure 1.3). The components can differ in different instruments; there can be different nebulizers used (e.g., concentric, low-flow self-aspirating, total consumption nebulizer, etc.), different mass separators (e.g., quadrupole, time of flight, magnetic sector), and different detectors (commonly used is a discrete dynode detector). The samples may be in a liquid form or solid when laser ablation (LA) is used for sample introduction (Thomas, 2003).

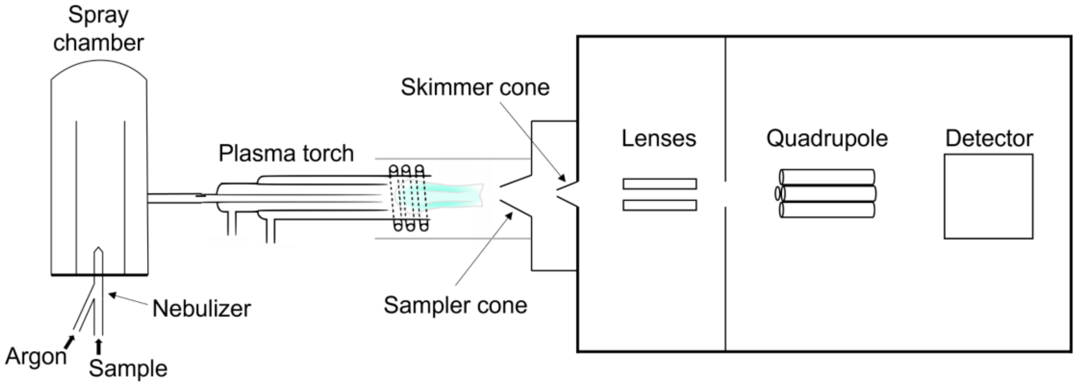

Figure 1.3: Schematic of the ICP-MS.

The sample is converted to fine aerosol in the nebulizer and is separated from larger droplets in the spray chamber. Plasma is generated by the interaction of a magnetic field with the flow of argon through a torch and has a temperature of around 10000 K. It is used to generate positively charged ions, which are then directed into the mass spectrometer through the interface region. This region is composed of two cones (sampler and skimmer cones), which guide the ions to the ion optics and then to the mass separator. In the mass separator, ions with a chosen mass to charge ratio (*m/z*) are selected and forwarded to a detector.

Different approaches can be used for quantification, such as external calibration and isotope dilution. One of the most accurate and precise approaches in elemental analysis is isotope dilution. In this approach, a natural abundance of two isotopes of an element is altered by adding a known amount of one of the isotopes. The limitations of this approach are that the investigated element must have more than one isotope, that it requires certified standards with enriched isotopes (which can be very expensive), and that it does not compensate for spectral interferences.

There are three types of interferences occurring in ICP-MS: spectral interferences, matrix interferences, and physical-based interferences (Thomas, 2003).

- *Spectral interferences*

  The most serious type of spectral interferences are polyatomic interferences, which are produced by combining two or more atomic ions. They can occur in relation to plasma gas, matrix, other elements in the sample, etc. In the argon plasma, polyatomic interferences caused by argon ions and their combinations are very common. Another type of spectral interference is doubly charged spectral interferences. Their formation is related to the ionization conditions in the plasma, and they are formed with a double positive charge instead of a normal single charge. There are different ways to compensate for spectral interferences, such as the removal of the matrix and the use of mathematical correction equations. However, another possibility is a collision-reaction cell technology, which prevents the formation of polyatomic and doubly charged interferences before the entrance to the mass analyzer. Hydrogen or helium can be used as a collision-reaction gas.

- *Matrix interferences*

  They include sample transport effect (it occurs because of dissolved solids or acid concentration in the sample and is caused by the sample's impact on droplet formation or droplet size selection), sample affecting the ionization conditions of the plasma and matrix-induced space-charge effects (poor transmission of trace levels of low-mass ions through the ion optics in the presence of large concentrations of high-mass matrix).

- *Physical-based interferences*

  They are defined as differences between sample and calibration standards and affect sample transport or nebulization. These differences can include viscosity, density, or matrix. Some solutions that overcome these issues include sample dilution and matrix matching. Internal standardization can help when the matrix is not entirely known.

Spectral interferences of polyatomic ions are not common for Pb, as its isotopes have high masses, where the formation of polyatomic species with overlapping *m/z* values is less likely. The main isobaric interference for Pb on mass 204 is ^{204}Hg. Some non-spectral interferences may also occur depending on the matrix (Komárek et al., 2008).

1.5.1.4 Multicollector inductively coupled plasma mass spectrometry (MC ICP-MS)

In MC ICP-MS, the principles of sample introduction and plasma formation are somewhat similar to those in an ICP-MS. However, the advantage of MC ICP-MS is its several detectors, which allow the detection of different masses at once, eliminating delays in detecting ions with different masses and consequently errors in measurement because of that.

MC ICP-MS has the same ion source as conventional ICP-MS – the Ar plasma, followed by ion lenses, an electrostatic analyzer (ESA), a magnetic sector analyzer, and multiple collectors for the measurement of ions (Figure 1.4). In the inductively coupled plasma, positively charged ions are formed, which are further accelerated across an electrical potential gradient and focused into a beam through a series of slits and electrostatically charged plates. Next, the ion beam passes through an energy filter, which produces a beam of ions with the same approximate energy. When the beam passes through the magnetic field, the ions separate based on their mass to charge ratio, and are then simultaneously measured by a series of collectors (Prohaska et al., 2014).

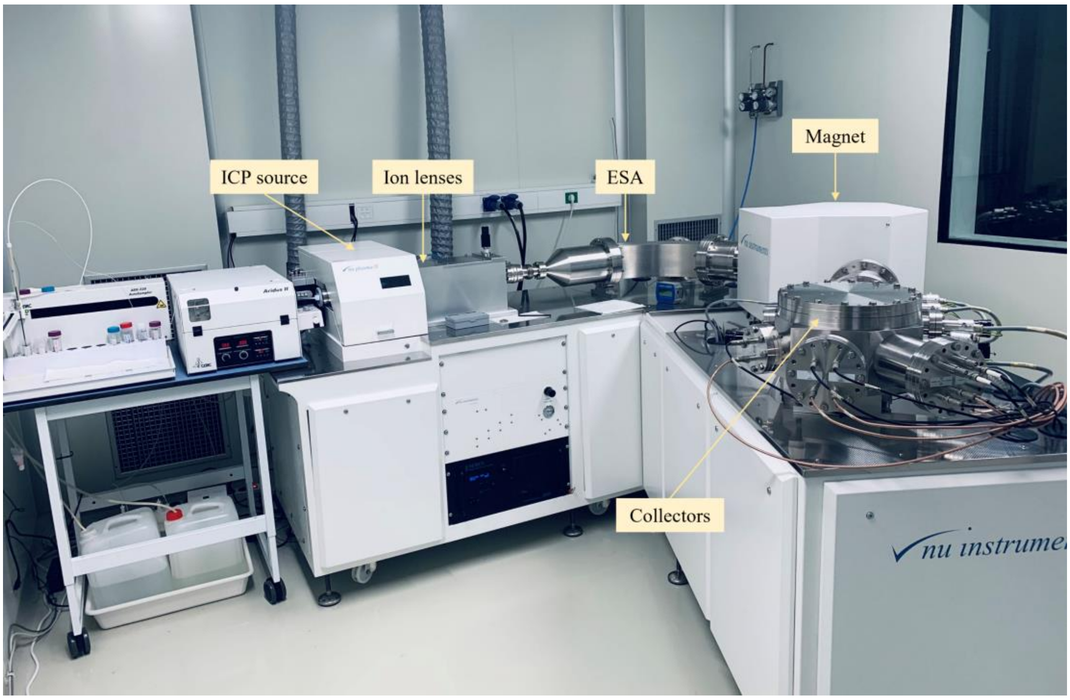

Figure 1.4: MC ICP-MS instrument and its parts.

During isotope ratio analysis with ICP-MS instruments, a phenomenon known as instrumental isotope fractionation (IIF) (also named mass discrimination effect or mass bias) occurs. IIF encompasses the cumulative effects in a mass spectrometer during sample introduction, ion formation, ion extraction, ion transmission, ion separation, and ion detection, resulting in a discrepancy between the measured isotope ratio and the true isotope ratio of a sample. IIF can arise from both mass-dependent and mass-independent effects, incorporating all discriminating factors. The preferential transmission of heavier isotopes is often considered a major cause of IIF among nuclides. In ICP-MS, the ionization source and the interface are believed to significantly contribute to IIF, primarily due to the substantial pressure drop between the ion source and the expansion region. For the correction of the IIF, different correction strategies can be applied (Prohaska et al., 2014).

- *Internal IIF correction*

  The conditions for using this approach are that isotopes used (either of the same or different elements) have similar fractionation behaviors and chemical properties. Elements, such as Sr, Nd, and Hf, have at least one pair of non-radiogenic isotopes, and their ratio has an assumed constant value, or at least has limited mass-related discrimination. Based on the comparison between the measured and assumed values of this ratio, a precise calculation of IIF can be made. However, Pb has only one non-radiogenic isotope (^{204}Pb), and because of that, other approaches for IFF correction are used. A benefit of isotope analysis with MC ICP-MS is that mass fractionation values for elements of similar mass are comparable. This enables the mass fractionation calculated for one element to be used to correct the IIF of another element. The IIF of Pb can be corrected with that of Tl (with non-radiogenic isotopes ^{203}Tl and ^{205}Tl) (Taylor et al., 2015).

- *External IIF correction*

  The procedure used for this correction is called the bracketing procedure. It means that before and after the sample, a solution of the isotope standard of the target element is measured. The measured values for each isotope ratio in the sample are then corrected for the difference in measured and certified value of the standards, measured before and after the sample. The matrix in the standard needs to be matched with that of a sample. For example, for Pb isotope ratio measurements, NIST SRM 981 is used as a calibrant (Prohaska et al., 2014).

- *Combination of internal and external IIF correction*

  This approach combines both correction strategies. For the Pb isotope ratio measurements, Tl is added to the samples before the measurement, and before and after the sample, a solution of NIST SRM 981 is measured. The advantage of this approach is that it allows a correction for short-term drifts in mass bias with internal correction (using Tl isotope ratio) and for mass bias correction using the same element (external bracketing procedure) (Prohaska et al., 2014).

- *Double-spike correction*

  This approach can be used for any element that has four or more isotopes. It involves a pair of artificially enhanced or spiked isotopes added to a part of the sample and measured separately from the pure sample – the "double-spike" procedure. Combining the data from the spiked and unspiked analyses allows the amount of fractionation in the unspiked fraction to be deconvolved. The isotope composition and concentration of the added double-spike have to be known. Before use, the isotope composition that will be added needs to be chosen, and also the proportion in which the sample and double-spike will be mixed (Rudge et al., 2009). The isotope composition and content of the element can be determined in one analysis by using an isotope dilution equation.

Additionally, certified reference materials (CRMs) need to be used to ensure the quality and comparability of results. Unfortunately, the Pb isotopic CRMs are currently not available for many environmental matrices.

1.5.2 Determination of metal-containing NPs

As metal-containing NPs form a growing category of substances found in the atmosphere, there is a need to better understand the impact of NPs on human health and their fate and behavior in the environment. Among the various analytical techniques available, single particle inductively coupled plasma mass spectrometry (spICP-MS) could be considered suitable for the analysis of metal-containing NPs in air.

1.5.2.1 Sample preparation

To introduce airborne NPs into the ICP-MS system, online sampling of NPs in the air using a rotating disk diluter (RDD) can be employed (Cen et al., 2024). However, offline sampling methods, such as PM collection on filters, are more commonly used. To analyze NPs on air filters by spICP-MS, appropriate sample preparation is required. In the study by Torregrosa et al. (2023), different extraction methods (such as direct immersion, hard cap espresso, ultrasound-assisted, and microwave-assisted extraction) and different extraction solvents (including trisodium citrate, ammonium hydroxide, potassium nitrate, etc.) were tested for the recovery of artificially deposited Au and Pt NPs on air filters. To the best of our knowledge, this is the only study to date that has investigated metal-containing NPs collected on air filters. On the other hand, other studies have investigated extraction procedures of PM_{10} and $PM_{2.5}$ from air filters and also the extraction of metal-containing NPs from different samples (e.g., soil, sediment, etc.). Folens et al. (2018) investigated the presence of Pt NPs in road dust collected in Belgium and Sweden with spICP-MS after ultrasound-assisted extraction in stormwater runoff. The results showed that Pt present in the leachate was entirely in the form of NPs. Roper et al. (2019) tested six different $PM_{2.5}$ filter extraction methods to investigate their potential effects on the composition and bioactivity of the samples. The results showed significant differences in element concentrations, and that extraction could change the chemical profile of the extracts. Bland et al. (2023) employed ultrasound-assisted extraction of $PM_{2.5}$ filters in deionized water to study $PM_{2.5}$ sources based on the composition of metal-containing particles. Baur et al. (2020) used surfactant-assisted extraction to extract incidental NPs from road runoff sediments collected from a road runoff treatment facility. The results showed that the method could be applied to different environmental samples potentially affected by road runoff (e.g., soil, sludge, water) and to analyze incidental NPs of small sizes and low concentrations. Goodman & Ranville (2023) used spICP-MS analysis of metal-containing NPs in stream sediments to study geochemical anomalies. The NPs were extracted using MilliQ water with small amounts of surfactant (11-mercaptoundeconoic acid), a shaker table, and a sonic bath. The results showed that this method could lower detection limits and enhance the detection of NPs in stream sediments, potentially leading to the collection of smaller field samples in mineralogic studies. Gómez-Pertusa et al. (2024) investigated the use of microwave-assisted extraction followed by spICP-MS determination of metal-containing NPs in soil. Different extraction solvents, such as MilliQ water, tetrasodium pyrophosphate, NaOH, and sodium citrate, were tested. The results showed that this method was appropriate for soil samples with different physicochemical properties and that it had similar accuracy and precision to other extraction methods (e.g., ultrasound, cloud point extraction).

1.5.2.2 Single particle inductively coupled plasma mass spectrometry (spICP-MS)

spICP-MS is a technique for sensitive and element-specific detection of NPs at environmentally low concentrations, which uses the established elemental analysis capabilities of ICP-MS but performs measurements on a per-particle basis (Laborda et al., 2014). The technique provides information about the chemical composition of NPs, and also about their size, number concentration, and size distribution. It allows the detection of both dissolved and particulate forms of an element. In principle, a liquid sample containing NPs must be diluted sufficiently to allow the NPs to enter the plasma individually, where they are vaporized, atomized, and ionized. The positively charged ion packets are then transported to the detector, where each short transient event measured in time-resolved analysis mode with a short dwell time represents a single NP. However, NPs enter the plasma randomly, and a measurement of two or more NPs within the dwell time can occur. The probability of this happening can be decreased with compromise conditions: short dwell time and low flux of NPs. spICP-MS enables the detection of metal-containing NPs as small as 20 nm, while the maximum recommended sizes are around (1–5) µm. Particle detection limits for spICP-MS reported in the literature are in the range of 10^6 particles/L (Laborda et al., 2013; Mitrano et al., 2012).

The number of measured pulses is directly correlated to particle number concentration and the intensity of the pulse with the mass of the element, or rather with the number of atoms in each NPs (Laborda et al., 2014). For the calculation of both particle number concentration and particle size, transport efficiency (η_n) needs to be known. It is defined as the ratio of the amount of analyte entering the plasma to the amount of analyte aspirated. Typical transport efficiencies reported in the literature are in the range of (1–10) % (Fréchette-Viens et al., 2017; Laborda et al., 2019). As transport efficiency is specific for each instrument, it needs to be determined individually and also regularly. For calculating transport efficiency, two methods are most commonly applied, the particle size method and particle frequency method (Pace et al., 2011). The first measures reference nanoparticles with known particle size, while the other measures reference nanoparticle suspension with known particle number concentration. In addition to the reference nanoparticle standard, the particle size method also needs a calibration curve of a dissolved element.

Particle number concentration (N_P) can be calculated using the equation (Degueldre et al., 2004; Degueldre, Favarger, Rossé, et al., 2006; Degueldre, Favarger, & Wold, 2006; Degueldre & Favarger, 2003, 2004):

$$N_P = \frac{f(I_P)}{q_{liq}\eta_n} \tag{1.1}$$

where $f(I_P)$ is the frequency of the particle events (no. of pulses/ms), q_{liq} is the sample flow rate (mL/ms), and η_n is the transport efficiency.

For the calculation of particle size, first, pulse intensity is correlated with the mass of the particle (m_P) with the following equation (Pace et al., 2011):

$$m_P = f_a^{-1}\left[\frac{\left(\left(I_P - I_{Bgd}\right)\eta_i\right) - b}{m}\right] \tag{1.2}$$

where f_a is the mass fraction of the analyzed element in the particle, η_i is the particle ionization efficiency, and m and b are the slope and intercept of the calibration curve (prepared with a dissolved elemental standard). For this equation, the assumption is that ions from a dissolved standard solution and ions from a nanoparticle will behave comparably past the plasma if they are composed of the same element. Another parameter to consider is particle ionization efficiency (η_i), which is a ratio of the ionization efficiency of the particle to the ionization efficiency of the corresponding dissolved element. As long as the particles are not bigger than 2 µm and the measured samples are sufficiently diluted, then plasma ionizes particles with a similar efficiency to a corresponding dissolved species. That means if these parameters are met, then η_i can be considered as 100 %.

Next, the mass of a spherical particle can be correlated to particle diameter (d) with the following equation (Pace et al., 2011):

$$d = \sqrt[3]{\left[\frac{6m_P}{\pi\rho}\right]} \tag{1.3}$$

where m_P is the mass of the particle, and ρ is the particle density.

Particle size for pure, spherical NPs can be obtained by calibration with NPs standard with a known diameter and the same chemical composition. If such a standard is not available, the dissolved standard of the measured element can be used (Pace et al., 2011) For size calculations of unknown particles, assumptions about particle chemical structure, density, and shape need to be made, or complementary techniques need to be used. The most common ones are electron microscopy, dynamic light scattering (DLS), and nanoparticle tracking analysis (Bolea et al., 2021).

Chapter 2

Aims and Hypothesis

Following the closure of the mine and smelter in the Upper Meža Valley and the implementation of remediation measures, the impact of pollutants on the environment and people began to decrease. Although the concentration of PTEs and especially Pb in the waters of the Meža River decreased over time, they are still present in the sediments in quite high concentrations. In addition, in recent years, an increase in Pb concentration in PM_{10} has been occasionally observed, which now poses a major challenge and potential risk to human health. By only monitoring the total concentration of PTEs in PM_{10} or environmental samples (soil, sand, sediments), it is almost impossible to determine their sources and fate in the environment and to assess the health risks they pose to humans. Therefore, the main purpose of the dissertation was to determine the source of Pb in PM_{10} from the Upper Meža Valley by applying advanced analytical techniques. First, the analytical method for the determination of Pb isotopic composition by MC ICP-MS in different environmental samples (river water, sediments, soils, mine waste, ores, minerals, sand from sandstones, dust roads and embankments, PM_{10}) was optimized and validated. Special attention was devoted to appropriate sample preparation and Pb isolation from the matrix. The method was then applied to real samples collected in the Upper Meža Valley, in which the total concentrations of different PTEs were also determined by ICP-MS. In this way, the local Pb sources were characterized. To investigate the concentration and size distribution of particles carrying Pb and other potentially present PTEs by spICP-MS, an analytical method for the extraction of NPs from PM_{10} samples was optimized and applied to the PM_{10} samples collected in the Upper Meža Valley.

Based on the aims of the doctoral dissertation, three hypotheses were formed:

- Multielemental and Pb isotope composition of PM_{10} from the Upper Meža Valley will display distinct patterns associated with their sources. These compositions will exhibit spatial and temporal variations corresponding to historical mining activities and current industrial practices.
- Ultrasound-assisted extraction followed by spICP-MS analysis is a useful method for the detection, quantification, and size characterization of metal-containing NPs in PM_{10} air filters. With it, the presence of Pb- and Zn-containing NPs in PM_{10} from the Upper Meža Valley will be proved.
- The combination of information on elemental, isotopic, and nanoparticulate forms of Pb in samples from the Upper Meža Valley will enable a better understanding of the fate of Pb in the environment and potential risks to residents.

Chapter 3

Materials and Methods

3.1 Sample Location, Collection, and Sample Preparation

The Upper Meža Valley is a narrow valley at 480 m a.s.l., situated between steep hills in northern Slovenia, adjacent to the border with Austria. It is relatively isolated, connected only by a regional road. It has rugged and varied relief, and the erosion of steep hills is prevented only by the forest. The Upper Meža Valley is surrounded by hills, where temperature inversions can often occur. Combination with poor atmospheric ventilation can increase the atmospheric pollution. The Upper Meža Valley has a long history of mining and smelting of Pb and Zn ore, and also the industry for secondary Pb production is present. The three main residential settlements in the area are Mežica, Črna na Koroškem, and Žerjav (Bavec et al., 2025; Bobnek Štaher, 2017; Miler & Gosar, 2013, 2019; Špes, 1998; Žibret et al., 2018). For this dissertation, different samples from the area were collected, including water and sediments from the Meža River and its tributaries, soil, sand, mine waste, road dust, ores, PM_{10}, and $PM_{2.5}$. Location and time of sampling for each sample are shown in Table A.1 (Appendix).

Various numbers of PM_{10} samples were collected in August, September, and October of 2018, at five different sampling locations (#1 – #5) in the Upper Meža Valley, in the settlements of Žerjav and Črna na Koroškem. An additional sampling was performed in Žerjav in March, April, May, June, and August of 2021 at Location #1 (Figure 3.1). At Location #1, a regular PM_{10} monitoring station is situated. Samples were not collected throughout the entire year, they were primarily collected in summer and fall to compare working and vacation days of the secondary Pb production industry and other activities in the valley. In addition to PM_{10}, $PM_{2.5}$ samples were also collected in 2018 at Location #4. Sampling of PM_{10} at Locations #1, #2, #3, #5, and of $PM_{2.5}$ at Location #4 was performed with a reference low-volume sampler Leckel SEQ 47/50, with pre-annealed 47 mm quartz fiber filters. The filters were automatically changed every 24 hours at a predetermined time. The airflow through the filter was 55.2 m^3/day. On the other hand, sampling of PM_{10} at Location #4 was performed with a high-volume DIGITEL DHA-80 sampler, with 150 mm quartz fiber filters. The filters were changed automatically every 24 hours at a predetermined time. The airflow through the filter was 720 m^3/day. The filter size and airflow did not impact the amount of PM collected, as the surface area-to-airflow ratio was comparable between the locations.

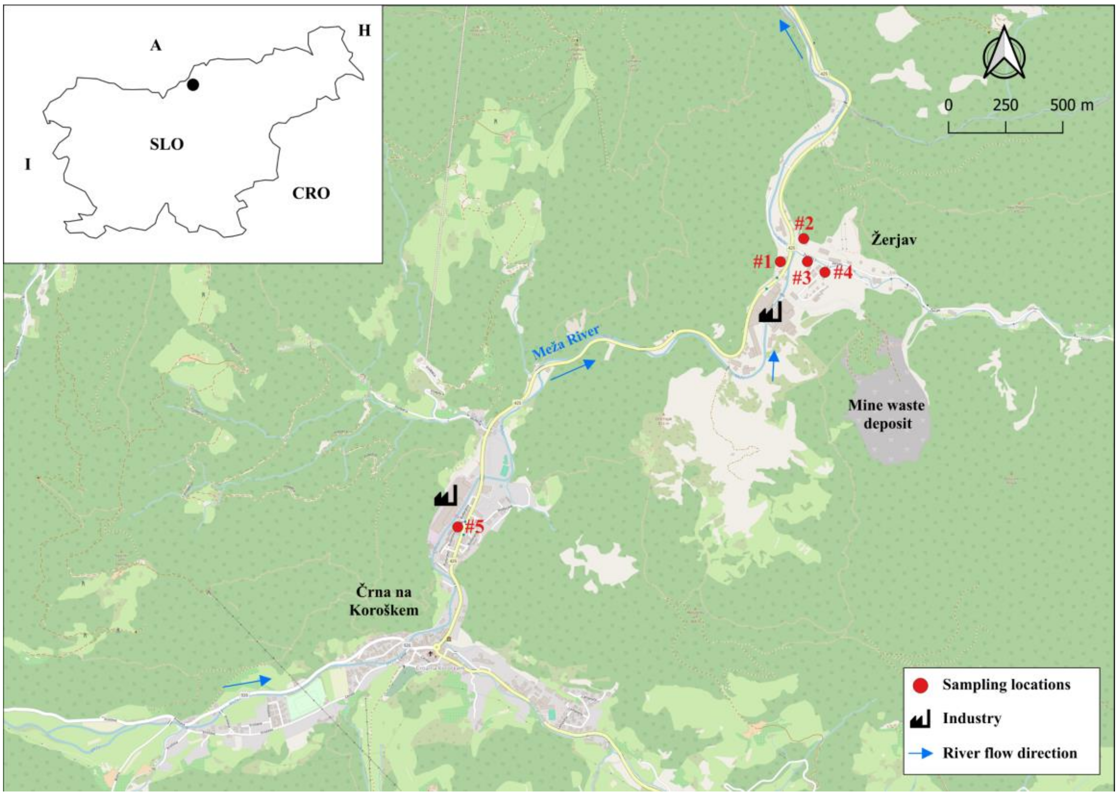

Figure 3.1: Sampling area with PM_{10} sampling locations.

For the determination of Zn- and Pb-containing NPs with spICP-MS filters from Location #1 (2021) and Location #4 (2018) were used (Table 3.1). For filters of smaller sizes (47 mm from Location #1), the entire filter was used for extraction and subsequent spICP-MS analysis, allowing for only one replicate. The filters of larger sizes (150 mm from Location #4) were cut into two circles before analysis, each with a diameter comparable to the smaller filters, enabling two replicates for analysis. All filters were dried overnight at 60 °C and weighed before the analysis. The optimized extraction procedure was applied, and the presence of Zn- and Pb-containing NPs in the filtered extracts was determined by spICP-MS analysis. In addition, total Zn and Pb concentrations in the extracts, filtered extracts, and filters after extraction were determined by ICP-MS analysis after acid digestion of the samples.

Table 3.1: Sampling date, location, and PM_{10} mass concentration of the PM_{10} samples from the Upper Meža Valley used for the determination of Zn- and Pb-containing NPs.

Sample	Sampling date	Sampling location	PM_{10} mass conc. (µg/m^3)
1a 1b	October 2018	Location #4	35
2a 2b	October 2018	Location #4	34
3a 3b	October 2018	Location #4	18
4	June 2021	Location #1	43
5	June 2021	Location #1	35

Sample	Sampling date	Sampling location	PM_{10} mass conc. (µg/m^3)
6	August 2021	Location #1	17
7	August 2021	Location #1	12

In addition to PM_{10} and $PM_{2.5}$, other types of samples, considered as potential sources of PTEs in PM_{10}, were also collected and analyzed, such as local soil, sand, sediment, mine waste, and exhaust from the Pb-recycling and Pb-battery production industry. For the purpose of this dissertation, soil, sand, sediment, and mine waste samples were considered as local background, and exhausts from the Pb-battery production industry were considered as an anthropogenic source. As an approximation of emissions from the Pb-battery production industry, components of Pb-batteries produced in the area were analyzed. There was 1 sample of Pb-grid and 3 samples of Pb-paste (composed of $PbSO_4$). Soil, sand, and mine waste samples were obtained from the Slovenian Environment Agency (ARSO). Samples of wulfenite, galenite, sphalerite, slate, andesite, and basalt were obtained from the University of Ljubljana, Faculty of Natural Sciences and Engineering, Department of Geology.

Water and sediment samples from the Meža River and its tributaries were collected once in January 2020. Water samples were collected at 7 locations along the Meža river: (1) Topla, (2) Črna 1, (3) Črna 2, (4) Žerjav 1, (5) Žerjav 2, (6) Mežica, (7) Podklanc, and on 3 tributaries: (8) Helena rivulet, (9) Jazbina rivulet, and (10) Junčar rivulet. The Meža River is 43 km long and is a typical Alpine river in its upper part, resulting in fast water flow. In its middle and lower part, water flow decreases due to a smaller slope and wider river bed. The average water flow of the Meža River is 9.2 m^3/s in January (dry season) and 15.4 m^3/s in April (wet season). Such fast water flow of the river results in a lack of fine sediments. Sediment samples were thus collected only at 5 locations: (2a) Črna 1, (3a) Črna 2, (5a) Žerjav 2, (7a) Podklanc, and (10a) Junčar rivulet. The sampling area and sampling sites are shown in Figure 3.2. Water samples were collected in 1 L plastic bottles, they were filtered through a 0.45 µm filter, acidified (1 mL of suprapur HNO_3 added to 1 L of the sample), and stored at 4 °C until analysis. As water samples were filtered before analysis, only concentrations of dissolved elements were determined. Sediment samples were collected with a plastic ladle, at least 200 g of it, and stored in 2 L plastic bottles together with water. In the laboratory, they were wet-sieved into different fractions (<2 mm, <0.250 mm, <0.150 mm, and <0.063 mm) and then dried to a constant mass at a temperature of 60 °C. For further analysis, two fractions were chosen: <0.150 mm and <0.063 mm.

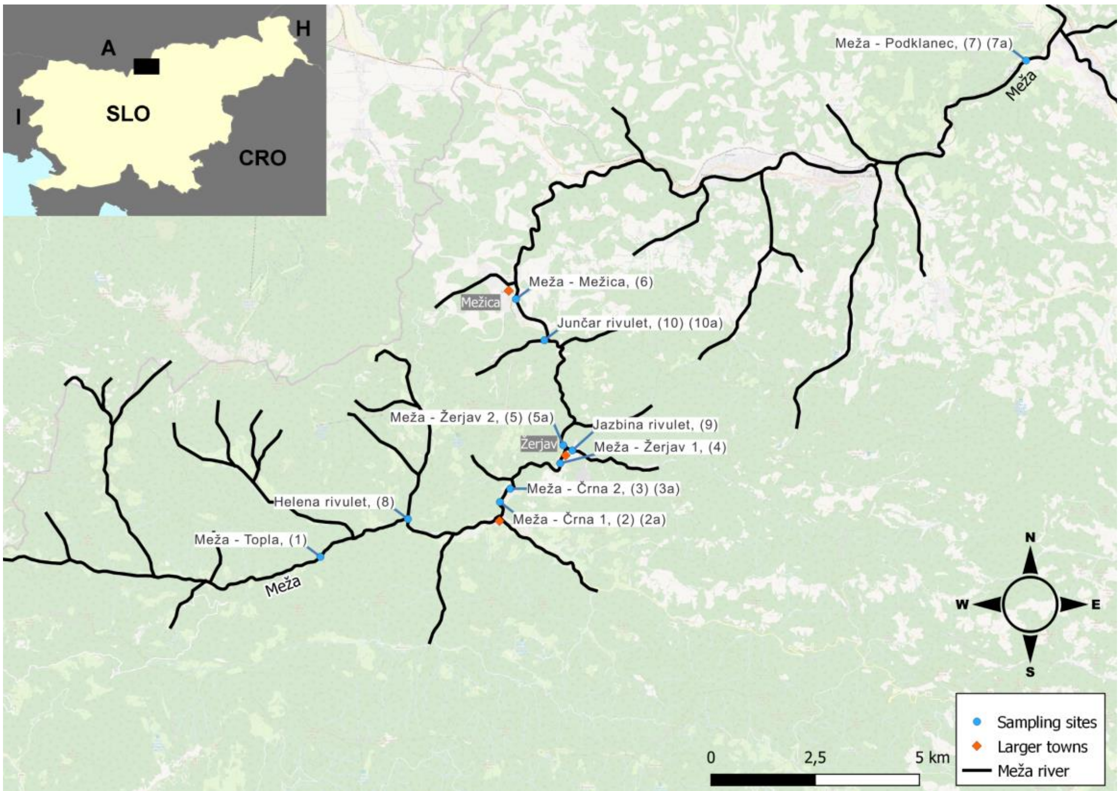

Figure 3.2: Sampling area with water and sediment sampling sites.

3.2 Instrumentation

Filters with PM_{10} and $PM_{2.5}$ were digested with the closed vessel microwave digestion system (UltraWAVE, Milestone, Sorisole, BG, Italy). Samples of sediment, soil, sand, mine waste, road dust, ore, and filters with PM_{10} for NPs determination were digested with the closed vessel microwave digestion system (MARS 6, CEM Corporation, Matthews, NC, USA). Samples of battery components were digested on a hotplate (C-MAG HP 10, IKA-Werke, Staufen, Germany). Total elemental concentrations were determined by conventional ICP-MS analysis using a 7700x quadrupole-ICP-MS instrument (Agilent Technologies, Tokyo, Japan). Extraction of NPs from filters was done in an ultrasonic bath (Sonis, Iskra PIO, Šentjernej, Slovenia), and NPs were determined by spICP-MS analysis using a 7900x quadrupole-ICP-MS instrument (Agilent Technologies). The shape, size, and elemental composition of NPs were determined by Verios G4 HP SEM (Thermo Fisher Scientific, Waltham, MA, USA), coupled with an AZtec Live EDS system (Oxford Instruments, Abingdon, UK). ICP-MS operating parameters for both conventional and single particle measuring modes were optimized daily for the highest sensitivity and are presented in Table 3.2. The Pb isotope ratios were determined by a Nu II Plasma MC ICP-MS from Nu Instruments (Ametek, Berwyn, MD, USA) coupled to a desolvation system (Aridus from Teledyne Cetac, Omaha, NE, USA) with a PFA nebulizer (100 µL/min) and nickel plasma cones for dry plasma. The instrument was optimized daily for the highest sensitivity and stability of the signal. General parameters are presented in Table 3.2.

Table 3.2: Operating parameters for PTEs concentration measurements with conventional ICP-MS, metal-containing NPs measurements with single particle ICP-MS, and Pb isotope measurements with MC ICP-MS.

	ICP-MS	
	Conventional mode	**Single particle mode**
Spray chamber	Scott double-pass	
Torch	Quartz torch with 2.5 mm injector	Quartz torch with 1.0 mm injector
Sampling and skimmer cones	Nickel	
Nebulizer	MiraMist, made of Teflon	MicroMist, made of glass
RF power	1550 W	
Plasma gas flow	15 L/min	
Auxiliary gas	0.90 L/min	
Nebulizer gas	1.05 L/min	0.70 L/min
Collision gas (He)	4.3 mL/min (^{66}Zn), No gas (^{208}Pb)	
Sample uptake rate	0.3 mL/min	
Dwell time	0.1 s	0.1 ms
Acquisition time	35 s	60 s (120* s)
Measured isotopes	^{66}Zn, ^{208}Pb	
	MC ICP-MS	
RF power	1300 W	
Plasma gas flow	13 L/min	
Auxiliary gas flow	0.80 L/min	
Nebulizer gas pressure	38 Psi	
Sampler cone	Ni, aperture diameter 0.9 mm	
Skimmer cone	Ni, aperture diameter 0.7 mm	
Integration time	10 s	
Number of cycles	25	
Number of blocks	2	
Mass assignment to Faraday cup detectors	H4 208 H3 207 H2 206 H1 205 Ax 204 L1 203 L2 202	

* For extracts in 1 % citric acid, acquisition time was prolonged to 120 s due to the low number of Zn- and Pb-containing NPs in the samples.

3.3 Reagents and Materials for Analytical Procedures

MilliQ water with a resistivity of 18.2 MΩ cm was obtained from a Direct-Q 5 system (Millipore, Watertown, MA, USA) and used for the preparation of samples and reagents. Hydrochloric acid (30 % (*w/w*) HCl, suprapur) and hydrofluoric acid (40 % (*w/w*) HF, suprapur), both obtained from Merck Ltd. (Darmstadt, Germany), nitric acid ((67–69) % (*w/w*) HNO_3, suprapur) of Carlo Erba Reagents Srl (Milan, Italy) and hydrogen peroxide (30 % (*w/w*) H_2O_2, suprapur) and boric acid (H_3BO_3, ultrapur) of Sigma-Aldrich (St. Louis, MO, USA) were used for sample digestion. For the determination of total elemental concentrations, an external calibration was used, prepared with the dilution of a multielement standard solution, Multi VI (ICP Standard Certipur, Merck Ltd.). As an accuracy check, certified reference materials of PM_{10}-like fine dust ERM-CZ120 (Institute for Reference Materials and Measurements, Geel, Belgium), channel sediment BCR 320R (Institute for Reference Materials and Measurements), loam soil ERM-CC141 (Institute for Reference Materials and Measurements) and certified reference material for trace elements in surface water SPS-SW1 (Spectrapure standards, Oslo, Norway) were used.

Water samples from the Meža River and its tributaries were filtered through 0.45 µm Minisart cellulose acetate membrane filters obtained from Sartorius (Göttingen, Germany).

For the optimization of Pb isolation from the matrix, three resins were tested, Pb Spec ((100–150) µm, Triskem International, Bruz, France), Sr Spec ((100–150) µm, Triskem International), and Dowex® 1X8 ((100–200) mesh, Acros Organics, Geel, Belgium). For testing different resins, a single-element standard solution of Pb (ICP Standard Certipur, Merck Ltd.), Pb isotopic standard SRM 981 (NIST, Gaithersburg, MD, USA), and different certified reference materials were used (PM_{10}-like fine dust ERM-CZ120, and loam soil ERM-CC141 obtained from the Institute for Reference Materials and Measurements, tomato leaves SRM 1573a, mussel tissue SRM 2976, and natural water SRM 1640a obtained from NIST).

For the optimization of the extraction procedure of Zn- and Pb-containing NPs, in-house PM_{10} filters were prepared using PM_{10} quartz fiber filters (MN QF-10, 47 mm, Macherey-Nagel, Düren, Germany) and certified reference material ERM-CZ120 (PM_{10}-like fine dust, obtained from Institute for Reference Materials and Measurements) with certified values for a total Zn concentration of 1240 mg/kg and a total Pb concentration of (113 ± 17) mg/kg. According to the certification report, the particle size distribution of the ERM-CZ120 material, as determined by dynamic light scattering (DLS) in a dispersion, which is only indicative of the aerodynamic diameter of the particles, consisted of 10 vol. % of particles below 1.75 µm, 16 vol. % below 2.49 µm, 50 vol. % below 7.59 µm, 84 vol. % below 15.01 µm, 90 vol. % below 20 µm (Piaścik et al., 2010). Sodium pyrophosphate ($Na_4P_2O_7 \times 10H_2O$, pro analysis) and ammonia solution (25 % (*w/w*) NH_3, suprapur) were obtained from Merck Ltd., and citric acid ($C_6H_8O_7$, AnalaR normapur) was obtained from VWR International (Leuven, Belgium). After extraction, samples were filtered through a (12–25) µm 589/1 black ribbon filter (Schleicher & Schuell GmbH, Dassel, Germany). A multielement standard solution, Multi VI, and single element standard solutions of Zn, Pb, and Au (ICP Standard Certipur, Merck Ltd.) were used for calibration. A gold nanoparticle (Au NP) suspension (BBI Solutions, Cardiff, UK), containing 56.8 mg/L of citric-acid-coated Au NPs with an average particle diameter of (50 ± 3) nm, was used daily for the determination of transport efficiency.

3.4 Total PTEs Determination in Samples from the Upper Meža Valley by ICP-MS

Total concentrations of PTEs (Pb, Zn, As, Cd, Li, Al, V, Cr, Mn, Fe, Co, Ni, Cu, Se, Rb, Sr, Mo, Ag, Sb, Ba, Tl, and U) in all the samples from the Upper Meža Valley were determined by ICP-MS. Before the measurements, the samples were digested.

Filters with PM_{10} and $PM_{2.5}$ were digested with a closed vessel microwave-assisted digestion following the standard *EN 14902 Ambient Air Quality. Standard Method for the Measurement of Pb, Cd, As, and Ni in the PM_{10} Fraction of Suspended Particulate Matter*, 2005. Filters were put into Teflon vessels, and a mixture of HNO_3 and H_2O_2 was added. The samples were subjected to one cycle of closed vessel microwave digestion at the maximum power of 1500 W. A clear solution was quantitatively transferred into a 100 mL measuring flask and filled to the mark with MilliQ water. The same procedure (acids only) was applied to a blank sample in every cycle.

Soil, sand, sediment, mine waste, ore samples, and CRMs of PM_{10}-like fine dust (ERM-CZ120), channel sediment (BCR 320R), and loam soil (ERM-CC141) were digested with a closed vessel microwave-assisted digestion following the method described by Zuliani et al. (2016). First, approximately 0.25 g of a sample was weighed into Teflon vessels. Afterwards, 4 mL of HNO_3, 1 mL of HCl, 2 mL of H_2O_2, and 2 mL of HF were added. The samples were subjected to the two-step microwave-assisted digestion, as described above. A clear solution was quantitatively transferred into 30 mL PP graduated tubes and filled to the mark with MilliQ water. The same procedure (acids only) was applied to a blank sample in every cycle.

To ensure that results from the two digestion procedures could be compared, 3 PM_{10} filters were also digested using the soil sample digestion method (which included HF). The concentrations of Pb, Zn, As, Cd, and Fe were comparable between the two digestion procedures. As expected, only Al showed a difference. Based on this comparison, Pb, Zn, As, Cd, and Fe concentrations were considered consistent across the different sample types.

Biological CRMs, tomato leaves (SRM 1573a) and mussel tissue (SRM 2976), were subjected to a closed vessel microwave-assisted digestion as follows: approximately 0.3 g of sample was weighed into Teflon vessels. Afterwards, 4 mL of HNO_3, 1 mL of H_2O_2, and 0.1 mL of HF were added. The samples were subjected to the following one cycle of closed vessel microwave digestion at the maximum power of 1600 W: ramping to temperature T = 140 °C in 15 min, holding at T = 140 °C for 5 min, ramping to T = 200 °C in 15 min, holding at T = 200 °C for 30 min. A clear solution was quantitatively transferred into 20 mL PP graduated tubes and filled to the mark with MilliQ water. The same procedure (acids only) was applied to a blank sample in every cycle.

Battery components were digested on a hotplate with 8 mol/L HNO_3. Approximately 0.05 g of a sample was weighed into 50 mL PP graduated tubes, and 15 mL of 8 mol/L HNO_3 was added. The closed tubes were put on a hotplate at around 85 °C for 6 h. As an accuracy check, certified reference material NIST SRM 981 Pb isotopic standard was subjected to the same digestion procedure as the samples.

Filters with PM_{10} used for metal-containing NPs determination were subjected to microwave-assisted digestion as follows: 5 mL of sample (ERM-CZ120 suspension, extracts, and filtered extracts) or the whole filter sample was transferred to the Teflon vessel. 2 mL of HNO_3, 1 mL of HCl, 1 mL of H_2O_2, and 1 mL of HF (for liquid samples) or 2 mL of HF (for filter samples) were added in the first step, and 6 mL of H_3BO_3 (4 % (*w/w*)) (for liquid samples) or 12.5 mL of H_3BO_3 (4 % (*w/w*)) (for filter samples) were added in the second step. The samples were subjected to the following two cycles of closed vessel microwave digestion at the maximum power of 1600 W: ramping to temperature T = 140 °C in

15 min, holding at T = 140 °C for 5 min, ramping to T = 200 °C in 20 min, holding at T = 200 °C for 60 min. After the first cycle, H_3BO_3 (4 % (*w/w*)) was added and the samples were subjected to the second cycle following the program: ramping to T = 140 °C in 15 min, holding at T = 140 °C for 5 min, ramping to T = 200 °C in 15 min, holding at T = 200 °C for 30 min. The clear solution obtained after digestion was quantitatively transferred to 30 mL PP graduated tubes and made up to the mark with MilliQ water. The same procedure (acids only) was applied to a blank sample in each cycle.

Before ICP-MS analysis, the samples were appropriately diluted with MilliQ water (resulting in a 1 % HNO_3 solution). Quantification was performed based on external calibration by measuring PTEs ionic standards prepared in 1 % HNO_3 in the concentration range of (0.5–500) µg/L and an online internal standard (25 µg/L Rh in 1 % HNO_3).

3.5 Pb Isotope Determination

Pb isotope ratios in all the samples were determined by MC ICP-MS. For the correction of instrumental mass bias, a combination of internal and external calibration was used. An appropriate amount of standard solution of Tl (NIST SRM 3158) was added to the samples before the measurement. The isotope standard reference material NIST SRM 981 was measured as a bracketing standard. Before the measurements, Pb was isolated from the matrix.

3.5.1 Isolation of Pb from the matrix

To obtain the best results, Pb isolation from the matrix was first optimized. Different certified reference materials (CRMs), such as PM_{10}-like fine dust (ERM-CZ120), loam soil (ERM-CC141), tomato leaves (SRM 1573a), and mussel tissue (SRM 2976), were first subjected to microwave-assisted digestion, as described in Chapter 3.4.

Samples then underwent separation of Pb from the matrix, using extraction chromatographic Pb Spec and Sr Spec resin, and ion exchange resin Dowex® 1X8. Before Pb extraction chromatography, samples had to be evaporated and re-dissolved in the required solvent, in 1 mol/L HNO_3, 8 mol/L HNO_3, or 0.5 mol/L HBr for Pb Spec, Sr Spec, and Dowex® 1X8 resin, respectively.

For the optimization of Pb isolation from the matrix, first, possible blanks of the procedure were tested by using only acid in the place of a sample (1 mol/L HNO_3, 8 mol/L HNO_3, and 0.5 mol/L HBr for Pb Spec, Sr Spec, and Dowex® 1X8 resin, respectively). Next, recovery rates of each resin were tested using a single-element standard solution of Pb (ICP Standard Certipur, Merck Ltd.). For Pb Spec, Sr Spec, and Dowex® 1X8 resin, solutions with 300 µg/L, 120 µg/L, and 150 µg/L Pb in 1 mol/L HNO_3, 8 mol/L HNO_3, and 0.5 mol/L HBr were prepared, respectively. For Pb elution from Pb Spec, Sr Spec, and Dowex® 1X8 resin, 0.1 mol/L ammonium oxalate, 8 mol/L HCl, and 6 mol/L HCl were used, respectively. The mass balance during the separation procedure was followed by measuring Pb concentration by ICP-MS.

After that, resins were tested with a CRM of tomato leaves (SRM 1573a). The influence of different parameters on the recovery rate was tested:

- duration of ultrasonic bath sonication: after first evaporation (2 h, 3 h, 4 h) and after second evaporation (4 h, 5 h, 6 h),
- volume of the sample (4 mL, 9 mL, 12 mL),
- end concentration of Pb in the sample (30 µg/L, 50 µg/L, 100 µg/L).

The final separation procedure of Pb from the matrix for each resin is shown in Figure 3.3.

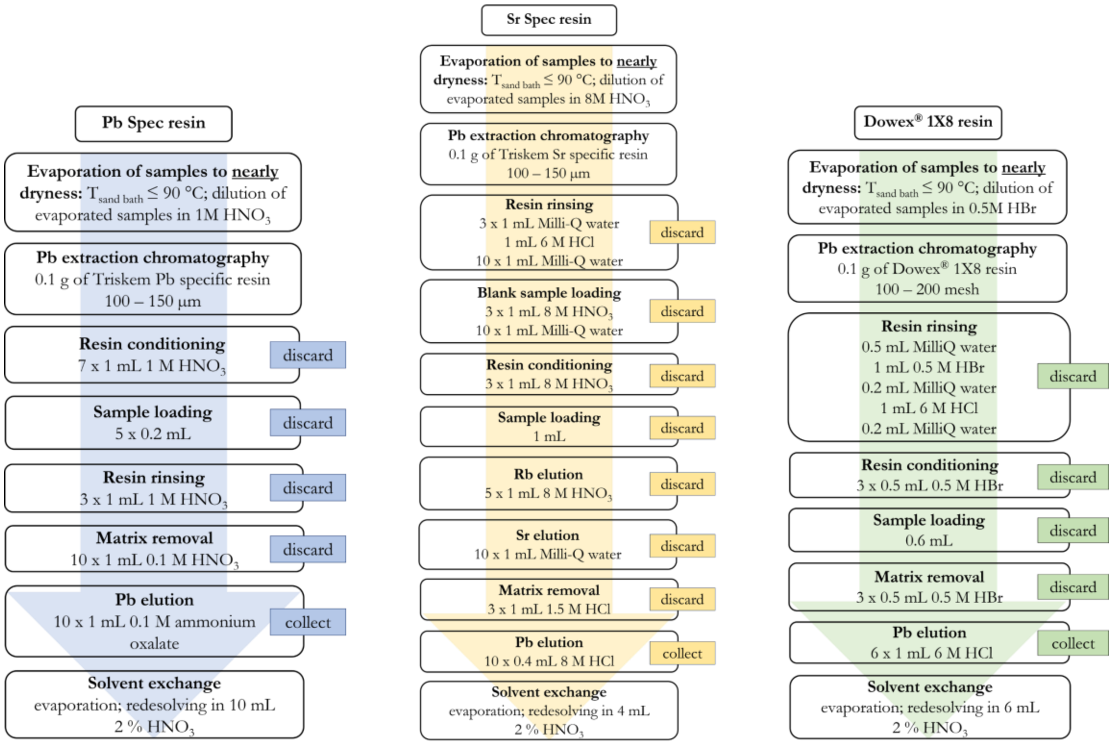

Figure 3.3: Schematic of Pb separation procedure for Pb Spec, Sr Spec, and Dowex® 1X8 resin.

With optimal parameters, the separation procedure was also tested on different CRMs containing Pb (PM_{10}-like fine dust ERM-CZ120, loam soil ERM-CC141, mussel tissue SRM 2976, and natural water SRM 1640a). The procedure for Dowex® 1X8 resin was additionally tested with Pb isotopic standard NIST SRM 981. In addition to Pb recovery rates, Pb isotope composition in all the CRMs after the separation was determined by MC ICP-MS.

For Pb isotope ratio determination in samples from the Upper Meža Valley, Pb was isolated from the matrix by using 0.1 g of ion exchange resin Dowex® 1X8 (100–200 mesh, Acros Organics). The procedure applied is described in more detail in Figure 3.3. An appropriate amount of sample was evaporated on a sand bath (T = (70–90) °C) and then re-dissolved in 0.6 mL of 0.5 mol/L HBr by sonication for 3 h, and then applied to the resin. Pb was washed out of the resin by 6 mol/L HCl. The samples were then again evaporated to dryness and re-dissolved in 6 mL of 2 % HNO_3 by sonication for 5 h. For each sample, a new resin was used. To control Pb recovery after separation, total Pb concentration was measured by ICP-MS.

3.6 Determination of Zn- and Pb-containing NPs

3.6.1 Extraction of NPs from PM_{10} filters

The procedure used for extracting metal-containing NPs from PM_{10} filters was based on the use of ultrasound sonication, which has been previously reported as an effective method for the extraction of PM from air filters (Bland et al., 2023; Pietrogrande et al., 2021; Torregrosa et al., 2023). The two parameters that were further optimized were the time of sonication and the type of extraction solvent (MilliQ water, 10 mM sodium pyrophosphate, 1 % citric acid, and 1 % aqueous ammonia solution), while the concentrations of extraction solvents used in this dissertation were adapted from a previously published work by Torregrosa et al. (2023). The sonication times of 0.5 h, 1 h, and 2 h were tested with 10 mM sodium pyrophosphate, which proved to be the most suitable extraction solvent. Optimization of the sonication time and extraction solvents was performed using the PM_{10} filters prepared in-house by applying the ERM-CZ120 suspension to the blank PM_{10} quartz fiber filters. The ERM-CZ120 suspension was prepared by weighing 20 mg of ERM-CZ120 powder into 50 mL of MilliQ water, resulting in a 0.4 mg/mL PM_{10}-like fine dust suspension. The suspension was sonicated using an ultrasonic bath, operated at 40 kHz for 30 min. 5 mL of the ERM-CZ120 suspension was applied to PM_{10} filters, retaining approximately 2 mg of PM_{10}-like fine dust. A schematic of the extraction optimization procedure is shown in Figure 3.4. The concentration of Zn and Pb not retained on the filter was determined by ICP-MS in the filtrate (i.e., solution passing through the filter), to which 20 µL of concentrated HNO_3 was added.

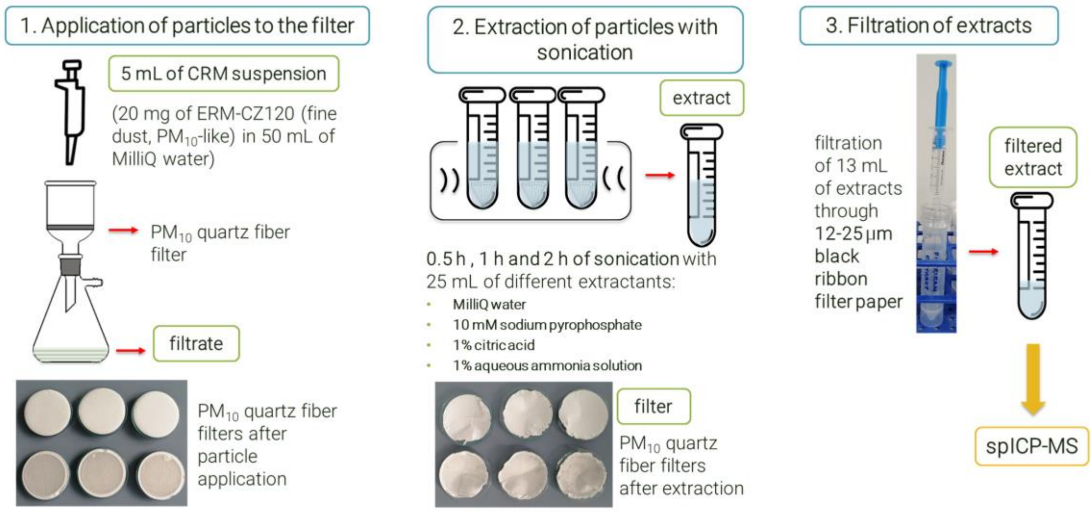

Figure 3.4: Schematic of the extraction optimization procedure.

The optimized extraction procedure involved placing dried quartz filters into the 50 mL PP graduated tubes to which 20 mL of 10 mM sodium pyrophosphate was added. Samples were subjected to bath sonication operated at 40 kHz frequency for 2 h. The extracts were afterward quantitatively transferred to 30 mL PP graduated tubes, while the filters and 50 mL tubes were rinsed with 5 mL of 10 mM sodium pyrophosphate, which was combined with the rest of the extract. After the extraction, the filters were transferred to watch glasses and dried overnight at 60 °C. During the extraction, the filters partially disintegrated, resulting in the presence of filter fibers in the extracts. As this could lead to clogging of the ICP-MS nebulizer, the fibers needed to be removed before spICP-MS analysis. Since the centrifugation could not remove quartz fibers from the extracts, filtration through (12–25) µm filters was applied. To minimize the risk of adsorptive losses of Zn- and Pb-containing NPs, the (12–25) µm filters were first pre-equilibrated. This involved passing 5 mL of MilliQ water and 1 mL of 10 mM sodium pyrophosphate through the filter and discarding the solution. This step was repeated three times to ensure proper filter pre-equilibration before filtering the extracts.

3.6.2 spICP-MS analysis of extracted NPs

Zn- and Pb-containing NPs in the filtered extracts were determined by spICP-MS. A multi-element batch was used for consecutive measurements of two elements in time-resolved mode. The signal intensity of the ^{66}Zn and ^{208}Pb isotopes was recorded consecutively for 60 s (for extraction with MilliQ, sodium pyrophosphate, and aqueous ammonia solution) or 120 s (for extraction with citric acid). A dwell time for each isotope was set to 0.1 ms. Before spICP-MS analysis, the sample extracts were diluted with MilliQ water (2x for extracts in MilliQ water and 1 % citric acid, 5x for extracts in 1 % aqueous ammonia solution, and 10x for extracts in 10 mM sodium pyrophosphate) to ensure that the number of particles detected during one acquisition time ranged between 100 and 2000. This adjustment aimed to detect a sufficient number of particles for statistical purposes while minimizing bias due to multiple particle events. Another consideration in selecting the optimal dilution factor was to maintain a low baseline signal, which could otherwise be increased due to spectral interferences and/or the presence of dissolved analytes (as in the case of the extraction with 1 % citric acid).

An accurate sample flow rate was determined daily by weighing MilliQ water introduced as a sample at a peristaltic pump speed of 0.1 rotations/s (N=3). The transport efficiency was determined daily according to the particle size method (Pace et al., 2011). This involved analyzing a 50 nm AuNP suspension prepared from a stock suspension (BBI Solutions, Cardiff, UK), which contained 56.8 mg/L of citric-acid-coated AuNPs with an average particle diameter of 50 ± 3 nm, diluted to a concentration of 0.142 µg/L. Additionally, ionic Au standards (prepared from a single Au ICP Standard Certipur form Merck Ltd.) were prepared at concentrations of 0 µg/L, 0.5 µg/L, 1.0 µg/L, and 5.0 µg/L. The particle size method was selected as the particle diameter of the AuNPs in the stock standard solution used to determine transport efficiency is less susceptible to change over time compared to the particle number concentration. The latter can decrease over the storage time of the AuNPs stock solution due to aggregation/agglomeration, particle settling, and/or particle adhesion to the container walls.

Particle mass quantification was based on calibration curves prepared from different concentration levels of ionic Zn and Pb standards (ranging from 0.5 µg/L to 100 µg/L). Particle mass was converted to particle diameter by assuming spherical mono-elemental particles consisting of Zn (Zn mass fraction 1.0, with a density of 7.13 g/cm^3) or Pb (Pb mass fraction 1.0, with a density of 11.35 g/cm^3). These assumptions introduce significant bias in determining particle sizes, potentially leading to their underestimation. As a result, the particle size information reported by spICP-MS in this dissertation is only qualitative. For creating particle size distribution graphs, bin sizes of 5 nm and 2 nm were used for Zn- and Pb-containing NPs, respectively.

Data processing was performed using the Single Nanoparticle Application Module within the MassHunter 5.2 Workstation Software (Version D.01.02, Build 708.1, Agilent Technologies) in the “Peak Integration Mode”. The smallest particle diameter observed in the particle size distribution of filter extracts was considered the minimum detectable particle diameter. The lowest signal intensity threshold above which events were considered to be NPs was set at a value corresponding to a particle diameter of 55 nm for Zn- and 18 nm for Pb-containing NPs. The application of the same threshold for all samples ensured that a direct comparison of particle mass and number concentrations, as well as median particle diameters, was possible between samples.

The mass fraction of Zn- and Pb-containing NPs was calculated by comparing the particle mass concentration determined by spICP-MS with the total mass concentration determined in digested samples by ICP-MS. The summary of all calculations used regarding NPs in this dissertation is presented in the Appendix (Eq. (A.1) – (A.10)).

3.6.3 SEM-EDS analysis of extracted NPs

As the spICP-MS technique requires information on the NP composition, shape, and density for accurate sizing, the shape, size, and elemental composition of Zn- and Pb-containing NPs in the filtered extracts were determined by scanning electron microscopy–energy dispersive spectroscopy (SEM-EDS) in the backscattered electron (BSE) and secondary electron (SE) modes. The droplets of samples prepared in MilliQ water were deposited on carbon tape or silicon plates and vacuum-dried. MilliQ water was used as a solvent for the SEM-EDS analysis of the samples, as drying the sample droplets in sodium pyrophosphate resulted in the formation of a thin film that hindered particle detection. It was therefore necessary to perform solvent exchange by centrifuging the samples or to extract particles from filters using MilliQ water. The uncoated samples were analyzed with a beam current of 0.8 nA, at an accelerating voltage of 20 kV, and a working distance of 5 mm. Particles containing Zn and Pb were identified using the BSE mode images. Their size was determined using the measuring tool included in the Thermo Fisher Scientific SEM software, while their elemental makeup was determined using the EDS X-ray point analysis available in the AZtec software. EDS measurements were performed with a resolution of around 1 µm, which did not allow the chemical composition of individual particles to be investigated at lower dimensions. Elemental analysis data were collected using acquisition times of 100 s, and the software was calibrated using premeasured universal standards included in the software, referenced to a Co standard.

3.7 Pearson Correlation Coefficient (PCC)

Pearson correlation coefficients (PCC) were calculated to determine possible correlations between Pb, Zn, Cd, and As in sediments and those dissolved in water. Also, they were calculated to assess potential correlations between the particle number or mass concentration and the total mass concentration of the corresponding elements determined in the PM_{10} samples from the Upper Meža Valley. They were calculated with Microsoft Excel (Office 2019). The correlation was marked as very strong if the coefficient was above 0.80.

3.8 Probable Effect Concentration Quotient (PEC-Q)

The Probable effect concentration quotient (PEC-Q) approach (Long et al., 2006) was used to assess the potential toxicity of investigated elements (Pb, Zn, Cd, As, Cr, and Ni) in Meža River sediments. It is expressed as:

$$PEC-Q = \frac{\sum_{i=1}^{n} \frac{[Me]_i}{PEC_i}}{n} \tag{3.1}$$

where $[Me]_i$ is the concentration of the element measured in the sediment sample, PEC_i is the corresponding PEC value (they were summarized after MacDonald et al. (2000)), and n is the total number of measured elements. Two critical values for PEC-Q were reported by Long et al. (2006). A PEC-Q value of 0.25 represents conditions at which the percentage incidence of toxicity exceeds 20 % in laboratory toxicity tests with marine (i.e., *Ampelisca abdita* and *Rhepoxynius abronius*) or freshwater (i.e., *Hyalella azteca*) organisms, while a PEC-Q value of 0.34 indicates at which sites a reduction in the abundances of amphipods, gastropods, and capitellid polychaetes is likely to occur.

3.9 Enrichment Factor (EF)

The enrichment factor (EF) for Pb, Zn, Cd, and As in PM_{10} and $PM_{2.5}$ samples was used for identifying their possible anthropogenic input. It was calculated using the following equation:

$$EF = \frac{(X/R)_{aerosol}}{(X/R)_{crust}} \tag{3.2}$$

where X represents the element of interest, R is the reference element, and $(X/R)_{aerosol}$ and $(X/R)_{crust}$ represent the concentration ratios of X and R in PM_{10} and $PM_{2.5}$ samples and the Earth's upper crust, respectively. Different elements can be used as reference elements, the most commonly Si, Al, and Fe, as they are abundant in the crust (Cesari et al., 2012; Enamorado-Báez et al., 2015). In this dissertation, Fe was used as a reference element. For the $(X/Fe)_{crust}$, an average value from all the measured samples of local soil was taken. Based on EF values, sources of elements are categorized into three groups: EF $<$ 10 contributions primarily from crustal source; 10 $<$ EF $<$ 100 contributions from mixed sources, crustal and anthropogenic; and EF $>$ 100 contributions primarily from anthropogenic source (Lee et al., 2017).

3.10 Binary Endmember Mixing Model of Pb Isotope Ratios

The relative contribution of a possible anthropogenic source to Pb in PM_{10} and $PM_{2.5}$ was calculated using an equation for the binary endmember mixing model (Monna et al., 1997):

$$Pb_{anthropogenic}(\%) = \frac{(^{206}Pb/^{207}Pb)_{sample} - (^{206}Pb/^{207}Pb)_{natural}}{(^{206}Pb/^{207}Pb)_{anthropogenic} - (^{206}Pb/^{207}Pb)_{natural}} x\ 100 \tag{3.3}$$

where $Pb_{anthropogenic}$ represents the contribution of a possible anthropogenic source in this mixing model, $(^{206}Pb/^{207}Pb)_{sample}$, $(^{206}Pb/^{207}Pb)_{natural}$, $(^{206}Pb/^{207}Pb)_{anthropogenic}$ are the isotopic signatures of PM_{10} and $PM_{2.5}$ samples, local natural background (in this case sediment, soil, sand and mine waste) and possible anthropogenic source (in this case exhausts from secondary Pb production industry), respectively. In the equation, only the $^{206}Pb/^{207}Pb$ ratio is written, however, similar binary endmember mixing models can also be used for other Pb isotope ratios.

Chapter 4

Results and Discussion

4.1 Total PTEs Concentrations

Total PTEs concentrations were determined in different samples from the Upper Meža Valley, including PM_{10}, $PM_{2.5}$, water and sediment from Meža River and its tributaries, soil, sand, road dust, mine waste, ore, and Pb-battery components. Before analyzing the real samples, the procedure for determining total PTEs concentrations was tested with different CRMs (PM_{10}-like fine dust ERM-CZ120, channel sediment BCR 320R, loam soil ERM-CC141, and certified reference material for trace elements in surface water SPS-SW1). The determined values for all materials were in good alignment with the certified values (Table 4.1).

Table 4.1: Concentrations of selected elements determined in CRMs PM_{10}-like fine dust (ERM-CZ120), channel sediment (BCR 320R), and loam soil (ERM-CC141) after microwave digestion, and in SPS-SW1 by ICP-MS. Results are expressed with the standard deviation of ten sample replicates.

ERM-CZ120	certified conc. (mg/kg)	determined conc. (mg/kg)
Cr	201	199 ± 4
Fe	38144	38000 ± 580
Ni	58 ± 7	58 ± 2
Zn	1240	1235 ± 8
As	7.1 ± 0.7	7.1 ± 0.6
Cd	0.90 ± 0.22	1.00 ± 0.15
Pb	113 ± 17	116 ± 3
BCR 320R	certified conc. (mg/kg)	determined conc. (mg/kg)
Cr	59 ± 4	58 ± 3
Fe	25700 ± 1300	26000 ± 1000
Ni	27.1 ± 2.2	27.8 ± 2.0
Zn	319 ± 20	321 ± 15
As	21.7 ± 2.0	22.5 ± 1.8
Cd	2.64 ± 0.18	2.59 ± 0.16
Pb	85 ± 5	84 ± 3

ERM-CC141	certified conc. (mg/kg)	determined conc. (mg/kg)
Cr	86 ± 8	85 ± 1
Fe*	65800	22400 ± 800
Ni	26.4 ± 2.4	25.8 ± 0.7
Zn	57 ± 4	60 ± 2
As	9.9 ± 1.5	10.4 ± 0.2
Cd	0.35 ± 0.05	0.36 ± 0.05
Pb	41 ± 4	38 ± 2
SPS-SW1	certified conc. (µg/L)	determined conc. (µg/L)
Cr	2.00 ± 0.02	1.99 ± 0.02
Fe	20 ± 1	20.4 ± 0.2
Ni	10.0 ± 0.1	10.0 ± 0.1
Zn	20	19.9 ± 0.4
As	10.0 ± 0.1	10.1 ± 0.1
Cd	0.50 ± 0.01	0.50 ± 0.01
Pb	5.0 ± 0.1	5.0 ± 0.1

* Certified concentration is for Fe_2O_3.

4.1.1 Concentrations of dissolved PTEs in water samples from the Meža River and its tributaries

Concentrations of dissolved Pb, Zn, Cd, and As determined in water samples from the Meža River and its tributaries are presented in Table 4.2, while concentrations of the dissolved elements Li, Al, V, Cr, Mn, Fe, Co, Ni, Cu, Se, Rb, Sr, Mo, Ag, Sb, Ba, Tl, and U are shown in Table A.2 (Appendix).

Table 4.2: Concentration of dissolved Pb, Zn, Cd, and As (µg/L) in water samples from the Meža River and its tributaries determined by ICP-MS. Results are expressed with the measurement standard deviation.

Sample Number	Sample Location	Pb	Zn	Cd	As
(1)	Meža–Topla	2.52 ± 0.09	4.33 ± 0.09	0.038 ± 0.004	1.29 ± 0.02
(2)	Meža–Črna 1	1.08 ± 0.03	5.70 ± 0.19	0.049 ± 0.005	0.624 ± 0.012
(3)	Meža–Črna 2	9.01 ± 0.27	7.39 ± 0.13	0.057 ± 0.004	0.637 ± 0.012
(4)	Meža–Žerjav 1	19.7 ± 0.7	11.4 ± 0.4	0.105 ± 0.005	1.11 ± 0.04
(5)	Meža–Žerjav 2	41.9 ± 1.9	28.5 ± 0.7	0.578 ± 0.011	7.28 ± 0.11
(6)	Meža–Mežica	21.7 ± 0.6	63.8 ± 1.1	0.631 ± 0.010	3.09 ± 0.05
(7)	Meža–Podklanc	8.08 ± 0.22	53.6 ± 1.1	0.238 ± 0.012	0.871 ± 0.032
(8)	Helena rivulet	51.7 ± 0.9	107 ± 1	0.523 ± 0.011	0.413 ± 0.009
(9)	Jazbina rivulet	4.37 ± 0.13	67.7 ± 1.8	0.258 ± 0.010	0.368 ± 0.013
(10)	Jundar rivulet	31.5 ± 0.7	89.5 ± 1.2	0.250 ± 0.009	0.533 ± 0.012

The average dissolved concentrations determined in water were ranked as follows: Zn (43.9 µg/L) > Pb (19.1 µg/L) > As (1.62 µg/L) > Cd (0.273 µg/L). Overall, dissolved Zn and Pb concentrations in the Meža River were lower than in its tributaries, while dissolved

As concentrations were higher than in the tributaries. The highest dissolved Zn and Pb concentrations were measured at the Helena rivulet (8), which runs past abandoned mine shafts and mine waste deposits from where it may leach these elements (Gosar & Miler, 2011). The highest concentration of dissolved As in water was measured at Meža–Žerjav 2 (5) and of dissolved Cd at Meža–Mežica (6). As both sampling sites were in settlement centers, the elevated concentrations of As and Cd could be a result of urban runoff.

The results of this dissertation confirmed that concentrations of PTEs in water decreased over time (Gošar et al., 2015; Kladnik, 2009). In 1979, the average Pb concentration in the Meža River was 700 mg/L (Kladnik, 2009), while in 2002 it was 75 µg/L (Gošar et al., 2015). In 2002, the average Zn concentration in the Meža River was 175 µg/L, while in 2015, both Zn and Pb concentrations were close to background concentrations (25 µg/L and 5 µg/L, respectively) (Gošar et al., 2015). However, in this dissertation, Pb concentrations were elevated at the Helena (8) and Jinčar (10) rivulets, both receiving waters from the closed mines and Žerjav 1 (4), Žerjav 2 (5), and Mežica (6). Zn concentrations were elevated at all three investigated tributaries and also at Žerjav 2 (5), Mežica (6), and Podklanc (7). Locations Žerjav 1 (4) and Žerjav 2 (5) are both near a Pb-recycling factory and under urban influence. In Mežica, there were elevated concentrations of PTEs in the area around a former ore processing plant (Fux & Gosar, 2007). The results indicate that elevated concentrations of Pb and other PTEs in the Meža River tributaries can still be a result of the leaching of material from landfills, as was suggested in the past (Gosar & Miler, 2011).

The average dissolved Pb concentration determined in this dissertation was higher than the threshold values determined by the EU Water Frame Directive (WFD) (7.2 µg/L) (*Directive 2008/105/EC*, 2008). The limits were exceeded at most sampling sites except at Topla (1), Črna 1 (2), and the Jazbina rivulet (9). In general, dissolved Zn concentration exceeded the established limit (50 µg/L) at half of the sampling sites (Mežica (6), Podklanc (7), Helena (8), Jazbina (9), and Junčar (10) rivulet). The average dissolved Cd concentration was below the limit of 0.6 µg/L, and it was exceeded only at Mežica (6). Average concentrations of dissolved As, Ni, Cu, and Cr at all sampling sites were well below the established limits of 25 µg/L, 20 µg/L, 5 µg/L, and 32 µg/L, respectively (*Directive 2008/105/EC*, 2008; *S.I. No. 272 of 2009*, 2009).

4.1.2 Total PTEs concentrations in sediment samples from the Meža River and its tributaries

Pb, Zn, Cd, and As concentrations determined in the <0.063 mm and <0.150 mm sediment fractions from the Meža River and its tributaries are presented in Table 4.3, while total concentrations of other elements (Li, Al, V, Cr, Mn, Fe, Co, Ni, Cu, Se, Rb, Sr, Mo, Ag, Sb, Ba, Tl, and U) are shown in Table A.3 (Appendix).

The highest determined average concentrations of elements in sediments (fraction <0.063 mm) were those of Pb (6348 mg/kg), followed by Zn (5037 mg/kg) > As (34.7 mg/kg) > Cd (29.8 mg/kg). In fraction <0.150 mm, they were ranked Zn (5073 mg/kg) > Pb (3581 mg/kg) > Cd (26.3 mg/kg) > As (23.6 mg/kg). In general, higher concentrations of Pb, Cd, and As were determined in the smaller fraction (<0.063 mm), while for Zn, they were higher in the larger fraction (<0.150 mm). The results for Pb from this dissertation have an opposite trend to the results from Fux & Gosar (2007), where all four elements were higher in the larger sediment fraction, and they were attributed to the mine tailings. Higher concentrations of Pb in the fraction <0.063 mm at Meža–Žerjav 2 (5a) could indicate that there could be another anthropogenic source present. The differences in elemental distribution among different particle sizes were observed between natural and anthropogenic sources (S. Zhang et al., 2002).

Table 4.3: Total concentration of Pb, Zn, Cd, and As (mg/kg) in two fractions (<0.063 mm and <0.150 mm) of sediment samples from the Meža River and its tributaries determined by ICP-MS. Results are expressed with the measurement standard deviation.

Sample Number	Sample Location	Fraction (mm)	Pb	Zn	Cd	As
(2a)	Meža–Črna 1	<0.063	1619 ± 1	2214 ± 21	13.2 ± 0.1	22.3 ± 0.3
		<0.150	2549 ± 277	2055 ± 24	10.3 ± 0.1	14.4 ± 0.3
(3a)	Meža–Črna 2*	<0.150	120 ± 1	375 ± 6	2.45 ± 0.01	10.3 ± 0.3
		<0.250	114 ± 3	646 ± 5	2.71 ± 0.04	11.0 ± 0.2
(5a)	Meža–Žerjav 2	<0.063	15609 ± 16	5206 ± 74	33.0 ± 0.1	56.5 ± 0.6
		<0.150	3895 ± 275	1702 ± 6	9.61 ± 0.13	20.4 ± 0.3
(7a)	Meža–Podklanc	<0.063	5814 ± 5	6658 ± 69	43.8 ± 0.1	30.5 ± 0.4
		<0.150	10032 ± 192	15956 ± 121	88.0 ± 0.7	44.3 ± 0.6
(10a)	Junčar rivulet	<0.063	2350 ± 1	6071 ± 61	29.3 ± 0.1	29.5 ± 0.7
		<0.150	1401 ± 26	5278 ± 13	21.4 ± 0.3	28.7 ± 0.1

* Meža–Črna 2, no fine sediment present.

Regarding the sampling locations, the highest PTEs concentrations were, in general, present at the Podklanc (7a) sampling location in the <0.150 mm fraction. In the <0.063 mm fraction, the highest Pb and As concentrations were measured at Meža–Žerjav 2 (5a), which is situated a few meters downstream from the industrial area and from the confluence with the Jazbina rivulet. The lowest concentrations of all four elements in fraction <0.063 mm were measured at Meža–Črna 1 (2a) and in fraction <0.150 mm at Meža–Črna 2 (3a). The Meža River is an Alpine type river, with high and fast water flow, which leads to the removal of sediment from the beginning of the river and its deposition in the lower, slower parts of the river (Gosar & Miler, 2011). That would explain why the lowest elemental concentrations were determined in samples from the higher parts of the river (Meža–Črna 1 (2a) and 2 (3a)), and the highest concentrations were determined at the lower parts (Meža–Podklanc (7a), Žerjav 2 (5a)), especially in the fraction <0.150 mm.

PTEs concentrations in sediments from the Meža Valley have been monitored throughout the years. In 1986, average Pb, Zn, and Cd concentrations in the Meža River were 970 mg/kg, 2700 mg/kg, and 8.7 mg/kg, respectively. Between 1986 and 1992, their concentrations dropped around 4-, 10-, and 8-times, respectively. However, they again increased around 2-, 4-, and 7-times, respectively, between 2004 and 2005 (Kladnik, 2009). Between 2007 and 2011, approximately similar concentrations in two fractions of the sediments were reported for Pb, Zn, Cd, and As (<0.063 mm and <0.125 mm). However, these concentrations were higher than in the past. Higher concentrations were observed in the larger fraction and also in the tributaries, indicating that their primary source was the material from the mines and mine tailings (Fux & Gosar, 2007; Gosar & Miler, 2011). In this dissertation, the minimum values for Pb, Zn, and As in both fractions were higher than reported by Gosar & Miler (2011), who sampled the sediments from 2005 on. The Zn values in the fraction <0.063 mm, in particular, were almost 10-times higher. This could indicate that leaching of the elements from mines and landfills is still present, as well as an industrial and urban influence.

4.1.3 Correlations between PTEs in water and sediments

Pearson correlation coefficients (PCC) were calculated to determine if a correlation between the elements found in sediments and water exists. Pearson correlation coefficients for Pb, Zn, and As concentrations in filtered water and sediment fraction <0.063 mm were 0.99, 0.97, and 0.98, respectively, which indicates a very strong correlation between elemental concentrations in filtered water and sediment fraction <0.063 mm. The smallest fraction has the highest specific area, and it can therefore adsorb the highest amount of elements (S. X. Wang et al., 2003). These elements can then be released into the water because of the fast and turbulent water flow of the Meža River. Meanwhile, the Pearson correlation coefficient for Cd was 0.51, and the correlation was not as strong as in the case of the other three elements. The main difference between Cd and other elements is that Cd is the least soluble and is mainly bound to immobile fractions. That is why lower concentrations of it can be released into the water (Svete et al., 2001).

In comparing the concentration of Pb, As, Zn, and Cd in the filtered water among themselves, a very strong correlation between Pb and As (0.98), Pb and Cd (0.95), and also between As and Cd (0.95) was observed (Table A.4 (Appendix)). In the sediment fraction <0.063 mm, a perfect correlation between Pb and As (1.00) and also between Zn and Cd (1.00) was observed. The latter indicates that Zn and Cd come from the natural environment since Cd is present in important concentrations in Zn ore (Miler & Gosar, 2012; Štrucl, 1984). In the sediment fraction <0.150 mm, all four elements were very strongly correlated with each other (PCC > 0.96). PTEs in the larger fraction may be a result of mine tailings being washed into the river, and since mine tailings contain all four elements, that can explain their correlation. On the other hand, the elements, especially Pb and As, present in the fine sediment fraction, indicate an additional input.

4.1.4 Probable effect concentration quotient (PEC-Q)

The probable effect concentration quotient (PEC-Q) approach was used to evaluate possible risk from the simultaneous presence of several PTEs (Pb, Zn, Cd, As, Cr, and Ni) in the Meža River sediments. PEC-Q values for sediments collected at the Meža River and its tributaries were calculated according to Eq. (3.1), with data in Table 4.3, and Table A.3 (Appendix). The results presented in Figure 4.1 A show that all collected sediments, regardless of the fraction, had PEC-Q values over the critical value of 0.34. Regarding the very high total elemental concentrations in sediment samples, high PEC-Q values were to be expected. The lowest PEC-Q value was at Črna 2 (3a) in fraction <0.150 mm (0.62), while the highest was at Podklanc (7a) in fraction <0.150 mm (27.0). In sediment samples from Črna 1 (2a), PEC-Q values in both fractions were closer together than in any other location. The biggest difference between fractions was observed at Žerjav 2 (5a), where PEC-Q values in the <0.063 mm fraction were higher than in the <0.150 mm fraction, which may indicate that PTEs in the smaller fraction of the sediments at this location pose a higher risk to the river system than those in the larger one. That also coincides with higher PTEs concentrations measured in the smaller fraction at the Žerjav 2 (5a) sampling location.

To identify whether other PTEs, namely Ni, As, Cr, and Cd, may cause potential adverse effects, Pb and Zn, which were present in the highest concentrations, were excluded from the evaluation of PEC-Q. Figure 4.1 B shows that PEC-Q values were lower when calculated without Pb and Zn, in most cases by more than half. The biggest difference in PEC-Q values was in the sediment sample from Žerjav 2 (5a) in the <0.063 mm fraction. However, the differences were not so large that the PEC-Q values would be under the critical value of 0.34, indicating that other PTEs also have a big impact on the quality of the river sediments. Despite very high PEC-Q values, the state of the Meža River is not as critical as these values indicate, as Pb, Zn, and Cd are mostly bound to more sparingly soluble fractions (Svete et al., 2001).

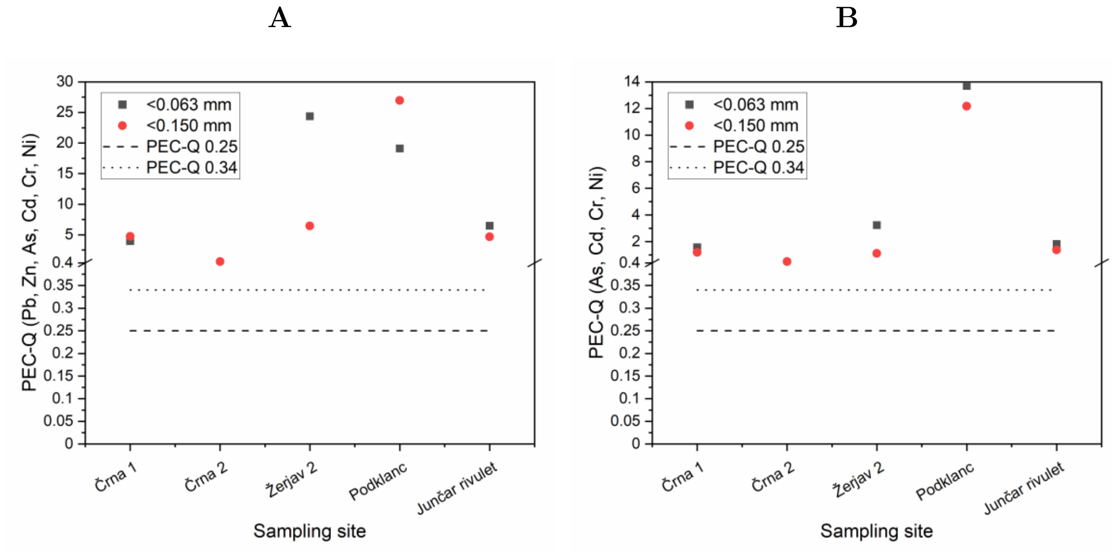

Figure 4.1: PEC-Q values for sediment samples A) with, and B) without the inclusion of Pb and Zn, collected along the Meža River and its tributaries. Horizontal lines correspond to PEC-Q values of 0.25 and 0.34.

4.1.5 Total PTEs concentrations in PM_{10}, $PM_{2.5}$, soil, sand, road dust, mine waste, ores, and Pb-battery components from the Upper Meža Valley

Pb, Zn, Cd, and As concentrations determined in PM_{10} samples from the Upper Meža Valley are presented in Figure 4.2, while total concentrations of other elements (Li, Al, V, Cr, Mn, Fe, Co, Ni, Cu, Se, Rb, Sr, Mo, Ag, Sb, Ba, Tl, and U) are shown in Table A.5 (Appendix).

The average PTEs concentrations in PM_{10} at the majority of locations were in the following order: Pb>Zn>Cd>As, except at Location #2, where Cd concentration was the lowest, and at Location #5, where Zn concentration was the highest. The highest average Pb and Cd concentrations were measured at Location #1, which is the National Environment Agency's (ARSO) monitoring station for PM_{10} particles in Žerjav, while the highest average Zn and As concentrations were measured at Location #2 and #5, respectively. The lowest average As and Cd concentrations were measured at Location #3. Žerjav is a settlement with around 340 inhabitants, situated between steep hills, and the distances between the sampling locations are small, except for Location #5, which is in the neighboring settlement. However, differences in elemental compositions in the Žerjav measurement stations were detected. Location #4 is the closest to the mine waste deposit, while Locations #1 and #5 are closest to the secondary Pb production site in Žerjav and Črna na Koroškem, respectively. Based on their position, a greater influence from the production exhaust can be expected.

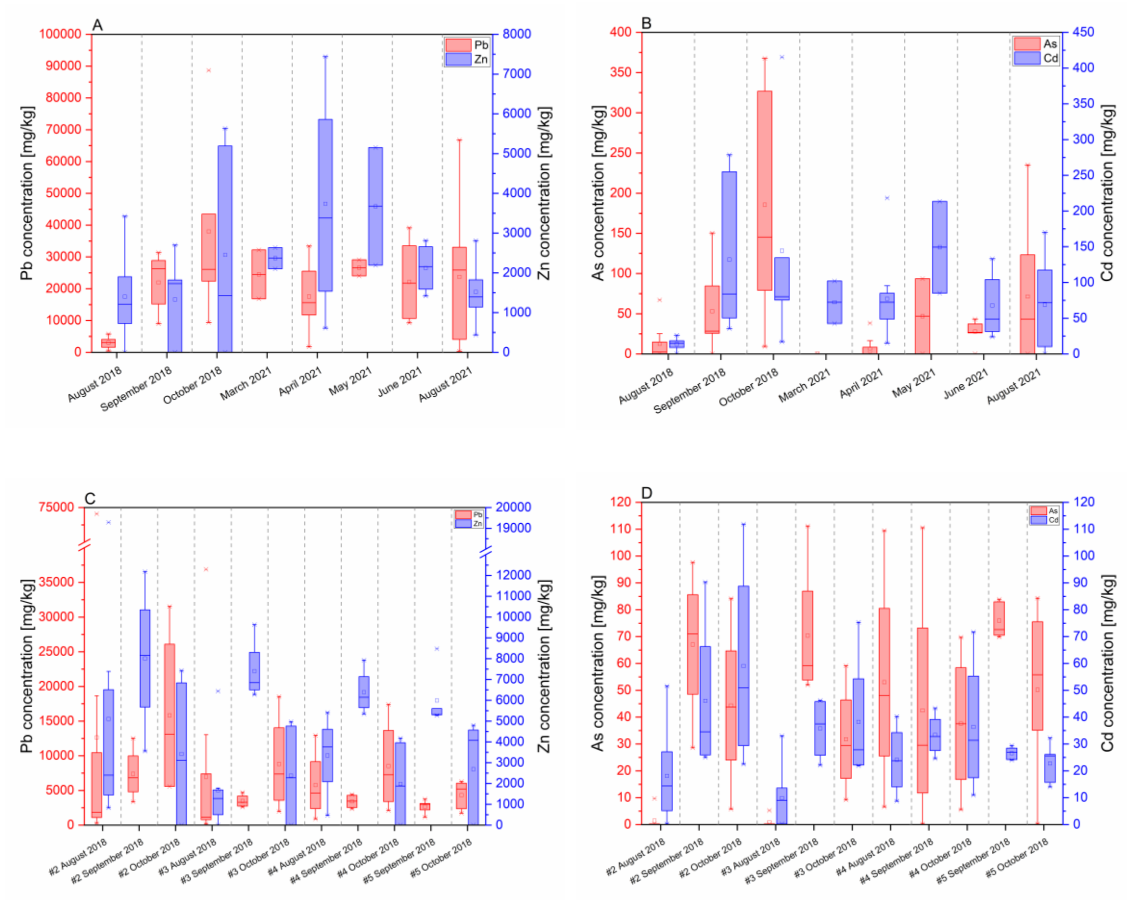

Figure 4.2: Temporal and spatial variations of Pb, Zn, As, and Cd concentrations in PM_{10} samples from the Upper Meža Valley. Figures A and B show Pb and Zn, and As and Cd concentrations at Location #1, respectively. Figures C and D show Pb and Zn, and As and Cd concentrations at Locations #2, #3, #4, and #5, respectively. Locations #1 – #4 were located in Žerjav, while Location #5 was in Črna na Koroškem.

From Figure 4.2, seasonal differences may be observed for all four elements, however, not significant. At Location #1, Pb and Zn concentrations were higher in 2021 compared to 2018, while this was not the case for As and Cd. The distribution of PM_{10} Pb concentrations was the largest among the analyzed samples, showing large daily and spatial variability. The annual average Pb concentrations in PM_{10} at Location #1 increased from 300 ng/m^3 in 2009 to 694 ng/m^3 in 2021 (Ivartnik et al., 2022). In 2021, the annual limit value was exceeded in 5 different months (Ivartnik et al., 2022). In June 2021, a high amount of desert dust was observed over the area, which caused increased concentrations of PM_{10} particles but did not influence the PTEs concentrations in the sampled particles.

Concentrations of PM_{10} collected at five different locations in 2018 and 2021 are shown in Figure 4.3. The highest particle concentration was determined in samples collected at Location #1 in June 2021. The daily limit value for PM_{10} recommended by WHO is 50 µg/m^3, while the annual limit value is 20 µg/m^3 (*WHO Global Air Quality Guidelines*, 2021). Of all the PM_{10} samples analyzed, the daily limit value was exceeded only once at Location #1 in June 2021. Similarly, based on the daily measurements of PM_{10} at Location #1 by ARSO, the daily limit value was exceeded 6 times in the whole year, 2 times in June (Bec et al., 2022).

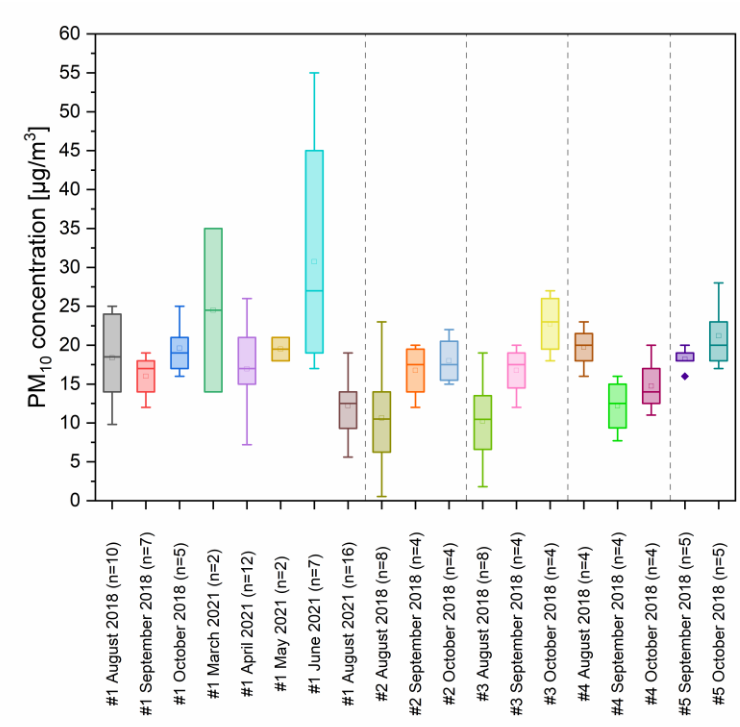

Figure 4.3: Spatial and temporal distribution of PM_{10} concentration in the Upper Meža Valley. Locations #1 – #4 were located in Žerjav, while Location #5 was in Črna na Koroškem.

When comparing average monthly PM_{10} concentrations in 2021 as determined by ARSO (Bec et al., 2022) at Location #1 and Ljubljana (the capital city of Slovenia), the PM_{10} concentrations at both locations were similar. In some months, the average monthly PM_{10} concentration was slightly higher in Žerjav (March, April, May, June), while in others it was slightly higher in Ljubljana (February, August, September, October, November, December). As a result of higher population density and various activities (including traffic), there are many sources of pollution in Ljubljana. Additionally, Ljubljana lies in a basin, where meteorological conditions (including low wind speeds) also prevent the removal of PM_{10} pollution. Despite similar average monthly PM_{10} concentrations at both locations, both daily and average annual Pb concentrations at Žerjav were significantly higher. Average annual Pb concentration in PM_{10} at Žerjav was 694 ng/m^3, while at Ljubljana it was 5.9 ng/m^3.

$PM_{2.5}$ samples were collected at one location (Location #4) in 2018. The average concentrations in three months were similar, and they were (11.1 ± 4.0) µg/m^3 in August, (11.4 ± 2.8) µg/m^3 in September, and (12.0 ± 6.0) µg/m^3 in October. The daily limit value for $PM_{2.5}$ recommended by WHO is 25 µg/m^3, while the annual limit value is 10 µg/m^3 (*WHO Global Air Quality Guidelines*, 2021). The daily limit value was not exceeded in the analyzed $PM_{2.5}$ samples. The average annual $PM_{2.5}$ concentration in 2018 in Ljubljana was 19 µg/m^3, while in 2021 it was 15 µg/m^3, as determined by ARSO (Bec et al., 2022). In both years, the annual limit value was exceeded. As there is no regular $PM_{2.5}$ monitoring station in Žerjav, no further comparisons could be made.

In addition to PM_{10} and water and sediments from the Meža River and its tributaries, total Pb, Zn, As, and Cd concentrations were also determined in soil, sand, road dust, ores, mine waste, and Pb-battery components. The elemental composition of Pb-battery components was used as a proxy for the exhaust from the secondary Pb production site.

The results are presented in Table 4.4, while total concentrations of other elements (Li, Al, V, Cr, Mn, Fe, Co, Ni, Cu, Se, Rb, Sr, Mo, Ag, Sb, Ba, Tl, and U) are shown in Table A.6 and Table A.7 (Appendix).

As expected, the highest Pb concentrations were found in Pb-battery components (Pb-grid, Pb-paste 1, Pb-paste 2, Pb-paste 3), and Pb ores and minerals, followed by mine waste samples, sediments from the Meža River and its tributaries (Table 4.3), and local sand, soil, and road dust. The highest average Zn concentration was found in sphalerite, followed by galenite and mine waste. Since As and Cd are typically impurities in Pb and Zn ores, their concentrations were significantly lower than that of Pb. The highest average As concentration was detected in wulfenite, while the lowest was in Pb-grid from Pb-batteries. The highest average Cd concentration was found in sphalerite, with the lowest in Pb-paste samples 1, 2, and 3.

In soil, Pb, Zn, As, and Cd concentrations were in the range of 32.6 mg/kg and 4153 mg/kg, 86.2 mg/kg and 6976 mg/kg, 6.13 mg/kg and 106 mg/kg, and 0.418 mg/kg and 46.1 mg/kg, respectively. The PTEs concentrations in the soil varied largely because some of the samples were taken at locations that underwent overlay with the uncontaminated soil. PTEs present in the soil are mostly a consequence of their release from mining and smelting activities that occurred for centuries as well as a result of bedrock rich with Pb and Zn ore (Žibret et al., 2018), while in sediments of Meža River and its tributaries mine waste deposits represent a significant source as shown in the study of Miler & Gosar (2012). Compared to published data for PTEs in soil and sediment from the Upper Meža Valley, the concentrations did not change significantly through the years (Finzgar et al., 2014; Gosar & Miler, 2011).

Table 4.4: Total concentration of Pb, Zn, Cd, and As (mg/kg) in different types of samples from the Upper Meža Valley determined by ICP-MS. Locations #1 – #4 of PM_{10} and $PM_{2.5}$ samples were located in Žerjav, while Location #5 was in Črna na Koroškem.

Sample Type	Number of samples	Pb				Zn				Cd				As			
		min	max	average	mean	min	max	average	mean	min	max	average	mean	min	max	average	mean
PM_{10}-Location #1	61	350	88689	20025	18992	<1.48	7439	2159	1777	<0.239	415	77.5	67.3	<0.231	368	48.1	20.6
PM_{10}-Location #2	16	256	74098	12124	5569	<1.48	19290	5409	4590	<0.239	112	35.3	25.9	<0.231	97.6	28.6	7.73
PM_{10}-Location #3	16	184	36891	6552	2747	<1.48	9633	3281	1692	<0.239	75.3	23.4	22.0	<0.231	111	26.0	7.21
PM_{10}-Location #4	12	900	17400	5899	4290	<1.48	7927	3906	3990	8.74	71.7	31.3	29.4	<0.231	111	44.4	40.1
$PM_{2.5}$-Location #4	12	575	7262	3302	3205	5554	13716	9408	8694	<0.239	68.4	28.6	22.3	<0.231	195	64.6	75.2
PM_{10}-Location #5	10	1165	6284	3482	3057	<1.48	8475	4340	5034	14.0	32.2	24.6	25.8	<0.231	84.4	63.1	71.6
Road dust	3	208	260	229	217	908	1010	965	978	4.31	5.03	4.76	4.93	11.3	12.7	11.9	11.7
Soil	26	32.6	4153	934	636	86.2	6976	1783	897	<0.239	46.1	10.9	4.78	6.13	106	23.0	20.1
Sand	11	48.0	11179	2607	1515	554	30004	8125	6352	6.25	118	40.7	29.8	6.10	113	30.5	20.1
Mine waste	4	578	28409	11994	9495	1281	88484	27711	10541	3.80	364	119	54.4	9.10	123	54.1	42.0
Wulfenite*	9	288006	621948	463745	563668	52.6	1232	375	218	1.91	15.3	8.56	7.98	733	1634	1169	1157
Galenite*	10	108187	916816	627484	585669	2401	114792	47196	41489	33.3	593	254	216	8.74	504	127	52.1
Sphalerite*	1			3703				691608				3408				148	
Slate*	2	90.2	95.5	92.9	92.9	2182	2213	2197	2197	4.37	4.49	4.43	4.43	16.7	17.0	16.8	16.8
Andesite*	2	115	581	348	348	91.3	149	120	120	<0.239	<0.239	<0.239	<0.239	1.51	2.14	1.83	1.83
Basalt*	2	44.2	66.9	55.6	55.6	169	175	172	172	<0.239	<0.239	<0.239	<0.239	3.15	3.17	3.16	3.16
Pb-grid	5	561234	726716	632046	605751	<1.48	<1.48	<1.48	<1.48	19.6	52.3	34.4	29.6	<0.231	0.551	0.295	0.231
Pb-paste 1	6	342742	693744	528714	552949	<1.48	<1.48	<1.48	<1.48	<0.239	0.532	0.358	0.341	<0.231	5.70	1.26	0.231
Pb-paste 2	6	326514	645829	469625	479761	<1.48	<1.48	<1.48	<1.48	<0.239	0.287	0.260	0.255	<0.231	4.59	1.33	0.563
Pb-paste 3	6	229887	805259	514034	495270	<1.48	<1.48	<1.48	<1.48	<0.239	0.414	0.341	0.355	<0.231	6.22	1.47	0.521

* Personal communication (Rogan Šmuc et al., 2025)

4.1.6 Enrichment factor (EF)

To estimate the potential anthropogenic input of Pb, Zn, Cd, and As in PM_{10} and $PM_{2.5}$ samples from the Upper Meža Valley, the enrichment factor (EF) was calculated according to Eq. (3.2) (Table 4.5). Although the mean upper continental crust values provided by Wedepohl (1995) are typically used for calculating $(X/Fe)_{crust}$, a different approach was adopted in this dissertation. Given the Upper Meža Valley's extensive history of Pb-ore mining and smelting, the local soil exhibits elevated concentrations of Pb, Zn, Cd, and As. Consequently, the average concentration values from all measured samples of the local soil were used to calculate the $(X/Fe)_{crust}$.

Table 4.5: Enrichment factors (EF) for Pb, Zn, As, and Cd in PM_{10} and $PM_{2.5}$ samples collected in the Upper Meža Valley at 5 locations in 2018 and 2021. Locations #1 – #4 were located in Žerjav, while Location #5 was in Črna na Koroškem. Results are expressed as an average of all the samples collected each month at one location, with standard deviation.

Location	Month	EF			
		Pb	Zn	As	Cd
#1 PM_{10}	August 2018	8.56 ± 4.84	1.91 ± 1.32	2.03 ± 3.52	3.27 ± 1.64
	September 2018	69.1 ± 18.3	2.16 ± 1.89	8.03 ± 7.37	33.6 ± 21.1
	October 2018	151 ± 129	5.42 ± 6.32	38.2 ± 33.8	49.0 ± 52.5
	March 2021	105 ± 78	4.63 ± 0.97	0.045 ± 0.016	26.8 ± 23.0
	April 2021	62.5 ± 28.2	7.56 ± 6.44	0.702 ± 1.255	23.0 ± 10.1
	May 2021	75.8 ± 36.8	5.74 ± 4.85	4.84 ± 6.78	31.4 ± 8.7
	June 2021	54.4 ± 42.7	2.47 ± 1.38	2.96 ± 2.31	15.2 ± 13.6
	August 2021	66.1 ± 44.8	2.50 ± 1.15	10.6 ± 11.7	16.9 ± 13.8
#2 PM_{10}	August 2018	5.69 ± 6.72	2.31 ± 0.91	0.159 ± 0.394	2.31 ± 2.54
	September 2018	13.4 ± 6.3	8.05 ± 4.69	6.66 ± 4.10	6.85 ± 2.94
	October 2018	64.5 ± 76.8	5.38 ± 6.22	7.95 ± 5.73	20.2 ± 22.3
#3 PM_{10}	August 2018	10.9 ± 15.1	1.67 ± 1.16	0.115 ± 0.241	2.35 ± 2.52
	September 2018	9.90 ±4.31	11.0 ± 5.0	10.1 ± 5.2	8.58 ± 4.00
	October 2018	58.9 ± 56.1	10.1 ± 11.9	12.1 ± 10.9	21.6 ± 16.9
#4 PM_{10}	August 2018	13.8 ± 8.4	4.58 ± 3.02	6.50 ± 4.01	5.68 ± 3.22
	September 2018	16.2 ± 5.8	15.5 ± 4.7	9.51 ± 10.98	13.4 ± 3.9
	October 2018	63.5 ± 67.4	7.73 ± 9.06	14.1 ± 11.6	23.9 ± 22.0
#4 $PM_{2.5}$	August 2018	16.1 ± 9.7	22.5 ± 6.2	18.5 ± 3.1	9.65 ± 8.14
	September 2018	13.5 ± 2.9	28.1 ± 4.3	0.074 ± 0.015	11.0 ± 2.0
	October 2018	25.8 ± 22.3	25.1 ± 8.2	29.8 ± 15.0	21.7 ± 12.7
#5 PM_{10}	September 2018	12.2 ± 4.2	14.3 ± 3.6	17.6 ± 1.8	10.6 ± 1.5
	October 2018	23.3 ± 15.3	9.50 ± 9.83	16.8 ± 10.5	11.7 ± 6.2

The lowest EF values were observed for Zn, followed by As. EF values below 10 suggested that the contribution to Zn and As was primarily from a crustal source, most likely from dust formed from the local soil. Higher EF values were observed for Cd and Pb, indicating a mixed source from both crustal and anthropogenic origins.

Examining the EFs for different months at Location #1, all four elements had EFs below 10 in August 2018. The EF for Zn remained below 10 in all other months, while As exhibited similar behavior, except for October 2018 and August 2021, when the EF ranged between 10 and 100. The EF for Cd consistently ranged between 10 and 100 across all other months. The EF for Pb exceeded 100 in October 2018 and March 2021, but fluctuated between 10 and 100 in other months. The EF values, particularly for Pb, showed high variability within and between months. For instance, the EF for Pb at Location #1 was below 10 in August 2018, but in August 2021, it was above 60. In 2018, 9.09 % of all the PM_{10} samples from Location #1 had EFs for Pb exceeding 100, which increased to 20.5 % in 2021, indicating a rising anthropogenic input.

4.2 Pb Isotope Composition

To determine the sources of Pb in PM_{10} from the Upper Meža Valley, the Pb isotope composition determined by MC ICP-MS was used. First, the procedure for Pb isolation from the matrix was optimized. Next, the optimized procedure was applied to real samples, including water and sediment from the Meža River and its tributaries, soil, sand, mine waste, ore, Pb-battery components, PM_{10}, and $PM_{2.5}$. Pb isotope ratios for each sample are shown in Table A.8 (Appendix). Then, the binary endmember mixing model was used to determine the contribution of each source to Pb in PM_{10}.

4.2.1 Optimization of Pb isolation from the matrix

First, possible blanks of the procedure were tested by using only acid in the place of a sample (1 mol/L HNO_3, 8 mol/L HNO_3, and 0.5 mol/L HBr for Pb Spec, Sr Spec, and Dowex® 1X8 resin, respectively). After the separation of Pb from the matrix, blank samples were measured on ICP-MS. The results showed that Pb concentration in blank samples was (0.276 ± 0.067) µg/L for Pb Spec, (0.461 ± 0.158) µg/L for Sr Spec, and (0.140 ± 0.046) µg/L for Dowex® 1X8 resin. As Pb concentrations in samples were significantly higher (on average around 50 µg/L) and blank concentrations were too low to be measured on MC ICP-MS, these were considered as acceptable blanks.

Next, the recovery rates of each resin were tested using a single-element standard solution of Pb, prepared in an appropriate medium for each resin. The recovery of the procedure with Pb Spec resin was (72.9 ± 4.9) %, with Sr Spec resin (35.8 ± 11.0) %, and with Dowex® 1X8 resin (92.3 ± 5.3) %. Testing with a standard solution of Pb revealed that different parameters in the procedure impacted the final Pb recovery. Possible losses of Pb for all three resins could occur during evaporation in a step for solvent exchange after the separation, so this step was tested next. The results showed that the biggest Pb losses in the procedure indeed occurred during this step. The biggest difference in recovery rate was with Sr Spec resin, and the smallest was with Dowex® 1X8 resin (Figure 4.4). To overcome these losses, different durations of the ultrasonic bath sonication were tested. The testing revealed that the best duration of the ultrasonic bath sonication after the first evaporation was 3 h, and after the second evaporation, 5 h. Pb recovery rates improved on average by 7 %, 30 %, and 1 % in the case of Pb Spec, Sr Spec, and Dowex® 1X8 resin, respectively.

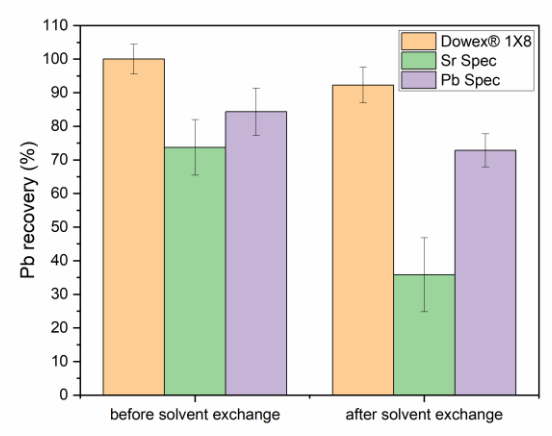

Figure 4.4: Difference in Pb recovery rates before and after solvent exchange. The average value and standard deviation were calculated from 5 replicates for each resin.

Even though the highest recovery rates were achieved with Dowex® 1X8 and Pb Spec resin, the latter turned out to be incompatible with MC ICP-MS, more specifically with the desolvation system (Aridus). Even though the samples after the Pb Spec resin were evaporated and re-dissolved in 2 % HNO_3, some of the ammonium oxalate must have remained in the samples as the Aridus membrane became completely permeable, resulting in none of the sample reaching the detectors. That is why only Dowex® 1X8 and Sr Spec resin were used in the next testing stage.

The next objective was to see if the results after changing different stages of the procedure for Pb separation from the matrix would be similar if, instead of a standard solution of Pb, a matrix CRM (SRM 1573a, tomato leaves) was used. The standard procedure was defined using the following parameters: ultrasonic bath sonication for 3 hours after the first evaporation and 5 hours after the second evaporation, a sample volume of 9 mL, and a final Pb concentration of 50 µg/L. Variations from the standard procedure included adjustments in these parameters: shorter sonication durations (2 hours after the first evaporation and 4 hours after the second), longer sonication durations (4 hours after the first evaporation and 6 hours after the second), sample volume variations (reduced to 4 mL or increased to 12 mL), and final Pb concentration variations (decreased to 30 µg/L or increased to 100 µg/L). The results in Figure 4.5 show that for Dowex® 1X8 resin, the standard procedure was already the optimal one because it had the highest Pb recovery rate. With all the changes in the parameters, the Pb recovery rate dropped, the lowest being with the lower end Pb concentration. In the case of Sr Spec resin, the highest Pb recovery rate was observed at a larger volume of the sample, which was 7.4 % better than that of the standard procedure. However, Dowex® 1X8 had better recovery rates overall.

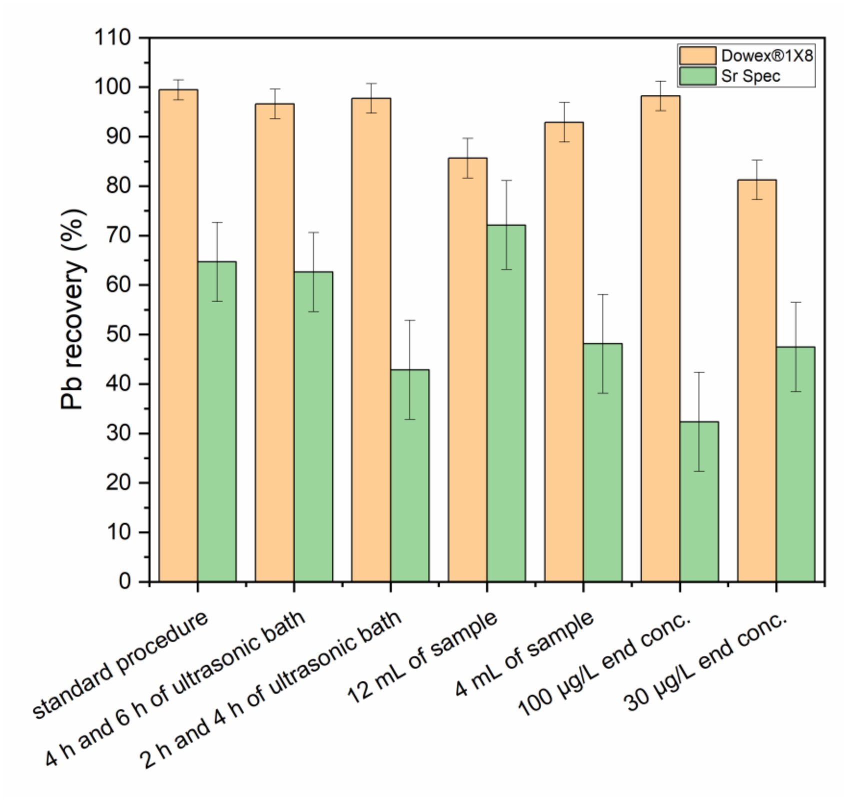

Figure 4.5: Difference in Pb recovery rates before and after solvent exchange. The average value and standard deviation were calculated from 3 replicates for each parameter.

After the optimal procedure parameters were chosen, resins were tested with different matrices to determine if the matrix had any effect on the Pb recovery rate. For this testing, different CRMs were selected, such as PM_{10}-like fine dust (ERM-CZ120), loam soil (ERM-CC141), mussel tissue (SRM 2976), natural water (SRM 1640a), and also real environmental samples, such as PM_{10} filters and soils. There was a difference in recovery rates observed, depending on different matrices (Figure 4.6). In general, the best recovery rates were observed with Dowex® 1X8 resin and with CRM tomato leaves, CRM natural water, and PM_{10} filter samples. The reason for lower Pb recovery rates with Sr spec resin might be that Sr Spec resin displays a lower Pb affinity than other resins (De Muynck et al., 2008). Also, it is very sensitive to organic matter, which interacts with the resin, clogging it and resulting in lower recovery rates, which was observed with Sr separation from plant matrices (H.-C. Liu et al., 2016).

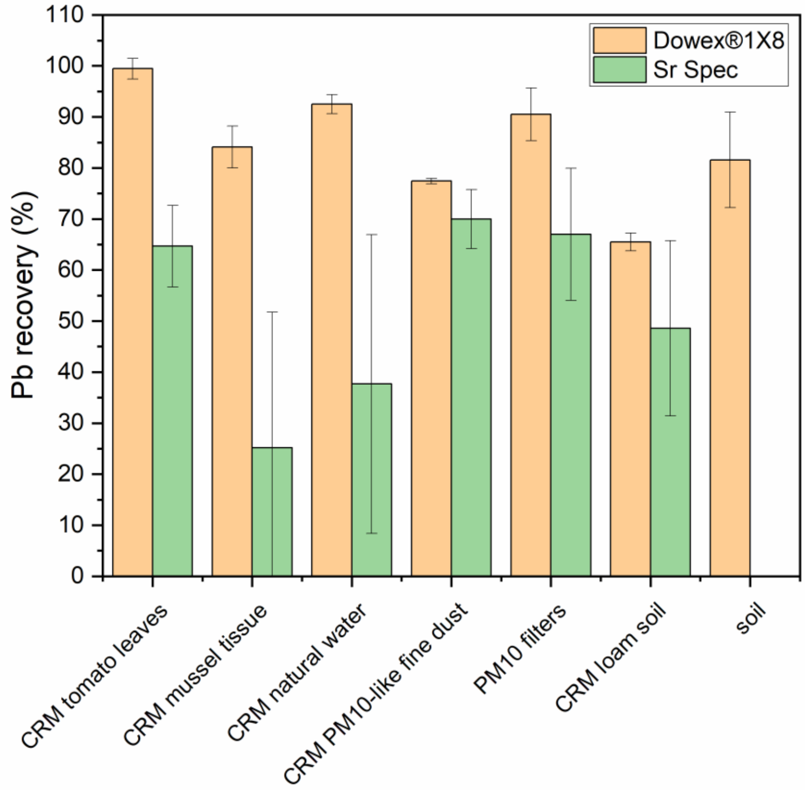

Figure 4.6: Pb recovery rates depending on different matrices for Dowex® 1X8 and Sr Spec resin. The average value and standard deviation were calculated from 5 replicates for each matrix.

Besides the impact of different parameters and resins on Pb recovery rates, their impact on Pb isotope composition was tested (Figure 4.7). Comparison of different pairs of Pb isotopes revealed that the best repeatability was achieved with Dowex® 1X8 for all matrices. The results showed that Pb isotope composition after separation with Dowex® 1X8 or Sr Spec resin in CRMs of tomato leaves (SRM 1573a), natural water (SRM 1640a), and PM_{10}-like fine dust (ERM-CZ120) was statistically the same, while Pb isotope composition in CRMs of loam soil (ERM-CC141) and mussel tissue (SRM 2976) was statistically different.

The $^{208}Pb/^{204}Pb$ value determined in CRM loam soil (ERM-CC141) after column separation on Dowex® 1X8 resin was 38.256 ± 0.039, the $^{207}Pb/^{204}Pb$ value was 15.636 ± 0.005, the $^{206}Pb/^{204}Pb$ value was 18.223 ± 0.033, the $^{208}Pb/^{206}Pb$ value was 2.099 ± 0.002, and the $^{206}Pb/^{207}Pb$ value was 1.165 ± 0.002.

The $^{208}Pb/^{204}Pb$ value determined in CRM PM_{10}-like fine dust (ERM-CZ120) after column separation on Dowex® 1X8 resin was 37.973 ± 0.081, the $^{207}Pb/^{204}Pb$ value was 15.611 ± 0.005, the $^{206}Pb/^{204}Pb$ value was 17.984 ± 0.081, the $^{208}Pb/^{206}Pb$ value was 2.111 ± 0.005, and the $^{206}Pb/^{207}Pb$ value was 1.152 ± 0.005.

The $^{208}Pb/^{204}Pb$ value determined in CRM natural water (SRM 1640a) after column separation on Dowex® 1X8 resin was 38.054 ± 0.020, the $^{207}Pb/^{204}Pb$ value was 15.593 ± 0.004, the $^{206}Pb/^{204}Pb$ value was 18.027 ± 0.011, the $^{208}Pb/^{206}Pb$ value was 2.111 ± 0.001, and the $^{206}Pb/^{207}Pb$ value was 1.156 ± 0.001.

The $^{208}Pb/^{204}Pb$ value determined in CRM tomato leaves (SRM 1573a) after column separation on Dowex® 1X8 resin was 38.893 ± 0.065, the $^{207}Pb/^{204}Pb$ value was 15.744 ±

0.022, the $^{206}Pb/^{204}Pb$ value was 19.080 ± 0.035, the $^{208}Pb/^{206}Pb$ value was 2.038 ± 0.005, and the $^{206}Pb/^{207}Pb$ value was 1.212 ± 0.003.

The $^{208}Pb/^{204}Pb$ value determined in CRM mussel tissue (SRM 2976) after column separation on Dowex® 1X8 resin was 38.002 ± 0.111, the $^{207}Pb/^{204}Pb$ value was 15.627 ± 0.018, the $^{206}Pb/^{204}Pb$ value was 17.987 ± 0.057, the $^{208}Pb/^{206}Pb$ value was 2.113 ± 0.001, and the $^{206}Pb/^{207}Pb$ value was 1.151 ± 0.002.

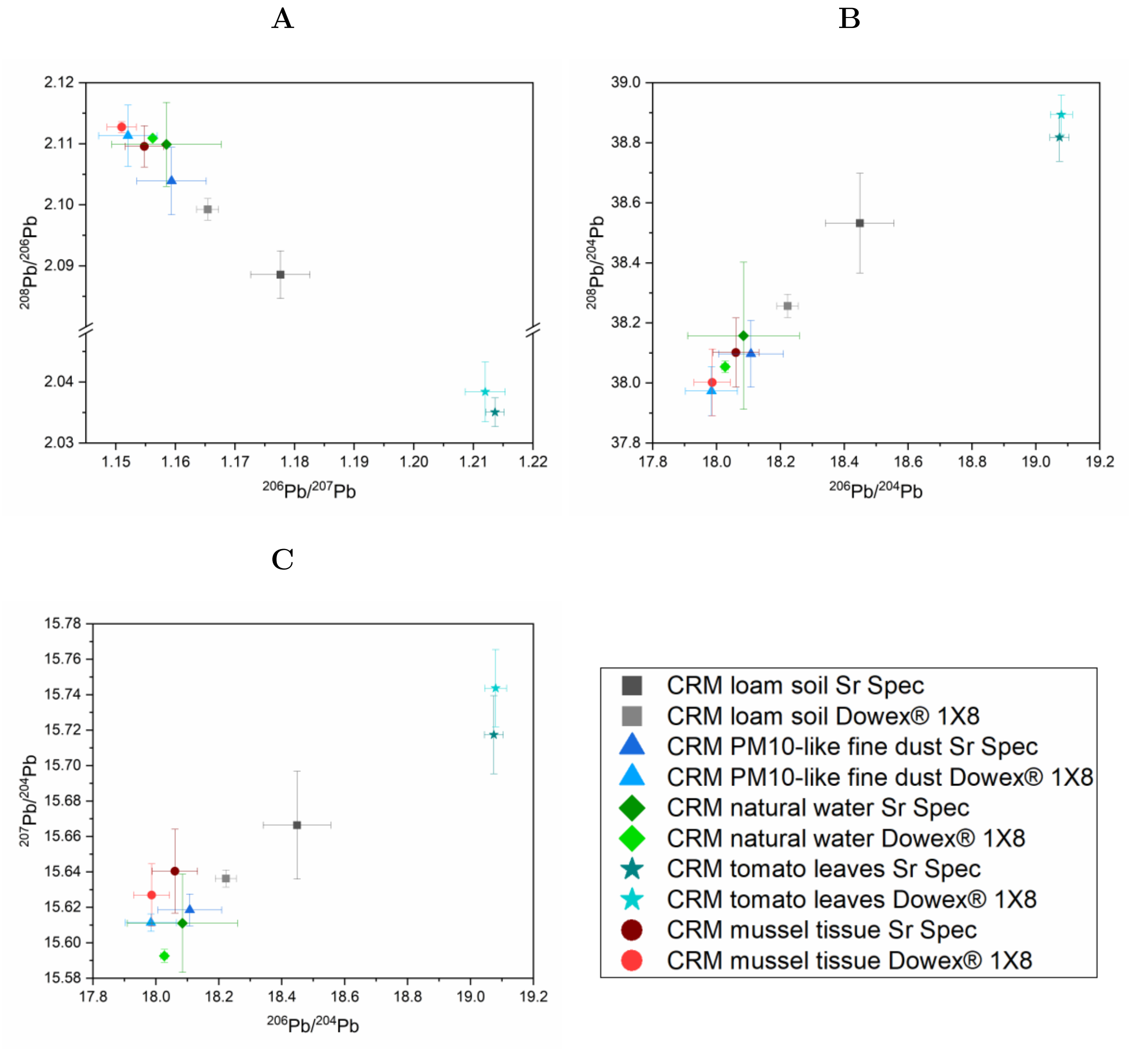

Figure 4.7: Pb isotope compositions of samples after Pb separation on Dowex® 1X8, and Sr Spec resin on a biplot of A) $^{208}Pb/^{206}Pb$ with $^{206}Pb/^{207}Pb$, B) $^{208}Pb/^{204}Pb$ with $^{206}Pb/^{204}Pb$, and C) $^{207}Pb/^{204}Pb$ with $^{206}Pb/^{204}Pb$. The average value and standard deviation were calculated from 5 replicates for each matrix.

The results of Pb isotope composition determined in different CRMs after column separation on Dowex® 1X8 resin were, in general, comparable to Pb isotope values obtained from the literature and GeoRem database (Jochum et al., 2005). The latter are gathered in Table 4.6. However, some differences were observed, which may have occurred due to the use of different instruments (in this dissertation, MC ICP-MS was used, while Honda (2021) and Judd & Swami (2010) used ICP-MS), and the possibility of using different mass bias corrections (in this dissertation, a combination of internal and external correction was used, while in GeoRem database that information is not specified).

Table 4.6: Pb isotope composition of different CRMs as reported in the literature.

CRM	$^{208}Pb/^{204}Pb$	$^{207}Pb/^{204}Pb$	$^{206}Pb/^{204}Pb$	$^{208}Pb/^{206}Pb$	$^{206}Pb/^{207}Pb$	Reference
ERM-CZ120	ND	ND	18.37 ± 0.07	2.096 ± 0.006	1.168 ± 0.002	Honda (2021)
SRM 1640a	38.183 ± 0.149	15.592 ± 0.064	18.218 ± 0.067	2.096 ± 0.001	1.169 ± 0.001	Jochum et al. (2005)
SRM 1573a	ND	ND	ND	2.021 ± 0.001	1.221 ± 0.001	Jochum et al. (2005)
	ND	ND	18.984 ± 0.153	2.024 ± 0.007	1.213 ± 0.003	Judd & Swami (2010)
SRM 2976	38.051 ± 0.010	15.612 ± 0.004	18.126 ± 0.004	2.099 ± 0.001	1.161 ± 0.001	Jochum et al. (2005)

ND - not determined

The procedure for Dowex® 1X8 resin was additionally tested with Pb isotope standard NIST SRM 981. The determined $^{208}Pb/^{204}Pb$ value was 36.735 ± 0.031 (certified 36.722), the $^{207}Pb/^{204}Pb$ value was 15.495 ± 0.010 (certified 15.492), the $^{206}Pb/^{204}Pb$ value was 16.942 ± 0.007 (certified 16.937), the $^{208}Pb/^{206}Pb$ value was 2.1683 ± 0.0009 (certified 2.1681), and the $^{206}Pb/^{207}Pb$ value was 1.093330 ± 0.000170 (certified 1.093326). The measured Pb isotope ratio values were in good agreement with the certified values, indicating that no isotope fractionation occurred during the procedure of Pb separation from the matrix.

4.2.2 Pb isotope composition of water and sediment samples from the Meža River and its tributaries

The Pb isotope composition of water and sediments (in two size fractions) from the Meža River and its tributaries was measured. The aim was to identify possible anthropogenic sources of Pb, especially regarding elevated Pb concentrations in the smaller fraction (<0.063 mm) of sediments. In Figure 4.8, the biplots of $^{207}Pb/^{204}Pb$ *vs.* $^{206}Pb/^{204}Pb$, $^{208}Pb/^{204}Pb$ *vs.* $^{206}Pb/^{204}Pb$, and $^{208}Pb/^{206}Pb$ *vs.* $^{206}Pb/^{207}Pb$ in water and sediments from the Meža River and its tributaries are presented.

It can be observed from Figure 4.8 A that the values for the Meža River water samples fall into four groups. In the first group are the samples from the locations Črna 2 (3), Žerjav 1 (4), and Žerjav 2 (5), with $^{207}Pb/^{204}Pb$ and $^{206}Pb/^{204}Pb$ ratios ranging from 15.592 to 15.608, and from 17.910 to 17.951, respectively. The three sampling locations are in the vicinity of a secondary Pb production industry. Similar Pb isotope ratios were also measured in PM_{10} particles from these areas. Pb can be present in river water because of atmospheric Pb being deposited into it, the significance of the input depends on Pb abundance in rain and aerosol solubility (Gaillardet et al., 2003). Additionally, Pb could also enter the river with the effluents from the surrounding industries. In the second group are values from sampling site Mežica (6) with $^{207}Pb/^{204}Pb$ and $^{206}Pb/^{204}Pb$ ratios of 15.640 and 18.167, respectively. Observation of Pb isotope ratios shows that the mixing of different Pb sources occurs. In the third group are values from sampling sites Črna 1 (2) and Podklanc (7) with higher $^{207}Pb/^{204}Pb$ and $^{206}Pb/^{204}Pb$ ratios (from 15.671 to 15.669, and from 18.313 to 18.329, respectively). Similar Pb isotope ratios were also measured in samples of local wulfenite, galenite, and attic dust that was attributed to the dust particles from the area (Miler & Gosar, 2019). In the fourth group, with the values of $^{207}Pb/^{204}Pb$ and $^{206}Pb/^{204}Pb$ ratios in the range 15.677 to 15.682, and 18.372 to 18.377, respectively, are samples collected at sampling sites Topla (1), and the tributaries (Helena rivulet (8), Jazbina rivulet (9), and Junčar rivulet (10)). The Pb isotope ratios coincide with samples of mine waste and sand. The samples from the fourth group (including the first sampling location on the Meža River) have the highest $^{207}Pb/^{204}Pb$ and $^{206}Pb/^{204}Pb$ ratios, while all the other samples that follow down the river have lower ratios. This is to some extent in compliance with findings from Gassama et al. (2021). The same grouping was also observed in biplots of $^{208}Pb/^{204}Pb$ *vs.* $^{206}Pb/^{204}Pb$ and $^{208}Pb/^{206}Pb$ *vs.* $^{206}Pb/^{207}Pb$, which are presented in Figure 4.8 B and C, respectively.

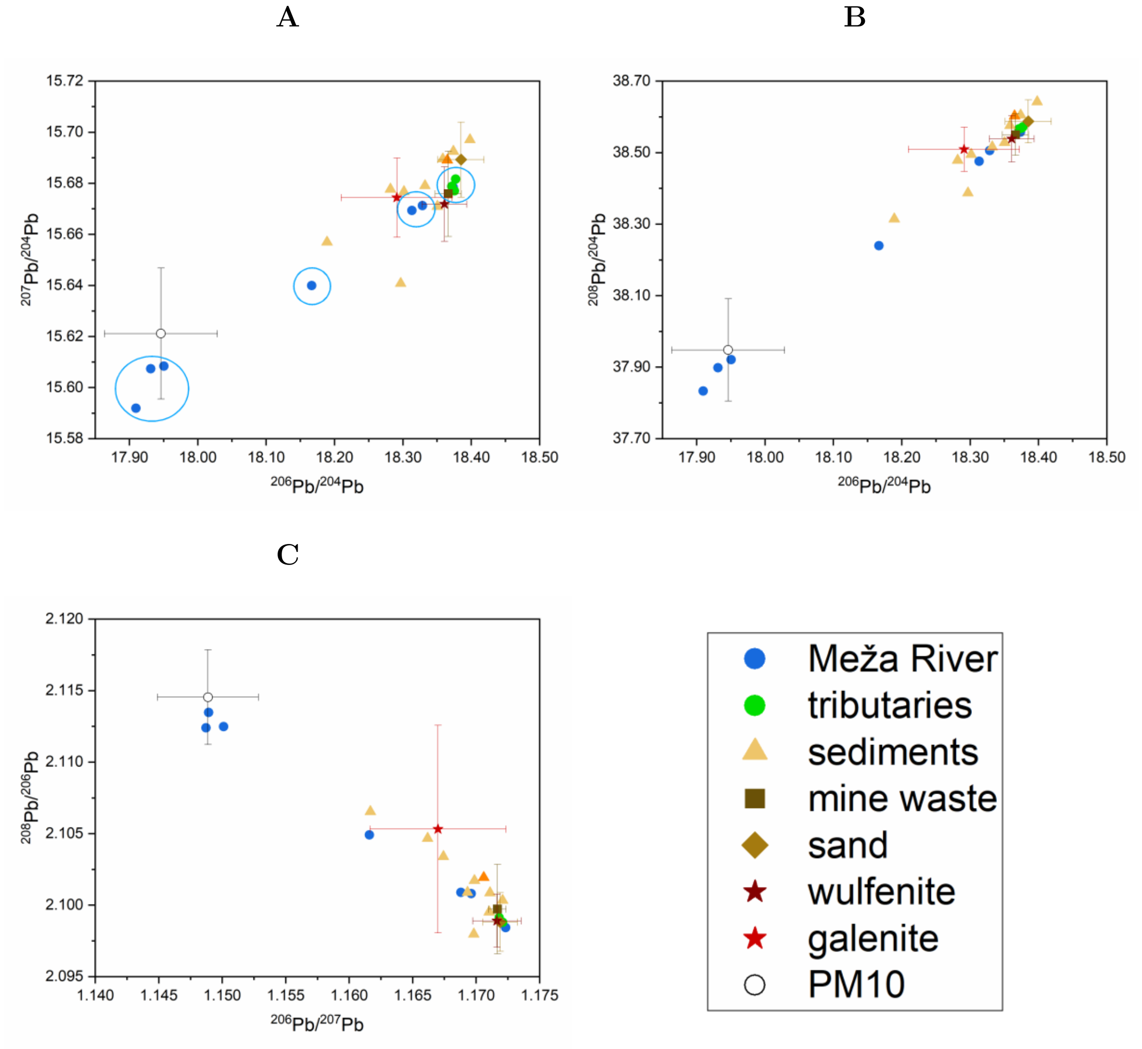

Figure 4.8: Pb isotope compositions of water and sediment samples from the Meža River and its tributaries on a biplot of A) $^{207}Pb/^{204}Pb$ *vs.* $^{206}Pb/^{204}Pb$, B) $^{208}Pb/^{204}Pb$ *vs.* $^{206}Pb/^{204}Pb$, and C) $^{208}Pb/^{206}Pb$ *vs.* $^{206}Pb/^{207}Pb$. The orange triangle marker for sediments represents the sample from Črna 2 with a fraction <0.250 mm.

Different Pb concentrations were observed between sediment fractions <0.063 mm and <0.150 mm. Based on the study of Zhang et al. (2002), an assumption was made that if Pb was from the same source, both fractions would have the same Pb isotope composition. As can be seen from Figure 4.9, the two sediment fractions had different Pb isotope compositions. The dispersion of Pb isotope ratios indicates that there may be other anthropogenic sources present besides local mining activities. The isotope composition of Pb in the <0.063 mm fraction is slightly shifted in the direction of PM_{10} particles and water samples from Žerjav 1 and 2 (lower $^{207}Pb/^{204}Pb$ and $^{206}Pb/^{204}Pb$ ratios), possibly indicating another source of Pb in the area. The sample with the lowest value of $^{206}Pb/^{204}Pb$ ratio is from Žerjav 2 (5a) (fraction <0.063 mm) and is close in value to the water sample taken at the Mežica (6) sampling site. As particles in the <0.063 mm fraction have a greater surface area, elements from the water tend to adsorb on them, in the case of Pb, even 10-times more than on larger fractions (Tansel & Rafiuddin, 2016). Pb isotope composition of sediments in the <0.150 mm fraction coincides with values of local mine waste, sand, and in some parts also with values of local ores, like wulfenite. A similar grouping was also observed in biplots of $^{208}Pb/^{204}Pb$ *vs.* $^{206}Pb/^{204}Pb$, and $^{208}Pb/^{206}Pb$ *vs.* $^{206}Pb/^{207}Pb$, which are presented in Figure 4.9 B and C, respectively.

A

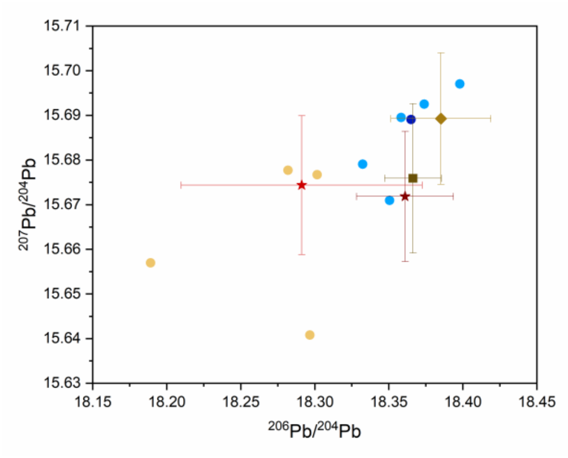

B

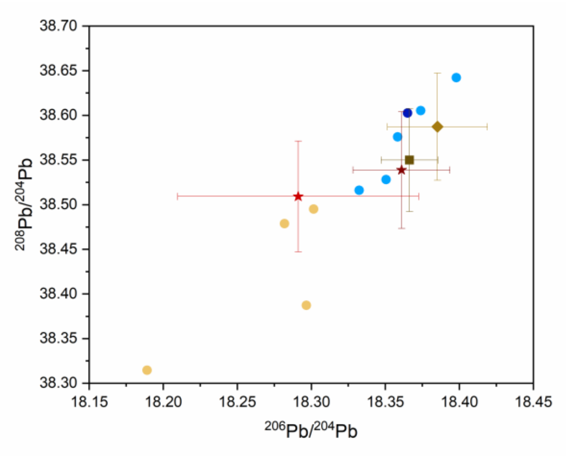

C

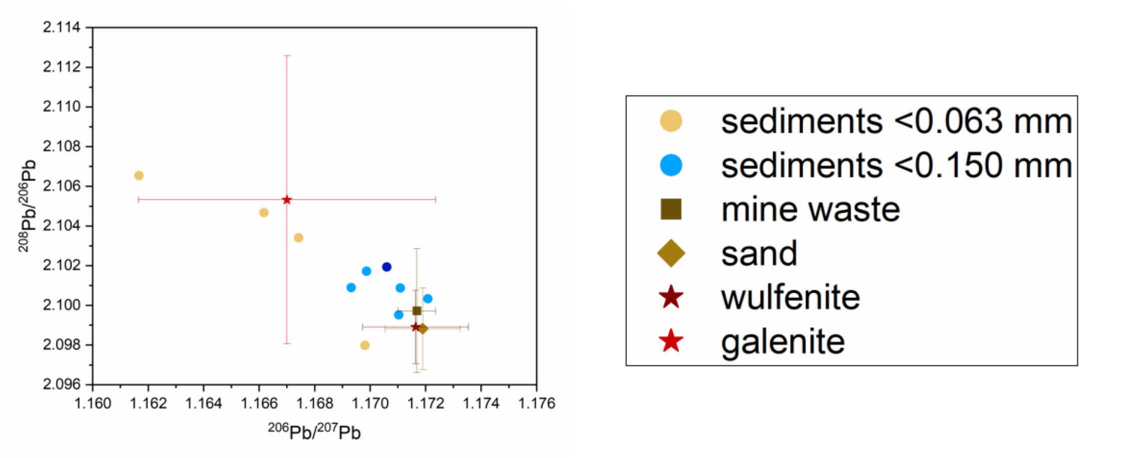

Figure 4.9: Pb isotope compositions of two sediment fractions (<0.063 mm and <0.150 mm) from the Meža River and its tributaries on a biplot of A) $^{207}Pb/^{204}Pb$ *vs.* $^{206}Pb/^{204}Pb$, B) $^{208}Pb/^{204}Pb$ *vs.* $^{206}Pb/^{204}Pb$, and C) $^{208}Pb/^{206}Pb$ *vs.* $^{206}Pb/^{207}Pb$. The dark blue circle marker for sediments <0.150 mm represents the sample from Črna 2, with a fraction <0.250 mm.

4.2.3 Pb isotope composition of PM_{10}, $PM_{2.5}$, soil, sand, road dust, mine waste, ores, and Pb-battery components from the Upper Meža Valley

Previous research in the Upper Meža Valley has predominantly focused on the distribution of PTEs and the environmental burden (Finzgar et al., 2014; Gošar et al., 2015; Gosar & Miler, 2011; Žibret et al., 2018). Some data on Pb isotope ratios have been previously reported (Miler et al., 2022; Miler & Gosar, 2019; Wagner et al., 2022), however, a comprehensive source apportionment of Pb in PM_{10} with the use of Pb isotopes and evaluation of the contributions of individual sources has not yet been performed. Based on the previous discussion, the Pb sources in PM_{10} samples couldn't be determined based on total PTEs concentrations. Therefore, Pb isotope composition was determined in PM_{10}, and different samples from the Upper Meža Valley were identified as potential Pb sources. The Pb isotope ratios and concentrations in PM_{10}, soil, sand, sediments, mine waste, and Pb-battery components are shown in Figure 4.10. The $^{206}Pb/^{207}Pb$ *vs.* [Pb] displays the separation of two different sources of Pb. One comes from the background environment ($^{206}Pb/^{207}Pb$ between 1.162 and 1.183) and the other from the secondary Pb production industry ($^{206}Pb/^{207}Pb$ between 1.120 and 1.153).

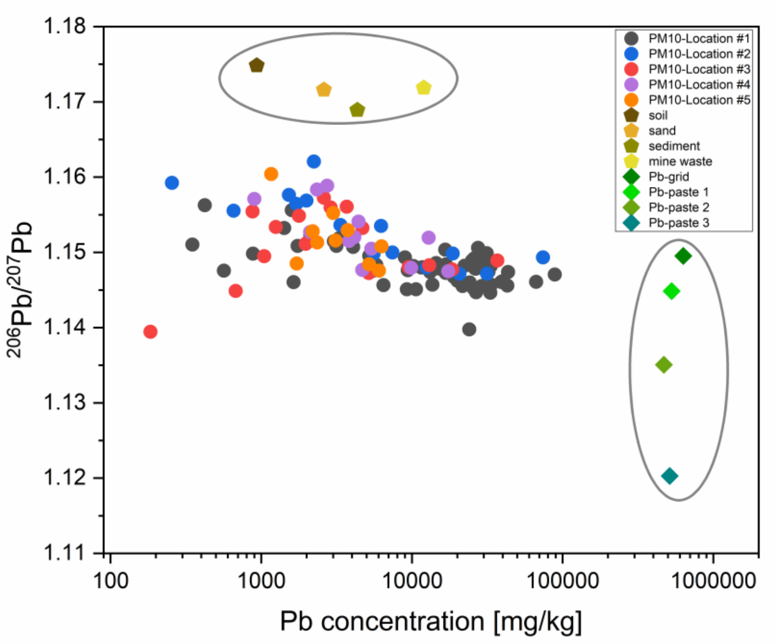

Figure 4.10: $^{206}Pb/^{207}Pb$ isotope ratios and Pb concentrations (log scale) of PM_{10} samples and potential Pb emission sources from the Upper Meža Valley. Locations #1 – #4 of PM_{10} samples were located in Žerjav, while Location #5 was in Črna na Koroškem.

The distribution of Pb isotope ratio values in the PM_{10} particles between the geogenic and anthropogenic sources is even more pronounced in the biplots of $^{208}Pb/^{206}Pb$ *vs.* $^{206}Pb/^{207}Pb$, $^{208}Pb/^{204}Pb$ *vs.* $^{207}Pb/^{204}Pb$, and $^{208}Pb/^{204}Pb$ *vs.* $^{206}Pb/^{204}Pb$, presented in Figure 4.11 A–C. $^{208}Pb/^{206}Pb$ and $^{206}Pb/^{207}Pb$ isotope ratios for leaded gasoline that was used around Europe (more specifically in the United Kingdom, France, Switzerland, and the Czech Republic) were summarized from Ettler et al. (2004), Komárek et al. (2008), Monna et al. (1995), and the references therein.

On the bottom right side of the plot in Figure 4.11 A are local environmental/background samples, such as sediment, soil, sand, mine waste, and ores. The Meža Valley is known for its Pb-Zn ore deposits. The Mežica ore deposit is predominantly composed of primary sulfide minerals, secondary oxide, and sulfide minerals. The deposit is a "Mississippi Valley" type (MVT) Pb-Zn ore deposit that is hosted in the Middle/Upper-Triassic Wetterstein platform carbonates (Gosar & Miler, 2011). Pb isotope ratios in galenite ores were 1.162–1.173, 38.360–38.564, 15.614–15.683, 18.205–18.377, 2.094–2.113, and for wulfenite 1.172–1.173, 38.456–38.574, 15.644–15.679, 18.344–18.374, 2.096–2.099 for $^{206}Pb/^{207}Pb$, $^{208}Pb/^{204}Pb$, $^{207}Pb/^{204}Pb$, $^{206}Pb/^{204}Pb$, $^{208}Pb/^{206}Pb$, respectively (Rogan Šmuc et al., 2025). Pb isotope ratios of galenite ores were in good agreement with the values reported by Miler & Gosar (2019), which were 38.5, 15.7, and 18.4 for $^{208}Pb/^{204}Pb$, $^{207}Pb/^{204}Pb$, and $^{206}Pb/^{204}Pb$, respectively. Mine waste is a mixture of Pb from different ores, and its isotope ratios are similar to those of galenite and wulfenite ores. Pb isotope ratios of mine waste determined in this dissertation were in good agreement with the values reported by Miler et al. (2022), who investigated the environmental impact of mine waste deposits in Slovenia. They analyzed mine waste samples from the Upper Meža Valley, Litija, and Pleše. The reported $^{208}Pb/^{204}Pb$, $^{207}Pb/^{204}Pb$, and $^{206}Pb/^{204}Pb$ ratios in three mine waste samples from the Upper Meža Valley were 38.7, 15.8, and 18.5–18.8, respectively.

Since most of the analyzed soils were of local origin, their Pb isotope ratios were similar to those of ores and mine waste, indicating that Pb smelting was an important source of Pb in soil. Pb isotope ratios of soils were in good agreement with the values reported by Wagner et al. (2022), who investigated the use of selective diffusive gradients in thin films for the simultaneous determination of Sr and Pb concentrations and isotope ratios in soils. The reported $^{206}Pb/^{207}Pb$, $^{208}Pb/^{204}Pb$, $^{207}Pb/^{204}Pb$, $^{206}Pb/^{204}Pb$, and $^{208}Pb/^{206}Pb$ ratios were 1.172, 38.517, 15.663, 18.360, and 2.098, respectively. However, in this dissertation, some samples were collected from sites where soil was exchanged (playgrounds, surroundings of kindergartens and schools). Their non-local origin was evident mostly from their lower Pb concentrations ((30–70) mg/kg) as well as from their slightly different values of Pb isotope ratios, which were 1.182, 38.792, 15.708, 18.568, 2.089 for $^{206}Pb/^{207}Pb$, $^{208}Pb/^{204}Pb$, $^{207}Pb/^{204}Pb$, $^{206}Pb/^{204}Pb$, $^{208}Pb/^{206}Pb$, respectively. These results are in agreement with findings by Ettler et al. (2004), who investigated soils that were heavily contaminated by Pb smelting. Samples were collected near a Pb smelter in Příbram (Czech Republic), where smelting of local ores was replaced by smelting of old Pb-batteries. Based on the Pb isotope composition and endmember mixing model, all of the Pb in topsoil was attributed to Pb from battery processing, and Pb from ore processing prevailed at a depth of 10 cm. The authors concluded that Pb smelting had the biggest impact on the contamination of soils in the area.

On the upper left side of the plot in Figure 4.11 A, the Pb isotope compositions of Pb-battery components are plotted, with $^{208}Pb/^{206}Pb$ and $^{206}Pb/^{207}Pb$ ratios ranging from 2.107 to 2.142, and from 1.120 to 1.153, respectively. Their Pb isotope ratio variability was higher than that of local environmental samples, as recycled Pb can come from different locations/parts of the world, which can have different Pb isotope compositions (L. Wang et al., 2021). The road dust had a Pb isotope composition similar to that of soil and mine waste, while the PM_{10} samples slightly differed from the local (background) samples and had the $^{208}Pb/^{206}Pb$ and $^{206}Pb/^{207}Pb$ isotope ratios ranging between 2.103 and 2.124, and from 1.139 to 1.162, respectively. They were situated between the two end members. A similar grouping was also observed in biplots of $^{208}Pb/^{204}Pb$ *vs.* $^{207}Pb/^{204}Pb$ and $^{208}Pb/^{204}Pb$ *vs.* $^{206}Pb/^{204}Pb$.

On the upper left side of the plot in Figure 4.11 A, the Pb isotope composition of leaded gasoline used in Europe is also plotted. Although leaded gasoline was a major source of Pb pollution in the past, since its prohibition, its contribution has diminished over time (Komárek et al., 2008; Walraven et al., 2014). Some studies have shown that even modern gasoline can contribute to Pb pollution, however, these studies were performed at remote or pristine locations, where every small contribution makes an impact (Astray et al., 2024; Chrastný et al., 2018). On the other hand, in areas with legacy Pb contamination due to mining and smelting and the presence of secondary Pb production industries, such small contributions are negligible and don't impact the overall Pb isotope compositions. In a location such as the Upper Meža Valley, where legacy Pb pollution still prevails and the secondary Pb production industry is also present, and where there is not a lot of traffic, unleaded gasoline is not expected to impact the Pb isotope composition of PM_{10} particles. There was also no significant difference observed in the Pb isotope composition of PM_{10} collected during the presence of desert dust, indicating that transboundary transport doesn't have a big impact on the Pb isotope composition of PM_{10} collected in the Upper Meža Valley.

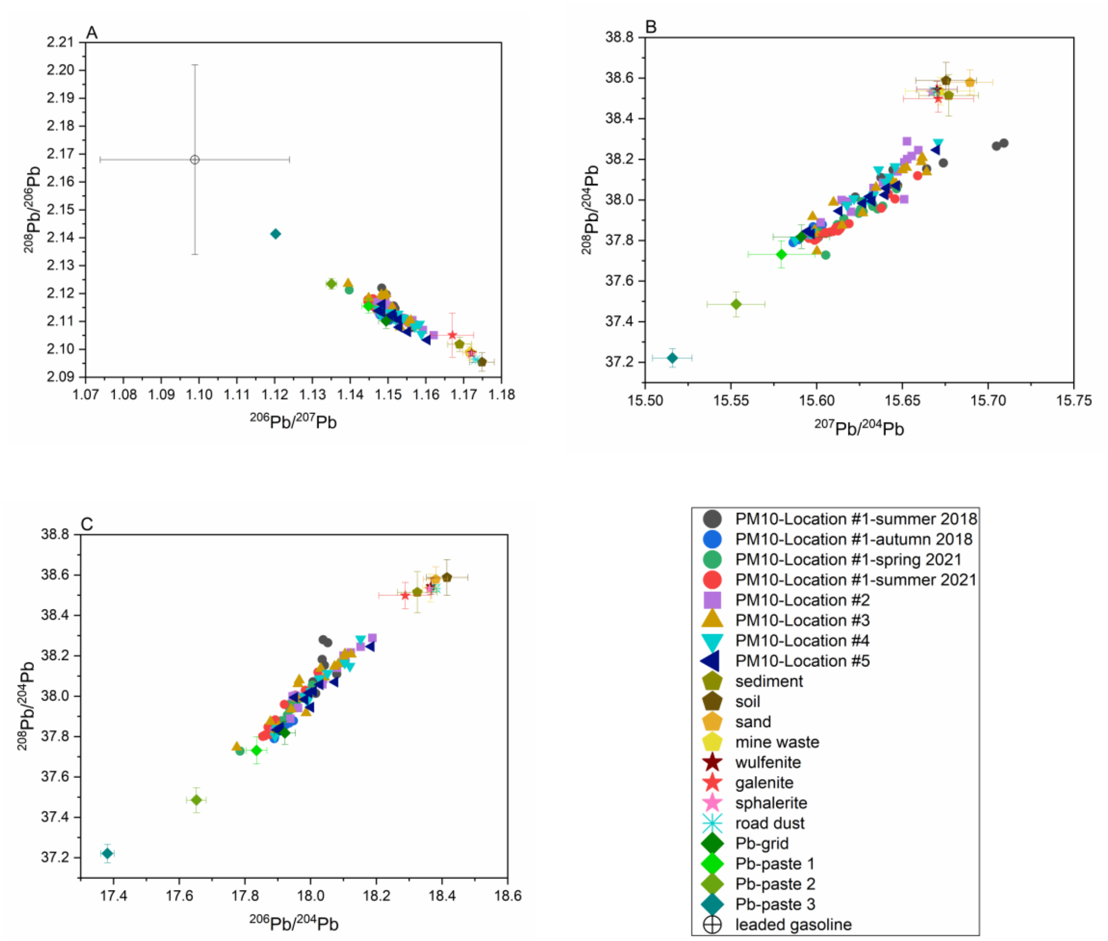

Figure 4.11: Biplots of A) $^{208}Pb/^{206}Pb$ *vs.* $^{206}Pb/^{207}Pb$, B) $^{208}Pb/^{204}Pb$ *vs.* $^{207}Pb/^{204}Pb$, and C) $^{208}Pb/^{204}Pb$ *vs.* $^{206}Pb/^{204}Pb$ for PM_{10} samples and potential Pb emission sources from the Upper Meža Valley. Locations #1 – #4 of PM_{10} samples were located in Žerjav, while Location #5 was in Črna na Koroškem.

The PM_{10} particles were sampled at 5 locations, of which 4 were in the same settlement (Žerjav) and one was from Črna na Koroškem. Both settlements were affected by mining activities in the valley as well as by the exhausts from industry related to the secondary

Pb production. Therefore, the concentration levels of PTEs and the Pb isotope composition in PM_{10} were similar between them. Also, between samples from Žerjav (Location #1, #2, #3, and #4), no difference was observed between those closer to the mine waste deposit and those near the secondary Pb production factory. Present observations do not agree with the findings from the study about particles in snow from the same region, where the authors found that the influence of the source decreases with distance (Miler & Gosar, 2013). The discrepancy between the findings may be attributed first to the size of the studied particles, as smaller particles may travel longer distances than the bigger ones, and secondly to the season of sampling, as precipitation can wash the atmosphere and contribute to quicker settlement of the particles. Contrary to spatial variability, some temporal differences were observed at Location #1 (PM_{10} monitoring station), although small, they were significant ($p < 0.05$) (Figure 4.12).

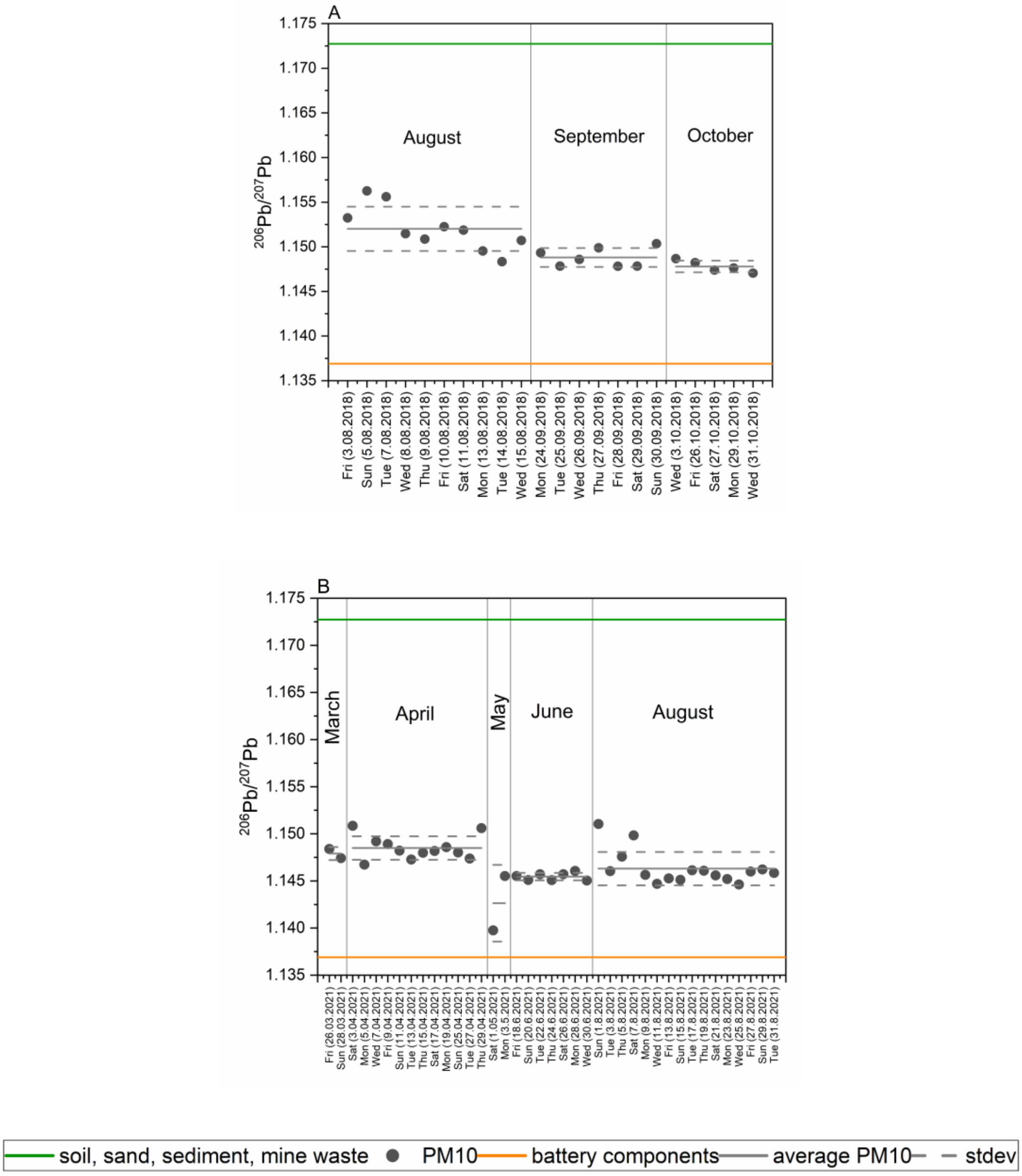

Figure 4.12: Temporal variability of $^{206}Pb/^{207}Pb$ isotope ratio in PM_{10} samples at Location #1 (in Žerjav) in A) 2018 and B) 2021.

Figure 4.12 shows slight monthly variability in both years. In 2018, the Pb isotope ratio values were closer to the background values compared to 2021. In September and October 2018, Pb isotope ratio values were closer to anthropogenic values compared to August, likely due to the summer holidays in August and the resulting decrease in secondary Pb production. At the beginning of 2021 (March and April), the COVID-19 restrictions may have caused the PM_{10} Pb isotope composition to lean towards background values compared to June and the second half of August, when the Pb isotope ratio values were lower and closer to anthropogenic values. Notably, in June, despite a significant influx of desert dust increasing particle concentration, the isotope composition of PM_{10} samples remained unchanged.

4.2.3.1 Comparison of PM_{10} and $PM_{2.5}$

At Location #4, both PM_{10} and $PM_{2.5}$ samples were collected independently to assess differences in total elemental concentrations and Pb isotope composition. Pb, Zn, Cd, and As concentrations determined in PM_{10} and $PM_{2.5}$ samples from the Upper Meža Valley are presented in Figure 4.13, while total concentrations of other elements (Li, Al, V, Cr, Mn, Fe, Co, Ni, Cu, Se, Rb, Sr, Mo, Ag, Sb, Ba, Tl, and U) are shown in Table A.5 (Appendix).

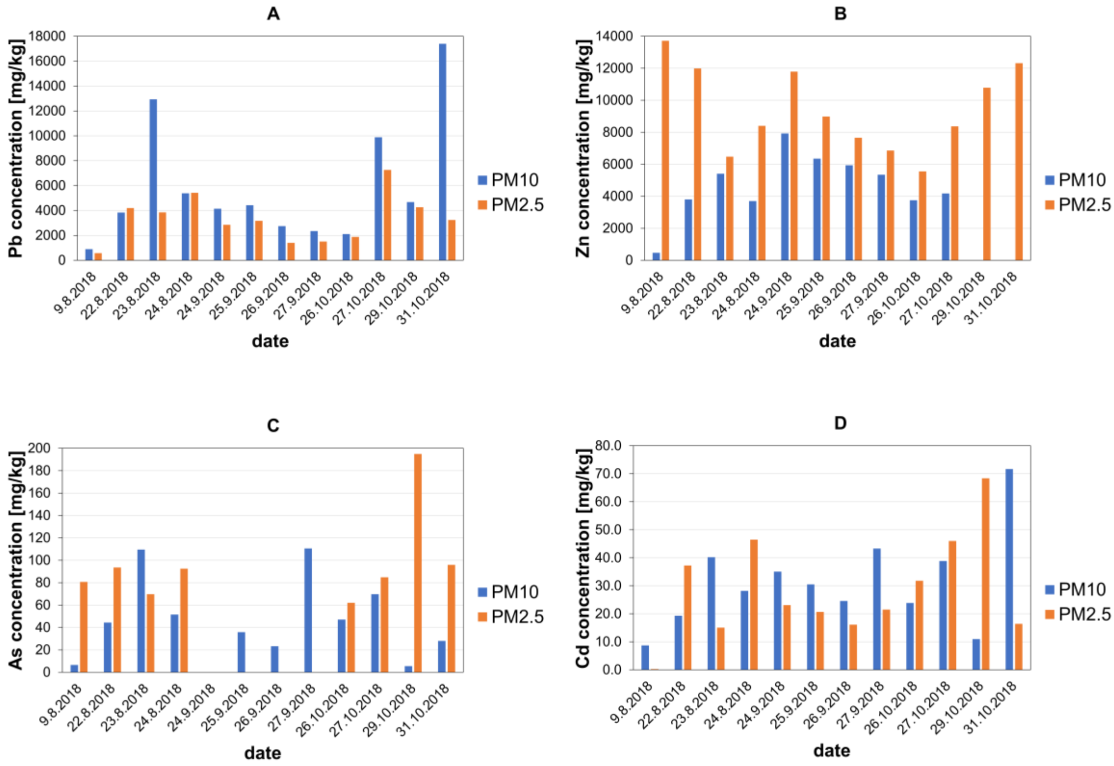

Figure 4.13: Total element concentration of A) Pb, B) Zn, C) As, and D) Cd in PM_{10} and $PM_{2.5}$ from Location #4 (in Žerjav) in the Upper Meža Valley.

While daily fluctuations were observed in the concentrations of Pb, As, and Cd, statistical analysis revealed no significant differences ($p > 0.05$) in the average concentrations of these elements between the two particulate size fractions. This suggests that the sources and atmospheric behaviour of these elements may be similar across coarse and fine particulate matter, which is similar to findings in smaller urban environments (Chatoutsidou & Lazaridis, 2022) and contrary to findings in megacities, where more of different industries can be present (Hao et al., 2018; K. Zhang et al., 2018). In contrast, Zn exhibited a significantly higher average concentration in $PM_{2.5}$ than in PM_{10} ($p < 0.05$), indicating a possible enrichment in finer particles. This is likely due to Zn's strong association with combustion-related processes, particularly from vehicular emissions, which predominantly contribute to the fine particle fraction (Pant et al., 2017; Pant & Harrison, 2012). When comparing average enrichment factors for Pb, Zn, As, and Cd in two particulate fractions (Table 4.5), only the average EF for Zn showed significantly higher enrichment in the $PM_{2.5}$ fraction ($p < 0.05$).

When comparing Pb isotope ratios between PM_{10} and $PM_{2.5}$, no significant differences were observed ($p > 0.05$), suggesting a common source or well-mixed origin of Pb in both fractions (Figure 4.14). This aligns with studies that have shown isotopic homogeneity in Pb across different particle sizes in urban atmospheres, particularly where industrial or legacy sources dominate (Hu et al., 2014; Souto-Oliveira et al., 2018). Therefore, the similarity in isotope composition reinforces the hypothesis that PM_{10} and $PM_{2.5}$ at this site are influenced by similar Pb sources.

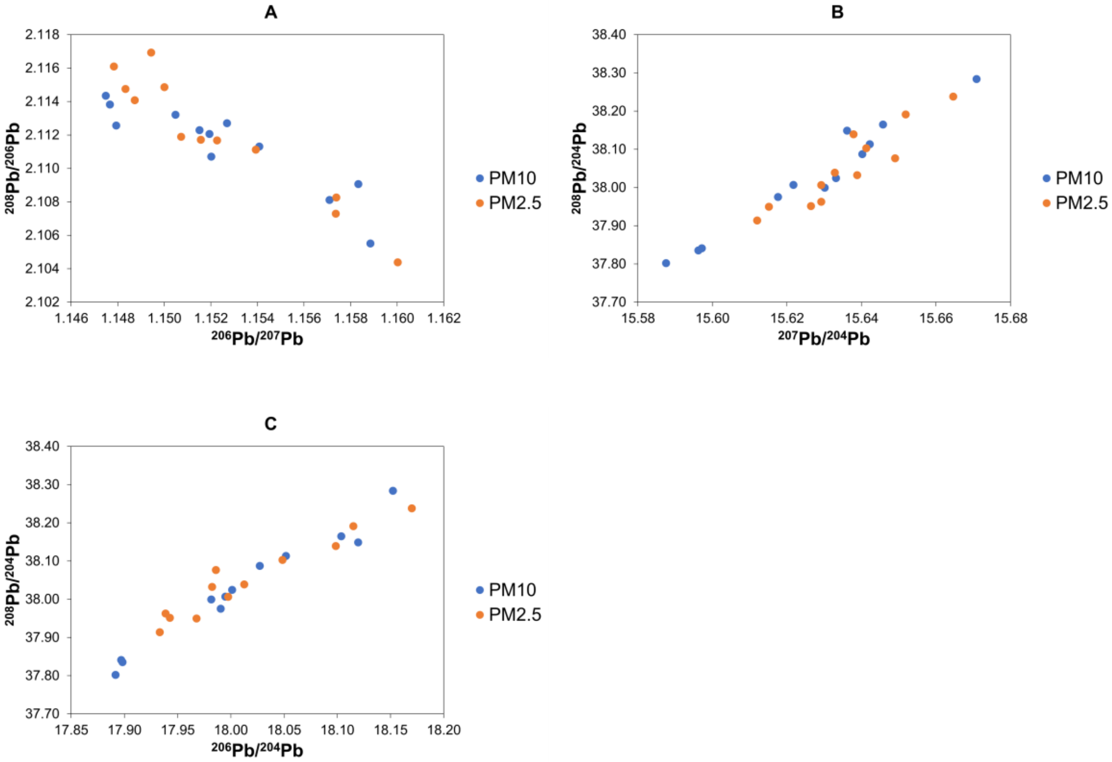

Figure 4.14: Biplots of A) $^{208}Pb/^{206}Pb$ *vs.* $^{206}Pb/^{207}Pb$, B) $^{208}Pb/^{204}Pb$ *vs.* $^{207}Pb/^{204}Pb$, and C) $^{208}Pb/^{204}Pb$ *vs.* $^{206}Pb/^{204}Pb$ for PM_{10} and $PM_{2.5}$ from Location #4 (in Žerjav) in the Upper Meža Valley.

4.2.4 Estimation of the Pb source's contribution by the mixing model

From the data presented so far, an exclusive origin of Pb only from the local background can be ruled out. To estimate the contributions of different sources of Pb in the PM_{10} samples, a binary endmember mixing model was adopted, and Eq. (3.3) was used for calculations (Monna et al., 1997). In this dissertation, two possible sources were identified, local environmental/background samples (sediment, soil, sand, mine waste) and an additional anthropogenic source (secondary Pb production industry). As it was not possible to determine individual Pb contributions to PM_{10} based on Pb isotope composition from sediment, soil, sand, and mine waste, as they have very similar isotope composition, these samples were grouped as local environmental/background samples. On the other hand, the anthropogenic source had a different Pb isotope composition. With the use of the $^{206}Pb/^{207}Pb$ ratio, the percent contribution to Pb in PM_{10} from anthropogenic source was calculated (Figure 4.15) and was around 69.3 % at Location #1, 55.8 % at Location #2, 61.5 % at Location #3, 56.4 % at Location #4, and 58.0 % at Location #5. The results showed that both natural and anthropogenic sources contribute to Pb in PM_{10}, however, the anthropogenic one prevailed. Similar results were obtained for other Pb isotope ratios. These results confirmed the assumption from the elemental composition of the PM_{10} at Location #1 to have a greater influence from the secondary Pb production exhaust, as it is situated nearby.

The anthropogenic contribution of Pb to PM at Location #4 was similar between PM_{10} and $PM_{2.5}$, the second being slightly but not significantly higher, at 57.0 %.

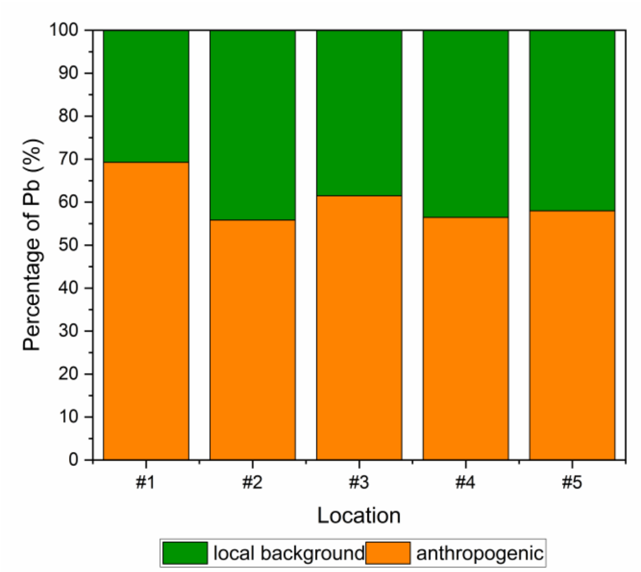

Figure 4.15: The percent contribution to Pb in PM_{10} from two sources, the anthropogenic source and local background. Locations #1 – #4 were located in Žerjav, while Location #5 was in Črna na Koroškem.

The data presented in this dissertation indicated a substantial contribution of anthropogenic sources to Pb in PM_{10}, with anthropogenic Pb accounting for between 55.8 % and 69.3 % across various locations. This highlights secondary Pb production, particularly from current activities such as Pb-recycling and battery production, as a major source of atmospheric Pb today. A study on mineralogical and elemental composition of snow deposits from the same region found that although approximately 85 % of PTE-bearing particles originated from present-day Pb-recycling, these particles represented only about 8.5 % of all deposited particles (Miler & Gosar, 2013; Žibret et al., 2018). This suggests that, nearly two decades ago, secondary Pb production had a relatively minor influence on overall environmental contamination, with legacy sources, such as historically deposited mine waste, still playing a significant role in contributing Pb-enriched particles to the atmosphere. The differences observed between this dissertation and the study by Miler & Gosar (2013) can be attributed to several interrelated factors. First, the sampling periods differed significantly: Miler and Gosar collected samples in February 2009, while samples for this dissertation were collected in August, September, and October of 2018 and March, April, May, June, and August of 2021. Over the intervening decade, activities related to battery recycling and production, and the availability of recycled materials, are likely to have increased. Methodological differences also play a role; Miler and Gosar employed SEM-EDS, whereas this dissertation used Pb isotope composition and an end-member mixing model, which may capture different aspects of Pb pollution. Furthermore, Pb sources were defined and categorised differently. Miler and Gosar distinguished between present-day Pb-recycling and historical sources, while in this dissertation, soil, sand, and mine waste were grouped into a broader local environmental or background category. These differences in analytical approach, time of sampling, and source classification highlight the complexity of tracing Pb pollution and underscore the need to address both historical and contemporary sources of environmental Pb contamination. However, Pb isotopes were proven as a reliable tool for source apportionment of PM_{10}, especially in areas with mining and smelting industries. For example, they were used by Félix et al. (2015), who investigated sources of atmospheric aerosol in the mining site in Hayden (Arizona, USA), which has a concentrator, smelter, and tailing facilities, and there are also various mines in the vicinity. The study was performed in two towns with a small population that are located in this area. The Pb isotope ratios revealed two different sources, the first originating from condensation of high-temperature vapours emitted from the smelter, and the second related to the background Pb present in the area.

On the other hand, Pb isotopes are mainly used in larger urban environments, where many different sources may contribute Pb to PM_{10}. In bigger cities, with higher population, a mix of multiple anthropogenic Pb sources can be expected, including mining, smelting, Pb-battery production, coal combustion, vehicle exhausts due to larger population and traffic, etc. F. Li et al. (2018) investigated the origin of Pb in urban dust samples from Hangzhou City (China). The Pb isotope ratios indicated that the main source of Pb in residential dust was coal combustion, while for road dust, it was vehicle exhaust emissions. Hu et al. (2014) determined coal emissions and smelting as an important source of Pb in street dust and atmospheric particles collected in Nanjing, a mega city in China. Aerosols from São Paulo city (Brazil) have a mix of different sources, mainly vehicular exhaust (including fuel combustion, tyre and brake wear), traffic dust resuspension, and industrial emissions from cement and fertilizer plants (Gioia et al., 2017). Based on Pb isotope composition, Chifflet et al. (2018) attributed Pb in PM_{10} from Haiphong, the third largest city in Vietnam, to soil dust, vehicle exhausts (including oil combustion), and Pb-Zn smelting, while Xu et al. (2012) identified five different sources of Pb in $PM_{2.5}$ from Xi'an (China), including coal combustion, vehicular emissions, industrial emissions, biomass burning and fugitive dust. Pb isotope composition of PM_{10}, situated between two end members, was observed by Dong et al. (2017), who investigated PM_{10} sampled in 2010 at two locations in central London (UK), with different traffic densities. The results showed no significant effect of traffic density on Pb isotope composition, suggesting similar sources at both locations. Additionally, the Pb isotope composition of PM_{10} fell between leaded gasoline (used in the UK before phasing out) and road dust. Even though two locations with different traffic densities were investigated, they were still both located in London, which is incomparably larger than any settlement in the Upper Meža Valley. This area has a specific situation, not comparable with large cities, as there are small settlements with a history of Pb ore mining and smelting, a secondary Pb production industry, and low traffic density. The environment is so loaded with Pb that smaller contributions from, e.g., coal combustion, traffic, and unleaded gasoline are not likely to have an impact on the Pb isotope composition of environmental samples. With the use of Pb isotopes in this dissertation, two predominant sources of Pb in PM_{10} were identified: local environmental/background samples (sediment, soil, sand, mine waste) and the secondary

Pb production industry, which were also suggested by previous research (Miler & Gosar, 2012, 2013, 2019).

4.3 NPs Determination by spICP-MS

To determine if any airborne metal-containing NPs were present in the Upper Meža Valley, a procedure for extracting NPs from PM_{10} filters was refined, and spICP-MS was used for their detection. As part of the extraction procedure optimization, the time of sonication, different extraction solvents, the impact of four extraction solvents on the transport efficiency, ICP-MS response, and linearity of ionic standard calibration curves were tested. The optimal procedure was then used on PM_{10} samples from the Upper Meža Valley.

4.3.1 Extraction procedure optimization

The first objective was to further improve the extraction of metal-containing NPs from PM_{10} samples based on the ultrasound-assisted procedure adapted from the existing literature (Bland et al., 2023; Pietrogrande et al., 2021; Torregrosa et al., 2023) for their subsequent analysis by spICP-MS. To the best of our knowledge, no certified reference materials for metal-containing NPs in a PM matrix or pristine (certified reference) standards for the target NPs exist for spiking the corresponding PM matrix. Therefore, the optimization of the extraction procedure was performed using a certified reference material of PM_{10}-like fine dust (ERM-CZ120), which closely mimics the composition of real PM_{10} samples and has a consistent and homogenous composition of Zn and Pb. However, this material is only certified for the total concentration of the target elements and lacks information on the potential presence or absence of these elements in nanoparticulate form. According to the certification report, the particle size distribution of ERM-CZ120 material, as determined by dynamic light scattering (DLS) in a dispersion, indicates the aerodynamic diameter of the particles, consisting of 10 vol. % of particles below 1.75 µm, 16 vol. % below 2.49 µm, 50 vol. % below 7.59 µm, 84 vol. % below 15.01 µm, 90 vol. % below 20 µm (Piaścik et al., 2010). However, the chemical composition of these particles and the percentage of particles smaller than 100 nm are unknown. The presence of NPs containing Zn and Pb was therefore assessed by spICP-MS analysis of the ERM-CZ120 material suspended in MilliQ water. For this assessment, dilution factors of 500x were applied for Zn- and Pb-containing NPs. The particle number and mass concentrations, particle diameter, and mass fraction of Zn- and Pb-containing NPs determined by spICP-MS in the ERM-CZ120 water suspension are given in Table 4.7. The mass concentration of Zn and Pb present in the ERM-CZ120 as NPs was found to be 65.3 mg of Zn-containing NPs per kg of the sample (representing 5.26 % of the total Zn content in ERM-CZ120) and 12.8 mg of Pb-containing NPs per kg of the sample (corresponding to 11.3 % of the total Pb content in ERM-CZ120). The mean particle sizes, calculated from particle mass based on the assumption of spherical mono-elemental particles, were determined to be 87 nm for Zn- and 32 nm for Pb-containing NPs. The particle number-based size distribution obtained by spICP-MS analysis of the ERM-CZ120 water suspension (Figure 4.16) shows that the sizes of Zn-containing NPs range from 55 nm to over 200 nm, while those of Pb-containing NPs range from 18 nm to more than 100 nm. However, different geometry and chemical composition would result in different particle diameters.

Table 4.7: Particle number and mass concentration, mean particle size, and mass fraction of NPs determined for Zn- and Pb-containing NPs in ERM-CZ120 suspended in different extraction solvents and analyzed by spICP-MS. The results represent the average values with a standard deviation of six replicates.

Extraction solvent	spICP-MS parameters	Zn-NPs	Pb-NPs
MilliQ water	Particle number conc. (particles/kg of dust)	(1.46 ± 0.24) E+13	(2.79 ± 0.57) E+13
	Particle mass conc. (mg/kg of dust)	65.3 ± 2.1	12.8 ± 2.3
	Mean particle size (nm)	87 ± 4	32 ± 3
	Mass fraction of NPs (%)	5.26 ± 0.17	11.3 ± 2.1
1 mM sodium pyrophosphate	Particle number conc. (particles/kg of dust)	(1.54 ± 0.21) E+13	(3.81 ± 0.48) E+13
	Particle mass conc. (mg/kg of dust)	90.1 ± 5.0	15.0 ± 4.0
	Mean particle size (nm)	98 ± 2	32 ± 1
	Mass fraction of NPs (%)	7.27 ± 0.41	13.3 ± 3.5
0.5 % citric acid	Particle number conc. (particles/kg of dust)	(6.54 ± 0.63) E+12	(9.16 ± 0.33) E+12
	Particle mass conc. (mg/kg of dust)	30.9 ± 5.8	3.83 ± 0.68
	Mean particle size (nm)	90 ± 5	34 ± 1
	Mass fraction of NPs (%)	2.49 ± 0.47	3.39 ± 0.60
0.2 % aqueous ammonia solution	Particle number conc. (particles/kg of dust)	(1.73 ± 0.13) E+13	(4.82 ± 0.42) E+13
	Particle mass conc. (mg/kg of dust)	93.6 ± 30.7	15.9 ± 4.0
	Mean particle size (nm)	96 ± 2	31 ± 1
	Mass fraction of NPs (%)	7.54 ± 2.48	14.1 ± 3.5

A

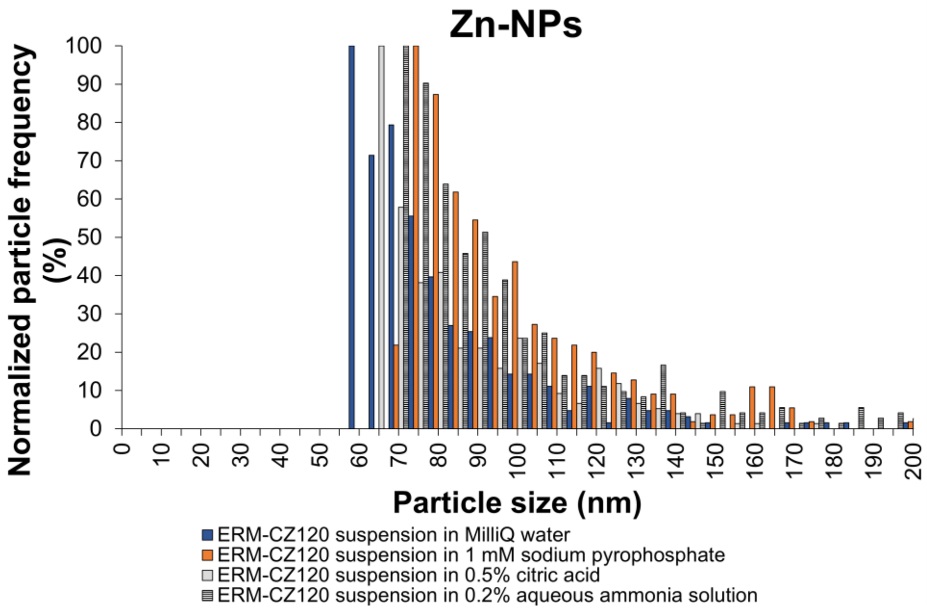

B

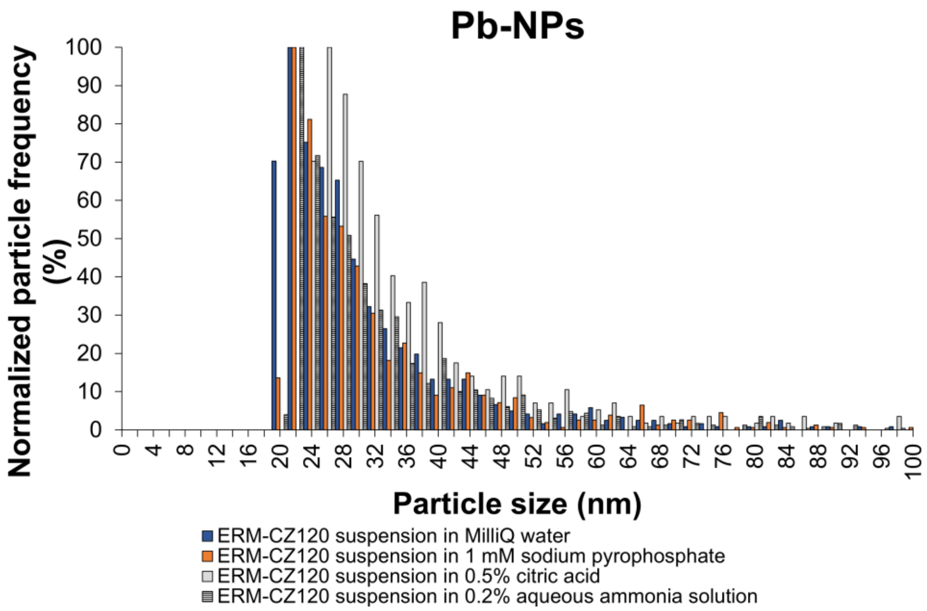

Figure 4.16: Particle size distribution obtained by spICP-MS for A) Zn- and B) Pb-containing NPs in ERM-CZ120 suspended in four different extraction solvents.

The particle number and mass concentrations, particle diameter, and mass fraction of Zn- and Pb-containing NPs were also determined in the ERM-CZ120 suspended in the corresponding extraction solvents (Table 4.7). The mass fraction of Zn- and Pb-containing NPs in ERM-CZ120 suspended in 1 mM sodium pyrophosphate and 0.2 % aqueous ammonia solution was comparable to that observed in MilliQ water, while it was significantly lower in 0.5 % citric acid, indicating either the dissolution or reduced stability of the particles in citric acid. A similar trend was generally observed for the particle number and mass concentration of Zn- and Pb-containing NPs in selected extraction solvents. The dissolution of Zn- and Pb-containing NPs in the 0.5 % citric acid can be considered negligible, as the baseline signals for Zn and Pb determined in the ERM-CZ120 suspension in citric acid were not significantly larger compared to those in MilliQ water (Figure A.1 and Figure A.2 (Appendix)). Additionally, the mean particle sizes of Zn- and Pb-containing NPs in the 0.5 % citric acid were similar to those observed in MilliQ water. From Table 4.7, it can be further observed that the mean particle size of Zn-containing NPs in a 1 mM sodium pyrophosphate and 0.2 % aqueous ammonia solution was slightly higher than that in MilliQ water, indicating their aggregation/agglomeration.

The particle size distribution of the ERM-CZ120 suspension in different extraction solvents was also determined by spICP-MS and is shown in Figure 4.16. It should be noted that the particle size distribution plots only show a selected size range for comparison purposes, even though Zn- and Pb-containing NPs as large as 300 nm and 200 nm, respectively, were also detected. The particle size distribution further confirmed the aggregation/agglomeration of Zn-containing NPs in sodium pyrophosphate and aqueous ammonia solution.

4.3.1.1 Investigating the impact of four extraction solvents on the transport efficiency, ICP-MS response, and linearity of ionic standard calibration curves

During the optimization of the extraction procedures, four different solvents were tested, including MilliQ water, 10 mM sodium pyrophosphate, 1 % citric acid, and 1 % aqueous ammonia solution. Given that the extraction solvent may affect the properties of metal-containing NPs, for instance, through their aggregation or dissolution, the influence of sodium pyrophosphate, citric acid, and aqueous ammonia solution on the particle properties was studied. For this purpose, the ERM-CZ120 material was suspended in the solutions of 1 mM sodium pyrophosphate, 0.5 % citric acid, and 0.2 % aqueous ammonia solution, representing the matrix of the corresponding extraction solvent, which was diluted 10-, 2-, and 5-times in MilliQ water after extraction, respectively. However, first, the impact of extraction solvents on the transport efficiency, ICP-MS response, and linearity of ionic standard calibration curves was thoroughly investigated. The first step was to evaluate whether ionic Zn and Pb standards, for the determination of the ICP-MS response, and Au NPs, for the determination of the transport efficiency, should be prepared in the extraction solvents or MilliQ water/0.1 % HNO_3. From Table 4.8, it can be seen that similar transport efficiencies ((3.0–4.3) %) were determined with the particle frequency and particle size methods, independent of the matrix used. The exception was observed for the transport efficiencies determined by the particle size method in 1 mM sodium pyrophosphate (5.7 %) and 0.2 % aqueous ammonia solution (2.1 %). This was related to the 63 % higher ICP-MS response for ionic Au in 1 mM sodium pyrophosphate and 42 % lower ICP-MS response for ionic Au in 0.2 % aqueous ammonia solution compared to MilliQ water. The ICP-MS responses for ionic Zn and Pb in 0.1 % HNO_3, 1 mM sodium pyrophosphate, and 0.5 % citric acid were similar but decreased by more than 96 % in 0.2 % aqueous ammonia solution. A reduced ICP-MS response in 0.2 % aqueous ammonia solution was most likely related to increased adhesion of ions to the surfaces of the sample container and/or the ICP-MS sample introduction system. However, this only affected the response of the ions and not the transport efficiency of the NPs (similar transport efficiencies based on the particle frequency method were observed in MilliQ water and 0.2 % aqueous ammonia solution). Therefore, for the measurements of NPs in MilliQ water, 1 mM sodium pyrophosphate, and 0.5 % citric acid, calibration curves were prepared from the matrix-matched ionic standards, whereas in the case of 0.2 % aqueous ammonia solution, ionic standards were prepared in 0.1 % aqueous HNO_3. The particle size method was selected to calculate the transport efficiency as the particle diameter of the Au NPs in the stock standard solution is less susceptible to change than the particle number concentration, which can decrease over time due to aggregation/agglomeration, particle settling, and/or particle adhesion to the container walls.

Table 4.8: Comparison of the transport efficiencies (calculated with particle frequency and particle size method by diluting Au NPs and ionic Au standards in relevant extraction solvents), and ICP-MS responses for ionic Au, Zn, and Pb standards with related R^2 values prepared in relevant extraction solvents. ICP-MS responses for ionic Au, Zn, and Pb standards prepared in 1 mM sodium pyrophosphate, 0.5 % citric acid, and 0.2 % aqueous ammonia solution are expressed as percentages in relation to the responses determined in MilliQ water. Results present the mean of the samples measured on two different days.

Extraction solvent	Transport efficiency (%)		Ionic Au		Ionic Zn		Ionic Pb	
	Particle frequency method	Particle size method	ICP-MS response (%)	R^2	ICP-MS response (%)	R^2	ICP-MS response (%)	R^2
MilliQ water*	3.7	3.5	100	0.9998	100	0.9998	100	0.9998
1 mM sodium pyrophosphate*	4.3	5.7	163	1	87.4	0.9999	90.8	0.9996
0.5 % citric acid	3.0	3.6	112	0.9993	126	1	103	0.9999
0.2 % aqueous ammonia solution	4.0	2.1	57.6	0.9984	3.77	0.9860	1.22	0.9986

* Ionic Zn and Pb standards were prepared in relevant matrices with the addition of 0.1 % HNO_3.

4.3.1.2 Optimization of extraction duration

The ERM-CZ120 material characterized for the presence of Zn- and Pb-containing NPs (described above) was applied to quartz fiber filters, and NPs were extracted into solution using the ultrasound-assisted extraction procedure, as described in Chapter 3.6.1. Different extraction durations (30 min, 1 h, 2 h) were tested using 10 mM sodium pyrophosphate as the extraction solvent to achieve the highest extraction efficiency (Figure 4.17). Sodium pyrophosphate was chosen as it gave the highest particle number concentration (along with aqueous ammonia solution) when analyzing the ERM-CZ120 suspensions (Table 4.7). While longer sonication times correlated with increased extraction of Pb-containing NPs, no clear trend was observed for Zn-containing NPs, leading to the conservative selection of a 2-hour sonication time for further testing.

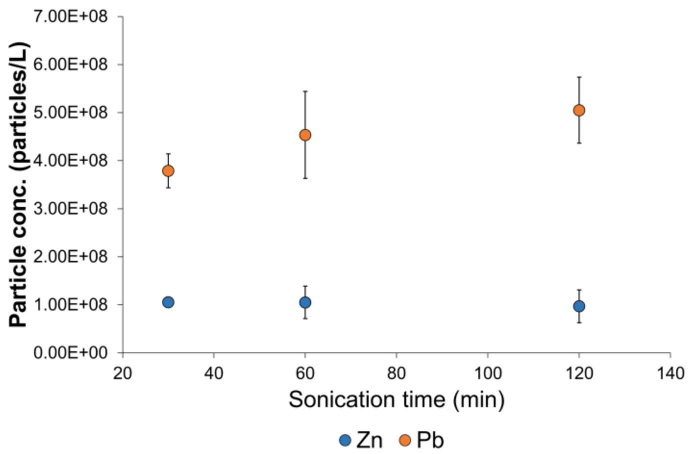

Figure 4.17: The particle number concentration of Zn- and Pb-containing NPs obtained by spICP MS in ERM-CZ120 extracted from PM_{10} filters using 10 mM sodium pyrophosphate and different sonication durations. Results represent the average values with a standard deviation of three replicates.

4.3.1.3 Optimization of extraction solvent

To further improve extraction efficiency, several solvents were tested, including MilliQ water, 10 mM sodium pyrophosphate, 1 % citric acid, and 1 % aqueous ammonia solution. After the extraction in different solvents, total Zn and Pb concentrations were first determined by ICP-MS in different fractions, including the filtrate (i.e., the solution that passed through the filter during the application of the ERM-CZ120 suspension), the extracts, and the filters after extraction, to follow the mass balance of the extraction procedure. The results presented in Figure 4.18 showed that most of the Zn and Pb were retained on the filters during the deposition of the ERM-CZ120 suspension, with only about 2 % passing through. This demonstrated that the quartz fiber filter with deposited ERM-CZ120 was a suitable test material for optimizing the procedure for extracting airborne NPs, offering a reliable approximation of the PM_{10} samples. The highest percentage of total Zn in the extract was achieved in 10 mM sodium pyrophosphate (90 %), while 1 % citric acid was most effective for Pb (66 %), followed by 10 mM sodium pyrophosphate (55 %). However, the standard deviation of the calculated fractions was high (up to 20 %), especially in the case of Zn, as some of the replicate measurements were below the detection limit.

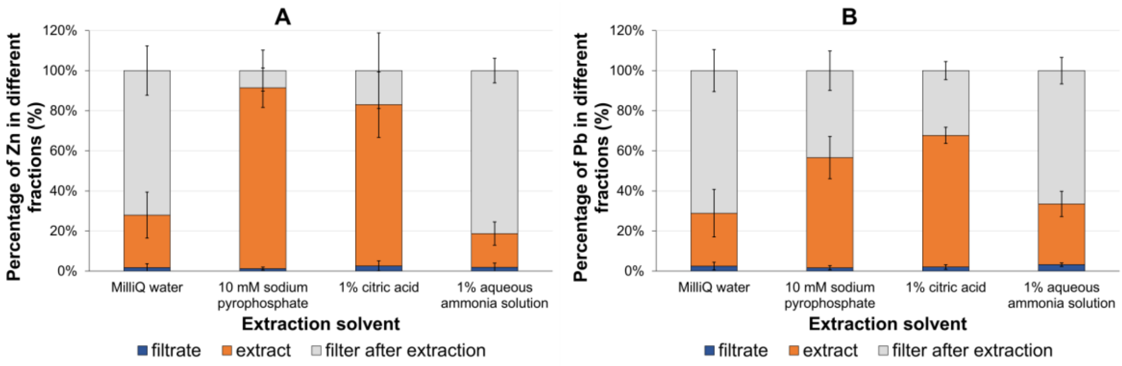

Figure 4.18: Percentage of total A) Zn and B) Pb concentration determined in different fractions after extraction of ERM-CZ120 from PM_{10} filters using different extraction solvents. The average value and standard deviation were calculated from 6 replicates for each extraction solvent. Zn and Pb concentrations determined in different fractions were normalized to the sum of Zn and Pb concentrations determined by ICP MS in all fractions.

To achieve higher accuracy and precision in quantifying Zn- and Pb-containing NPs in air samples at environmentally low concentrations, a spICP-MS technique was applied, offering more sensitive detection of NPs compared to the ICP-MS determination of total element content (Table 4.9).

Table 4.9: Particle size LOD, particle number concentration LOD, and particle mass concentration LOD determined for Zn- and Pb-containing NPs in different extraction solvents by spICP-MS and total mass concentration LOD determined for Zn and Pb in different extraction solvents by ICP-MS. Total mass concentration, particle number, and mass concentration LOD were calculated as 3.3 times the standard deviation of concentrations measured in six blank samples.

Extraction solvent	Zn				Pb			
	Particle size LOD (nm)	Particle number conc. LOD (particles/kg)	Particle mass conc. LOD (mg/kg)	Total mass conc. LOD (mg/kg)	Particle size LOD (nm)	Particle number conc. LOD (particles/kg)	Particle mass conc. LOD (mg/kg)	Total mass conc. LOD (mg/kg)
MilliQ water	55 – 65	1.47 E+11	0.680	23.0	18 – 25	1.04 E+11	0.047	1.12
10 mM sodium pyrophosphate	64 – 68	1.74 E+11	1.11	22.4	20	1.64 E+11	0.054	1.89
1 % citric acid	60 – 114*	6.03 E+09	0.143	4.66	19 – 41*	4.07 E+09	0.003	3.84
1 % aqueous ammonia solution	65	7.95 E+11	3.75	23.9	19 – 20	3.43 E+11	0.127	0.823

*Higher size LOD values for Zn- and Pb-containing NPs in 1 % citric acid are the result of particle dissolution, which led to the elevated ionic background and consequently higher particle detection threshold.

Before spICP-MS analysis, the extracts were filtered through a (12–25) µm filter to remove the fibers of the partially disintegrated quartz filters. The unwanted retention of NPs on the (12–25) µm filter was checked by comparing the number of particles in the filtered ERM-CZ120 water suspension with those in the unfiltered suspension. The results showed that (68 ± 9) % of the Zn- and Pb-containing particles passed through the filter, with good filtration repeatability and without altering the particle size distribution (Figure 4.19).

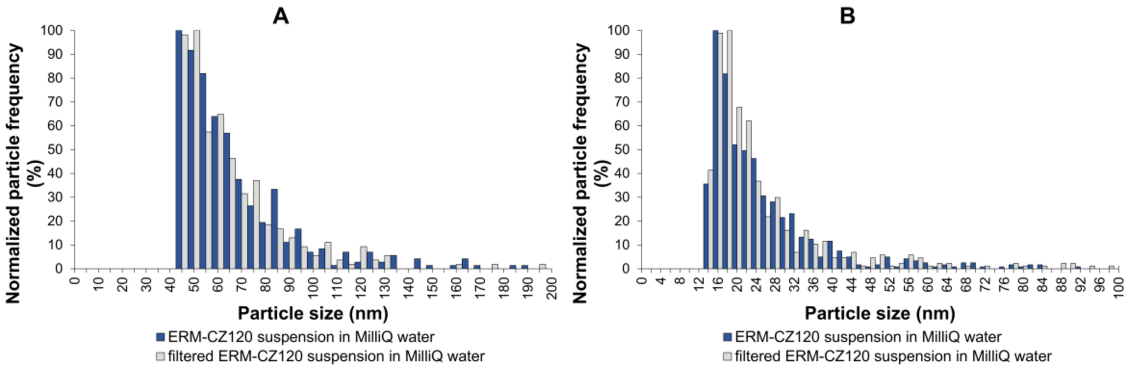

Figure 4.19: Particle size distribution of A) Zn- and B) Pb-containing NPs in unfiltered and filtered (through a (12–25) µm filter) ERM-CZ120 suspension in MilliQ water.

After filtration, the particle concentrations and size distributions of Zn- and Pb-containing NPs extracted from PM_{10} samples were determined by spICP-MS. Table 4.10 shows the extraction recoveries of Zn- and Pb-containing NPs extracted from PM_{10} filters with ERM-CZ120 using the four extraction solvents. The extraction recovery was calculated by comparing the concentration of Zn- and Pb-containing NPs in the extracts, as determined by spICP-MS, with their expected concentration in the ERM-CZ120 sample deposited on the quartz filter, following the Eq. (A.9) and Eq. ((A.10). The highest extraction recoveries based on particle mass concentrations for Zn- and Pb-containing NPs were achieved in 10 mM sodium pyrophosphate (9.14 % and 14.0 %, respectively), followed by 1 % aqueous ammonia solution (6.61 % and 7.21 %, respectively), while the lowest extraction recoveries were obtained in 1 % citric acid (2.95 % for Zn- and 2.92 % for Pb-containing NPs). A similar trend was observed for particle number concentrations, with sodium pyrophosphate showing the highest efficiency (11.0 % for Zn- and 21.8 % for Pb-containing NPs). These results differ from the findings of Torregrosa et al. (2023), who reported better recoveries of PtNPs from micro quartz filters using direct immersion in a 1 % aqueous ammonia solution ((20.1 ± 1.3) %) and a (9 ± 2) % recovery in 1 % disodium pyrophosphate. Similar to our findings, the lowest recovery was reported for 1% citric acid ((1.12 ± 0.18) %). In the same study, the authors reported (84 ± 2) % recoveries achieved after ultrasound-assisted extraction of PtNPs from filters in ammonia solution. This is significantly higher compared to the extraction recoveries obtained in this dissertation after applying ultrasound-assisted extraction of ERM-CZ120 from filters in 10 mM sodium pyrophosphate. It is important to note that the recoveries reported by Torregrosa et al. (2023) were obtained for suspensions of manufactured single-element NPs applied to air filters. In contrast, in this dissertation, certified reference material resembling PM_{10}-like fine dust was used, which more accurately reflects the composition of real PM_{10} samples. Specifically, matrix effects from airborne PM retained on the filter can influence the accuracy and precision of NPs determination, as also demonstrated by Torregrosa et al. (2023). Therefore, it is more appropriate to compare our method's performance with studies that have extracted and detected metal-containing NPs from more realistic environmental samples. For example, Folens et al. (2018) quantified PtNPs in road dust by spICP-MS following an ultrasonication extraction procedure using stormwater runoff for leaching. The authors reported an extraction efficiency of 2.7 %, which is as low as those obtained in this dissertation. Similarly, Avramescu et al. (2024) reported an extraction efficiency of (1.28

± 0.14) % for a road dust composite spiked with CeO_2 NPs following water extraction with sonication. The authors selected water as an extractant to isolate only the readily bioavailable NPs from the road dust. In this dissertation, higher extraction recoveries for Zn- and Pb-containing NPs in PM_{10} samples were achieved using sodium pyrophosphate, which enhances NPs extraction and promotes their dispersion. In summary, the recoveries observed in this dissertation cannot be considered low, especially when compared to the studies referenced above, which report similar or lower extraction efficiencies for various types of NPs from different environmental samples.

Table 4.10: Extraction recovery, mean particle size, and mass fraction of Zn- and Pb-containing NPs in ERM-CZ120 extracted from PM_{10} filters using different extraction solvents. Results represent the average values with a standard deviation of six replicates.

Extraction solvent	Zn				Pb			
	Extraction recovery[a] (%)				Extraction recovery[a] (%)			
	Based on particle number conc.	Based on particle mass conc.	Mean particle size (nm)	Mass fraction of NPs[b] (%)	Based on particle number conc.	Based on particle mass conc.	Mean particle size (nm)	Mass fraction of NPs[b] (%)
MilliQ water	5.25 ± 3.14	3.57 ± 1.36	82 ± 4	3.80 ± 0.30	6.84 ± 3.14	4.24 ± 2.01	30 ± 1	6.99 ± 4.19
10 mM sodium pyrophosphate	11.0 ± 2.9	9.14 ± 2.69	94 ± 2	1.96 ± 0.67	21.8 ± 3.0	14.0 ± 3.4	28 ± 1	7.12 ± 0.88
1 % citric acid	0.737 ± 0.189	2.95 ± 1.29	152 ± 10	0.157 ± 0.075	0.857 ± 0.166	2.92 ± 1.18	54 ± 4	0.185 ± 0.062
1 % aqueous ammonia solution	11.2 ± 4.2	6.61 ± 2.45	85 ± 1	5.46 ± 1.64	8.85 ± 2.95	7.21 ± 1.98	29 ± 1	29.6 ± 10.9

[a]Extraction recovery was calculated following Eq. (A.9) and Eq. (A.10).
[b]Mass fraction of NPs was calculated following Eq. (A.8).

The influence of different extraction solvents on the size and size distribution of the extracted NPs was further investigated. The mean particle sizes (Table 4.10) and particle size distributions (Figure 4.20) of Zn- and Pb-containing NPs in ERM-CZ120 extracted from PM_{10} filters with MilliQ water, 10 mM sodium pyrophosphate, and 1 % aqueous ammonia solution were similar to those in ERM-CZ120 suspended in the corresponding extraction solvents (Table 4.7). This suggests that extraction in these solvents had little impact on particle size, meaning it did not cause significant aggregation, dissolution, or selective size fractionation. In contrast, extraction with 1 % citric acid resulted in significantly larger mean particle sizes (152 nm for Zn- and 54 nm for Pb-containing NPs) compared to other extraction solvents and the ERM-CZ120 suspended in 0.5 % citric acid (90 nm for Zn- and 34 nm for Pb-containing NPs, Table 4.7). The size distribution for particles extracted with 1 % citric acid also shifted towards larger sizes (Figure 4.20 C, G), most likely due to partial dissolution of Zn- and Pb-containing NPs, as evidenced by the increased baseline signal for Zn and Pb after extraction (Figure 4.21). Consequently, a higher particle detection threshold had to be applied, resulting in elevated size LOD (114 nm for Zn- and 41 nm for Pb-containing NPs after extraction with 1 % citric acid, versus approximately 65 nm for Zn- and 20 nm for Pb-containing NPs after extraction with other solvents) (Table 4.9).

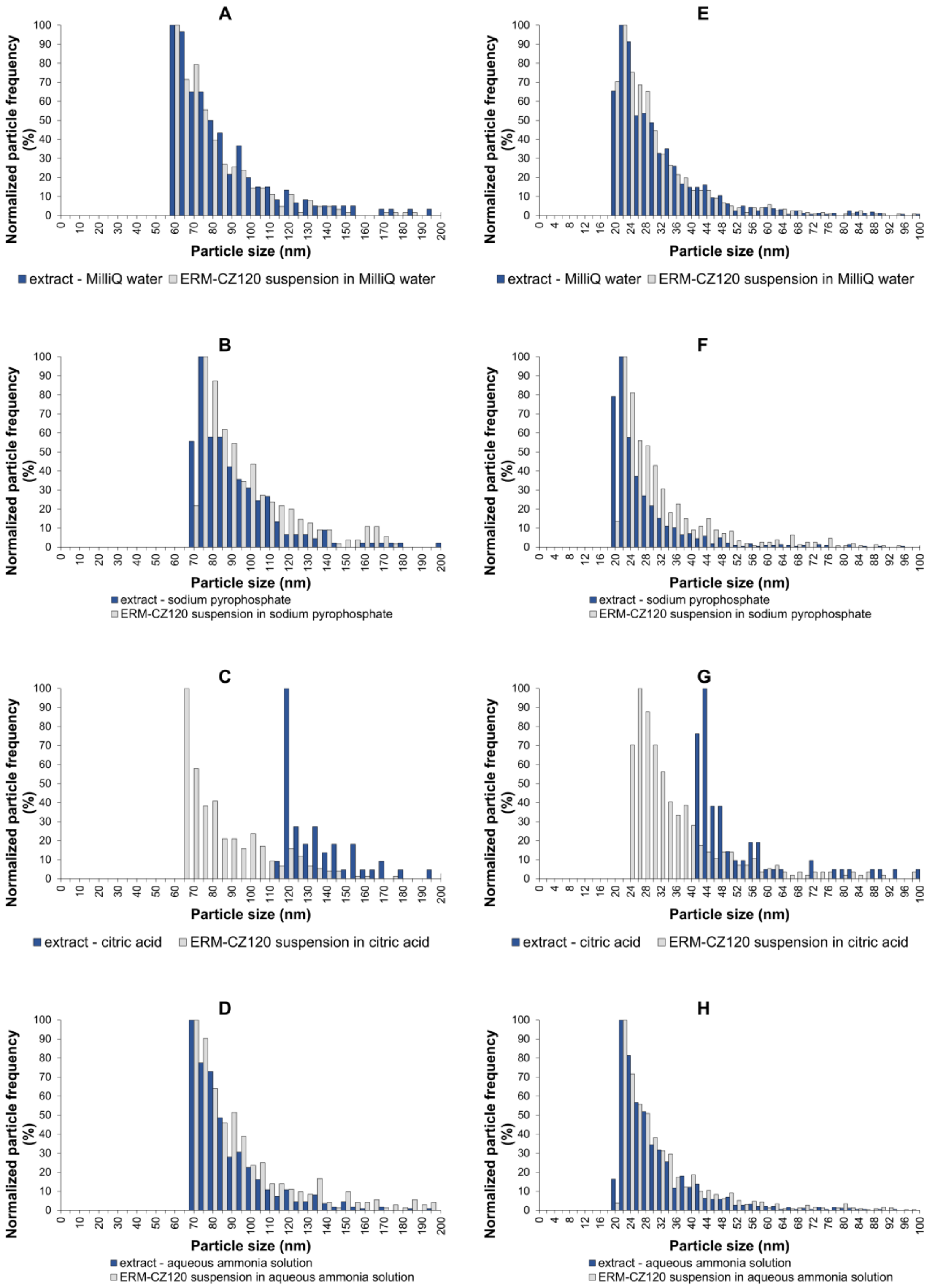

Figure 4.20: Particle size distribution obtained by spICP-MS for Zn- and Pb-containing NPs in ERM-CZ120 extracted from PM_{10} filters using different extraction solvents. Zn-containing NPs are presented in Figures A–D, and Pb-containing NPs are presented in Figures E–H. The particle size distribution of ERM-CZ120 suspended in the relevant extraction solvent is presented for comparison (grey histograms).

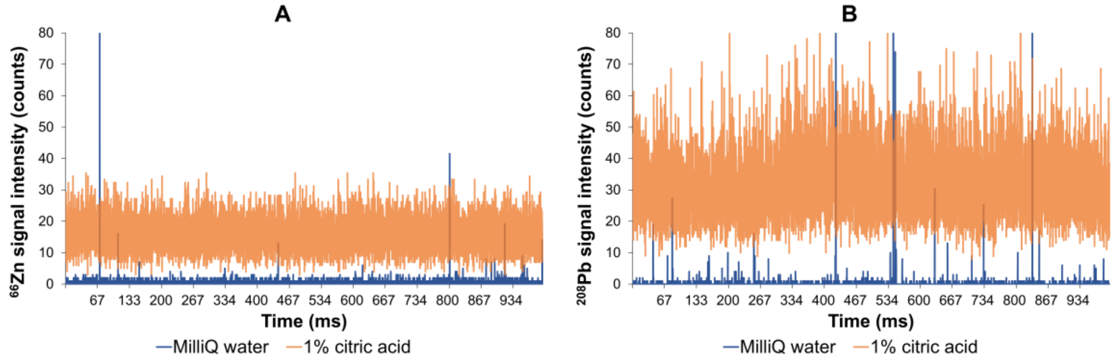

Figure 4.21: Time scans for A) Zn and B) Pb signal obtained by spICP-MS in the ERM-CZ120 extracted from PM_{10} filters using MilliQ water and 1 % citric acid.

As can be further evidenced from Table 4.10, the mass fraction of Zn- and Pb-containing NPs was the highest in 1 % aqueous ammonia solution (average 5.46 % for Zn and 29.6 % for Pb), followed by MilliQ water (average 3.80 % for Zn and 6.99 % for Pb) and 10 mM sodium pyrophosphate (on average 1.96 % for Zn and 7.12 % for Pb), and the lowest in 1 % citric acid (on average 0.157 % for Zn and 0.185 % for Pb). The mass fractions of Zn- and Pb-containing NPs in ERM-CZ120 after extraction from the filters (e.g., 3.80 % for Zn- and 6.99 % for Pb-containing NPs in MilliQ water) were generally lower than those obtained for the suspensions in the corresponding extraction solvents (e.g., 5.26 % for Zn- and 11.3 % for Pb-containing NPs in MilliQ water) (Table 4.7). This could indicate selective particle size fractionation during the application of the ERM-CZ120 suspension to the quartz filters, partial loss of particles due to filtration of the extract through a (12–25) µm filter, and/or particle dissolution during extraction (in the case of 1 % citric acid).

Summing up, the highest percentages of extracted Zn and Pb, in both total and nanoparticulate fractions, were obtained using 10 mM sodium pyrophosphate without affecting the particle size distribution. The optimized extraction procedure, therefore, involved sonication of the PM_{10} filter in 10 mM sodium pyrophosphate for 2 h, followed by filtration of the extract through a (12–25) µm filter that had been pre-conditioned with the extraction solution.

4.3.2 Investigating PM_{10} samples from the Upper Meža Valley for the presence of metal-containing NPs

The optimized procedure was applied to determine metal-containing NPs in PM_{10} samples from the Upper Meža Valley. First, the total element concentration in seven PM_{10} samples was determined. Next, the presence of metal-containing NPs in the extracts of PM_{10} samples was assessed with spICP-MS analysis, and complemented with SEM-EDS analysis.

4.3.2.1 Determination of total element concentration in PM_{10} samples from the Upper Meža Valley

The total Zn and Pb mass concentration in seven PM_{10} samples, collected at different locations and times (Table 3.1), was determined by summing the element concentrations measured in the extracts and filters after extraction (see Eq. (A.1) – Eq. (A.4)). The total Zn and Pb concentrations in the collected PM_{10} samples ranged from 857 mg/kg to 1848 mg/kg and from 3798 mg/kg to 26413 mg/kg, respectively, as shown in Table 4.11.

The total concentrations of both Zn and Pb were significantly higher on the filters collected in June and August 2021 at Location #1 (samples 4, 5, 6, and 7) compared to the filters collected in October 2018 at Location #4 (samples 1, 2, and 3). The observed differences in Zn and Pb concentrations may be attributed to the location and/or the presence of desert dust, which was elevated in June 2021. In June 2021, the Slovenian Environment Agency reported increased PM_{10} levels, along with elevated concentrations of some elements, particularly Al and Fe, due to the presence of desert dust across Slovenia (Bec et al., 2022). The latter could lead to an increased amount of PM_{10} to which elements can be attached (Loskot et al., 2024; Q. Wang et al., 2011).

Table 4.11: Total Zn and Pb mass concentrations, particle number and mass concentration, mean particle size, and mass fraction of Zn- and Pb-containing NPs in PM_{10} samples collected in the Upper Meža Valley. Total Zn and Pb mass concentrations were determined by ICP-MS with a repeatability better than 3 %, while the other parameters were determined by spICP-MS and represent the average values with the standard deviation of two replicates.

		Zn			
Sample	Total mass conc. (mg/kg)	Particle number conc. (particles/kg)	Particle mass conc. (mg/kg)	Mean particle size (nm)	Mass fraction of NPs (%)
1a	857 ± 26	(2.30 ± 0.81) E+12	29.8 ± 18.0	105 ± 6	3.47
1b	964 ± 29	(2.31 ± 0.12) E+12	36.6 ± 14.4	106 ± 2	3.79
2a	1122 ± 34	(2.93 ± 0.28) E+12	9.76 ± 2.19	89 ± 2	0.870
2b	921 ± 28	(2.72 ± 0.72) E+12	16.2 ± 1.2	96 ± 1	1.76
3a	998 ± 30	(2.13 ± 0.81) E+12	8.20 ± 3.06	88 ± 7	0.822
3b	1028 ± 31	(1.87 ± 0.00) E+12	6.15 ± 0.58	90 ± 3	0.598
4	1476 ± 44	(7.47 ± 1.38) E+12	30.1 ± 1.6	90 ± 5	2.04
5	1676 ± 50	(6.31 ± 2.30) E+12	26.1 ± 1.2	92 ± 8	1.55
6	1335 ± 40	(5.05 ± 0.75) E+12	33.1 ± 3.6	100 ± 4	2.48
7	1848 ± 55	(6.67 ± 0.75) E+12	39.0 ± 4.6	96 ± 3	2.11
		Pb			
Sample	Total mass conc. (mg/kg)	Particle number conc. (particles/kg)	Particle mass conc. (mg/kg)	Mean particle size (nm)	Mass fraction of NPs (%)
1a	5560 ± 167	(1.54 ± 0.25) E+14	30.6 ± 3.4	27 ± 0	0.550
1b	5883 ± 176	(1.72 ± 0.18) E+14	26.3 ± 6.2	26 ± 0	0.447
2a	4372 ± 131	(1.61 ± 0.06) E+14	32.0 ± 12.4	27 ± 1	0.732
2b	4251 ± 128	(1.46 ± 0.06) E+14	30.8 ± 1.6	27 ± 0	0.724
3a	3942 ± 118	(1.88 ± 0.15) E+14	40.1 ± 34.2	25 ± 2	1.02
3b	3798 ± 114	(1.76 ± 0.24) E+14	65.4 ± 37.4	28 ± 2	1.72
4	14733 ± 442	(3.36 ± 0.45) E+14	131 ± 10	30 ± 1	0.888
5	18846 ± 565	(3.23 ± 0.03) E+14	123 ± 49	30 ± 1	0.650
6	26413 ± 792	(2.04 ± 0.09) E+14	81.3 ± 1.7	30 ± 0	0.308
7	22925 ± 688	(1.96 ± 0.05) E+14	65.2 ± 22.4	30 ± 1	0.285

To compare the obtained results with the annual limit value of Pb in airborne PM, set to 500 ng/m^3 (*Directive 2008/105/EC*, 2008; *WHO Global Air Quality Guidelines*, 2021), the total Zn and Pb mass concentrations per volume of filtered air were calculated for each PM_{10} sample collected in the Upper Meža Valley (Table 4.12). The average annual values for Location #4 (samples 1–3) and Location #1 (samples 4–7) were calculated and compared to the annual limit value of Pb in airborne PM. The average total Pb concentration at Location #4 (the year 2018) was 139 ng/m^3, while at Location #1 (the year 2021) it was 504 ng/m^3. Samples 4 and 5, with Pb concentrations of 634 ng/m^3 and 660 ng/m^3, respectively, were the only samples to exceed the annual limit value for Pb, which aligns with the presence of desert dust and elevated PM_{10} levels. Similarly, the average total Zn concentration was higher in 2021 (41.8 ng/m^3 at Location #1) than in 2018 (28.3 ng/m^3 at Location #4). Nevertheless, these values provide no insight, as there is currently no established or recommended annual limit value for Zn in airborne PM.

Table 4.12: Total Zn and Pb mass concentrations, particle number, and mass concentration of Zn- and Pb-containing NPs in PM_{10} samples collected in the Upper Meža Valley, calculated per volume of filtered air. Total Zn and Pb mass concentrations were determined by ICP-MS with a repeatability better than 3 %, while the other parameters were determined by spICP-MS and represent the average values with the standard deviation of two replicates.

Sample	Zn			Pb		
	Total mass conc. (ng/m^3)	Particle number conc. (particles/m^3)	Particle mass conc. (ng/m^3)	Total mass conc. (ng/m^3)	Particle number conc. (particles/m^3)	Particle mass conc. (ng/m^3)
1a	30.0 ± 0.9	(8.05 ± 2.84) E+04	1.04 ± 0.63	195 ± 6	(5.39 ± 0.88) E+06	1.07 ± 0.12
1b	33.7 ± 1.0	(8.09 ± 0.42) E+04	1.28 ± 0.50	206 ± 6	(6.02 ± 0.63) E+06	0.921 ± 0.217
2a	38.2 ± 1.1	(9.96 ± 0.95) E+04	0.332 ± 0.074	149 ± 4	(5.47 ± 0.20) E+06	1.09 ± 0.42
2b	31.3 ± 0.9	(9.25 ± 2.45) E+04	0.551 ± 0.041	145 ± 4	(4.96 ± 0.20) E+06	1.05 ± 0.05
3a	18.0 ± 0.5	(3.83 ± 1.46) E+04	0.148 ± 0.055	71.0 ± 2.1	(3.38 ± 0.27) E+06	0.722 ± 0.616
3b	18.5 ± 0.6	(3.37 ± 0.00) E+04	0.111 ± 0.010	68.4 ± 2.1	(3.17 ± 0.43) E+06	1.18 ± 0.67
4	63.5 ± 1.9	(3.21 ± 0.59) E+05	1.29 ± 0.07	634 ± 19	(1.44 ± 0.19) E+07	5.63 ± 0.43
5	58.7 ± 1.8	(2.21 ± 0.81) E+05	0.914 ± 0.042	660 ± 20	(1.13 ± 0.01) E+07	4.31 ± 1.72
6	22.7 ± 0.7	(8.59 ± 1.28) E+04	0.563 ± 0.061	449 ± 13	(3.47 ± 0.15) E+06	1.38 ± 0.03
7	22.2 ± 0.7	(8.00 ± 0.90) E+04	0.468 ± 0.055	275 ± 8	(2.35 ± 0.06) E+06	0.782 ± 0.269

4.3.2.2 Determination of metal-containing NPs extracted from PM_{10} samples of the Upper Meža Valley

The presence of metal-containing NPs in the extracts of PM_{10} samples from the Upper Meža Valley was assessed by using the optimized extraction procedure, followed by spICP-MS analysis. The analysis confirmed the presence of Zn- and Pb-containing NPs in all of the analyzed extracts, indicating their occurrence in PM_{10} samples. The corresponding particle number and mass concentration, mean particle size, and mass fraction of the extracted Zn- and Pb-containing NPs are presented in Table 4.11. The highest number concentrations of Zn- and Pb-containing NPs were observed in PM_{10} samples 4, 5, 6, and 7, all from Location #1. The particle number concentrations of Zn-containing NPs ranged between 1.87E+12 particles/kg (Location #4) and 7.47E+12 particles/kg (Location #1), and between 1.46E+14 particles/kg (Location #4) and 3.36E+14 particles/kg (Location #1) for Pb-containing NPs. There was a significant difference (t-test, $p < 0.05$) between the particle number concentration of Zn-containing NPs in PM_{10} samples collected in June and August 2021 (4, 5, 6, 7) and October 2018 (1, 2, 3). The mass concentrations of Zn-containing NPs ranged between 6.15 mg/kg (Location #4) and 39.0 mg/kg (Location #1), and between 26.3 mg/kg (Location #4) and 131 mg/kg (Location #1) for Pb-containing NPs. A significant difference (t-test, $p < 0.05$) was observed in the particle mass concentration of Pb-containing NPs between PM_{10} samples collected from Location #4 and those from Location #1. In contrast, the mass concentrations of Zn-containing NPs did not differ significantly between the two locations.

Although there are currently no guidelines available specifying the allowable concentration of airborne metal-containing NPs, their presence in PM can pose a potential risk to human health. Recent reports have indicated that particle number concentration in a volume of air is a better measure of exposure than particle mass concentration and that an important parameter in the toxicity of NPs is their surface area (Rabajczyk et al., 2020). Our results revealed notable particle number concentrations for both Pb- and Zn-containing NPs, with higher average concentrations observed at Location #1 in 2021 (1.77 E+05 particles/m^3 for Zn- and 7.89 E+06 particles/m^3 for Pb-containing NPs) compared to Location #4 in 2018 (7.09 E+04 particles/m^3 for Zn-containing NPs and 4.73 E+06 particles/m^3 for Pb-containing NPs) (Table 4.12).

The calculation of the Pearson correlation coefficient (PCC) to evaluate potential relationships among various particle parameters (including particle mass and number concentration, as well as total element concentration) in each PM_{10} sample revealed a very strong correlation between the number and mass concentrations of Pb-containing NPs (PCC = 0.95). Additionally, total Zn concentration exhibited a very strong correlation with the number concentration of Zn-containing NPs (PCC = 0.91), while total Pb concentration showed a strong correlation with the mass concentration of Pb-containing NPs (PCC = 0.64).

The mean particle size of Zn-containing NPs ranged from 88 nm to 106 nm, and from 25 nm to 30 nm for Pb-containing NPs. The mass fraction of (nano)particulate Zn extracted from PM_{10} samples ranged from 0.598 % to 3.79 %. The highest mass fraction of Zn NPs was found in sample 1, consistent with the presence of larger Zn-containing NPs in this sample (Figure 4.22 A). In contrast, the size distribution of Pb-containing NPs (Figure 4.22 B) and the percentage of Pb present in NP form ((0.285–1.72) %) across different samples showed smaller variability. Interestingly, the mass fraction of Pb-containing NPs in the collected PM_{10} samples was significantly lower than in the ERM-CZ120 extracts ((7.12 ± 0.88) %, Table 4.10). This suggests that Pb in the PM_{10} samples from the Upper Meža Valley was likely bound to coarser airborne particles (Miler & Gosar, 2019), which were less efficiently extracted into the solution, leading to a smaller mass fraction of Pb-containing NPs. There was no significant difference (t-test, $p > 0.05$) between the mass fraction of Zn- and Pb-containing NPs in PM_{10} samples collected in June and August 2021 (4, 5, 6, 7) and October 2018 (1, 2, 3).

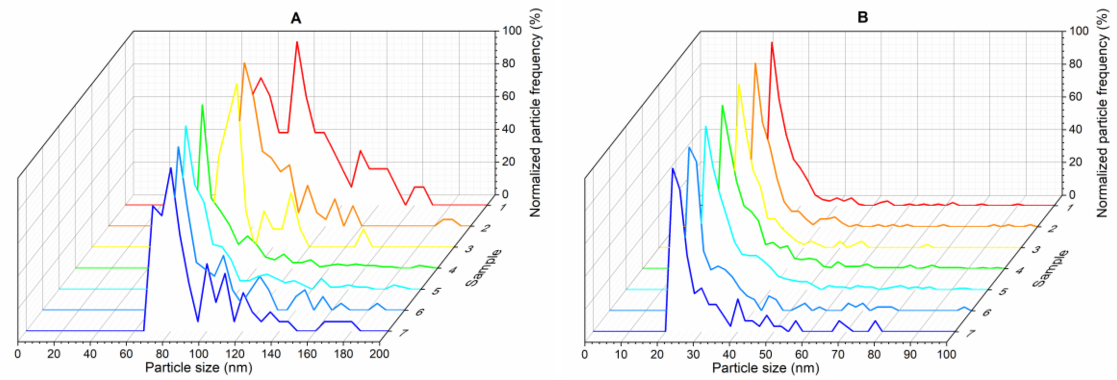

Figure 4.22: Particle size distribution of A) Zn-, and B) Pb-containing NPs in PM_{10} samples collected in the Upper Meža Valley. The samples were extracted from PM_{10} filters using an optimized extraction procedure and analyzed by spICP-MS.

To further assess the anthropogenic contribution to the Zn- and Pb-containing NPs in the studied PM_{10} samples, both particle mass concentrations as well as total element concentrations were normalized to the total aluminum (Al) concentration, determined in each sample. The samples were compared based on the location (or year of sampling) and whether the desert dust was present at the time of sampling. The ratios of total concentrations (Zn/Al and Pb/Al) and particle mass concentrations (Zn NPs/Al and Pb NPs/Al) differed across samples collected on different days (Table 4.13). At Location #4, sample 3 had the highest Zn/Al, Pb/Al, and Pb NPs/Al ratios, while its Zn NPs/Al ratio was comparable with those of samples 1 and 2. Sample 3 also showed the highest Pb NPs/Al ratio among all 7 samples. This suggests the anthropogenic contribution of Pb-containing NPs in sample 3 is more likely. At Location #1, sample 6 had the highest values for all four ratios, again indicating an anthropogenic origin of these particles. No significant difference was observed between samples collected in 2018 and 2021, likely due to the high variability in daily measurements. When comparing samples 4 and 5 (collected during the presence of desert dust) with other samples, they showed lower Zn/Al, Pb/Al, Zn NPs/Al ratios, with similar or lower Pb NPs/Al ratios. However, the only significant difference (t-test, $p < 0.05$) was observed for the Zn NPs/Al ratio.

Table 4.13: Total Zn and Pb concentrations (Zn/Al and Pb/Al) and mass concentrations of Zn- and Pb-containing NPs (Zn NPs/Al and Pb NPs/Al) normalized to total Al concentrations, determined in each PM_{10} sample.

Sample	Zn/Al	Pb/Al	Zn NPs/Al	Pb NPs/Al
1a	0.152	0.986	0.0053	0.0054
1b	0.222	1.35	0.0084	0.0061
2a	0.204	0793	0.0018	0.0058
2b	0.236	1.09	0.0042	0.0079
3a	0.796	3.14	0.0065	0.0320
3b	0.729	2.69	0.0044	0.0464
4	0.055	0.548	0.0011	0.0049
5	0.082	0.922	0.0013	0.0060
6	0.175	3.45	0.0043	0.0106
7	ND	ND	ND	ND

ND - not determined

4.3.2.3 SEM-EDS analysis of metal-containing NPs extracted from PM_{10} samples of the Upper Meža Valley

To complement the spICP-MS results, extracts of PM_{10} filters from the Upper Meža Valley were analyzed by SEM-EDS to determine the shape, size, and elemental composition of (nano)particles that contained Zn and Pb. The analysis revealed that Zn- and Pb-containing particles of different sizes, shapes, and elemental compositions were present in all the investigated samples, and representative SEM-EDS images of particles detected in samples 2, 6, and 7 are presented in Figure 4.23. Most particles were multi-elemental, with the most frequently detected elements being Pb, Zn, S, O, Fe, Sn, Cr, and Ca. Based on the EDS spectra, Pb-containing particles were almost solely composed of Pb sulfate (Figure 4.23 A–C), while Zn was found in oxides with minor amounts of Ca and Al impurities (Figure 4.23 H) or Fe-Al oxides with minor amounts of Zn, Cr, and Mg impurities (Figure 4.23 G, I). Some particles also contained minor atomic percentages of both Pb and Zn (Figure 4.23 D–F). For the samples shown in Figure 4.23 A, E, and F, the high Si content in the EDS spectra was a result of both the silicon plate used as a base for sample droplet deposition and the silicon filter fibers. The chemical composition of metal-containing particles can indicate their sources, as demonstrated by studies of metal-bearing phases in attic and household dust (Miler & Gosar, 2019) and snow (Miler & Gosar, 2013) from the Upper Meža Valley area. According to these studies, the presence of Pb sulfate particles in samples from this dissertation may suggest primary Pb-smelting, while Fe-oxides with traces of Zn, Cu, and Pb may be associated with mining and mechanical processing of mine waste (Miler & Gosar, 2012). However, SEM-EDS can only provide rough qualitative data on particle composition, which alone is insufficient to accurately identify the origin of these particles. Instead, the Pb isotope composition can serve as a more reliable tool for determining the sources of Pb pollution.

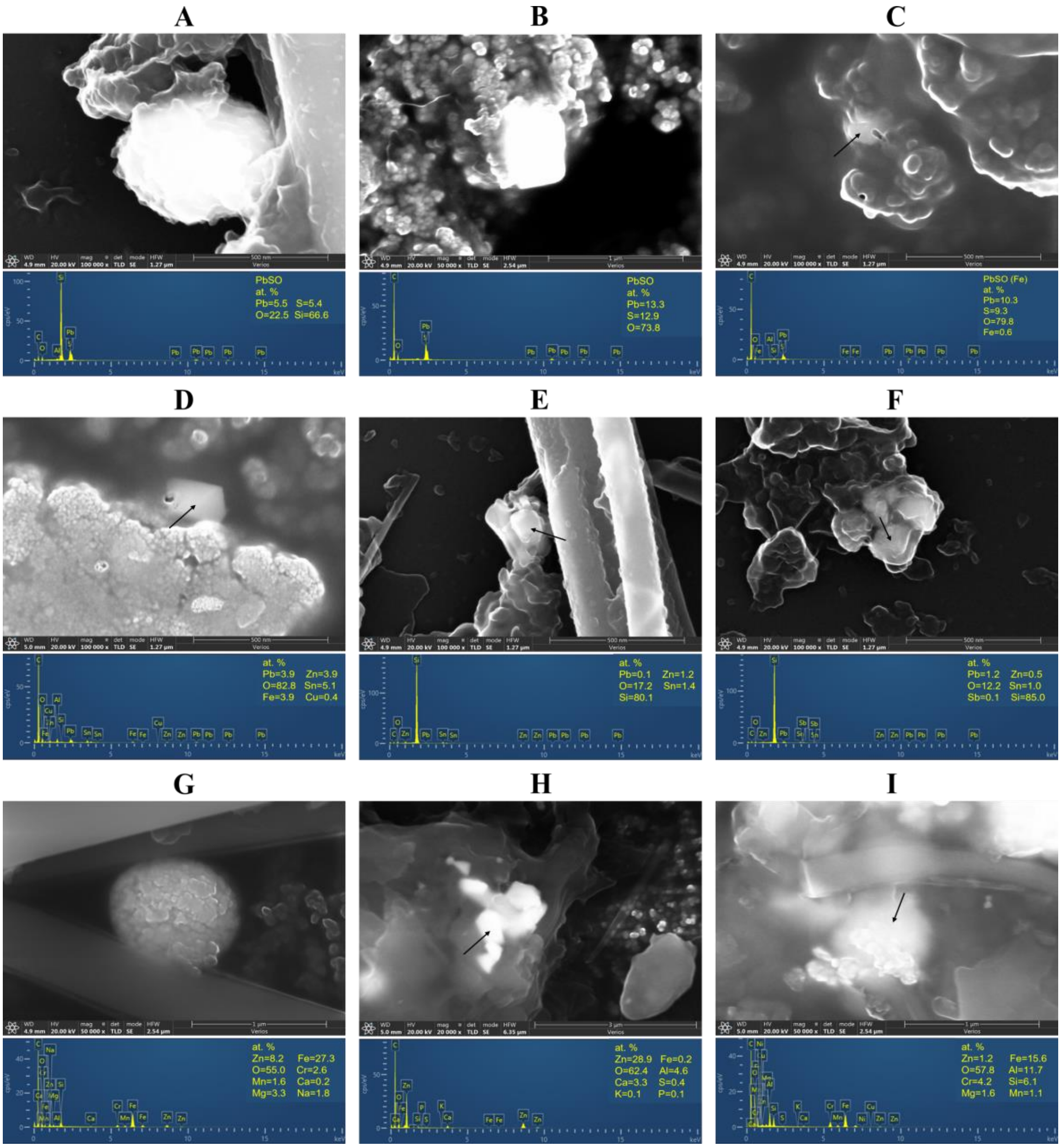

Figure 4.23: SEM images, EDS spectra, and elemental composition of particles in filtered extracts of PM_{10} samples from the Upper Meža Valley. Pb-containing particles are presented in Figures A–C, a mix of both in Figures D–F, and Zn-containing particles are presented in Figures G–I.

SEM images in Figure 4.23 further show that both Zn- and Pb-containing particles exhibited spherical and rectangular shapes. Pb-containing particles were predominantly arranged individually, while Zn-containing and mixed Pb-Zn particles were also aggregated. Although larger particles and the aggregates/agglomerates (in the µm range) were present, for this dissertation, the focus was only on particles in the nanometer scale to allow comparison with the spICP-MS results, which can only detect particles up to a few 100 nm. SEM-EDS identified particle sizes ranging from 93 nm to 900 nm (Figure 4.23), which were larger than the particles detected by spICP-MS analysis. Comparing SEM results with spICP-MS data is not straightforward due to biases in particle size determination from spICP-MS, which relies on assumptions about particle composition, density, and shape that are often unknown in environmental samples. The mean particle sizes determined by spICP-MS in the PM_{10} filter extracts from the Upper Meža Valley (Table 4.11) were therefore only indicative, based on the assumption of spherical particles consisting solely of Zn or Pb, while EDS spectra revealed that particles were primarily sulphates and oxides with minor Zn and/or Pb content. As the molar fraction of the element in NP decreases (from NPs containing the pure element to NPs containing relevant sulphates/oxides), the particle diameter calculated by spICP-MS increases.

For example, assuming a Pb sulfate ($PbSO_4$) composition of Pb-containing NPs with a mass fraction of Pb 0.684 and density of 6.29 g/cm^3, the mean particle diameter would increase by a factor of 1.37 compared to the PbNPs, resulting in a mean particle diameter of (37 ± 1) nm and particle size distribution containing particles as large as 100 nm (Figure 4.24). However, even the recalculated sizes of $PbSO_4$ particles determined by spICP-MS were, in general, still smaller than those observed by SEM (Figure 4.23 A–C).

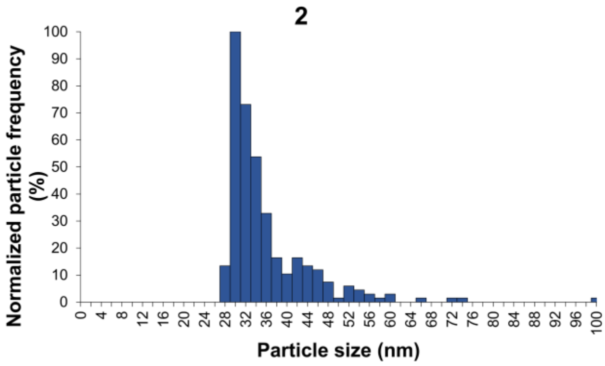

Figure 4.24: Particle size distribution of Pb-containing NPs in the PM_{10} sample 2 collected in the Upper Meža Valley. The particle size distribution was obtained by spICP-MS, assuming the $PbSO_4$ composition of the particles.

The discrepancies between the two techniques in terms of particle sizes can also be explained by the difficulties posed by the sample composition, combined with the physical limitations of the SEM-EDS technique. The PM_{10} filter samples were composed of many particles of different compositions and sizes, of which only a small number contained Pb and Zn, while many were composed of Fe, Sn, and Ag, making their identification by Z-contrast in the SEM-BSE mode difficult. As the SEM technique requires dry samples due to the high vacuum environment of the microscope chamber, the drying of the sample suspensions could also have led to increased particle size due to recrystallization. Additionally, drying the sample droplets in sodium pyrophosphate resulted in the formation of a thin film that hindered particle detection (Figure 4.25). Consequently, it was necessary to perform solvent exchange by centrifuging the samples or to extract particles from filters using MilliQ water. The characterization of small particles was then further complicated by the resolution of the EDS (~1 µm), which presents a significant challenge in analyzing such real environmental samples by SEM-EDS. In conclusion, the aforementioned limitations of spICP-MS and SEM-EDS highlight the need to combine both techniques for comprehensive analysis of airborne metal-containing NPs at low environmental concentrations.

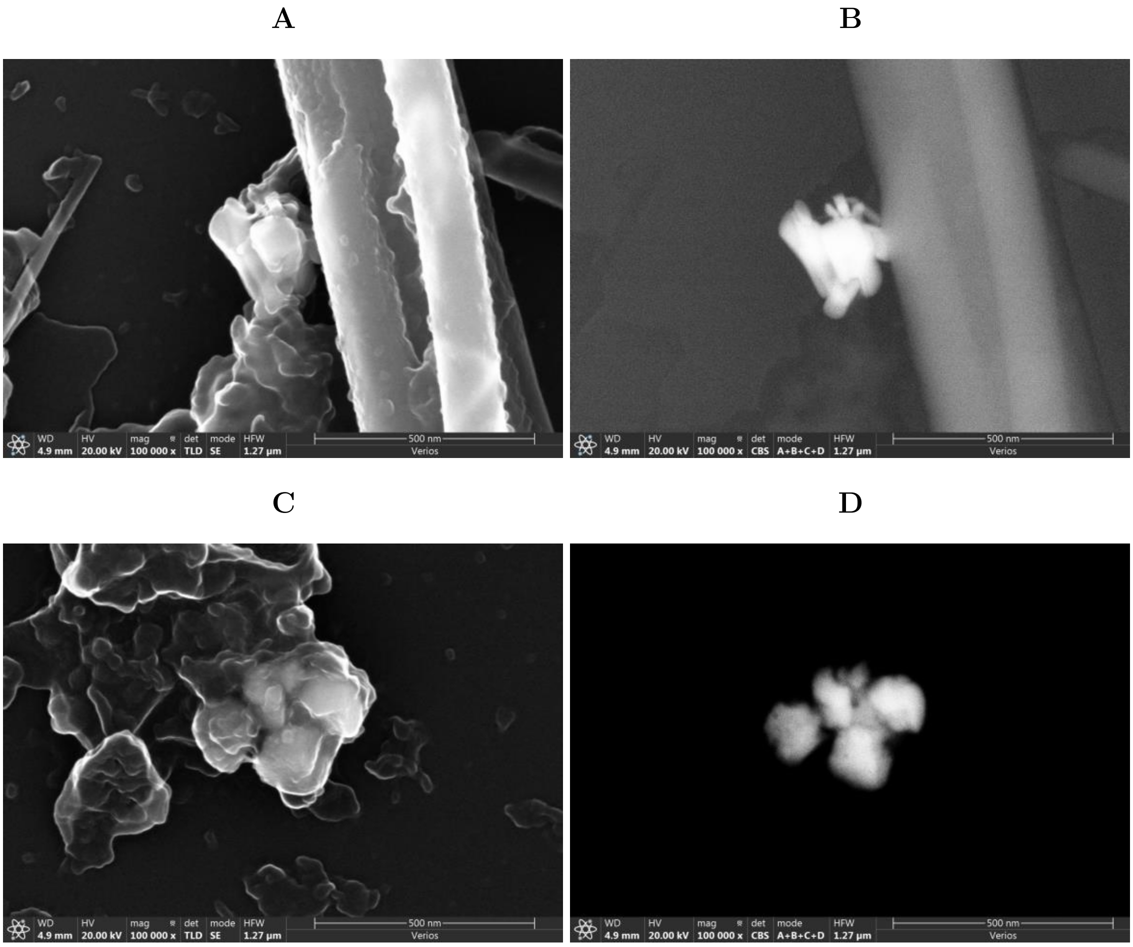

Figure 4.25: Secondary electron (SE) (Figures A and C) and backscattered (BSE) (Figures B and D) SEM images of Zn- and Pb-containing (nano)particles in filtered extracts of PM_{10} samples from the Upper Meža Valley, after solvent exchange. In the SE images, a layer that formed during sample drying is observed covering the particles. This exacerbated the challenge of detecting Zn- and Pb-containing (nano)particles in the BSE mode, where a combination of high contrast and low brightness was used to search the sample for particles composed of heavier elements (Figures B and D).

Chapter 5

Conclusions

This dissertation aimed to determine PTEs concentrations and Pb isotope composition of PM_{10} from the Upper Meža Valley, and based on the results, try to determine possible sources of Pb. For that, different environmental and anthropogenic samples were analyzed. High PTEs concentrations, especially of Pb, were determined in the majority of samples, including all PM_{10} collected at five different locations in 2018 and 2021. Temporal variations in PTEs concentrations were minor, with an increase in Pb and Zn at Location #1 in 2021 compared to 2018, but no significant change for As and Cd. Although the highest PM_{10} levels were recorded in June 2021 due to desert dust, there was no influence on the PTEs concentrations.

Pb isotope composition was used for the first time on the samples from the Upper Meža Valley for detailed source apportionment of individual source contributions. Local environmental samples, including sediment, soil, sand, road dust, mine waste, and ores, from the Upper Meža Valley exhibited similar Pb isotope ratios due to their common origin from the MVT Pb-Zn ore deposit. Pb-battery components displayed a broader range of Pb isotope ratios, reflecting their diverse origins. PM_{10} samples from Žerjav and Črna na Koroškem showed similar Pb isotope compositions, with minimal differences observed over time at Location #1, despite spatial similarities in Pb sources. In 2018, Pb isotope ratios were closer to background values in August, likely due to reduced operations of secondary Pb production during the summer holidays. In early 2021, COVID-19 restrictions may have caused the PM_{10} Pb isotope composition to align more with background values, contrasting with the lower, anthropogenic-level ratios observed in June and late August. Despite a significant influx of desert dust in June and increasing particle concentrations, the isotope composition of PM_{10} remained stable. The dissertation showed that Pb in PM_{10} originated from both local environmental sources (such as soil, sand, and mine waste) and anthropogenic sources, with the latter contributing significantly. Using a binary endmember mixing model, it was determined that anthropogenic Pb contributed between 55.8 % and 69.3 % of the Pb in PM_{10} across various locations. This suggests that present-day human activities, particularly near secondary Pb production sites, are major sources of Pb pollution in PM_{10}.

The presence of metal-containing NPs was evaluated for the first time in PM_{10} from the Upper Meža Valley. To investigate the concentration and size distribution of particles carrying Pb and other potentially present PTEs by spICP-MS, an analytical method for the extraction of NPs from PM_{10} samples was refined. The results of the extraction optimization showed that the two-hour ultrasound-assisted extraction of PM_{10} filters in 10 mM sodium pyrophosphate was the most suitable for subsequent quantification and size characterization of the extracted Zn- and Pb-containing NPs by spICP-MS. Before spICP-MS analysis, an additional step including the filtration of extracts through (12–25) µm filter paper was applied to prevent nebulizer clogging. The results showed that most of the Zn- and Pb-containing particles passed through the filter and that filtration did not significantly change the particle size distribution. The optimized extraction procedure followed by spICP-MS detection was applied for quantification and size characterization of Zn- and Pb-containing NPs in the PM_{10} samples collected in the Upper Meža Valley. The mass fraction of Zn-containing NPs on filters was between 0.598 % and 3.79 %, and between 0.285 % and 1.72 % for Pb-containing NPs. In accordance with the total Zn and Pb concentrations, the average particle number concentrations per volume of filtered air were higher for both Pb- and Zn-containing NPs at Location #1 in 2021 compared to Location #4 in 2018. Furthermore, the SEM-EDS analysis of particles extracted from PM_{10} filters collected in the Upper Meža Valley confirmed the presence of particles of different sizes (in the size range between 100 nm up to a few µm), shapes (spherical and rectangular) and chemical compositions (mostly in the form of sulfates and oxides that at least partially contained Zn and/or Pb, or had these elements attached to their surface).

The combination of information on elemental, isotopic, and nanoparticulate forms of Pb in samples from the Upper Meža Valley provided important information for a better understanding of the fate of Pb in the environment and potential risks to residents. However, the discrepancies in some of the findings in this dissertation compared to other studies underscore the need for comprehensive approaches to understand and address both historical and current sources of environmental Pb pollution. This conclusion can be applied not only to the small local scale studies as this one in the Upper Meža Valley, but also globally, where the Pb source appointment is even more complex.

To complement and expand on the research in the Upper Meža Valley presented in this dissertation, an important future perspective would be to investigate the isotope composition of Pb in nanoparticulate form. This analysis could help to determine whether the metal-containing NPs originate from local environmental sources or are the result of anthropogenic activities. Utilizing time of flight (TOF) ICP-MS would be particularly advantageous for this purpose, as it allows for the simultaneous measurement of different isotopes within individual nanoparticles in very short time intervals. Additionally, assessing the levels of Pb and its isotope composition in the blood of surrounding residents and workers could provide valuable insights. Comparing these results with the Pb isotope composition of environmental and industrial samples analyzed in this dissertation could reveal potential correlations between exposure sources and Pb in blood. Such investigations could not only deepen the understanding of the sources and pathways of Pb exposure but also inform the public health strategies aimed at reducing the risks associated with environmental contamination.

Appendix A

Supplementary Material

A.1 Location and Time of Sampling

Table A.1: Location and time of sampling of water, sediment, soil, sand, road dust, mine waste, PM_{10}, $PM_{2.5}$, and ore samples from the Upper Meža Valley.

Sample	Type	Location	Time
(1)	Water	Meža–Topla	January 2020
(2)		Meža–Črna 1	
(3)		Meža–Črna 2	
(4)		Meža–Žerjav 1	
(5)		Meža–Žerjav 2	
(6)		Meža–Mežica	
(7)		Meža–Podklanc	
(8)		Helena rivulet	
(9)		Jazbina rivulet	
(10)		Junčar rivulet	
(2a)	Sediment	Meža–Črna 1	January 2020
(3a)		Meža–Črna 2*	
(5a)		Meža–Žerjav 2	
(7a)		Meža–Podklanc	
(10a)		Junčar rivulet	
Soil 1	Soil	Žerjav 1 – playground	2018
Soil 2		Žerjav 1 – playground	2018
Soil 3		Žerjav 1 – playground	2018
Soil 4		Žerjav 1 – playground	2018
Soil 5		Žerjav 1 – playground	2018
Soil 6		Žerjav 1– playground	2018
Soil 7		Žerjav 2 – kindergarten	2018
Soil 8		Žerjav 3 – garden, lawn	2018
Soil 9		Žerjav 3 – garden, lawn	2019
Soil 10		Rudarjevo 1 – playground	2008
Soil 11		Rudarjevo 2 – garden	2009
Soil 12		Rudarjevo 3 – garden	2009
Soil 13		Rudarjevo 4 – playground	2009
Soil 14		Rudarjevo 4 – playground	2009

Sample	Type	Location	Time
Soil 15	Soil	Rudarjevo 5 – playground	2013
Soil 16		Rudarjevo 5 – playground	2013
Soil 17		Rudarjevo 6 – playground	2013
Soil 18		Rudarjevo 6 – playground	2013
Soil 19		Rudarjevo 7 – playground	2013
Soil 20		Rudarjevo 7 – playground	2013
Soil 21		Rudarjevo 7 – playground	2013
Soil 22		Rudarjevo 8 – garden	2015
Soil 23		Rudarjevo 8 – garden	2015
Soil 24		Mušenik – garden, lawn	2018
Soil 25		Mušenik – garden, lawn	2018
Soil 26		Mušenik – garden	2018
Sand 1	Sand	Žerjav 2 – kindergarten, sandbox	2018
Sand 2		Žerjav 4 – parking lot	2019
Sand 3		Žerjav 5 – playground	2009
Sand 4		Rudarjevo 9 – yard	2009
Sand 5		Koprivna - yard	2008
Sand 6		Rudarjevo 10 – yard	2009
Sand 7		Rudarjevo 11 – yard	2009
Sand 8		Rudarjevo – for road sanding	2011
Sand 9		Črna na Koroškem 1 – road bank	2011
Sand 10		Črna na Koroškem 2 – road sand	2013
Sand 11		Mušenik – yard	2018
Mine waste 1	Mine waste	Žerjav – mine shaft	2017
Mine waste 2		Žerjav – landfill	2018
Mine waste 3		Mušenik – landfill	2011
Mine waste 4		Mušenik – landfill	2011
PM_{10}-1	PM_{10}	#1 – Žerjav	August 2018
PM_{10}-2		#1 – Žerjav	August 2018
PM_{10}-3		#1 – Žerjav	August 2018
PM_{10}-4		#1 – Žerjav	August 2018
PM_{10}-5		#1 – Žerjav	August 2018
PM_{10}-6		#1 – Žerjav	August 2018
PM_{10}-7		#1 – Žerjav	August 2018
PM_{10}-8		#1 – Žerjav	August 2018
PM_{10}-9		#1 – Žerjav	August 2018
PM_{10}-10		#1 – Žerjav	August 2018
PM_{10}-11		#1 – Žerjav	September 2018
PM_{10}-12		#1 – Žerjav	September 2018
PM_{10}-13		#1 – Žerjav	September 2018
PM_{10}-14		#1 – Žerjav	September 2018
PM_{10}-15		#1 – Žerjav	September 2018

Sample	Type	Location	Time
PM_{10}-16	PM_{10}	#1 – Žerjav	September 2018
PM_{10}-17		#1 – Žerjav	September 2018
PM_{10}-18		#1 – Žerjav	October 2018
PM_{10}-19		#1 – Žerjav	October 2018
PM_{10}-20		#1 – Žerjav	October 2018
PM_{10}-21		#1 – Žerjav	October 2018
PM_{10}-22		#1 – Žerjav	October 2018
PM_{10}-23		#1 – Žerjav	March 2021
PM_{10}-24		#1 – Žerjav	March 2021
PM_{10}-25		#1 – Žerjav	April 2021
PM_{10}-26		#1 – Žerjav	April 2021
PM_{10}-27		#1 – Žerjav	April 2021
PM_{10}-28		#1 – Žerjav	April 2021
PM_{10}-29		#1 – Žerjav	April 2021
PM_{10}-30		#1 – Žerjav	April 2021
PM_{10}-31		#1 – Žerjav	April 2021
PM_{10}-32		#1 – Žerjav	April 2021
PM_{10}-33		#1 – Žerjav	April 2021
PM_{10}-34		#1 – Žerjav	April 2021
PM_{10}-35		#1 – Žerjav	April 2021
PM_{10}-36		#1 – Žerjav	April 2021
PM_{10}-37		#1 – Žerjav	May 2021
PM_{10}-38		#1 – Žerjav	May 2021
PM_{10}-39		#1 – Žerjav	June 2021
PM_{10}-40		#1 – Žerjav	June 2021
PM_{10}-41		#1 – Žerjav	June 2021
PM_{10}-42		#1 – Žerjav	June 2021
PM_{10}-43		#1 – Žerjav	June 2021
PM_{10}-44		#1 – Žerjav	June 2021
PM_{10}-45		#1 – Žerjav	June 2021
PM_{10}-46		#1 – Žerjav	August 2021
PM_{10}-47		#1 – Žerjav	August 2021
PM_{10}-48		#1 – Žerjav	August 2021
PM_{10}-49		#1 – Žerjav	August 2021
PM_{10}-50		#1 – Žerjav	August 2021
PM_{10}-51		#1 – Žerjav	August 2021
PM_{10}-52		#1 – Žerjav	August 2021
PM_{10}-53		#1 – Žerjav	August 2021
PM_{10}-54		#1 – Žerjav	August 2021
PM_{10}-55		#1 – Žerjav	August 2021
PM_{10}-56		#1 – Žerjav	August 2021
PM_{10}-57		#1 – Žerjav	August 2021
PM_{10}-58		#1 – Žerjav	August 2021
PM_{10}-59		#1 – Žerjav	August 2021
PM_{10}-60		#1 – Žerjav	August 2021
PM_{10}-61		#1 – Žerjav	August 2021

Sample	Type	Location	Time
PM_{10}-62		#2 – Žerjav	August 2018
PM_{10}-63		#2 – Žerjav	August 2018
PM_{10}-64		#2 – Žerjav	August 2018
PM_{10}-65		#2 – Žerjav	August 2018
PM_{10}-66		#2 – Žerjav	August 2018
PM_{10}-67		#2 – Žerjav	August 2018
PM_{10}-68		#2 – Žerjav	August 2018
PM_{10}-69		#2 – Žerjav	August 2018
PM_{10}-70		#2 – Žerjav	September 2018
PM_{10}-71		#2 – Žerjav	September 2018
PM_{10}-72		#2 – Žerjav	September 2018
PM_{10}-73		#2 – Žerjav	September 2018
PM_{10}-74		#2 – Žerjav	October 2018
PM_{10}-75		#2 – Žerjav	October 2018
PM_{10}-76		#2 – Žerjav	October 2018
PM_{10}-77		#2 – Žerjav	October 2018
PM_{10}-78		#3 – Žerjav	August 2018
PM_{10}-79		#3 – Žerjav	August 2018
PM_{10}-80		#3 – Žerjav	August 2018
PM_{10}-81		#3 – Žerjav	August 2018
PM_{10}-82		#3 – Žerjav	August 2018
PM_{10}-83		#3 – Žerjav	August 2018
PM_{10}-84		#3 – Žerjav	August 2018
PM_{10}-85	PM_{10}	#3 – Žerjav	August 2018
PM_{10}-86		#3 – Žerjav	September 2018
PM_{10}-87		#3 – Žerjav	September 2018
PM_{10}-88		#3 – Žerjav	September 2018
PM_{10}-89		#3 – Žerjav	September 2018
PM_{10}-90		#3 – Žerjav	October 2018
PM_{10}-91		#3 – Žerjav	October 2018
PM_{10}-92		#3 – Žerjav	October 2018
PM_{10}-93		#3 – Žerjav	October 2018
PM_{10}-94		#4 – Žerjav	August 2018
PM_{10}-95		#4 – Žerjav	August 2018
PM_{10}-96		#4 – Žerjav	August 2018
PM_{10}-97		#4 – Žerjav	August 2018
PM_{10}-98		#4 – Žerjav	September 2018
PM_{10}-99		#4 – Žerjav	September 2018
PM_{10}-100		#4 – Žerjav	September 2018
PM_{10}-101		#4 – Žerjav	September 2018
PM_{10}-102		#4 – Žerjav	October 2018
PM_{10}-103		#4 – Žerjav	October 2018
PM_{10}-104		#4 – Žerjav	October 2018
PM_{10}-105		#4 – Žerjav	October 2018
PM_{10}-106		#5 – Črna na Koroškem	September 2018
PM_{10}-107		#5 – Črna na Koroškem	September 2018

Sample	Type	Location	Time
PM_{10}-108	PM_{10}	#5 – Črna na Koroškem	September 2018
PM_{10}-109		#5 – Črna na Koroškem	September 2018
PM_{10}-110		#5 – Črna na Koroškem	September 2018
PM_{10}-111		#5 – Črna na Koroškem	October 2018
PM_{10}-112		#5 – Črna na Koroškem	October 2018
PM_{10}-113		#5 – Črna na Koroškem	October 2018
PM_{10}-114		#5 – Črna na Koroškem	October 2018
PM_{10}-115		#5 – Črna na Koroškem	October 2018
$PM_{2.5}$-1	$PM_{2.5}$	#4 – Žerjav	August 2018
$PM_{2.5}$-2		#4 – Žerjav	August 2018
$PM_{2.5}$-3		#4 – Žerjav	August 2018
$PM_{2.5}$-4		#4 – Žerjav	August 2018
$PM_{2.5}$-5		#4 – Žerjav	September 2018
$PM_{2.5}$-6		#4 – Žerjav	September 2018
$PM_{2.5}$-7		#4 – Žerjav	September 2018
$PM_{2.5}$-8		#4 – Žerjav	September 2018
$PM_{2.5}$-9		#4 – Žerjav	October 2018
$PM_{2.5}$-10		#4 – Žerjav	October 2018
$PM_{2.5}$-11		#4 – Žerjav	October 2018
$PM_{2.5}$-12		#4 – Žerjav	October 2018
RD-1	Road dust	Črna na Koroškem	September 2018
RD-2		Črna na Koroškem	September 2018
RD-3		Črna na Koroškem	September 2018
W1	Wulfenite*	Upper Meža Valley	2021
W3			
W3			
W4			
W5			
W6			
W7			
W8			
W9			
G1	Galenite*	Revir Union	2021
G2		Revir Union	
G3		Žerjav	
G4		Žerjav	
G5		Žerjav	
G6		Topla	
G7		Topla	
G8		Topla	
G9		Topla	
G10		Topla	
Sp1	Sphalerite*	Revir Fridrih	2021
Sl1	Slate*	Revir Moring	2021
Sl2			

Sample	Type	Location	Time
A1	Andesite*	Reht	2021
A2			
B1	Basalt*	Javorje	2021
B2			

*Personal communication (Rogan Šmuc et al., 2025)

A.2 Summary of All Calculations Used Regarding NPs

- **Total mass concentration of Zn or Pb in PM_{10} samples**

$$Total\ concentration\ (\frac{mg}{kg}) = \frac{m_{combined}}{m_{dust\ on\ filter}} \tag{A.1}$$

The total mass concentration of Zn or Pb on the filter was calculated by comparing the combined mass of Zn or Pb ($m_{combined}$, mg) with the mass of dust deposited on the filter ($m_{dust\ on\ filter}$, kg). The combined mass was calculated following (A.2):

$$m_{combined}(mg) = m_{extract} + m_{filter} \tag{A.2}$$

where $m_{extract}$ represents the mass of Zn or Pb in the extract (mg), and m_{filter} represents the mass of Zn or Pb left on the filter after the extraction (mg). Mass in the extract was calculated following Eq. (A.3), while mass on the filter after extraction was calculated following Eq. (A.4):

$$m_{extract}(mg) = CONC_{extract}\ x\ V_{extract} \tag{A.3}$$

where $CONC_{extract}$ represents a concentration of Zn or Pb determined in digested extract (ng/mL), and $V_{extract}$ is a volume of extract (mL).

$$m_{filter}(mg) = CONC_{filter}\ x\ V_{digested\ filter} \tag{A.4}$$

where $CONC_{filter}$ represents a concentration of Zn or Pb determined in the solution obtained from the digested filter after extraction (ng/mL), and $V_{digested\ filter}$ is the volume of the solution obtained from the digested filter (mL).

- **Particle number concentration of Zn- or Pb-containing NPs in the PM_{10} samples**

Particle number concentration in PM_{10} samples (particles/kg) was calculated following Eq. (A.5):

$$Particle\ number\ conc.\left(\frac{particles}{kg}\right) = \frac{\frac{particle\ conc.}{1000}\ x\ V_{extract}}{m_{dust\ on\ filter}}\ x\ 1000000 \tag{A.5}$$

where *particle conc.* represents particle number concentration of Zn- or Pb-containing NPs determined in extracts by spICP-MS (particles/L), $V_{extract}$ is a volume of extract (mL), and $m_{dust\ on\ filter}$ is mass of dust deposited on the filter (mg).

- **Particle mass concentration of Zn- or Pb-containing NPs in the PM_{10} samples**

Particle mass concentration (mg/kg) was calculated following Eq. (A.6):

$$Particle\ mass\ conc.\left(\frac{mg}{kg}\right) = \frac{\frac{mass\ conc.}{1000}\ x\ V_{extract}}{m_{dust\ on\ filter}} \tag{A.6}$$

where *mass conc.* represents particle mass concentration of Zn- or Pb-containing NPs determined in extracts by spICP-MS (ng/L), $V_{extract}$ is a volume of extract (mL), and $m_{dust\ on\ filter}$ is mass of dust deposited on the filter (mg).

- **Particle mass concentration of Zn- or Pb-containing NPs in ERM-CZ120**

Particle mass concentration (mg/kg) in ERM-CZ120 prepared by weighing 20 mg of ERM-CZ120 powder into 50 ml of MilliQ water was calculated following Eq. (A.7):

$$Particle\ mass\ conc.\left(\frac{mg}{kg}\right) = \frac{\frac{mass\ conc.}{1000}\ x\ V_{ERM-CZ120}}{m_{ERM-CZ120}} \tag{A.7}$$

where *mass conc.* represents particle mass concentration of Zn- or Pb-containing NPs determined in ERM-CZ120 water suspension by spICP-MS (ng/L), $V_{ERM\text{-}CZ120}$ is a volume of ERM-CZ120 water suspension (50 mL), and $m_{ERM\text{-}CZ120}$ is the mass of ERM-CZ120 dust (20 mg).

- **Mass fraction of Zn- or Pb-containing NPs in PM_{10} samples**

$$Mass\ fraction\ of\ NPs\ (\%) = \frac{particle\ mass\ concentration}{total\ concentration}\ x\ 100 \tag{A.8}$$

The mass fraction of NPs (%) was calculated by comparing particle mass concentration of Zn- or Pb-containing NPs determined in extracts by spICP-MS (mg/kg) with the total mass concentration of Zn or Pb determined in acid-digested PM_{10} samples by conventional ICP-MS (mg/kg).

- **Extraction recovery**

$$Extraction\ recovery\ (\%) = \frac{CONC_{NPs\ in\ extract}}{CONC_{NPs\ deposited\ on\ filter}}\ x\ 100 \tag{A.9}$$

The extraction recovery (%) was calculated by comparing the mass concentration of Zn- and Pb-containing NPs in the extract, as determined by spICP-MS ($CONC_{NPs\ in\ extract}$, mg/kg), with their expected concentration in the ERM-CZ120 sample deposited on the quartz filter ($CONC_{NPs\ deposited\ on\ filter}$, mg/kg). The latter was calculated following Eq. (A.10):

$$CONC_{NPs\ deposited\ on\ filter} = CONC_{NPs\ in\ ERM-CZ120\ suspension}\ x\ \frac{V_{deposited\ ERM-CZ120\ suspension}}{V_{extract}} \quad (A.10)$$

based on the concentration of Zn- and Pb-containing NPs in the ERM-CZ120 suspended in the corresponding extraction solvent ($CONC_{NPs\ in\ ERM-CZ120\ suspension}$, mg/kg) – see Eq. (A.7), the volume of the suspension deposited on a filter ($V_{deposited\ ERM-CZ120\ suspension}$, mL), and the volume of the extract ($V_{extract}$, mL).

A.3 Total Element Concentrations in Filtered Water and Sediment Samples from the Meža River and Its Tributaries

Table A.2: Total element concentrations (µg/L) in filtered water samples from the Meža River, determined by ICP-MS. Results are expressed with the measurement standard deviation.

Sample number	(1)	(2)	(3)	(4)	(5)	(6)	(7)	(8)	(9)	(10)
Sample location	Meža - Topla	Meža – Črna 1	Meža – Črna 2	Meža Žerjav 1	Meža – Žerjav 2	Meža - Mežica	Meža - Podklanc	Helena rivulet	Jazbina rivulet	Junčar rivulet
Li	1.27 ± 0.05	1.19 ± 0.03	1.22 ± 0.02	1.32 ± 0.06	1.70 ± 0.09	1.35 ± 0.05	1.80 ± 0.07	0.560 ± 0.022	0.865 ± 0.036	0.665 ± 0.049
Al	57.5 ± 0.8	10.7 ± 0.4	10.8 ± 0.4	10.3 ± 0.3	12.1 ± 0.5	9.16 ± 0.27	15.5 ± 0.2	3.35 ± 0.24	4.42 ± 0.12	6.20 ± 0.11
V	0.687 ± 0.013	0.580 ± 0.005	0.565 ± 0.010	0.510 ± 0.013	0.588 ± 0.015	0.466 ± 0.005	0.660 ± 0.015	0.346 ± 0.006	0.403 ± 0.008	1.78 ± 0.05
Cr	0.429 ± 0.008	0.345 ± 0.003	0.358 ± 0.008	0.374 ± 0.006	0.489 ± 0.005	0.432 ± 0.008	0.571 ± 0.014	0.299 ± 0.004	0.353 ± 0.005	0.324 ± 0.006
Mn	4.94 ± 0.16	0.852 ± 0.016	1.13 ± 0.05	1.74 ± 0.08	3.29 ± 0.11	2.74 ± 0.05	6.61 ± 0.09	0.213 ± 0.016	0.541 ± 0.039	0.868 ± 0.050
Fe	64.1 ± 1.3	8.56 ± 0.10	8.75 ± 0.04	9.05 ± 0.20	20.2 ± 0.3	16.1 ± 0.6	44.9 ± 0.8	3.06 ± 0.07	4.60 ± 0.09	5.28 ± 0.21
Co	0.082 ± 0.007	0.022 ± 0.005	0.023 ± 0.004	0.030 ± 0.004	0.077 ± 0.002	0.063 ± 0.006	0.102 ± 0.005	0.032 ± 0.002	0.022 ± 0.003	0.027 ± 0.003
Ni	0.245 ± 0.008	0.324 ± 0.011	0.245 ± 0.003	0.325 ± 0.011	1.38 ± 0.02	1.12 ± 0.02	1.09 ± 0.02	0.370 ± 0.009	0.366 ± 0.006	0.508 ± 0.009
Cu	0.392 ± 0.012	0.302 ± 0.008	0.291 ± 0.018	0.492 ± 0.022	0.824 ± 0.016	0.815 ± 0.027	1.00 ± 0.04	0.866 ± 0.048	0.339 ± 0.016	0.501 ± 0.016
Se	0.637 ± 0.021	0.816 ± 0.036	0.711 ± 0.029	0.950 ± 0.037	0.871 ± 0.026	0.915 ± 0.045	0.688 ± 0.031	0.640 ± 0.023	0.740 ± 0.018	0.589 ± 0.022
Rb	0.688 ± 0.031	0.595 ± 0.015	0.628 ± 0.017	0.915 ± 0.034	1.25 ± 0.02	0.704 ± 0.028	1.01 ± 0.03	0.481 ± 0.006	0.290 ± 0.005	0.414 ± 0.010
Sr	39.1 ± 0.8	98.2 ± 1.7	113 ± 2	143 ± 2	142 ± 4	108 ± 3	118 ± 1	106 ± 1	87.4 ± 0.7	85.4 ± 1.3
Mo	0.202 ± 0.028	0.236 ± 0.024	0.339 ± 0.014	0.745 ± 0.043	3.60 ± 0.13	1.76 ± 0.08	2.87 ± 0.10	0.207 ± 0.020	0.580 ± 0.029	0.354 ± 0.024
Ag	0.0020 ± 0.0004	0.0015 ± 0.0008	0.0016 ± 0.0006	0.0026 ± 0.0007	0.0038 ± 0.0008	0.0019 ± 0.0006	0.0023 ± 0.0014	0.0018 ± 0.0011	0.0026 ± 0.0015	0.0014 ± 0.0011
Sb	11.1 ± 0.9	17.4 ± 1.4	31.7 ± 1.4	101 ± 7	255 ± 6	246 ± 5	77.7 ± 2.4	39.5 ± 2.2	60.3 ± 2.1	65.4 ± 2.6
Ba	5.13 ± 0.23	9.99 ± 0.29	10.6 ± 0.1	12.1 ± 0.2	11.7 ± 0.3	19.3 ± 0.3	21.8 ± 0.4	8.33 ± 0.11	15.7 ± 0.1	15.1 ± 0.3
Tl	0.010 ± 0.002	0.012 ± 0.003	0.023 ± 0.002	0.035 ± 0.004	0.196 ± 0.012	0.096 ± 0.012	0.118 ± 0.003	0.045 ± 0.003	0.067 ± 0.003	0.103 ± 0.004
U	0.227 ± 0.013	0.254 ± 0.004	0.293 ± 0.005	0.213 ± 0.003	0.232 ± 0.008	0.602 ± 0.011	0.566 ± 0.018	0.678 ± 0.034	0.727 ± 0.020	0.934 ± 0.034

Table A.3: Total element concentrations (mg/kg) in sediment samples from the Meža River, determined by ICP-MS. Results are expressed with the measurement standard deviation.

Sample number	(2a)		(3a)		(5a)		(7a)		(10a)	
Sample location	Meža – Črna 1		Meža – Črna 2		Meža – Žerjav 2		Meža - Podklanc		Jünčar rivulet	
Fraction (mm)	<0.063	<0.150	<0.150	<0.250	<0.063	<0.150	<0.063	<0.150	<0.063	<0.150
Li	43.1 ± 0.1	ND	42.3 ± 0.1	ND	30.1 ± 0.1	ND	35.0 ± 0.1	ND	7.69 ± 0.01	ND
Al	61717 ± 45	86442 ± 376	54120 ± 23	80931 ± 920	41092 ± 66	59489 ± 379	51249 ± 50	64469 ± 985	11910 ± 12	8700 ± 53
V	160 ± 1	ND	90.2 ± 0.1	ND	174 ± 1	ND	292 ± 1	ND	54.1 ± 0.1	ND
Cr	206 ± 1	148 ± 5	55.6 ± 0.1	58.0 ± 0.6	342 ± 1	115 ± 1	3900 ± 21	2482 ± 45	24.4 ± 0.1	18.4 ± 0.3
Mn	1170 ± 1	ND	606 ± 1	ND	1433 ± 1	ND	1463 ± 2	ND	387 ± 1	ND
Fe	56008 ± 490	79386 ± 1511	33962 ± 213	49373 ± 107	81431 ± 866	53946 ± 215	90157 ± 383	166545 ± 1148	11297 ± 115	9583 ± 39
Co	19.9 ± 0.1	ND	12.7 ± 0.1	ND	20.8 ± 0.1	ND	38.8 ± 0.1	ND	3.00 ± 0.01	ND
Ni	51.8 ± 0.1	44.8 ± 0.4	33.2 ± 0.1	28.3 ± 0.3	73.4 ± 0.1	42.6 ± 1.0	482 ± 1	355 ± 7	12.2 ± 0.1	8.80 ± 0.06
Cu	33.3 ± 0.1	ND	28.0 ± 0.1	ND	81.5 ± 0.1	ND	168 ± 1	ND	13.0 ± 0.1	ND
Se	2.83 ± 1.07	ND	2.10 ± 1.09	ND	5.77 ± 2.47	ND	5.75 ± 1.71	ND	1.87 ± 1.42	ND
Rb	77.1 ± 0.1	ND	73.6 ± 0.1	ND	39.9 ± 0.1	ND	59.2 ± 0.1	ND	15.5 ± 0.1	ND
Sr	229 ± 1	ND	201 ± 1	ND	229 ± 1	ND	199 ± 1	ND	160 ± 1	ND
Mo	32.8 ± 0.1	25.6 ± 0.5	2.52 ± 0.01	1.08 ± 0.04	130 ± 1	19.4 ± 0.1	344 ± 1	191 ± 3	68.4 ± 0.1	27.1 ± 0.3
Ag	0.429 ± 0.004	< DL	0.222 ± 0.002	< DL	2.02 ± 0.01	< DL	0.664 ± 0.002	< DL	0.496 ± 0.004	< DL
Sb	1184 ± 3	ND	239 ± 1	ND	23482 ± 26	ND	4672 ± 4	ND	751 ± 3	ND
Ba	628 ± 1	ND	277 ± 1	ND	754 ± 1	ND	926 ± 1	ND	1199 ± 1	ND
Tl	0.624 ± 0.001	ND	0.462 ± 0.001	ND	0.733 ± 0.004	ND	2.26 ± 0.01	ND	1.12 ± 0.01	ND
U	6.17 ± 0.01	ND	2.39 ± 0.01	ND	7.80 ± 0.01	ND	5.96 ± 0.01	ND	10.8 ± 0.1	ND

ND - not determined

A.4 Pearson Correlation Matrix

Table A.4: A) Pearson correlation matrix for metal concentrations in filtered water samples from the Meža River (µg/L). B) Pearson correlation matrix for metal concentrations in sediment samples from the Meža River, fraction <0.063 mm (mg/kg). C) Pearson correlation matrix for metal concentrations in sediment samples from the Meža River, fraction <0.150 mm (mg/kg).

		Pb	Zn	As	Cd
A)					
	Pb	1			
	Zn	0.22	1		
	As	**0.98**	0.18	1	
	Cd	**0.95**	0.48	**0.95**	1
B)					
	Pb	1			
	Zn	0.47	1		
	As	**1.00**	0.41	1	
	Cd	0.45	**1.00**	0.39	1
C)					
	Pb	1			
	Zn	**0.96**	1		
	As	**0.99**	**0.98**	1	
	Cd	**0.96**	**1.00**	**0.98**	1

A.5 Total Element Concentrations in PM_{10} and $PM_{2.5}$ Samples from the Upper Meža Valley

Table A.5: Total element concentrations (mg/kg) in PM_{10} and $PM_{2.5}$ samples from the Upper Meža Valley, determined by ICP-MS. Results are expressed as an average of all the samples from one location, with standard deviation.

Sample location	#1	#2	#3	#4	#4	#5
Sample type	PM_{10}	PM_{10}	PM_{10}	PM_{10}	$PM_{2.5}$	PM_{10}
Li	1.05 ± 4.69	4.63 ± 9.18	4.29 ± 7.50	0.613 ± 0.760	5.21 ± 8.15	6.34 ± 4.66
Al	11197 ± 10484	16180 ± 16029	10434 ± 6997	8663 ± 9397	5075 ± 2677	6878 ± 9397
V	65.9 ± 23.0	157 ± 313	95.2 ± 108.5	38.9 ± 24.9	35.0 ± 33.7	31.7 ± 22.9
Cr	189 ± 70	517 ± 951	337 ± 377	219 ± 68	208 ± 141	167 ± 37
Mn	241 ± 85	1597 ± 1729	299 ± 191	634 ± 469	176 ± 38	175 ± 66
Fe	10767 ± 4773	24733 ± 26170	11879 ± 7462	8960 ± 6510	6208 ± 2676	7266 ± 5144
Co	2.02 ± 5.59	4.24 ± 5.87	7.96 ± 11.59	6.30 ± 5.03	16.8 ± 9.2	12.3 ± 6.4
Ni	112 ± 112	198 ± 324	166 ± 198	77.1 ± 41.8	219 ± 475	85.4 ± 13.4
Cu	218 ± 333	214 ± 144	155 ± 133	130 ± 65	658 ± 1227	695 ± 1568
Se	33.4 ± 64.9	20.7 ± 52.7	15.3 ± 29.8	20.6 ± 43.2	15.7 ± 24.5	17.7 ± 15.6
Rb	15.7 ± 14.1	52.9 ± 84.7	29.3 ± 25.0	36.9 ± 15.2	36.9 ± 13.3	42.0 ± 8.6
Sr	26.3 ± 60.2	120 ± 168	114 ± 163	100 ± 79	233 ± 169	208 ± 107
Mo	58.7 ± 75.5	210 ± 371	236 ± 323	53.0 ± 22.8	207 ± 219	43.9 ± 17.5
Ag	1.19 ± 5.03	2.75 ± 5.02	4.29 ± 6.48	1.89 ± 4.70	5.32 ± 8.85	8.50 ± 6.10
Sb	994 ± 1005	2191 ± 4937	1022 ± 1773	1326 ± 1130	1816 ± 1283	527 ± 310
Ba	815 ± 468	1536 ± 3181	993 ± 1386	181 ± 109	401 ± 232	1476 ± 2909
Tl	2.32 ± 4.39	5.63 ± 10.37	7.03 ± 10.24	4.86 ± 6.70	8.11 ± 11.53	11.1 ± 7.3
U	0.490 ± 2.552	4.91 ± 10.03	5.75 ± 9.35	3.10 ± 5.37	7.62 ± 10.55	9.61 ± 6.62

A.6 Total Element Concentrations in Soil, Sand, Mine Waste, Road Dust, Pb-battery Components, and Ores from the Upper Meža Valley

Table A.6: Total element concentrations (mg/kg) in soil, sand, mine waste, road dust, and Pb-battery components from the Upper Meža Valley, determined by ICP-MS. Results are expressed as an average of all the analysed samples, with standard deviation.

Sample type	Soil	Sand	Mine waste	Road dust	Pb-grid	Pb-paste 1	Pb-paste 2	Pb-paste 3
Li	ND	ND	ND	12.8 ± 2.6	ND	0.431 ± 0.032	0.336 ± 0.056	0.461 ± 0.104
Al	60237 ± 22751	15563 ± 15626	30842 ± 29247	27258 ± 2069	72.4 ± 4.4	<DL	7.08 ± 1.37	3.39 ± 1.34
V	ND	ND	ND	72.1 ± 3.8	<DL	0.010 ± 0.005	0.011 ± 0.005	<DL
Cr	85.5 ± 53.4	112 ± 170	76.3 ± 53.0	122 ± 7	ND	<DL	<DL	<DL
Mn	ND	ND	ND	823 ± 32	ND	<DL	<DL	<DL
Fe	40503 ± 11662	21102 ± 16969	54073 ± 29007	24313 ± 1424	<DL	<DL	<DL	<DL
Co	ND	ND	ND	8.34 ± 0.56	ND	0.014 ± 0.007	<DL	<DL
Ni	44.5 ± 25.7	83.0 ± 131.0	52.9 ± 19.7	24.2 ± 1.1	ND	<DL	<DL	<DL
Cu	ND	ND	ND	23.3 ± 1.4	<DL	3.00 ± 0.08	2.02 ± 0.16	2.82 ± 0.22
Se	ND	ND	ND	2.17 ± 2.03	ND	<DL	<DL	<DL
Rb	ND	ND	ND	36.2 ± 2.6	<DL	0.044 ± 0.009	<DL	<DL
Sr	ND	ND	ND	123 ± 4	<DL	<DL	<DL	<DL
Mo	7.73 ± 10.29	41.8 ± 60.6	47.8 ± 43.0	4.28 ± 0.69	<DL	1.28 ± 0.07	0.880 ± 0.072	1.14 ± 0.09
Ag	4.00 ± 7.27	1.63 ± 1.66	1.54 ± 1.66	<DL	15.3 ± 0.2	3.27 ± 0.08	3.22 ± 0.33	2.81 ± 0.13
Sb	ND	ND	ND	0.631 ± 0.087	<DL	4.12 ± 0.28	3.29 ± 2.40	3.20 ± 3.16
Ba	ND	ND	ND	183 ± 12	<DL	<DL	7.94 ± 0.16	13.1 ± 2.4
Tl	ND	ND	ND	0.428 ± 0.029	9.67 ± 0.28	3.71 ± 0.48	8.44 ± 2.20	11.8 ± 2.5
U	ND	ND	ND	1.97 ± 0.11	ND	<DL	<DL	<DL

ND - not determined

Table A.7: Total element concentrations (mg/kg) in ore samples from the Upper Meža Valley, determined by ICP-MS. Results are expressed as an average of all the analysed samples, with standard deviation.

Sample type	Wulfenite*	Galenite*	Sphalerite**	Slate*	Andesite*	Basalt*
Li	<DL	<DL	0.319 ± 0.038	66.6 ± 0.8	34.5 ± 0.1	20.0 ± 0.3
Al	213 ± 137	709 ± 638	404 ± 7	96556 ± 4321	98995 ± 1615	86118 ± 3705
V	766 ± 343	0.902 ± 1.010	1.09 ± 0.09	128 ± 1	87.0 ± 6.0	405 ± 7
Cr	33.3 ± 17.1	2.74 ± 1.83	9.68 ± 0.28	98.9 ± 2.9	57.9 ± 0.2	30.0 ± 0.5
Mn	45.5 ± 46.6	41.8 ± 30.7	70.7 ± 2.4	427 ± 19	530 ± 9	1431 ± 7
Fe	1656 ± 2120	23023±22009	7235 ± 119	43828 ± 395	29970 ± 2000	10566 ± 2481
Co	0.264 ± 0.169	0.357 ± 0.226	0.308 ± 0.058	18.8 ± 0.4	7.75 ± 0.64	50.5 ± 0.2
Ni	3.59 ± 2.58	6.85 ± 2.38	8.13 ± 0.20	68.6 ± 4.0	13.3 ± 2.6	54.8 ± 5.2
Cu	4.96 ± 5.00	7.11 ± 10.48	276 ± 4	56.8 ± 4.5	2.32 ± 1.00	93.3 ± 1.1
Se	0.866 ± 0.100	1.41 ± 0.67	<DL	<DL	<DL	2.26 ± 1.32
Rb	0.282 ± 0.149	1.06 ± 0.57	0.583 ± 0.320	177 ± 3	78.9 ± 3.0	14.3 ± 1.1
Sr	5.46 ± 1.85	46.6 ± 82.4	5.27 ± 0.88	106 ± 1	231 ± 8	798 ± 47
Mo	171386±59122	43.9 ± 62.4	0.287 ± 0.055	1.33 ± 0.18	1.50 ± 0.04	1.45 ± 0.01
Ag	0.292 ±0.088	0.951 ± 1.350	9.15 ± 0.45	<DL	0.226 ± 0.013	0.472 ± 0.039
Sb	2.07 ± 1.70	41.4 ± 62.9	<DL	1.24 ± 0.04	0.457 ± 0.181	1.18 ± 0.10
Ba	1.23 ± 0.32	18.8 ± 31.7	6.54 ± 0.39	321 ± 20	550 ± 9	202 ± 8
Tl	0.436 ± 0.094	34.6 ± 34.2	17.1 ± 0.5	0.797 ± 0.099	0.436 ± 0.151	0.047 ± 0.012
U	0.567 ± 0.264	0.797 ± 0.898	0.101 ± 0.008	2.87 ± 0.13	1.19 ± 0.10	1.20 ± 0.01

* Personal communication (Rogan Šmuc et al., 2025)

** Results are expressed with the measurement standard deviation, as only one sample of sphalerite was analyzed.

A.7 Pb Isotope Ratios of Water, Sediment, Soil, Sand, Road Dust, Mine Waste, Pb-battery Components, PM_{10}, $PM_{2.5}$, and Ore Samples from the Upper Meža Valley

Table A.8: Pb isotope ratios of water, sediment, soil, sand, road dust, mine waste, Pb-battery components, PM_{10}, $PM_{2.5}$, and ore samples from the Upper Meža Valley. Results are expressed with the measurement standard deviation.

Water	$^{208}Pb/^{204}Pb$	$^{207}Pb/^{204}Pb$	$^{206}Pb/^{204}Pb$	$^{208}Pb/^{206}Pb$	$^{206}Pb/^{207}Pb$
(1)	38.557 ± 0.015	15.678 ±0.005	18.374 ± 0.006	2.098 ± 0.001	1.172 ± 0.001
(2)	38.505 ± 0.020	15.671 ± 0.003	18.329 ± 0.010	2.101 ± 0.001	1.170 ± 0.001
(3)	37.833 ± 0.024	15.592 ± 0.007	17.910 ± 0.005	2.112 ± 0.001	1.149 ± 0.001
(4)	37.921 ± 0.016	15.608 ± 0.006	17.951 ± 0.003	2.112 ± 0.001	1.150 ± 0.001
(5)	37.898 ± 0.009	15.607 ± 0.003	17.931 ± 0.003	2.113 ± 0.001	1.149 ± 0.001
(6)	38.240 ± 0.042	15.640 ± 0.012	18.167 ± 0.010	2.105 ± 0.001	1.162 ± 0.001
(7)	38.476 ± 0.033	15.669 ± 0.011	18.313 ± 0.007	2.101 ± 0.001	1.169 ± 0.001
(8)	38.566 ± 0.010	15.679 ± 0.002	18.372 ± 0.003	2.099 ± 0.001	1.172 ± 0.001
(9)	38.569 ± 0.012	15.677 ± 0.004	18.376 ± 0.008	2.099 ± 0.001	1.172 ± 0.001
(10)	38.572 ± 0.006	15.682 ± 0.001	18.377 ± 0.001	2.099 ± 0.001	1.172 ± 0.001
Sediment	$^{208}Pb/^{204}Pb$	$^{207}Pb/^{204}Pb$	$^{206}Pb/^{204}Pb$	$^{208}Pb/^{206}Pb$	$^{206}Pb/^{207}Pb$
(2a) <0.063 mm	38.479 ± 0.002	15.678 ± 0.001	18.282 ± 0.002	2.105 ± 0.001	1.166 ± 0.001
(2a) <0.150 mm	38.605 ± 0.002	15.692 ± 0.001	18.374 ± 0.001	2.101 ± 0.001	1.171 ± 0.001
(3a) <0.150 mm	38.642 ± 0.004	15.697 ± 0.001	18.398 ± 0.002	2.100 ± 0.001	1.172 ± 0.001
(3a) <0.250 mm	38.603 ± 0.002	15.689 ± 0.001	18.365 ± 0.002	2.102 ± 0.001	1.171 ± 0.001
(5a) <0.063 mm	38.315 ± 0.002	15.657 ± 0.001	18.189 ± 0.001	2.107 ± 0.001	1.162 ± 0.001
(5a) <0.150 mm	38.576 ± 0.002	15.690 ± 0.001	18.358 ± 0.001	2.102 ± 0.001	1.170 ± 0.001
(7a) <0.063 mm	38.495 ± 0.002	15.677 ± 0.001	18.302 ± 0.002	2.103 ± 0.001	1.167 ± 0.001
(7a) <0.150 mm	38.528 ± 0.002	15.671 ± 0.001	18.351 ± 0.001	2.100 ± 0.001	1.171 ± 0.001
(10a) <0.063 mm	38.387 ± 0.003	15.641 ± 0.001	18.297 ± 0.002	2.098 ± 0.001	1.170 ± 0.001
(10a) <0.150 mm	38.516 ± 0.002	15.679 ± 0.001	18.332 ± 0.002	2.101 ± 0.001	1.169 ± 0.001
Soil	$^{208}Pb/^{204}Pb$	$^{207}Pb/^{204}Pb$	$^{206}Pb/^{204}Pb$	$^{208}Pb/^{206}Pb$	$^{206}Pb/^{207}Pb$
Soil 1	38.543 ± 0.013	15.672 ± 0.004	18.370 ± 0.003	2.098 ± 0.001	1.172 ± 0.001
Soil 2	38.558 ± 0.010	15.666 ± 0.001	18.402 ± 0.001	2.097 ± 0.001	1.175 ± 0.001
Soil 3	38.573 ± 0.010	15.677 ± 0.001	18.383 ± 0.001	2.098 ± 0.001	1.173 ± 0.001
Soil 4	38.582 ± 0.024	15.681 ± 0.007	18.387 ± 0.005	2.098 ± 0.001	1.173 ± 0.001
Soil 5	38.570 ± 0.030	15.669 ± 0.012	18.386 ± 0.007	2.098 ± 0.001	1.173 ± 0.001
Soil 6	38.599 ± 0.048	15.663 ± 0.018	18.431 ± 0.006	2.094 ± 0.001	1.177 ± 0.001
Soil 7	38.555 ± 0.011	15.673 ± 0.003	18.374 ± 0.002	2.098 ± 0.001	1.172 ± 0.001
Soil 8	38.567 ± 0.007	15.674 ± 0.004	18.379 ± 0.004	2.098 ± 0.001	1.173 ± 0.001
Soil 9	38.650 ± 0.010	15.703 ± 0.002	18.409 ± 0.001	2.100 ± 0.001	1.172 ± 0.001
Soil 10	38.502 ± 0.001	15.654 ± 0.001	18.363 ± 0.001	2.097 ± 0.001	1.173 ± 0.001
Soil 11	38.587 ± 0.001	15.684 ± 0.001	18.391 ± 0.001	2.098 ± 0.001	1.173 ± 0.001
Soil 12	38.594 ± 0.001	15.683 ± 0.001	18.426 ± 0.001	2.095 ± 0.001	1.175 ± 0.001
Soil 13	38.798 ± 0.001	15.709 ± 0.001	18.562 ± 0.001	2.090 ± 0.001	1.182 ± 0.001
Soil 14	38.676 ± 0.001	15.676 ± 0.001	18.462 ± 0.001	2.095 ± 0.001	1.178 ± 0.001
Soil 15	38.505 ± 0.001	15.650 ± 0.001	18.387 ± 0.001	2.094 ± 0.001	1.175 ± 0.001
Soil 16	38.518 ± 0.001	15.670 ± 0.001	18.354 ± 0.001	2.099 ± 0.001	1.171 ± 0.001

Soil	$^{208}Pb/^{204}Pb$	$^{207}Pb/^{204}Pb$	$^{206}Pb/^{204}Pb$	$^{208}Pb/^{206}Pb$	$^{206}Pb/^{207}Pb$
Soil 17	38.589 ± 0.001	15.686 ± 0.001	18.389 ± 0.001	2.098 ± 0.001	1.172 ± 0.001
Soil 18	38.532 ± 0.001	15.669 ± 0.001	18.377 ± 0.001	2.097 ± 0.001	1.173 ± 0.001
Soil 19	38.810 ± 0.001	15.708 ± 0.001	18.584 ± 0.001	2.088 ± 0.001	1.18 ± 0.0013
Soil 20	38.768 ± 0.001	15.709 ± 0.001	18.557 ± 0.001	2.089 ± 0.001	1.181 ± 0.001
Soil 21	38.486 ± 0.001	15.646 ± 0.001	18.408 ± 0.001	2.091 ± 0.001	1.177 ± 0.001
Soil 22	38.618 ± 0.001	15.688 ± 0.001	18.482 ± 0.001	2.089 ± 0.001	1.178 ± 0.001
Soil 23	38.545 ± 0.001	15.670 ± 0.001	18.393 ± 0.001	2.096 ± 0.001	1.174 ± 0.001
Soil 24	38.565 ± 0.001	15.676 ± 0.001	18.388 ± 0.001	2.097 ± 0.001	1.173 ± 0.001
Soil 25	38.537 ± 0.001	15.663 ± 0.001	18.403 ± 0.001	2.094 ± 0.001	1.175 ± 0.001
Soil 26	38.458 ± 0.001	15.646 ± 0.001	18.348 ± 0.001	2.096 ± 0.001	1.173 ± 0.001
Sand	$^{208}Pb/^{204}Pb$	$^{207}Pb/^{204}Pb$	$^{206}Pb/^{204}Pb$	$^{208}Pb/^{206}Pb$	$^{206}Pb/^{207}Pb$
Sand 1	38.548 ± 0.028	15.671 ± 0.004	18.379 ± 0.009	2.097 ± 0.001	1.173 ± 0.001
Sand 2	38.676 ± 0.010	15.706 ± 0.001	18.415 ± 0.001	2.100 ± 0.001	1.173 ± 0.001
Sand 3	38.570 ± 0.002	15.687 ± 0.001	18.367 ± 0.001	2.100 ± 0.001	1.171 ± 0.001
Sand 4	38.658 ± 0.010	15.702 ± 0.001	18.428 ± 0.001	2.098 ± 0.001	1.174 ± 0.001
Sand 5	38.643 ± 0.010	15.702 ± 0.001	18.389 ± 0.001	2.101 ± 0.001	1.171 ± 0.001
Sand 6	38.546 ± 0.002	15.677 ± 0.001	18.365 ± 0.001	2.099 ± 0.001	1.171 ± 0.001
Sand 7	38.529 ± 0.001	15.678 ± 0.001	18.335 ± 0.001	2.101 ± 0.001	1.170 ± 0.001
Sand 8	38.615 ± 0.001	15.708 ± 0.001	18.434 ± 0.001	2.095 ± 0.001	1.174 ± 0.001
Sand 9	38.568 ± 0.001	15.687 ± 0.001	18.398 ± 0.001	2.096 ± 0.001	1.173 ± 0.001
Sand 10	38.475 ± 0.001	15.689 ± 0.001	18.317 ± 0.001	2.100 ± 0.001	1.168 ± 0.001
Sand 11	38.537 ± 0.001	15.676 ± 0.001	18.361 ± 0.001	2.099 ± 0.001	1.171 ± 0.001
Mine waste	$^{208}Pb/^{204}Pb$	$^{207}Pb/^{204}Pb$	$^{206}Pb/^{204}Pb$	$^{208}Pb/^{206}Pb$	$^{206}Pb/^{207}Pb$
Mine waste 1	38.575 ± 0.001	15.684 ± 0.001	18.366 ± 0.001	2.103 ± 0.001	1.171 ± 0.001
Mine waste 2	38.582 ± 0.001	15.684 ± 0.001	18.373 ± 0.001	2.100 ± 0.001	1.172 ± 0.001
Mine waste 3	38.436 ± 0.002	15.642 ± 0.001	18.332 ± 0.001	2.097 ± 0.001	1.172 ± 0.001
Mine waste 4	38.548 ± 0.001	15.678 ± 0.001	18.387 ± 0.001	2.097 ± 0.001	1.173 ± 0.001
Pb-battery	$^{208}Pb/^{204}Pb$	$^{207}Pb/^{204}Pb$	$^{206}Pb/^{204}Pb$	$^{208}Pb/^{206}Pb$	$^{206}Pb/^{207}Pb$
Pb-grid a	37.886 ± 0.003	15.618 ± 0.001	17.921 ± 0.003	2.114 ± 0.001	1.147 ± 0.001
Pb-grid b	37.747 ± 0.002	15.574 ± 0.001	17.888 ± 0.002	2.110 ± 0.001	1.149 ± 0.001
Pb-grid c	37.786 ± 0.002	15.583 ± 0.001	17.909 ± 0.002	2.110 ± 0.001	1.149 ± 0.001
Pb-grid d	37.869 ± 0.013	15.593 ± 0.006	17.976 ± 0.006	2.107 ± 0.001	1.153 ± 0.001
Pb-grid e	37.804 ± 0.002	15.587 ± 0.001	17.916 ± 0.002	2.110 ± 0.001	1.149 ± 0.001
Pb-paste 1 a	37.794 ± 0.003	15.606 ± 0.001	17.827 ± 0.002	2.120 ± 0.001	1.142 ± 0.001
Pb-paste 1 b	37.633 ± 0.002	15.551 ± 0.001	17.805 ± 0.002	2.114 ± 0.001	1.145 ± 0.001
Pb-paste 1 c	37.685 ± 0.004	15.566 ± 0.001	17.822 ± 0.001	2.114 ± 0.001	1.145 ± 0.001
Pb-paste 1 d	37.814 ± 0.024	15.592 ± 0.007	17.897 ± 0.004	2.113 ± 0.001	1.148 ± 0.001
Pb-paste 1 e	37.745 ± 0.002	15.585 ± 0.001	17.834 ± 0.002	2.116 ± 0.001	1.144 ± 0.001
Pb-paste 1 f	37.717 ± 0.002	15.577 ± 0.001	17.825 ± 0.002	2.116 ± 0.001	1.144 ± 0.001
Pb-paste 2 a	37.514 ± 0.002	15.565 ± 0.001	17.650 ± 0.002	2.125 ± 0.001	1.134 ± 0.001
Pb-paste 2 b	37.451 ± 0.002	15.542 ± 0.001	17.644 ± 0.001	2.122 ± 0.001	1.135 ± 0.001
Pb-paste 2 c	37.460 ± 0.002	15.549 ± 0.001	17.634 ± 0.001	2.124 ± 0.001	1.134 ± 0.001
Pb-paste 2 d	37.586 ± 0.011	15.574 ± 0.005	17.712 ± 0.004	2.122 ± 0.001	1.137 ± 0.001
Pb-paste 2 e	37.496 ± 0.001	15.561 ± 0.001	17.640 ± 0.001	2.126 ± 0.001	1.134 ± 0.001
Pb-paste 2 f	37.408 ± 0.002	15.528 ± 0.001	17.635 ± 0.001	2.121 ± 0.001	1.136 ± 0.001
Pb-paste 3 a	37.211 ± 0.001	15.514 ± 0.001	17.376 ± 0.001	2.142 ± 0.001	1.120 ± 0.001
Pb-paste 3 b	37.189 ± 0.002	15.510 ± 0.001	17.364 ± 0.001	2.142 ± 0.001	1.120 ± 0.001

Pb-battery	$^{208}Pb/^{204}Pb$	$^{207}Pb/^{204}Pb$	$^{206}Pb/^{204}Pb$	$^{208}Pb/^{206}Pb$	$^{206}Pb/^{207}Pb$
Pb-paste 3 c	37.211 ± 0.001	15.514 ± 0.001	17.375 ± 0.001	2.142 ± 0.001	1.120 ± 0.001
Pb-paste 3 d	37.306 ± 0.025	15.535 ± 0.006	17.422 ± 0.002	2.141 ± 0.001	1.121 ± 0.001
Pb-paste 3 e	37.233 ± 0.001	15.522 ± 0.001	17.380 ± 0.001	2.142 ± 0.001	1.120 ± 0.001
Pb-paste 3 f	37.177 ± 0.001	15.501 ± 0.001	17.372 ± 0.001	2.140 ± 0.001	1.121 ± 0.001
PM_{10}	$^{208}Pb/^{204}Pb$	$^{207}Pb/^{204}Pb$	$^{206}Pb/^{204}Pb$	$^{208}Pb/^{206}Pb$	$^{206}Pb/^{207}Pb$
PM_{10}-1	38.014 ± 0.003	15.623 ± 0.001	18.015 ± 0.001	2.110 ± 0.001	1.153 ± 0.001
PM_{10}-2	38.110 ± 0.005	15.637 ± 0.002	18.079 ± 0.002	2.108 ± 0.001	1.156 ± 0.001
PM_{10}-3	38.148 ± 0.002	15.645 ± 0.001	18.078 ± 0.001	2.110 ± 0.001	1.156 ± 0.001
PM_{10}-4	38.182 ± 0.001	15.674 ± 0.001	18.035 ± 0.001	2.116 ± 0.001	1.151 ± 0.001
PM_{10}-5	38.072 ± 0.001	15.647 ± 0.001	18.007 ± 0.001	2.114 ± 0.001	1.151 ± 0.001
PM_{10}-6	38.075 ± 0.001	15.642 ± 0.001	18.023 ± 0.001	2.113 ± 0.001	1.152 ± 0.001
PM_{10}-7	38.153 ± 0.001	15.664 ± 0.001	18.042 ± 0.001	2.115 ± 0.001	1.152 ± 0.001
PM_{10}-8	38.265 ± 0.001	15.705 ± 0.001	18.052 ± 0.001	2.120 ± 0.001	1.150 ± 0.001
PM_{10}-9	38.280 ± 0.001	15.709 ± 0.001	18.038 ± 0.001	2.122 ± 0.001	1.148 ± 0.001
PM_{10}-10	37.994 ± 0.002	15.616 ± 0.001	17.969 ± 0.001	2.114 ± 0.001	1.151 ± 0.001
PM_{10}-11	37.863 ± 0.001	15.599 ± 0.001	17.928 ± 0.001	2.112 ± 0.001	1.149 ± 0.001
PM_{10}-12	37.797 ± 0.001	15.587 ± 0.001	17.890 ± 0.001	2.113 ± 0.001	1.148 ± 0.001
PM_{10}-13	37.829 ± 0.001	15.595 ± 0.001	17.911 ± 0.001	2.112 ± 0.001	1.149 ± 0.001
PM_{10}-14	37.868 ± 0.001	15.598 ± 0.001	17.935 ± 0.001	2.111 ± 0.001	1.150 ± 0.001
PM_{10}-15	37.825 ± 0.001	15.594 ± 0.001	17.898 ± 0.001	2.113 ± 0.001	1.148 ± 0.001
PM_{10}-16	37.790 ± 0.001	15.586 ± 0.001	17.889 ± 0.001	2.112 ± 0.001	1.148 ± 0.001
PM_{10}-17	37.879 ± 0.001	15.603 ± 0.001	17.948 ± 0.001	2.110 ± 0.001	1.150 ± 0.001
PM_{10}-18	37.848 ± 0.001	15.600 ± 0.001	17.918 ± 0.001	2.112 ± 0.001	1.149 ± 0.001
PM_{10}-19	37.857 ± 0.004	15.602 ± 0.002	17.913 ± 0.002	2.113 ± 0.001	1.148 ± 0.001
PM_{10}-20	37.804 ± 0.004	15.589 ± 0.001	17.887 ± 0.001	2.114 ± 0.001	1.147 ± 0.001
PM_{10}-21	37.825 ± 0.001	15.594 ± 0.001	17.896 ± 0.001	2.114 ± 0.001	1.148 ± 0.001
PM_{10}-22	37.822 ± 0.001	15.595 ± 0.001	17.887 ± 0.001	2.114 ± 0.001	1.147 ± 0.001
PM_{10}-23	37.969 ± 0.001	15.633 ± 0.001	17.952 ± 0.001	2.115 ± 0.001	1.148 ± 0.001
PM_{10}-24	37.969 ± 0.001	15.639 ± 0.001	17.943 ± 0.001	2.116 ± 0.001	1.147 ± 0.001
PM_{10}-25	38.055 ± 0.001	15.647 ± 0.001	18.006 ± 0.001	2.113 ± 0.001	1.151 ± 0.001
PM_{10}-26	37.956 ± 0.001	15.635 ± 0.001	17.929 ± 0.001	2.117 ± 0.001	1.147 ± 0.001
PM_{10}-27	37.956 ± 0.001	15.626 ± 0.001	17.956 ± 0.001	2.114 ± 0.001	1.149 ± 0.001
PM_{10}-28	37.980 ± 0.001	15.632 ± 0.001	17.959 ± 0.001	2.115 ± 0.001	1.149 ± 0.001
PM_{10}-29	37.907 ± 0.001	15.616 ± 0.001	17.929 ± 0.001	2.114 ± 0.001	1.148 ± 0.001
PM_{10}-30	37.879 ± 0.001	15.612 ± 0.001	17.911 ± 0.001	2.115 ± 0.001	1.147 ± 0.001
PM_{10}-31	37.942 ± 0.001	15.627 ± 0.001	17.939 ± 0.001	2.115 ± 0.001	1.148 ± 0.001
PM_{10}-32	37.934 ± 0.001	15.625 ± 0.001	17.939 ± 0.001	2.115 ± 0.001	1.148 ± 0.001
PM_{10}-33	37.948 ± 0.001	15.625 ± 0.001	17.946 ± 0.001	2.114 ± 0.001	1.149 ± 0.001
PM_{10}-34	37.937 ± 0.001	15.625 ± 0.001	17.937 ± 0.001	2.115 ± 0.001	1.148 ± 0.001
PM_{10}-35	37.843 ± 0.001	15.601 ± 0.001	17.899 ± 0.001	2.114 ± 0.001	1.147 ± 0.001
PM_{10}-36	37.991 ± 0.001	15.626 ± 0.001	17.979 ± 0.001	2.113 ± 0.001	1.151 ± 0.001
PM_{10}-37	37.728 ± 0.001	15.605 ± 0.001	17.785 ± 0.001	2.121 ± 0.001	1.140 ± 0.001
PM_{10}-38	37.815 ± 0.001	15.601 ± 0.001	17.871 ± 0.001	2.116 ± 0.001	1.146 ± 0.001
PM_{10}-39	37.840 ± 0.002	15.605 ± 0.001	17.874 ± 0.001	2.117 ± 0.001	1.146 ± 0.001
PM_{10}-40	37.845 ± 0.001	15.610 ± 0.001	17.873 ± 0.001	2.117 ± 0.001	1.145 ± 0.001
PM_{10}-41	37.824 ± 0.001	15.601 ± 0.001	17.874 ± 0.001	2.116 ± 0.001	1.146 ± 0.001
PM_{10}-42	37.809 ± 0.001	15.600 ± 0.001	17.862 ± 0.001	2.117 ± 0.001	1.145 ± 0.001

PM_{10}	$^{208}Pb/^{204}Pb$	$^{207}Pb/^{204}Pb$	$^{206}Pb/^{204}Pb$	$^{208}Pb/^{206}Pb$	$^{206}Pb/^{207}Pb$
PM_{10}-43	37.814 ± 0.001	15.599 ± 0.001	17.871 ± 0.001	2.116 ± 0.001	1.146 ± 0.001
PM_{10}-44	37.826 ± 0.001	15.601 ± 0.001	17.879 ± 0.001	2.116 ± 0.001	1.146 ± 0.001
PM_{10}-45	37.804 ± 0.001	15.599 ± 0.001	17.860 ± 0.001	2.117 ± 0.001	1.145 ± 0.001
PM_{10}-46	38.119 ± 0.002	15.659 ± 0.001	18.023 ± 0.001	2.115 ± 0.001	1.151 ± 0.001
PM_{10}-47	37.960 ± 0.001	15.638 ± 0.001	17.920 ± 0.001	2.118 ± 0.001	1.146 ± 0.001
PM_{10}-48	38.005 ± 0.002	15.646 ± 0.001	17.954 ± 0.001	2.117 ± 0.001	1.148 ± 0.001
PM_{10}-49	38.029 ± 0.001	15.642 ± 0.001	17.984 ± 0.001	2.115 ± 0.001	1.150 ± 0.001
PM_{10}-50	37.883 ± 0.001	15.619 ± 0.001	17.892 ± 0.001	2.117 ± 0.001	1.146 ± 0.001
PM_{10}-51	37.848 ± 0.001	15.613 ± 0.001	17.871 ± 0.001	2.118 ± 0.001	1.145 ± 0.001
PM_{10}-52	37.862 ± 0.001	15.614 ± 0.001	17.882 ± 0.001	2.117 ± 0.001	1.145 ± 0.001
PM_{10}-53	37.856 ± 0.001	15.613 ± 0.001	17.878 ± 0.001	2.117 ± 0.001	1.145 ± 0.001
PM_{10}-54	37.871 ± 0.001	15.613 ± 0.001	17.894 ± 0.001	2.116 ± 0.001	1.146 ± 0.001
PM_{10}-55	37.862 ± 0.001	15.611 ± 0.001	17.891 ± 0.001	2.116 ± 0.001	1.146 ± 0.001
PM_{10}-56	37.835 ± 0.001	15.605 ± 0.001	17.876 ± 0.001	2.116 ± 0.001	1.146 ± 0.001
PM_{10}-57	37.843 ± 0.001	15.608 ± 0.001	17.874 ± 0.001	2.117 ± 0.001	1.145 ± 0.001
PM_{10}-58	37.802 ± 0.001	15.599 ± 0.001	17.854 ± 0.001	2.117 ± 0.001	1.145 ± 0.001
PM_{10}-59	37.820 ± 0.001	15.598 ± 0.001	17.875 ± 0.001	2.116 ± 0.001	1.146 ± 0.001
PM_{10}-60	37.811 ± 0.001	15.596 ± 0.001	17.875 ± 0.001	2.115 ± 0.001	1.146 ± 0.001
PM_{10}-61	37.821 ± 0.001	15.599 ± 0.001	17.873 ± 0.001	2.116 ± 0.001	1.146 ± 0.001
PM_{10}-62	38.185 ± 0.001	15.651 ± 0.001	18.106 ± 0.001	2.109 ± 0.001	1.157 ± 0.001
PM_{10}-63	38.289 ± 0.002	15.653 ± 0.001	18.188 ± 0.001	2.105 ± 0.001	1.162 ± 0.001
PM_{10}-64	38.217 ± 0.002	15.655 ± 0.001	18.122 ± 0.001	2.109 ± 0.001	1.158 ± 0.001
PM_{10}-65	38.141 ± 0.001	15.647 ± 0.001	18.080 ± 0.001	2.110 ± 0.001	1.156 ± 0.001
PM_{10}-66	38.245 ± 0.003	15.659 ± 0.001	18.152 ± 0.001	2.107 ± 0.001	1.159 ± 0.001
PM_{10}-67	38.201 ± 0.001	15.653 ± 0.001	18.100 ± 0.001	2.110 ± 0.001	1.156 ± 0.001
PM_{10}-68	37.993 ± 0.001	15.618 ± 0.001	17.957 ± 0.001	2.116 ± 0.001	1.150 ± 0.001
PM_{10}-69	38.000 ± 0.001	15.615 ± 0.001	17.946 ± 0.001	2.117 ± 0.001	1.149 ± 0.001
PM_{10}-70	37.836 ± 0.001	15.598 ± 0.001	17.905 ± 0.001	2.113 ± 0.001	1.148 ± 0.001
PM_{10}-71	37.942 ± 0.003	15.620 ± 0.001	17.962 ± 0.001	2.112 ± 0.001	1.150 ± 0.001
PM_{10}-72	38.059 ± 0.004	15.633 ± 0.002	18.036 ± 0.002	2.110 ± 0.001	1.154 ± 0.001
PM_{10}-73	38.085 ± 0.005	15.639 ± 0.002	18.038 ± 0.002	2.111 ± 0.001	1.154 ± 0.001
PM_{10}-74	37.890 ± 0.006	15.602 ± 0.002	17.938 ± 0.002	2.112 ± 0.001	1.150 ± 0.001
PM_{10}-75	38.004 ± 0.002	15.651 ± 0.001	17.954 ± 0.001	2.117 ± 0.001	1.147 ± 0.001
PM_{10}-76	37.840 ± 0.001	15.598 ± 0.001	17.899 ± 0.001	2.114 ± 0.001	1.148 ± 0.001
PM_{10}-77	37.828 ± 0.001	15.595 ± 0.001	17.889 ± 0.001	2.115 ± 0.001	1.147 ± 0.001
PM_{10}-78	38.159 ± 0.001	15.652 ± 0.001	18.084 ± 0.001	2.110 ± 0.001	1.155 ± 0.001
PM_{10}-79	38.148 ± 0.002	15.650 ± 0.001	18.073 ± 0.001	2.111 ± 0.001	1.155 ± 0.001
PM_{10}-80	38.094 ± 0.003	15.644 ± 0.001	18.043 ± 0.001	2.111 ± 0.001	1.153 ± 0.001
PM_{10}-81	37.875 ± 0.006	15.615 ± 0.001	17.877 ± 0.005	2.118 ± 0.001	1.145 ± 0.001
PM_{10}-82	37.747 ± 0.007	15.600 ± 0.001	17.775 ± 0.006	2.124 ± 0.001	1.139 ± 0.001
PM_{10}-83	37.988 ± 0.002	15.610 ± 0.001	17.960 ± 0.002	2.120 ± 0.001	1.149 ± 0.001
PM_{10}-84	38.080 ± 0.001	15.646 ± 0.001	17.966 ± 0.001	2.120 ± 0.001	1.148 ± 0.001
PM_{10}-85	38.061 ± 0.001	15.635 ± 0.001	17.962 ± 0.001	2.119 ± 0.001	1.149 ± 0.001
PM_{10}-86	37.918 ± 0.007	15.598 ± 0.002	17.987 ± 0.002	2.108 ± 0.001	1.153 ± 0.001
PM_{10}-87	38.208 ± 0.004	15.661 ± 0.001	18.124 ± 0.001	2.108 ± 0.001	1.157 ± 0.001
PM_{10}-88	38.210 ± 0.002	15.662 ± 0.001	18.105 ± 0.001	2.110 ± 0.001	1.156 ± 0.001
PM_{10}-89	38.187 ± 0.005	15.661 ± 0.002	18.102 ± 0.002	2.109 ± 0.001	1.156 ± 0.001

PM_{10}	$^{208}Pb/^{204}Pb$	$^{207}Pb/^{204}Pb$	$^{206}Pb/^{204}Pb$	$^{208}Pb/^{206}Pb$	$^{206}Pb/^{207}Pb$
PM_{10}-90	38.137 ± 0.006	15.664 ± 0.002	18.031 ± 0.002	2.115 ± 0.001	1.151 ± 0.001
PM_{10}-91	37.936 ± 0.004	15.627 ± 0.001	17.941 ± 0.002	2.115 ± 0.001	1.148 ± 0.001
PM_{10}-92	37.834 ± 0.001	15.598 ± 0.001	17.894 ± 0.001	2.114 ± 0.001	1.147 ± 0.001
PM_{10}-93	37.851 ± 0.001	15.599 ± 0.001	17.902 ± 0.001	2.114 ± 0.001	1.148 ± 0.001
PM_{10}-94	38.164 ± 0.002	15.646 ± 0.001	18.104 ± 0.001	2.108 ± 0.001	1.157 ± 0.001
PM_{10}-95	38.024 ± 0.003	15.633 ± 0.001	18.001 ± 0.001	2.112 ± 0.001	1.152 ± 0.001
PM_{10}-96	38.007 ± 0.003	15.622 ± 0.001	17.995 ± 0.001	2.112 ± 0.001	1.152 ± 0.001
PM_{10}-97	37.999 ± 0.002	15.630 ± 0.001	17.982 ± 0.001	2.113 ± 0.001	1.150 ± 0.001
PM_{10}-98	37.975 ± 0.003	15.618 ± 0.001	17.991 ± 0.001	2.111 ± 0.001	1.152 ± 0.001
PM_{10}-99	38.113 ± 0.004	15.642 ± 0.002	18.052 ± 0.002	2.111 ± 0.001	1.154 ± 0.001
PM_{10}-100	38.149 ± 0.003	15.636 ± 0.001	18.120 ± 0.001	2.106 ± 0.001	1.159 ± 0.001
PM_{10}-101	38.284 ± 0.004	15.671 ± 0.001	18.152 ± 0.002	2.109 ± 0.001	1.158 ± 0.001
PM_{10}-102	38.087 ± 0.004	15.640 ± 0.001	18.027 ± 0.001	2.113 ± 0.001	1.153 ± 0.001
PM_{10}-103	37.802 ± 0.005	15.588 ± 0.002	17.892 ± 0.002	2.113 ± 0.001	1.148 ± 0.001
PM_{10}-104	37.835 ± 0.001	15.596 ± 0.001	17.898 ± 0.001	2.114 ± 0.001	1.148 ± 0.001
PM_{10}-105	37.841 ± 0.001	15.597 ± 0.001	17.897 ± 0.001	2.114 ± 0.001	1.147 ± 0.001
PM_{10}-106	38.025 ± 0.005	15.640 ± 0.002	18.009 ± 0.002	2.111 ± 0.001	1.152 ± 0.001
PM_{10}-107	38.058 ± 0.004	15.641 ± 0.001	18.029 ± 0.001	2.111 ± 0.001	1.153 ± 0.001
PM_{10}-108	37.945 ± 0.005	15.613 ± 0.002	18.001 ± 0.001	2.108 ± 0.001	1.153 ± 0.001
PM_{10}-109	38.070 ± 0.004	15.647 ± 0.001	18.074 ± 0.001	2.106 ± 0.001	1.155 ± 0.001
PM_{10}-110	38.246 ± 0.004	15.670 ± 0.001	18.184 ± 0.001	2.103 ± 0.001	1.160 ± 0.001
PM_{10}-111	37.984 ± 0.003	15.627 ± 0.001	17.983 ± 0.001	2.112 ± 0.001	1.151 ± 0.001
PM_{10}-112	38.017 ± 0.005	15.631 ± 0.002	17.995 ± 0.002	2.113 ± 0.001	1.151 ± 0.001
PM_{10}-113	37.994 ± 0.006	15.632 ± 0.002	17.952 ± 0.002	2.116 ± 0.001	1.149 ± 0.001
PM_{10}-114	37.833 ± 0.001	15.597 ± 0.001	17.898 ± 0.001	2.114 ± 0.001	1.148 ± 0.001
PM_{10}-115	37.846 ± 0.001	15.595 ± 0.001	17.908 ± 0.001	2.113 ± 0.001	1.148 ± 0.001
$PM_{2.5}$	$^{208}Pb/^{204}Pb$	$^{207}Pb/^{204}Pb$	$^{206}Pb/^{204}Pb$	$^{208}Pb/^{206}Pb$	$^{206}Pb/^{207}Pb$
$PM_{2.5}$-1	38.238 ± 0.003	15.665 ± 0.001	18.170 ± 0.001	2.104 ± 0.001	1.160 ± 0.001
$PM_{2.5}$-2	38.076 ± 0.006	15.649 ± 0.002	17.986 ± 0.002	2.117 ± 0.001	1.149 ± 0.001
$PM_{2.5}$-3	38.006 ± 0.002	15.629 ± 0.001	17.998 ± 0.001	2.112 ± 0.001	1.152 ± 0.001
$PM_{2.5}$-4	37.949 ± 0.002	15.615 ± 0.001	17.968 ± 0.001	2.112 ± 0.001	1.151 ± 0.001
$PM_{2.5}$-5	38.032 ± 0.003	15.639 ± 0.001	17.983 ± 0.001	2.115 ± 0.001	1.150 ± 0.001
$PM_{2.5}$-6	38.039 ± 0.003	15.633 ± 0.001	18.013 ± 0.001	2.112 ± 0.001	1.152 ± 0.001
$PM_{2.5}$-7	38.191 ± 0.005	15.652 ± 0.002	18.115 ± 0.002	2.108 ± 0.001	1.157 ± 0.001
$PM_{2.5}$-8	38.139 ± 0.004	15.638 ± 0.002	18.099 ± 0.002	2.107 ± 0.001	1.157 ± 0.001
$PM_{2.5}$-9	38.103 ± 0.005	15.641 ± 0.002	18.049 ± 0.002	2.111 ± 0.001	1.154 ± 0.001
$PM_{2.5}$-10	37.951 ± 0.004	15.626 ± 0.001	17.943 ± 0.001	2.115 ± 0.001	1.148 ± 0.001
$PM_{2.5}$-11	37.963 ± 0.004	15.629 ± 0.001	17.939 ± 0.001	2.116 ± 0.001	1.148 ± 0.001
$PM_{2.5}$-12	37.913 ± 0.003	15.612 ± 0.001	17.933 ± 0.001	2.114 ± 0.001	1.149 ± 0.001
Road dust	$^{208}Pb/^{204}Pb$	$^{207}Pb/^{204}Pb$	$^{206}Pb/^{204}Pb$	$^{208}Pb/^{206}Pb$	$^{206}Pb/^{207}Pb$
RD-1	38.517 ± 0.001	15.665 ± 0.001	18.372 ± 0.001	2.096 ± 0.001	1.173 ± 0.001
RD-2	38.534 ± 0.001	15.670 ± 0.001	18.379 ± 0.001	2.097 ± 0.001	1.173 ± 0.001
RD-3	38.550 ± 0.001	15.671 ± 0.001	18.393 ± 0.001	2.096 ± 0.001	1.174 ± 0.001
Wulfenite*	$^{208}Pb/^{204}Pb$	$^{207}Pb/^{204}Pb$	$^{206}Pb/^{204}Pb$	$^{208}Pb/^{206}Pb$	$^{206}Pb/^{207}Pb$
W1	38.542 ± 0.065	15.670 ± 0.020	18.366 ± 0.016	2.099 ± 0.002	1.172 ± 0.001
W3	38.456 ± 0.014	15.644 ± 0.005	18.344 ± 0.004	2.096 ± 0.001	1.173 ± 0.001
W3	38.559 ± 0.045	15.676 ± 0.015	18.373 ± 0.012	2.099 ± 0.001	1.172 ± 0.001

Wulfenite*	$^{208}Pb/^{204}Pb$	$^{207}Pb/^{204}Pb$	$^{206}Pb/^{204}Pb$	$^{208}Pb/^{206}Pb$	$^{206}Pb/^{207}Pb$
W4	38.502 ± 0.004	15.657 ± 0.001	18.354 ± 0.001	2.098 ± 0.004	1.172 ± 0.001
W5	38.565 ± 0.020	15.676 ± 0.006	18.371 ± 0.005	2.099 ± 0.001	1.172 ± 0.001
W6	38.574 ± 0.026	15.679 ± 0.008	18.374 ± 0.006	2.099 ± 0.001	1.172 ± 0.001
W7	38.567 ± 0.018	15.677 ± 0.006	18.371 ± 0.004	2.099 ± 0.001	1.172 ± 0.001
W8	38.561 ± 0.028	15.675 ± 0.008	18.370 ± 0.007	2.099 ± 0.001	1.172 ± 0.001
W9	38.569 ± 0.031	15.677 ± 0.009	18.372 ± 0.007	2.099 ± 0.001	1.172 ± 0.001
Galenite*	$^{208}Pb/^{204}Pb$	$^{207}Pb/^{204}Pb$	$^{206}Pb/^{204}Pb$	$^{208}Pb/^{206}Pb$	$^{206}Pb/^{207}Pb$
G1	38.360 ± 0.001	15.614 ± 0.001	18.318 ± 0.001	2.094 ± 0.001	1.173 ± 0.001
G2	38.560 ± 0.035	15.674 ± 0.011	38.368 ± 0.009	2.099 ± 0.001	1.172 ± 0.001
G3	38.555 ± 0.040	15.675 ± 0.012	18.374 ± 0.011	2.098 ± 0.001	1.172 ± 0.001
G4	38.562 ± 0.030	15.676 ± 0.009	18.375 ± 0.007	2.099 ± 0.001	1.172 ± 0.001
G5	38.564 ± 0.026	15.677 ± 0.009	18.377 ± 0.006	2.098 ± 0.001	1.172 ± 0.001
G6	38.488 ± 0.046	15.682 ± 0.014	18.216 ± 0.010	2.113 ± 0.001	1.162 ± 0.001
G7	38.443 ± 0.004	15.668 ± 0.001	18.205 ± 0.001	2.112 ± 0.001	1.162 ± 0.001
G8	38.474 ± 0.040	15.678 ± 0.013	18.213 ± 0.009	2.112 ± 0.001	1.162 ± 0.001
G9	38.486 ± 0.055	15.682 ± 0.018	18.216 ± 0.013	2.113 ± 0.001	1162 ± 0.001
G10	38.489 ± 0.053	15.683 ± 0.017	18.217 ± 0.012	2.113 ± 0.002	1.162 ± 0.001
Sphalerite*	$^{208}Pb/^{204}Pb$	$^{207}Pb/^{204}Pb$	$^{206}Pb/^{204}Pb$	$^{208}Pb/^{206}Pb$	$^{206}Pb/^{207}Pb$
Sp1	38.530 ± 0.001	15.667 ± 0.001	18.362 ± 0.001	2.098 ± 0.001	1.172 ± 0.001
Slate*	$^{208}Pb/^{204}Pb$	$^{207}Pb/^{204}Pb$	$^{206}Pb/^{204}Pb$	$^{208}Pb/^{206}Pb$	$^{206}Pb/^{207}Pb$
Sl1	38.515 ± 0.003	15.625 ± 0.001	18.431 ± 0.002	2.090 ± 0.001	1.180 ± 0.001
Sl2	38.516 ± 0.001	15.626 ± 0.001	18.429 ± 0.001	2.090 ± 0.001	1.179 ± 0.001
Andesite*	$^{208}Pb/^{204}Pb$	$^{207}Pb/^{204}Pb$	$^{206}Pb/^{204}Pb$	$^{208}Pb/^{206}Pb$	$^{206}Pb/^{207}Pb$
A1	38.642 ± 0.100	15.620 ± 0.062	18.438 ± 0.049	2.096 ± 0.002	1.181 ± 0.004
A2	38.593 ± 0.105	15.566 ± 0.074	18.433 ± 0.103	2.094 ± 0.002	1.184 ± 0.004
Basalt*	$^{208}Pb/^{204}Pb$	$^{207}Pb/^{204}Pb$	$^{206}Pb/^{204}Pb$	$^{208}Pb/^{206}Pb$	$^{206}Pb/^{207}Pb$
B1	39.061 ± 0.085	15.749 ± 0.017	18.825 ± 0.093	2.075 ± 0.006	1.195 ± 0.007
B2	39.030 ± 0.100	15.770 ± 0.083	18.651 ± 0.086	2.093 ± 0.019	1.183 ± 0.014

*Personal communication (Rogan Šmuc et al., 2025)

A.8 Time Scan for Zn and Pb Signal Obtained by spICP-MS in the ERM-CZ120 Suspensions

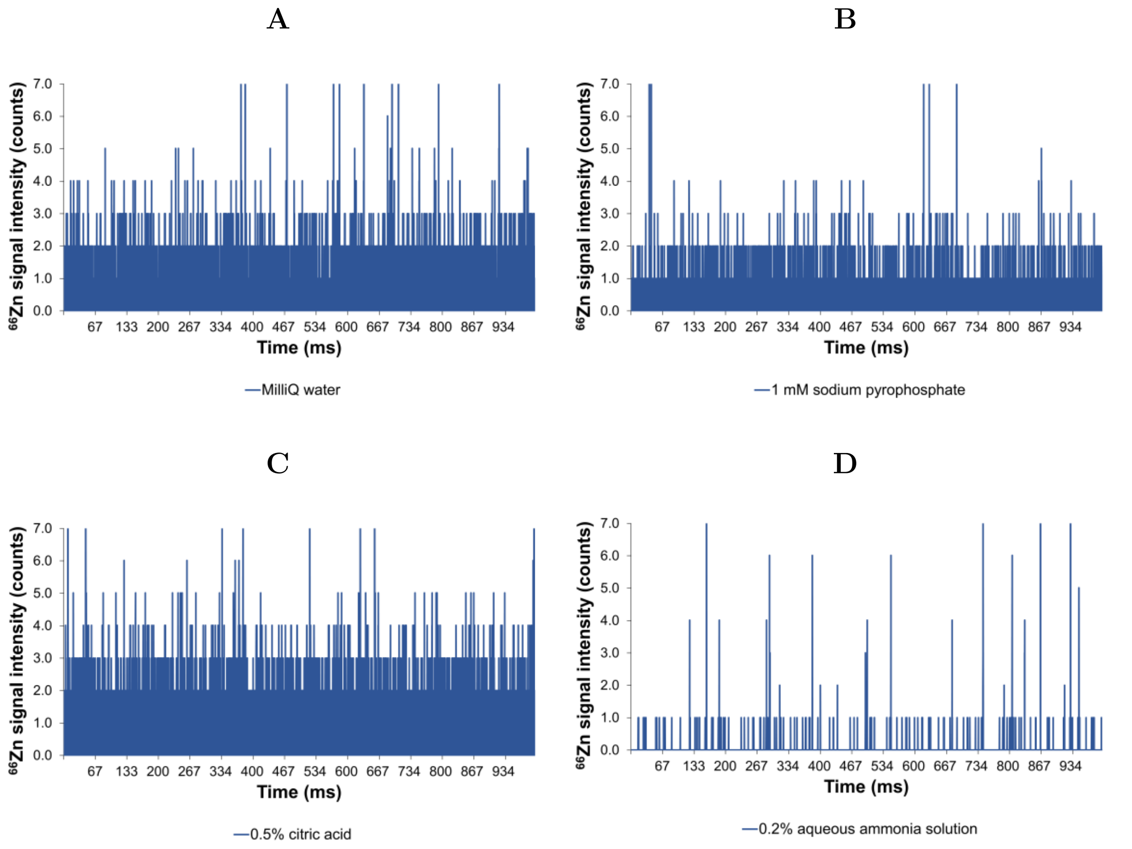

Figure A.1: Time scan for Zn signal obtained by spICP-MS in the ERM-CZ120 suspended in A) MilliQ water, B) 1 mM sodium pyrophosphate, C) 0.5 % citric acid, and D) 0.2 % aqueous ammonia solution.

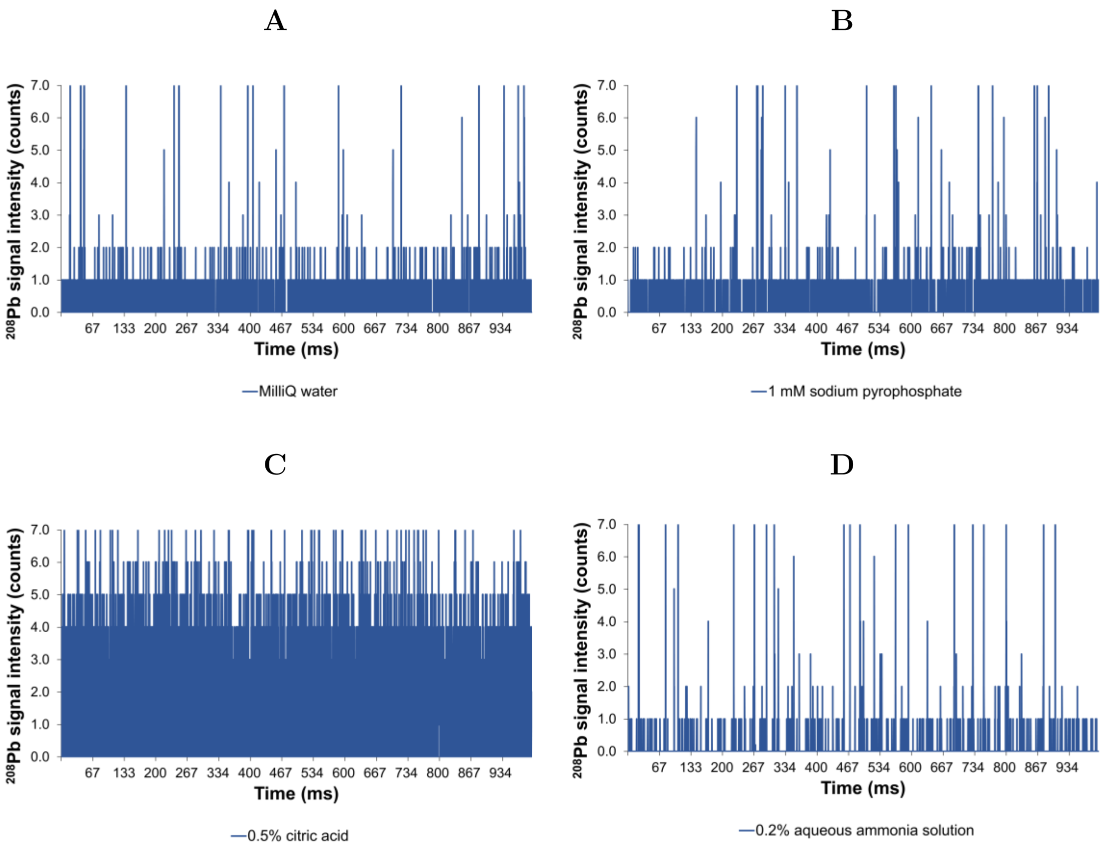

Figure A.2: Time scan for Pb signal obtained by spICP-MS in the ERM-CZ120 suspended in A) MilliQ water, B) 1 mM sodium pyrophosphate, C) 0.5 % citric acid, and D) 0.2 % aqueous ammonia solution.

References

Apte, J. S., Marshall, J. D., Cohen, A. J., & Brauer, M. (2015). Addressing Global Mortality from Ambient PM $_{2.5}$. *Environmental Science & Technology*, *49*(13), 8057–8066. https://doi.org/10.1021/acs.est.5b01236

Astray, B., Šípková, A., Baragaño, D., Pechar, J., Krejci, R., Komárek, M., & Chrastný, V. (2024). Measuring Pb isotope ratios in fresh snow filtrate refines the apportioning of contaminant sources in the Arctic. *Environmental Pollution*, *345*, 123457. https://doi.org/10.1016/j.envpol.2024.123457

Avramescu, M.-L., Casey, K., Levesque, C., Chen, J., Wiseman, C., & Beauchemin, S. (2024). Identification and quantification of trace metal(loid)s in water-extractable road dust nanoparticles using SP-ICP-MS. *Science of The Total Environment*, *924*, 171720. https://doi.org/10.1016/j.scitotenv.2024.171720

Baur, S., Reemtsma, T., Stärk, H.-J., & Wagner, S. (2020). Surfactant assisted extraction of incidental nanoparticles from road runoff sediment and their characterization by single particle-ICP-MS. *Chemosphere*, *246*, 125765. https://doi.org/10.1016/j.chemosphere.2019.125765

Bavec, Š., Čeru, T., Kirinčič, S., Ivartnik, M., Golja, V., Turšič, J., Teran, K., & Miler, M. (2025). Interdisciplinary Assessment of Children's Lead Exposure in Residential Areas Degraded by Mining (Upper Meža Valley, Slovenia). *Exposure and Health*. https://doi.org/10.1007/s12403-025-00716-1

Beane, S. J., Comber, S. D. W., Rieuwerts, J., & Long, P. (2016). Abandoned metal mines and their impact on receiving waters: A case study from Southwest England. *Chemosphere*, *153*, 294–306. https://doi.org/10.1016/j.chemosphere.2016.03.022

Bec, D., Ciglenečki, D., Dolšak Lavrič, P., Gjerek, M., Koleša, T., Logar, M., Matavž, L., Murovec, M., Rus, M., & Žabkar, R. (2022). *Kakovost zraka v Sloveniji v letu 2021*. ARSO.

Beeston, M. P., Teun Van Elteren, J., Simon Šelih, V., & Fairhurst, R. (2010). Characterization of artificially generated PbS aerosols and their use within a respiratory bioaccessibility test. *The Analyst*, *135*(2), 351–357. https://doi.org/10.1039/B910429A

Beritić, T. (1952). *Izveštaj o terenskem istraživanju u rudniku i topionici olova u Mežicama*. Zagreb, Institut za higienu rada Jugoslovanske akademije znanosti i umetnosti.

Bing-Quan, Z., Yu-Wei, C., & Jian-Hua, P. (2001). Lead isotope geochemistry of the urban environment in the Pearl River Delta. *Applied Geochemistry*, *16*(4), 409–417. https://doi.org/10.1016/S0883-2927(00)00047-0

Bland, G. D., Battifarano, M., Liu, Q., Yang, X., Lu, D., Jiang, G., & Lowry, G. V. (2023). Single-Particle Metal Fingerprint Analysis and Machine Learning Pipeline for Source Apportionment of Metal-Containing Fine Particles in Air. *Environmental Science & Technology Letters*, *10*(11), 1023–1029. https://doi.org/10.1021/acs.estlett.2c00835

Bobnek Štaher, T. (2017). *Spremembe stanja okolja v Zgornji Mežiški dolini od 90. Let do danes in mnenje prbivalcev* [Magistrsko delo]. Univerza na Primorskem, Fakulteta za humanistične študije.

Bodor, K., Micheu, M. M., Keresztesi, Á., Birsan, M.-V., Nita, I.-A., Bodor, Z., Petres, S., Korodi, A., & Szép, R. (2021). Effects of PM10 and Weather on Respiratory and Cardiovascular Diseases in the Ciuc Basin (Romanian Carpathians). *Atmosphere*, *12*(2), 289. https://doi.org/10.3390/atmos12020289

Bolea, E., Jimenez, M. S., Perez-Arantegui, J., Vidal, J. C., Bakir, M., Ben-Jeddou, K., Gimenez-Ingalaturre, A. C., Ojeda, D., Trujillo, C., & Laborda, F. (2021). Analytical applications of single particle inductively coupled plasma mass spectrometry: A comprehensive and critical review. *Analytical Methods*, *13*(25), 2742–2795. https://doi.org/10.1039/D1AY00761K

Bollhöfer, A., & Rosman, K. J. R. (2001). Isotopic source signatures for atmospheric lead: The Northern Hemisphere. *Geochimica et Cosmochimica Acta*, *65*(11), 1727–1740. https://doi.org/10.1016/S0016-7037(00)00630-X

Cen, T., Torrent, L., Testino, A., & Ludwig, C. (2024). Rotating disk diluter hyphenated with single particle ICP-MS as an online dilution and sampling platform for metallic nanoparticles characterization in ambient aerosol. *Journal of Aerosol Science*, *175*, 106283. https://doi.org/10.1016/j.jaerosci.2023.106283

Cesari, D., Contini, D., Genga, A., Siciliano, M., Elefante, C., Baglivi, F., & Daniele, L. (2012). Analysis of raw soils and their re-suspended PM10 fractions: Characterisation of source profiles and enrichment factors. *Applied Geochemistry*, *27*(6), 1238–1246. https://doi.org/10.1016/j.apgeochem.2012.02.029

Chatoutsidou, S. E., & Lazaridis, M. (2022). Mass concentrations and elemental analysis of PM2.5 and PM10 in a coastal Mediterranean site: A holistic approach to identify contributing sources and varying factors. *Science of The Total Environment*, *838*, 155980. https://doi.org/10.1016/j.scitotenv.2022.155980

Chifflet, S., Amouroux, D., Bérail, S., Barre, J., Van, T. C., Baltrons, O., Brune, J., Dufour, A., Guinot, B., & Mari, X. (2018). Origins and discrimination between local and regional atmospheric pollution in Haiphong (Vietnam), based on metal(loid) concentrations and lead isotopic ratios in PM10. *Environmental Science and Pollution Research*, *25*(26), 26653–26668. https://doi.org/10.1007/s11356-018-2722-7

Chrastný, V., Šillerová, H., Vítková, M., Francová, A., Jehlička, J., Kocourková, J., Aspholm, P. E., Nilsson, L. O., Berglen, T. F., Jensen, H. K. B., & Komárek, M. (2018). Unleaded gasoline as a significant source of Pb emissions in the Subarctic. *Chemosphere*, *193*, 230–236. https://doi.org/10.1016/j.chemosphere.2017.11.031

Csavina, J., Field, J., Taylor, M. P., Gao, S., Landázuri, A., Betterton, E. A., & Sáez, A. E. (2012). A review on the importance of metals and metalloids in atmospheric dust and aerosol from mining operations. *Science of The Total Environment*, *433*, 58–73. https://doi.org/10.1016/j.scitotenv.2012.06.013

De Muynck, D., Cloquet, C., & Vanhaecke, F. (2008). Development of a new method for Pb isotopic analysis of archaeological artefacts using single-collector ICP-dynamic reaction cell-MS. *J. Anal. At. Spectrom.*, *23*(1), 62–71. https://doi.org/10.1039/B709461B

Degueldre, C., & Favarger, P.-Y. (2003). Colloid analysis by single particle inductively coupled plasma-mass spectroscopy: A feasibility study. *Colloids and Surfaces A: Physicochemical and Engineering Aspects*, *217*(1–3), 137–142. https://doi.org/10.1016/S0927-7757(02)00568-X

Degueldre, C., & Favarger, P.-Y. (2004). Thorium colloid analysis by single particle inductively coupled plasma-mass spectrometry. *Talanta*, *62*(5), 1051–1054. https://doi.org/10.1016/j.talanta.2003.10.016

Degueldre, C., Favarger, P.-Y., & Bitea, C. (2004). Zirconia colloid analysis by single particle inductively coupled plasma–mass spectrometry. *Analytica Chimica Acta*, *518*(1–2), 137–142. https://doi.org/10.1016/j.aca.2004.04.015

Degueldre, C., Favarger, P.-Y., Rossé, R., & Wold, S. (2006). Uranium colloid analysis by single particle inductively coupled plasma-mass spectrometry. *Talanta*, *68*(3), 623–628. https://doi.org/10.1016/j.talanta.2005.05.006

Degueldre, C., Favarger, P.-Y., & Wold, S. (2006). Gold colloid analysis by inductively coupled plasma-mass spectrometry in a single particle mode. *Analytica Chimica Acta*, *555*(2), 263–268. https://doi.org/10.1016/j.aca.2005.09.021

Dewan, N., Majestic, B. J., Ketterer, M. E., Miller-Schulze, J. P., Shafer, M. M., Schauer, J. J., Solomon, P. A., Artamonova, M., Chen, B. B., Imashev, S. A., & Carmichael, G. R. (2015). Stable isotopes of lead and strontium as tracers of sources of airborne particulate matter in Kyrgyzstan. *Atmospheric Environment*, *120*, 438–446. https://doi.org/10.1016/j.atmosenv.2015.09.017

Directive 2008/50/EC of the European Parliament and of the Council of 21 May 2008 on ambient air quality and cleaner air for Europe. (2008). European Union.

Directive 2008/105/EC of the European Parliament and of the Council of 16 December 2008. (2008). European Union. https://doi.org/10.1007/978-1-137-54482-7_26

Dong, S., Ochoa Gonzalez, R., Harrison, R. M., Green, D., North, R., Fowler, G., & Weiss, D. (2017). Isotopic signatures suggest important contributions from recycled gasoline, road dust and non-exhaust traffic sources for copper, zinc and lead in PM10 in London, United Kingdom. *Atmospheric Environment*, *165*, 88–98. https://doi.org/10.1016/j.atmosenv.2017.06.020

Doufexi, M., Gamvroula, D. E., & Alexakis, D. E. (2022). Elements' Content in Stream Sediment and Wildfire Ash of Suburban Areas in West Attica (Greece). *Water*, *14*(3), 310. https://doi.org/10.3390/w14030310

EN 14902 Ambient air quality. Standard method for the measurement of Pb, Cd, As, and Ni in the PM10 fraction of suspended particulate matter. (2005).

Enamorado-Báez, S. M., Gómez-Guzmán, J. M., Chamizo, E., & Abril, J. M. (2015). Levels of 25 trace elements in high-volume air filter samples from Seville (2001–2002): Sources, enrichment factors and temporal variations. *Atmospheric Research*, *155*, 118–129. https://doi.org/10.1016/j.atmosres.2014.12.005

Epova, E. N., Bérail, S., Séby, F., Barre, J. P. G., Vacchina, V., Médina, B., Sarthou, L., & Donard, O. F. X. (2020). Potential of lead elemental and isotopic signatures for authenticity and geographical origin of Bordeaux wines. *Food Chemistry*, *303*, 125277. https://doi.org/10.1016/j.foodchem.2019.125277

Erel, Y., Dubowski, Y., Halicz, L., Erez, J., & Kaufman, A. (2001). Lead Concentrations and Isotopic Ratios in the Sediments of the Sea of Galilee. *Environmental Science & Technology*, *35*(2), 292–299. https://doi.org/10.1021/es0013172

Essien, J. P., Antai, S. P., & Olajire, A. A. (2009). Distribution, Seasonal Variations and Ecotoxicological Significance of Heavy Metals in Sediments of Cross River Estuary Mangrove Swamp. *Water, Air, and Soil Pollution*, *197*(1–4), 91–105. https://doi.org/10.1007/s11270-008-9793-x

Ettler, V. (2016). Soil contamination near non-ferrous metal smelters: A review. *Applied Geochemistry*, *64*, 56–74. https://doi.org/10.1016/j.apgeochem.2015.09.020

Ettler, V., Mihaljevic, M., & Komárek, M. (2004). ICP-MS measurements of lead isotopic ratios in soils heavily contaminated by lead smelting: Tracing the sources of pollution. *Analytical and Bioanalytical Chemistry*, *378*(2), 311–317. https://doi.org/10.1007/s00216-003-2229-y

European communities environmental objectives (surface waters) regulations 2009. (2009). European Union.

European Environment Agency Glossary. (2025). https://www.eea.europa.eu/help/glossary/eea-glossary

Evans, J. A., Pashley, V., Richards, G. J., Brereton, N., & Knowles, T. G. (2015). Geogenic lead isotope signatures from meat products in Great Britain: Potential for use in food authentication and supply chain traceability. *Science of The Total Environment*, *537*, 447–452. https://doi.org/10.1016/j.scitotenv.2015.07.133

Félix, O. I., Csavina, J., Field, J., Rine, K. P., Sáez, A. E., & Betterton, E. A. (2015). Use of lead isotopes to identify sources of metal and metalloid contaminants in atmospheric aerosol from mining operations. *Chemosphere*, *122*, 219–226. https://doi.org/10.1016/j.chemosphere.2014.11.057

Finzgar, N., Jez, E., Voglar, D., & Lestan, D. (2014). Spatial distribution of metal contamination before and after remediation in the Meza Valley, Slovenia. *Geoderma*, *217–218*, 135–143. https://doi.org/10.1016/j.geoderma.2013.11.011

Folens, K., Van Acker, T., Bolea-Fernandez, E., Cornelis, G., Vanhaecke, F., Du Laing, G., & Rauch, S. (2018). Identification of platinum nanoparticles in road dust leachate by single particle inductively coupled plasma-mass spectrometry. *Science of The Total Environment*, *615*, 849–856. https://doi.org/10.1016/j.scitotenv.2017.09.285

Fréchette-Viens, L., Hadioui, M., & Wilkinson, K. J. (2017). Practical limitations of single particle ICP-MS in the determination of nanoparticle size distributions and dissolution: Case of rare earth oxides. *Talanta*, *163*, 121–126. https://doi.org/10.1016/j.talanta.2016.10.093

Fugaš, M. (1977). *Biological significance of some metals as air pollutants. Part I Lead. Environmental health effects research series EPA-600/1-77-041*. Research Triangle Park, US Environmental Protection Agency.

Fux, J., & Gosar, M. (2007). Lead and other heavy metals in stream sediments in the area of Meža valley. *Geologija*, *50*(2), 347–360. https://doi.org/10.5474/geologija.2007.025

Gaillardet, J., Viers, J., & Dupré, B. (2003). 5.09—Trace Elements in River Waters. In H. D. Holland & K. K. Turekian (Eds.), *Treatise on Geochemistry* (pp. 225–272). Pergamon. https://doi.org/10.1016/B0-08-043751-6/05165-3

Gassama, N., Curie, F., Vanhooydonck, P., Bourrain, X., & Widory, D. (2021). Determining the Regional Geochemical Background for Dissolved Trace Metals and Metalloids in Stream Waters: Protocol, Results and Limitations—The Upper Loire River Basin (France). *Water*, *13*(13), 1845. https://doi.org/10.3390/w13131845

Gioia, S. M. C. L., Babinski, M., Weiss, D. J., Spiro, B., Kerr, A. A. F. S., Veríssimo, T. G., Ruiz, I., & Prates, J. C. M. (2017). An isotopic study of atmospheric lead in a megacity after phasing out of leaded gasoline. *Atmospheric Environment*, *149*, 70–83. https://doi.org/10.1016/j.atmosenv.2016.10.049

Gómez-Pertusa, C., García-Poyo, M. C., Grindlay, G., Pedraza, R., Yáñez, M. A., & Gras, L. (2024). Determination of metallic nanoparticles in soils by means spICP-MS after a microwave-assisted extraction treatment. *Talanta*, *272*, 125742. https://doi.org/10.1016/j.talanta.2024.125742

Goodman, A. J., & Ranville, J. F. (2023). Single particle inductively coupled plasma mass spectrometry: A new method to detect geochemical anomalies in stream sediments. *Journal of Geochemical Exploration*, *251*, 107231. https://doi.org/10.1016/j.gexplo.2023.107231

Gošar, D., Costa, M. R., Ferreira, A., & Štrucl, S. F. (2015). Assessment of past and present water quality in closed Mežica Pb-Zn Mine (Slovenia). *Comunicações Geológicas*, *102*(1), 65–69.

Gosar, M., & Miler, M. (2011). Anthropogenic metal loads and their sources in stream sediments of the Meža River catchment area (NE Slovenia). *Applied Geochemistry*, *26*(11), 1855–1866. https://doi.org/10.1016/j.apgeochem.2011.06.009

Graney, J. R., Edgerton, E. S., & Landis, M. S. (2019). Using Pb isotope ratios of particulate matter and epiphytic lichens from the Athabasca Oil Sands Region in Alberta, Canada to quantify local, regional, and global Pb source contributions. *Science of The Total Environment*, *654*, 1293–1304. https://doi.org/10.1016/j.scitotenv.2018.11.047

Gray, J. E., Pribil, M. J., Van Metre, P. C., Borrok, D. M., & Thapalia, A. (2013). Identification of contamination in a lake sediment core using Hg and Pb isotopic compositions, Lake Ballinger, Washington, USA. *Applied Geochemistry*, *29*, 1–12. https://doi.org/10.1016/j.apgeochem.2012.12.001

Gregorač, F. (1965). Bogatenje Mežiške rude. 300 let mežiških rudnikov. *Društvo Rudarjev, Metalurgov in Geologov Mežica*, 167–180.

Griffiths, A., Packman, H., Leung, Y.-L., Coles, B. J., Kreissig, K., Little, S. H., Van De Flierdt, T., & Rehkämper, M. (2020). Evaluation of Optimized Procedures for High-Precision Lead Isotope Analyses of Seawater by Multiple Collector Inductively Coupled Plasma Mass Spectrometry. *Analytical Chemistry*, *92*(16), 11232–11241. https://doi.org/10.1021/acs.analchem.0c01780

Hao, Y., Meng, X., Yu, X., Lei, M., Li, W., Shi, F., Yang, W., Zhang, S., & Xie, S. (2018). Characteristics of trace elements in PM2.5 and PM10 of Chifeng, northeast China: Insights into spatiotemporal variations and sources. *Atmospheric Research*, *213*, 550–561. https://doi.org/10.1016/j.atmosres.2018.07.006

Honda, M. (2021). Multielement quantification and Pb isotope analysis of the certified reference material ERM-CZ120 for fine particulate matter. *GEOCHEMICAL JOURNAL*, *55*(6), 355–371. https://doi.org/10.2343/geochemj.2.0642

Hu, X., Sun, Y., Ding, Z., Zhang, Y., Wu, J., Lian, H., & Wang, T. (2014). Lead contamination and transfer in urban environmental compartments analyzed by lead levels and isotopic compositions. *Environmental Pollution*, *187*, 42–48. https://doi.org/10.1016/j.envpol.2013.12.025

Irrgeher, J., & Prohaska, T. (2016). Application of non-traditional stable isotopes in analytical ecogeochemistry assessed by MC ICP-MS - A critical review. *Analytical and Bioanalytical Chemistry*, *408*(2), 369–385. https://doi.org/10.1007/s00216-015-9025-3

Ivartnik, M., Pavlič, H., Hudopisk, N., Simetinger, M., Ploder, J., Hočevar, B., Pogorevc, N., Kajnih, N., Glavica, V., & Ferlin, I. (2022). *Poročilo o izvajanju programa ukrepov za izboljšanje kakovosti okolja v Zgornji Mežiški dolini za leto 2022*. NIJZ OE Ravne.

Ivartnik, M., Pavlič, H., Hudopisk, N., Simetinger, M., Ploder, J., & Hrenič, Š. (2017). *Poročilo o izvajanju programa ukrepov za izboljšanje kakovosti okolja v Zgornji Mežiški dolini za leti 2016 in 2017*. NIJZ OE Ravne.

Ivartnik, M., Pavlič, H., Hudopisk, N., Simetinger, M., Ploder, J., & Kajnih, N. (2019). *B Poročilo o izvajanju programa ukrepov za izboljšanje kakovosti okolja v Zgornji Mežiški dolini za leto 2019*. NIJZ OE Ravne.

Ivartnik, M., Pavlič, H., Hudopisk, N., Simetinger, M., Vindiš, T., & Hrenič, Ž. (2019). *A Poročilo o izvajanju programa ukrepov za izboljšanje kakovosti okolja v Zgornji Mežiški dolini za leto 2018*. NIJZ OE Ravne.

Ivartnik, M., Pavlič, H., Hudopisk, N., Švetak, G., Simetinger, M., Hočevar, B., Ploder, J., & Vindiš, T. (2015). *Poročilo o izvajanju programa ukrepov za izboljšanje kakovosti okolja v Zgornji Mežiški dolini za programsko obdobje 2013/2014*. NIJZ OE Ravne.

Ivartnik, M., Pavlič, H., & Korošec, G. (2012). *Poročilo o izvajanju programa ukrepov za izboljšanje kakovosti okolja v Zgornji Mežiški dolini v letu 2012*. NIJZ OE Ravne.

Jeevanandam, J., Barhoum, A., Chan, Y. S., Dufresne, A., & Danquah, M. K. (2018). Review on nanoparticles and nanostructured materials: History, sources, toxicity and regulations. *Beilstein Journal of Nanotechnology*, *9*, 1050–1074. https://doi.org/10.3762/bjnano.9.98

Jez, E., & Lestan, D. (2015). Prediction of blood lead levels in children before and after remediation of soil samples in the upper Meza Valley, Slovenia. *Journal of Hazardous Materials*, *296*, 138–146. https://doi.org/10.1016/j.jhazmat.2015.04.049

Jochum, K. P., Nohl, U., Herwig, K., Lammel, E., Stoll, B., & Hofmann, A. W. (2005). GeoReM: A New Geochemical Database for Reference Materials and Isotopic Standards. *Geostandards and Geoanalytical Research*, *29*(3), 333–338. https://doi.org/10.1111/j.1751-908X.2005.tb00904.x

Judd, C. D., & Swami, K. (2010). ICP-MS determination of lead isotope ratios in legal and counterfeit cigarette tobacco samples. *Isotopes in Environmental and Health Studies*, *46*(4), 484–494. https://doi.org/10.1080/10256016.2010.528839

Kladnik, Š. (2009). *Primerjava aktualnega stanja okolja v Zgornji Mežiški dolini z razmerami v preteklih desetletjih* [Diplomsko delo]. Univerza v Ljubljani, Filozofska fakulteta, Oddelek za geografijo.

Koleša, T., Turšič, J., & Fašing, J. (2008). *Monitoring zunanjega zraka v Zgornji Mežiški dolini*. ARSO.

Komárek, M., Ettler, V., Chrastný, V., & Mihaljevič, M. (2008). Lead isotopes in environmental sciences: A review. *Environment International*, *34*(4), 562–577. https://doi.org/10.1016/j.envint.2007.10.005

Kong, H., Teng, Y., Song, L., Wang, J., & Zhang, L. (2018). Lead and strontium isotopes as tracers to investigate the potential sources of lead in soil and groundwater: A case study of the Hun River alluvial fan. *Applied Geochemistry*, *97*, 291–300. https://doi.org/10.1016/j.apgeochem.2018.08.022

Kushwaha, A., Hans, N., Kumar, S., & Rani, R. (2018). A critical review on speciation, mobilization and toxicity of lead in soil-microbe-plant system and bioremediation strategies. *Ecotoxicology and Environmental Safety*, *147*, 1035–1045. https://doi.org/10.1016/j.ecoenv.2017.09.049

Laborda, F., Bolea, E., & Jiménez-Lamana, J. (2014). Single Particle Inductively Coupled Plasma Mass Spectrometry: A Powerful Tool for Nanoanalysis. *Analytical Chemistry*, *86*(5), 2270–2278. https://doi.org/10.1021/ac402980q

Laborda, F., Gimenez-Ingalaturre, A. C., Bolea, E., & Castillo, J. R. (2019). Single particle inductively coupled plasma mass spectrometry as screening tool for detection of particles. *Spectrochimica Acta Part B: Atomic Spectroscopy*, *159*, 105654. https://doi.org/10.1016/j.sab.2019.105654

Laborda, F., Jiménez-Lamana, J., Bolea, E., & Castillo, J. R. (2013). Critical considerations for the determination of nanoparticle number concentrations, size and number size distributions by single particle ICP-MS. *Journal of Analytical Atomic Spectrometry*, *28*(8), 1220. https://doi.org/10.1039/c3ja50100k

Larrose, A., Coynel, A., Schäfer, J., Blanc, G., Massé, L., & Maneux, E. (2010). Assessing the current state of the Gironde Estuary by mapping priority contaminant distribution and risk potential in surface sediment. *Applied Geochemistry*, *25*(12), 1912–1923. https://doi.org/10.1016/j.apgeochem.2010.10.007

Lee, S., Han, C., Shin, D., Hur, S. D., Jun, S. J., Kim, Y.-T., Byun, D.-S., & Hong, S. (2017). Characteristics of elemental and Pb isotopic compositions in aerosols (PM10-

2.5) at the Ieodo Ocean Research Station in the East China Sea. *Environmental Pollution*, *231*, 154–164. https://doi.org/10.1016/j.envpol.2017.08.007

Li, F., Jinxu, Y., Shao, L., Zhang, G., Wang, J., & Jin, Z. (2018). Delineating the origin of Pb and Cd in the urban dust through elemental and stable isotopic ratio: A study from Hangzhou City, China. *Chemosphere*, *211*, 674–683. https://doi.org/10.1016/j.chemosphere.2018.07.199

Li, F.-L., Liu, C.-Q., Yang, Y.-G., Bi, X.-Y., Liu, T.-Z., & Zhao, Z.-Q. (2012). Natural and anthropogenic lead in soils and vegetables around Guiyang city, southwest China: A Pb isotopic approach. *Science of The Total Environment*, *431*, 339–347. https://doi.org/10.1016/j.scitotenv.2012.05.040

Liu, C., Chen, R., Sera, F., Vicedo-Cabrera, A. M., Guo, Y., Tong, S., Coelho, M. S. Z. S., Saldiva, P. H. N., Lavigne, E., Matus, P., Valdes Ortega, N., Osorio Garcia, S., Pascal, M., Stafoggia, M., Scortichini, M., Hashizume, M., Honda, Y., Hurtado-Díaz, M., Cruz, J., … Kan, H. (2019). Ambient Particulate Air Pollution and Daily Mortality in 652 Cities. *New England Journal of Medicine*, *381*(8), 705–715. https://doi.org/10.1056/NEJMoa1817364

Liu, H.-C., Chung, C.-H., You, C.-F., & Chiang, Y.-H. (2016). Determination of 87Sr/86Sr and δ88/86Sr ratios in plant materials using MC-ICP-MS. *Analytical and Bioanalytical Chemistry*, *408*(2), 387–397. https://doi.org/10.1007/s00216-015-9070-y

Long, E. R., Ingersoll, C. G., & MacDonald, D. D. (2006). Calculation and Uses of Mean Sediment Quality Guideline Quotients: A Critical Review. *Environmental Science & Technology*, *40*(6), 1726–1736. https://doi.org/10.1021/es058012d

Loskot, J., Jezbera, D., Nalezinková, M., Šmejkalová, A. H., Fernandes, D., & Komárek, J. (2024). Impact of Saharan dust on particulate matter characteristics in an urban and a natural locality in Central Europe. *Scientific Reports*, *14*(1), 32002. https://doi.org/10.1038/s41598-024-83603-0

Lowry, G. V., Gregory, K. B., Apte, S. C., & Lead, J. R. (2012). Transformations of Nanomaterials in the Environment. *Environmental Science & Technology*, *46*(13), 6893–6899. https://doi.org/10.1021/es300839e

MacDonald, D. D., Ingersoll, C. G., & Berger, T. A. (2000). Development and Evaluation of Consensus-Based Sediment Quality Guidelines for Freshwater Ecosystems. *Archives of Environmental Contamination and Toxicology*, *39*(1), 20–31. https://doi.org/10.1007/s002440010075

Miler, M., Bavec, Š., & Gosar, M. (2022). The environmental impact of historical Pb-Zn mining waste deposits in Slovenia. *Journal of Environmental Management*, *308*, 114580. https://doi.org/10.1016/j.jenvman.2022.114580

Miler, M., & Gosar, M. (2012). Characteristics and potential environmental influences of mine waste in the area of the closed Mežica Pb–Zn mine (Slovenia). *Journal of Geochemical Exploration*, *112*, 152–160. https://doi.org/10.1016/j.gexplo.2011.08.012

Miler, M., & Gosar, M. (2013). Assessment of Metal Pollution Sources by SEM/EDS Analysis of Solid Particles in Snow: A Case Study of Žerjav, Slovenia. *Microscopy and Microanalysis*, *19*(6), 1606–1619. https://doi.org/10.1017/S1431927613013202

Miler, M., & Gosar, M. (2019). Assessment of contribution of metal pollution sources to attic and household dust in Pb-polluted area. *Indoor Air*, *29*(3), 487–498. https://doi.org/10.1111/ina.12548

Mitrano, D. M., Barber, A., Bednar, A., Westerhoff, P., Higgins, C. P., & Ranville, J. F. (2012). Silver nanoparticle characterization using single particle ICP-MS (SP-ICP-

MS) and asymmetrical flow field flow fractionation ICP-MS (AF4-ICP-MS). *Journal of Analytical Atomic Spectrometry*, *27*(7), 1131. https://doi.org/10.1039/c2ja30021d

Monna, F., Benothman, D., & Luck, J. (1995). Pb isotopes and Pb, Zn and Cd concentrations in the rivers feeding a coastal pond (Thau, southern France): Constraints on the origin(s) and flux(es) of metals. *Science of The Total Environment*, *166*(1–3), 19–34. https://doi.org/10.1016/0048-9697(95)04514-2

Monna, F., Lancelot, J., Croudace, I. W., Cundy, A. B., & Lewis, J. T. (1997). Pb Isotopic Composition of Airborne Particulate Material from France and the Southern United Kingdom: Implications for Pb Pollution Sources in Urban Areas. *Environmental Science & Technology*, *31*(8), 2277–2286. https://doi.org/10.1021/es960870+

Morgan, T. J., George, A., Boulamanti, A. K., Álvarez, P., Adanouj, I., Dean, C., Vassilev, S. V., Baxter, D., & Andersen, L. K. (2015). Quantitative X-ray Fluorescence Analysis of Biomass (Switchgrass, Corn Stover, Eucalyptus, Beech, and Pine Wood) with a Typical Commercial Multi-Element Method on a WD-XRF Spectrometer. *Energy & Fuels*, *29*(3), 1669–1685. https://doi.org/10.1021/ef502380x

Mourdikoudis, S., Pallares, R. M., & Thanh, N. T. K. (2018). Characterization techniques for nanoparticles: Comparison and complementarity upon studying nanoparticle properties. *Nanoscale*, *10*(27), 12871–12934. https://doi.org/10.1039/C8NR02278J

National programe on environmental protection, Official Gazette RS 83/99. (1999). Republic of Slovenia.

Needleman, H. (2004). Lead Poisoning. *Annual Review of Medicine*, *55*(1), 209–222. https://doi.org/10.1146/annurev.med.55.091902.103653

Ordinance on areas of maximum environmental impact and on the program of measures to improve the quality of the environment in the upper Meža Valley, Official Gazette RS 119/07. (2007). Republic of Slovenia.

Pace, H. E., Rogers, N. J., Jarolimek, C., Coleman, V. A., Higgins, C. P., & Ranville, J. F. (2011). Determining Transport Efficiency for the Purpose of Counting and Sizing Nanoparticles via Single Particle Inductively Coupled Plasma Mass Spectrometry. *Analytical Chemistry*, *83*(24), 9361–9369. https://doi.org/10.1021/ac201952t

Pan, L., Fang, G., Wang, Y., Wang, L., Su, B., Li, D., & Xiang, B. (2018). Potentially Toxic Element Pollution Levels and Risk Assessment of Soils and Sediments in the Upstream River, Miyun Reservoir, China. *International Journal of Environmental Research and Public Health*, *15*, 2364. https://doi.org/10.3390/ijerph15112364

Pant, P., & Harrison, R. M. (2012). Critical review of receptor modelling for particulate matter: A case study of India. *Atmospheric Environment*, *49*, 1–12. https://doi.org/10.1016/j.atmosenv.2011.11.060

Pant, P., Shi, Z., Pope, F. D., & Harrison, R. M. (2017). Characterization of Traffic-Related Particulate Matter Emissions in a Road Tunnel in Birmingham, UK: Trace Metals and Organic Molecular Markers. *Aerosol and Air Quality Research*, *17*(1), 117–130. https://doi.org/10.4209/aaqr.2016.01.0040

Perraud, V., Bruns, E. A., Ezell, M. J., Johnson, S. N., Yu, Y., Alexander, M. L., Zelenyuk, A., Imre, D., Chang, W. L., Dabdub, D., Pankow, J. F., & Finlayson-Pitts, B. J. (2012). Nonequilibrium atmospheric secondary organic aerosol formation and growth. *Proceedings of the National Academy of Sciences*, *109*(8), 2836–2841. https://doi.org/10.1073/pnas.1119909109

Philip Horwitz, E., Dietz, M. L., Rhoads, S., Felinto, C., Gale, N. H., & Houghton, J. (1994). A lead-selective extraction chromatographic resin and its application to the isolation of lead from geological samples. *Analytica Chimica Acta*, *292*(3), 263–273. https://doi.org/10.1016/0003-2670(94)00068-9

Piaścik, M., Perez Przyk, E., & Held, A. (2010). *The certification of the mass fractions of arsenic, cadmium, nickel and lead in fine dust (PM10-like matrix): Certified reference material ERM-CZ120*. Publications Office, European Commission. Joint Research Centre. Institute for Reference Materials and Measurements. https://data.europa.eu/doi/10.2787/31636

Pietrogrande, M. C., Bacco, D., Trentini, A., & Russo, M. (2021). Effect of filter extraction solvents on the measurement of the oxidative potential of airborne PM2.5. *Environmental Science and Pollution Research*, *28*(23), 29551–29563. https://doi.org/10.1007/s11356-021-12604-7

Pin, C., Gannoun, A., & Dupont, A. (2014). Rapid, simultaneous separation of Sr, Pb, and Nd by extraction chromatography prior to isotope ratios determination by TIMS and MC-ICP-MS. *J. Anal. At. Spectrom.*, *29*(10), 1858–1870. https://doi.org/10.1039/C4JA00169A

Prestor, J., Štrucl, S., & Pungartnik, M. (2003). Mežica lead and zinc mine closure impact on hydrogeological conditions in upper Meža valley. *RMZ - Materials and Geoenvironment*, *50*(1), 313–316.

Prohaska, T., Irrgeher, J., Zitek, A., & Jakubowski, N. (Eds.). (2014). *Sector Field Mass Spectrometry for Elemental and Isotopic Analysis*. The Royal Society of Chemistry. https://doi.org/10.1039/9781849735407

Prpić-Majić, D. (1982). *Povečana apsorpcija olova u radnika, pomočnog i tehničkog osoblja 'OZD Rudniki svinca in topilnica Mežica'. Izvještaj IMI-P-47.* Zagreb, Institut za medicinska istraživanja i medicinu rada.

Rabajczyk, A., Zielecka, M., Porowski, R., & Hopke, P. K. (2020). Metal nanoparticles in the air: State of the art and future perspectives. *Environmental Science: Nano*, *7*(11), 3233–3254. https://doi.org/10.1039/D0EN00536C

Rečnik, A., Zavašnik, J., & Fajmut-Štrucl, S. (2014). The Mežica mine, Koroška (Slovenia). *The Mineralogical Record*, *45*(5), 507–548.

Regulation on drinking water, Official Gazette RS 19/04. (2004). Republic of Slovenia.

Results of the three-month air monitoring in the upper Meža Valley. (2007). ARSO.

Rogan Šmuc, N., Žerdoner, T., Zuliani, T., & et al. (2025). *Personal Communication, not published.*

Roper, C., Delgado, L. S., Barrett, D., Massey Simonich, S. L., & Tanguay, R. L. (2019). PM $_{2.5}$ Filter Extraction Methods: Implications for Chemical and Toxicological Analyses. *Environmental Science & Technology*, *53*(1), 434–442. https://doi.org/10.1021/acs.est.8b04308

Rudge, J. F., Reynolds, B. C., & Bourdon, B. (2009). The double spike toolbox. *Chemical Geology*, *265*(3–4), 420–431. https://doi.org/10.1016/j.chemgeo.2009.05.010

Sanderson, P., Delgado-Saborit, J. M., & Harrison, R. M. (2014). A review of chemical and physical characterisation of atmospheric metallic nanoparticles. *Atmospheric Environment*, *94*, 353–365. https://doi.org/10.1016/j.atmosenv.2014.05.023

Shiel, A. E., Weis, D., & Orians, K. J. (2010). Evaluation of zinc, cadmium and lead isotope fractionation during smelting and refining. *Science of The Total Environment*, *408*(11), 2357–2368. https://doi.org/10.1016/j.scitotenv.2010.02.016

Souto-Oliveira, C. E., Babinski, M., Araújo, D. F., & Andrade, M. F. (2018). Multi-isotopic fingerprints (Pb, Zn, Cu) applied for urban aerosol source apportionment and discrimination. *Science of The Total Environment*, *626*, 1350–1366. https://doi.org/10.1016/j.scitotenv.2018.01.192

Špes, M. (1998). Degradacija okolja kot dejavnik diferenciacije urbane pokrajine. *Geographica Slovenica*, *30.*

Štrucl, I. (1984). Geološke, geokemične in mineraloške značilnosti rude in prikamenine svinčevo-cinkovih orudenenj mežiškega rudišča. *Geologija*, *27*, 215–327.

Svete, P., Milačič, R., & Pihlar, B. (2001). Partitioning of Zn, Pb and Cd in river sediments from a lead and zinc mining area using the BCR three-step sequential extraction procedure. *Journal of Environmental Monitoring*, *3*(6), 586–590. https://doi.org/10.1039/b106311c

Tansel, B., & Rafiuddin, S. (2016). Heavy metal content in relation to particle size and organic content of surficial sediments in Miami River and transport potential. *International Journal of Sediment Research*, *31*(4), 324–329. https://doi.org/10.1016/j.ijsrc.2016.05.004

Taylor, R. N., Ishizuka, O., Michalik, A., Milton, J. A., & Croudace, I. W. (2015). Evaluating the precision of Pb isotope measurement by mass spectrometry. *Journal of Analytical Atomic Spectrometry*, *30*(1), 198–213. https://doi.org/10.1039/C4JA00279B

Thalassinos, G., Petropoulos, S. A., Grammenou, A., & Antoniadis, V. (2023). Potentially Toxic Elements: A Review on Their Soil Behavior and Plant Attenuation Mechanisms against Their Toxicity. *Agriculture*, *13*, 1684. https://doi.org/10.3390/agriculture13091684

Thomas, R. (2003). *Practical Guide to ICP-MS*. CRC Press. https://doi.org/10.1201/9780203027073

Torregrosa, D., Grindlay, G., De La Guardia, M., Gras, L., & Mora, J. (2023). Determination of metallic nanoparticles in air filters by means single particle inductively coupled plasma mass spectrometry. *Talanta*, *252*, 123818. https://doi.org/10.1016/j.talanta.2022.123818

Uzu, G., Sobanska, S., Sarret, G., Muñoz, M., & Dumat, C. (2010). Foliar Lead Uptake by Lettuce Exposed to Atmospheric Fallouts. *Environmental Science & Technology*, *44*(3), 1036–1042. https://doi.org/10.1021/es902190u

Vanhaecke, F., & Degryse, P. (Eds.). (2012). *Isotopic Analysis: Fundamentals and Applications Using ICP-MS*. Wiley.

Wagner, S., Santner, J., Irrgeher, J., Puschenreiter, M., Happel, S., & Prohaska, T. (2022). Selective Diffusive Gradients in Thin Films (DGT) for the Simultaneous Assessment of Labile Sr and Pb Concentrations and Isotope Ratios in Soils. *Analytical Chemistry*, *94*(16), 6338–6346. https://doi.org/10.1021/acs.analchem.2c00546

Walraven, N., Van Os, B. J. H., Klaver, G. Th., Middelburg, J. J., & Davies, G. R. (2014). Reconstruction of historical atmospheric Pb using Dutch urban lake sediments: A Pb isotope study. *Science of The Total Environment*, *484*, 185–195. https://doi.org/10.1016/j.scitotenv.2014.02.062

Wang, C., Liu, S., Zhao, Q., Deng, L., & Dong, S. (2012). Spatial variation and contamination assessment of heavy metals in sediments in the Manwan Reservoir, Lancang River. *Ecotoxicology and Environmental Safety*, *82*, 32–39. https://doi.org/10.1016/j.ecoenv.2012.05.006

Wang, J., Chen, T., Zhang, W., Zhao, Y., Yang, S., & Chen, A. (2020). Tracing the geographical origin of rice by stable isotopic analyses combined with chemometrics. *Food Chemistry*, *313*, 126093. https://doi.org/10.1016/j.foodchem.2019.126093

Wang, L., Jin, Y., Weiss, D. J., Schleicher, N. J., Wilcke, W., Wu, L., Guo, Q., Chen, J., O'Connor, D., & Hou, D. (2021). Possible application of stable isotope compositions for the identification of metal sources in soil. *Journal of Hazardous Materials*, *407*, 124812. https://doi.org/10.1016/j.jhazmat.2020.124812

Wang, Q., Zhuang, G., Li, J., Huang, K., Zhang, R., Jiang, Y., Lin, Y., & Fu, J. S. (2011). Mixing of dust with pollution on the transport path of Asian dust—Revealed from the aerosol over Yulin, the north edge of Loess Plateau. *Science of The Total Environment*, *409*(3), 573–581. https://doi.org/10.1016/j.scitotenv.2010.10.032

Wang, S. X., Zhang, S. Z., & Shan, X.-Q. (2003). Fractionation of heavy metals in different particle-size sediments and its relationship with heavy metal pollution. *Bulletin of Environmental Contamination and Toxicology*, *71*, 873–880.

Wedepohl, K. H. (1995). The composition of the continental crust. *Geochimica et Cosmochimica Acta*, *59*(7), 1217–1232.

Wen, H., Zhang, Y., Cloquet, C., Zhu, C., Fan, H., & Luo, C. (2015). Tracing sources of pollution in soils from the Jinding Pb–Zn mining district in China using cadmium and lead isotopes. *Applied Geochemistry*, *52*, 147–154. https://doi.org/10.1016/j.apgeochem.2014.11.025

WHO global air quality guidelines. Particulate matter (PM2.5 and PM10), ozone, nitrogen dioxide, sulfur dioxide and carbon monoxide. (2021). World Health Organization.

Xu, H. M., Cao, J. J., Ho, K. F., Ding, H., Han, Y. M., Wang, G. H., Chow, J. C., Watson, J. G., Khol, S. D., Qiang, J., & Li, W. T. (2012). Lead concentrations in fine particulate matter after the phasing out of leaded gasoline in Xi'an, China. *Atmospheric Environment*, *46*, 217–224. https://doi.org/10.1016/j.atmosenv.2011.09.078

Yang, Y., Vance, M., Tou, F., Tiwari, A., Liu, M., & Hochella, M. F. (2016). Nanoparticles in road dust from impervious urban surfaces: Distribution, identification, and environmental implications. *Environmental Science: Nano*, *3*(3), 534–544. https://doi.org/10.1039/C6EN00056H

Yoshinaga, J., Yamasaki, K., Yonemura, A., Ishibashi, Y., Kaido, T., Mizuno, K., Takagi, M., & Tanaka, A. (2014). Lead and other elements in house dust of Japanese residences – Source of lead and health risks due to metal exposure. *Environmental Pollution*, *189*, 223–228. https://doi.org/10.1016/j.envpol.2014.03.003

Zhang, K., Chai, F., Zheng, Z., Yang, Q., Zhong, X., Fomba, K. W., & Zhou, G. (2018). Size distribution and source of heavy metals in particulate matter on the lead and zinc smelting affected area. *Journal of Environmental Sciences*, *71*, 188–196. https://doi.org/10.1016/j.jes.2018.04.018

Zhang, S., Wang, S., & Shan, X. (2002). DISTRIBUTION AND SPECIATION OF HEAVY METALS IN SURFACE SEDIMENTS FROM GUANTING RESERVOIR, BEIJING. *Journal of Environmental Science and Health, Part A*, *37*(4), 465–478. https://doi.org/10.1081/ESE-120003228

Zhao, Z.-Q., Zhang, W., Li, X.-D., Yang, Z., Zheng, H.-Y., Ding, H., Wang, Q.-L., Xiao, J., & Fu, P.-Q. (2015). Atmospheric lead in urban Guiyang, Southwest China: Isotopic source signatures. *Atmospheric Environment*, *115*, 163–169. https://doi.org/10.1016/j.atmosenv.2015.05.049

Žibret, G., Gosar, M., Miler, M., & Alijagić, J. (2018). Impacts of mining and smelting activities on environment and landscape degradation—Slovenian case studies. *Land Degradation & Development*, *29*(12), 4457–4470. https://doi.org/10.1002/ldr.3198

Zuliani, T., Mladenovič, A., Ščančar, J., & Milačič, R. (2016). Chemical characterisation of dredged sediments in relation to their potential use in civil engineering. *Environmental Monitoring and Assessment*, *188*(4), 234. https://doi.org/10.1007/s10661-016-5239-x

Zupan, M., Grčman, H., Tič, I., Hodnik, A., Kralj, T., Šporar, M., Rupreht, J., Šinkovec, M., Lapajne, S., Šijanec, V., Ilc, Z., Gogić Knezić, S., Mohorovič, B., Istenič, B., Kralj, T., Rojec, L., Rojec, M., Zupan, M., & Šijanec, M. (2008). *Raziskave onesnaženosti tal Slovenije, poročilo za leto 2007.* Biotehniška fakulteta UL.

Bibliography

Publications Related to the Thesis

Journal Articles

Goltnik, T., Burger, J., Kranjc, I., Turšič, J., & Zuliani, T. (2022). Potentially toxic elements and Pb isotopes in mine-draining Meža River catchment (NE Slovenia). *Water*, 14(7), 998-1-998-13. DOI: 10.3390/w14070998

Žerdoner, T., Vidmar, J., Arah, B., & Zuliani, T. (2025). Determination of airborne metal-containing nanoparticles in a historic mining area using single particle ICP-MS. *Analyst*, Online edition (in press). DOI: 10.1039/d5an00480b

Žerdoner, T., Burger, J., Kranjc, I., Turšič, J., & Zuliani, T. (2025). Revealing Long-Term Anthropogenic Influence on PM_{10} Through Lead Isotope Signatures in a Post-Mining Region. *Atmospheric Environment,* under review.

Conference Papers

Goltnik, T., & Zuliani, T. (2021). Development of an analytical method for the determination of the isotopic composition of Pb in environmental samples. In *Throughout knowledge towards a green new world: book of abstracts. 13th Jožef Stefan International Postgraduate School Students' Conference*. Ljubljana, Slovenia: Jožef Stefan International Postgraduate School, Jožef Stefan Institute.

Goltnik, T., & Zuliani, T. (2021). Identification of Pb sources in the upper Mežica Valley based on Pb isotope composition. In *Goldschmidt Virtual Conference*. European Association of Geochemistry and the Geochemical Society.

Goltnik, T., Burger, J., Kranjc, I., Turšič, J., & Zuliani, T. (2021). Pb isotopic composition in environmental samples from Upper Meža Valley. In *Book of abstracts: 27th Annual Meeting of the Slovenian Chemical Society*. Portorož, Slovenia: Slovenian Chemical Society.

Goltnik, T., Burger, J., Kranjc, I., Turšič, J., & Zuliani, T. (2022). Elemental and Pb isotope composition in water and sediments from the Meža river catchment. *In Book of abstracts: 14th Jožef Stefan International Postgraduate School Students' Conference*. Kamnik, Slovenia: Jožef Stefan International Postgraduate School, Jožef Stefan Institute.

Goltnik, T., Nikezić, M., Hauptman, Ž., Gračanin, N., Dolenec, M., Rogan Šmuc, N., Benedik, L., & Zuliani, T. (2022). Precise determination of isotope ratios of non-traditional elements in solid environmental samples. In *Book of abstracts: 28th Annual Meeting of the Slovenian Chemical Society*. Portorož, Slovenia: Slovenian Chemical Society.

Nikezić, M., Goltnik, T., Furdek, M., Ivanić, M., Fiket, Ž., Meić, A., Zgrablić, Ž., & Zuliani, T. (2022). Determination of $^{87}Sr/^{86}Sr$ ratio in truffles from Istria, Croatia. In *Book of* *abstracts: 28th Annual Meeting of the Slovenian Chemical Society.* Portorož, Slovenia: Slovenian Chemical Society.

Goltnik, T., Burger, J., Koleša,. T., Kranjc, I., Turšič, J., & Zuliani, T. (2023). Use of lead isotope composition for source tracing of air particulate matter from Upper Meža Valley. *In European Winter Conference on Plasma Spectrochemistry: Book of abstracts.* Ljubljana, Slovenia: National Institute of Chemistry.

Žerdoner, T., Vidmar, J., & Zuliani, T. (2023). Optimization of extraction of Pb nanoparticles from PM_{10} filters for single particle ICP-MS analysis. In *Book of abstracts: 29th Annual Meeting of the Slovenian Chemical Society.* Portorož, Slovenia: Slovenian Chemical Society.

Zuliani, T., Nikezić, M., & Žerdoner, T. (2024). Stable non-traditional isotopes as tracers for the identification of contaminant sources. In *Meeting point of the science and practice in the fields of corrosion, materials and environmental protection: proceedings.* Beograd, Serbia. Serbian Society of Corrosion and Materials Protection.

Other Publications

Zuliani, T., Vidmar, J., Goltnik, T., Nikezć, M., Ščančar, J., & Milačič, R. (2023). Unlocking the mysteries of trace elements: their quantification, speciation and isotope ratio determination: *lecture at Montanuniversität Leoben, Department für Chemie, Leoben, Austria.*

Zuliani, T., Žerdoner, T., & Nikezć, M. (2023). Non-traditional isotopes: exploring new avenues in environmental and geoscience research: *lecture at Instiut Ruđer Bošković, Zagreb, Croatia.*

Žerdoner, T., Zuliani, T., & Vidmar, J. (2024). Optimization of a method for determination of Zn- and Pb-containing nanoparticles in PM_{10} by sp-ICP-MS: *lecture at Strokovno srečanje uporabnikov ICP-MS opreme, ICP-MS Seminar 2024, Ljubljana, Slovenia.*

Zuliani, T., Vidmar, J., Nikezić, M., Žerdoner, T., Leban, P., Marković, K., Marković, S., Ščančar, J., Milačič, R. (2024). Studying the biogeochemical cycling of elements by the use of ICP-MS: *lecture at Strokovno srečanje uporabnikov ICP-MS opreme, ICP-MS Seminar 2024, Ljubljana, Slovenia.*

Biography

Tjaša Žerdoner was born on 2.11.1993 in Slovenj Gradec, Slovenia. She finished Gymnasium Velenje in 2012 and started her Bachelor's Degree studies at the Faculty of Chemistry and Chemical Technology at the University of Ljubljana. During her studies, she had practical training at the National Institute of Chemistry, working on the synthesis of TiO_2 particles with a flower-shaped nanostructure that can be used in the photocatalytic fission of water. In 2018, she obtained her Bachelor's Degree in Chemistry, titled "Low-temperature synthesis and self-cleaning efficiency of TiO_2-ZrO_2 thin films on glass and metal substrates". In 2018, she enrolled in a Master's Study program at the Faculty of Chemistry and Chemical Engineering at the University of Maribor. During her studies, she had practical training at the National Laboratory for Health, Environment and Food, Maribor, at the Laboratory for Water Analysis, where she was introduced to various analytical techniques for determining the general parameters and composition of water. She also participated in the PKP project (Po kreativni poti do znanja / On the creative path to knowledge) "Support in testing and analysis of curcumin formulations (TEST-AN KURKUMA)". In 2020, she obtained her Master's Degree in Chemistry, titled "Removal of trace organic contaminants from model wastewater using forward osmosis". Then she continued with her PhD studies at the Jožef Stefan International Postgraduate School, doctoral study program Ecotechnologies, under the supervision of assoc. prof. dr. Tea Zuliani and was employed as a young researcher at the Jožef Stefan Institute, at the Department of Environmental Sciences. Her research focused on the source appointment of lead (Pb) present in airborne particulate matter (PM_{10}) by determination of total elemental concentrations, Pb isotopes, and metal-containing nanoparticles in PM_{10}, as well as different environmental samples from the Upper Meža Valley.